# Strength Enhancement of Prestressed Concrete Dapped-End Girders

**Dr.Shatha Dhia Mohammed**
Lecturer
College of Engineering- University of Baghdad
Email:Shathadhia@yahoo.com

**Dr. Thamer Khudair Mahmoud**
Professor
College of Engineering- University of Baghdad
Email:thamir.azawi@gmail.com

## ABSTRACT

This paper presents the application of nonlinear finite element models in the analysis of dapped-ends pre-stressed reinforced concrete girders under static loading by using ANSYS software. The girder dimensions are (4.90 m span, 0.40 m depth, 0.20 m width, 0.20 m nib depth, and 0.10 m nib length) and the parameters considered in this research are the pre-stress effect, and strand profile (straight and draped).

The numerical results are compared with the experimental results of the same girders. The comparisons are carried out in terms of initial prestress effect, load- deflection curve, and failure load. Good agreement was obtained between the analytical and experimental results. Even that, the numerical model was stiffer than the experimental, but; there were a good agreements in both trends and values. The difference varies in the range (5-12)% for the deflection. Results have shown that the pre-stress force has increased the static ultimate load capacity by (35%) in case of straight strand and by (97%) in case of draped strand

**Key words:** dapped-end girder, finite element, prestress.

# تعزيز مقاومة الروافد الخرسانية المسبقة الجهد ذات النهايات المستدقة

**شذى ضياء محمد**
مدرس
كلية الهندسة - جامعة بغداد

**د.ثامر خضير محمود**
استاذ
كلية الهندسة - جامعة بغداد

## الخلاصة

يقدم هذا البحث دراسة التحليل الغير خطي باستخدام نظرية العناصر المحددة لتحليل العتبات الخرسانية المسبقة الجهد ذات النهايات المستدقة تحت تاثير الاحمال الاستاتيكية باستخدام برنامج (ANSYS). ابعاد العتب المحلل كانت (4.90 م للفضاء, 0.40 م عمق , 0.20 م عرض , 0.20 م عمق النهاية المستدقة و 0.10 م طول النهاية المستدقة ) . قام البحث بدراسة تاثير كل منذ قوة الاجهاد و مسار حبال الشد ( مستقيمة , منحنية) على التحمل الاقصى للعتب .

تمت مقارنة النتائج العددية مع ما يماثلها من نتائج عملية وقد كانت المقارنة بدلالة الانحناء الاولي الناتج عن قوة الشد , منحني القوة-الهطول و حمل الفشل وقد اظهرت المقارنة تقاربا جيدا بين النتائج النظرية و مثيلاتها العملية. وعلى الرغم من كون النموذج الممثل باستخدام نظرية العناصر المحددة كان اكثر جساءة من مثيله عمليا الا ان النتائج اظهرت توافقا جيدا من ناحيتي النزعة والقيم القصوى تتراوح بين (5-12)%. كما وجد بان قوة الاجهاد المسبق تزيد من مقدار الحمل الاقصى بنسبة ( 35%) لحالات حبال الشد ذات المسار المستقيم و بنسبة (97%) لحالات المسار المنحني.

**الكلمات الرئيسية:** الروافد ذات النهايات المستدقة, العناصر المحددة, الاجهاد المسبق

## 1. INTRODUCTION

The severe stress concentration at the re-entrant corner of the dapped- end girders, due to unusual shape, didn't restrict the extensively using of such girders in different types of structures. It is a better choice for better lateral stability; since it lowers the deck center of gravity by indentation supporting corbel into the depth of the supported girders. The re-entrant corner, certainly, can be considered as the weakest location in the dapped-ends girder. It requires special details of reinforcement, otherwise, a rapid diagonal tension cracks may propagate and a failure will acquire with few or no warning.

Many of researches had been started since 1969 when Reynold, **Reynold, G. C., 1969,** developed suitable reinforcement details evolving a design procedure for dapped-end members. Then after many researches were made to study the shear capacity and behavior of RC dapped-end beams, **Ajina, J. M., 1986, Herzinger, R. and El-Badry, M. M. ,2002, Liem, S. K., 1983, Mohamed, R. N. and Elliott, K. S., 2008, Reynold, G. C., 1969, Wang, Q. , Guo, Z. and Hoogenboom, P.C.J., 2005**. PCI, ACI and STM design method were considered to detect the most sufficient and economic design of dapped-end beam, **Ahmed, S. et al, 2013, Barton, D. L., 1988, Huang, P.C, J.J Myers and A. Nanni, 2000, Mader, B. S., 1999, Mattock, A. H., and Theryo, T., 1986** . There were also many researches that studied the effect of different reinforcement details on the response of dapped-end beam, **Herzinger, R. and El-Badry, M. M. ,2002, Mattock, A. H., and Theryo, T., 1986**. The effect of geometric layout of the dapped- end (nib height and width) were also considered in some researches, **Chung, J. C. J, 1985, Khan, M. A., 1981**.

## 2. FINITE ELEMENT TYPES CONSIDERED IN THE PRESENT STUDY

The concrete will be modeled using Solid65 element. This element has eight nodes with three degrees of freedom at each node (translations in the nodal x, y, and z directions). Plastic deformation, cracking in three orthogonal directions, and crushing are the most important capability of this element that made it a suitable choice to model concrete material. **Fig. 1** shows the schematic drawing of this element.

Steel reinforcement and steel strand are modelled using Link8 element. This element is a 3D spar element and it has two nodes with three degrees of freedom at each node (translations in the nodal *x*, y and z directions) as shown in **Fig. 2**. This element is also capable to represent an initial strain and plastic deformation at high stress level.

The Solid45 element is used for modelling the steel plates at the supports and loading locations to prevent stress concentration and to provide stress distribution over supports and loading areas. The element is defined with eight nodes having three degrees of freedom at each node – translations in the nodal x, y, and z directions. The geometry and node locations for this element type are shown in **Fig. 3**.

## 3. MATERIAL PROPERTIES

The required parameters to identify the material models are listed in **Table 1**. Regarding Solid65 element (set No. 1), the model includes density, linear isotropic and multi-linear isotropic properties to properly model concrete material. The compressive uniaxial stress-strain relationship for the concrete model (multi-linear isotropic) was obtained using the following equations, **MacGregor, 1992.**

$$f = \frac{E_c \varepsilon}{1+\left(\frac{\varepsilon}{\varepsilon_o}\right)^2} \quad (1)$$

$$\varepsilon_o = \frac{2f_c'}{E_c} \quad (2)$$

$$E = \frac{f}{\varepsilon} \quad (3)$$

Where:
$f$ = Stress at any strain.
$\varepsilon$ = Strain at stress $f$.
$\varepsilon_o$ = Strain at the ultimate compressive strength $fc'$.
$E$ = Modulus of elasticity.

Based on Hook's law and Eq. (1), the adopted stress-strain relationship for concrete used in this study, **Fig. 4 (b)** was that as suggested by **Jindal, A., 2012, Wolanski, B. S., 2001, and Kachlakev, D. I., 2005**. The curves start at zero stress and strain while the first points (defined at 0.3 $fc'$) was calculated in the linear range, Eq. (3). The rest points (2-6) were calculated from Eq. (1) with $\varepsilon_o$ obtained from Eq. (2).

Model numbers 2, and 3 refer to Link8 element. This element was used for all steel reinforcement and it is assumed to be bilinear isotropic behavior at nonlinear stage. Bilinear isotropic material is also based on the Von Mises failure criteria. This model requires the yield stress ($f_y$), as well as the hardening modulus of the steel to be defined.

Material model number 4 refers to the Solid45 element used for the steel plates at loading points and at supports. Therefore, this element is modeled as a linear isotropic element.

Material model number 5 represents the properties of pre-stressing steel. It was modeled as multilinear isotropic material following the von Mises failure criteria. The pre-stressing steel was modeled using a multilinear stress-strain curve developed using the following equations, **Wolanski, B. S.,2001.**

$$\varepsilon_{ps} \leq 0.008\ ; \quad f_{ps} = 28\,000\ \varepsilon_{ps}\ ksi \tag{4}$$

$$\varepsilon_{ps} > 0.008\ ; \quad f_{ps} = 286 - \frac{0.075}{(\varepsilon_{ps} - 0.0065)} < 0.98 f_{ps}\ ksi \tag{5}$$

## 4. GEOMETRY AND FINITE ELEMENT MODELING

Three simply supported dapped-ends girders that had the same geometric layout, flexural and shear reinforcement (**Fig. 5, Fig. 6 and Table 2)** are analyzed using ANSYS finite elements model. All the tested beams were designed, according to PCI Design Handbook 6th Edition [16] requirements to fail at their ends.

The dapped-ends girders, anchorages, load plates, and support plates were modeled as volumes. The combined volumes are shown in **Fig.7** for both straight and draped strand profiles, respectively, while the layout of the generated draped duct is sown in **Fig. 8**.

The use of a rectangular or square mesh is recommended for Solid65 element to obtain good results, **Wolanski, B. S., 2001**. However, the presence of the duct, reduces the possibility to mesh the circular hole properly. Therefore, finer the mesh was set for elements as possible near the duct. The overall mesh of the concrete, load and support plate volumes is shown in **Fig. 9** for the straight and draped strands, respectively. Lines were created so that they pass through the nodes of the reinforcement bars, then after a mesh line command was adopted to generate the reinforcement elements. However, the necessary mesh attributes as described above need to be set before each section of the reinforcement is created. **Fig. 10 and Fig. 11** show the overall mesh of the steel reinforcement for a straight and draped strands, respectively.

## 5. VALIDATION OF THE FINITE ELEMENT MODEL

In order to validate the finite element modeling of reinforced and prestressed dapped-ends concrete beams , the finite element model using ANSYS program has been applied to analyze a compatible concrete beams tested in by **Mohammed, S. D., and Mahmoud, T. K., 2014**. The predicted results are compared with the experimental results. The comparison includes prestress effect, load-deflection relation, and failure load.

### 5.1 Pre-stress effect

The deflections obtained from experimental work **(Mohammed, S. D., and Mahmoud, T. K., 2014)**, hand calculations, and from the FE analysis due to the pre-stress effect are given in **Table 3** (no hand calculation was considered for cases of draped strand profile). **Fig. 12** shows the deflected shape due to pre-stress effect for each tested specimens. From **Table 3** it is clear that there is a good agreement between the experimental, hand calculations. The difference varies between (1%) and (6%).

### 5.2 Load - deflection relation.

The results obtained from the FE analysis for the load – deflection relation are presented in **Fig. 13** while **Fig.14** shows the contour lines of the deflection at the failure stage. The presentation also includes a comparison between the experimental **(Mohammed, S. D., and Mahmoud, T. K., 2014)** and numerical results. Even that the numerical models were stiffer than the experimental, but; there were a good agreement in both trend and amplitude that varies between (5%) and (12%).

### 5.3 Load at failure

In the finite element analysis, the continuity in the solution process, depends on the concepts of rigid body motion. The small load increment solution continues until there is a dis-converge in results. **Table 4** gives the failure load as obtained from the FE analysis and the experimental work **(Mohammed, S. D., and Mahmoud, T. K., 2014)** for each modeled specimens.

## 6. RESPONSE AND BEHAVIOUR OF DAPPED-END REINFORCEMENT

Five positions were adopted to get better understanding for the response and behaviour of the dapped-end reinforcement that is recommended by the PCI**, PCI Design Handbook 6$^{th}$ Edition 2004,** as shown in **Fig. 15**. The effect of the pre-stressing presses was investigated, **Fig. 16** shows the advantage of the draped strand profile on the response of shear and flexure reinforcement ( $A_h$, $A_v$, $A_s$, $A_{sh}$, and $A_{s'h}$) It is clear that in case of draped strand, the reinforcement yields when approaching the failure stage which indicates a good strengthening for the concrete.

The crack patterns, for each modeled specimen, as obtained from ANSYS program are shown in **Fig.17**. These cracks were selected at the failure stage. It is clear that the initial crack generated at the re-entrant corner of the dapped-ends girder and extends then after toward the applied load. This is compatible with the experiment test results by **Mohammed, S. D., and Mahmoud, T. K., 2014**.

## 7. CONCLUSIONS

Based on the predicted results from the finite element analysis, the following conclusions may be drown:

1. There was no significant difference in the effect of pre-stress force, for both straight and draped strand profile, on the response of flexural reinforcement ($A_s$, $A_h$, and $A_{s'h}$) up to crack

stage. Then after the strain load curves show a separation due to the stiffening effect of draped pre-stress force.

2. The behavior and response of shear reinforcement ($A_v$ and $A_{sh}$) under the effect of straight and draped strand profile are similar to that of flexural reinforcement of the dapped-ends girder.

3. Straight pre-stress profile shows about (35%) more effect on the response of shear reinforcement ($A_{sh}$) than other types of shear reinforcement ($A_v$).

4. A similar crack pattern in all specimens was detected. Cracks started with the initiation of diagonal re-entrant crack, followed by nib inclined crack and diagonal tension crack (developed in the full-depth of the girder).

5. The general behavior of the finite element model presented by the load- deflection shows a good agreement in both trend and amplitude.

6. The finite element model behavior was stiffer than that of the tested specimen due to the effect of bond slip between the concrete and steel bars and the effect of micro cracks which were excluded in the finite element analysis. The overestimation in the failure load as calculated by the finite element analysis was (4-11)%.

## REFERENCE


- Ahmed, S. et al, 2013, *Evaluation of the Shear Strength of Dapped Ended Beam*, Life Science Journal, Vol. 10, No. 3, PP. 1038-1044.

- Ajina, J. M., 1986, *Effect of Steel Fibers on Precast Dapped-End Beam*, CMS Thesis, South Dakota State University, Brookings, SD.

- Barton, D. L., 1988, *Detailing of Structural Concrete Dapped End Beams*, MS Thesis, University of Texas at Austin, Austin, TX.

- Chung, J. C-J, 1985, *Effect of Depth of Nib on Strength of a Dapped-End Beam*, MS Thesis, University of Weshington, Seattle, WA.

- Herzinger, R. , El-Badry, M. M. ,2002, *Use of Stud Shear Reinforcement in Concrete Beams with Dapped Ends*, 4th Structural Specialty Conference of the Canadian Society for Civil Engineering, Montréal, Québec, Canada 5-8 June 2002 .

- Huang, P.C, J.J Myers and A. Nanni, 2000, *Dapped-End Strengthening in Precast Prestressed Concrete Double Tee Beams with FRP Composites*, Proc., 3rd Inter. Conf. on Advanced Composite Materials in Bridges and Structures, Ottawa, Canada, J. Humar and A.G. Razaqpur, Editors, 15-18 Aug. 2000, pp. 545-552.

- Jindal, A., 2012, *Finite Element Modeling of Reinforced Concrete Exterior Beam-Column Joint Retrofitted with Externally Bonded Fiber Reinforced Polymer (FRP)*, M.Sc. Thesis, Thapar University, Patiala, India.
- Kachlakev, D. I., 2005, *Finite Element Analysis and Model Validation of Shear Deficient Reinforced Concrete Beams Strengthened With GFRP Laminates*, California Polytechnic State University.

- Khan, M. A., 1981, *A Study of the Behavior of Reinforced Concrete Dapped-End Beams*, M. Sc Thesis, University of Washington, Seattle, WA, PP. 145.

- Liem, S. K., 1983, *Maximum Shear Strength of dapped-End or corbel*, MS Thesis, Concordia University, Montreal, Quebec, Canada.

- Mader, B. S., 1999, *Detailing Dapped Ends of Pretensioned Concrete Beams*, MS. Thesis, University of Texas at Austin, Austin, TX.

- MacGregor, J. G., 1992, *Reinforced Concrete Mechanics and Design*, Prentice-Hall, Inc., Englewood Cliffs, NJ, PP 848.

- Mattock, A. H., and Theryo, T., 1986, *Strength of Members with Dapped Ends*, PCI Research Project No. 6, Final Report, Precast/Prestressed Concrete Institute, Chicago, IL.

- Mohamed, R. N. and Elliott, K. S., 2008, *Shear Strength of Short Recess Precast Dapped end Beams Made of Steel Fiber Self-Compacting Concrete*, 33rd Conference on OUR WORLD IN CONCRETE & STRUCTURES: 25 – 27 August 2008, Singapore.

- Mohammed, S. D., and Mahmoud, T. K., 2014. *Effect of Prestress Force on the Strength of Dapped-End Reinforced Concrete Beams*, ACCMES Conference, June 2014 (Japan).

- PCI, 2004, *PCI Design Handbook - Precast and Prestressed Concrete*, Sixth Edition, Precast/Prestressed Concrete Instituted, Chicago, Illinois.

- Reynold, G. C., 1969, *The Strength of Half-Joints in Reinforced Concrete Beams*, TRA 415, Cement and Concrete Association, London, United Kingdom, June, PP. 9.

- Wang, Q. , Guo, Z. and Hoogenboom, P.C.J., 2005, *Experimental Investigation on the Shear Capacity of RC Dapped end Beams and Design Recommendations*, Structural Engineering and Mechanics, Vol. 21, No. 2, PP. 221- 235.

- Wolanski, B. S., 2001, *Flexural Behavior of Reinforced and Pre-Stressed Beam Using Finite Element Analysis*, M. Sc. Thesis, Marquette University.

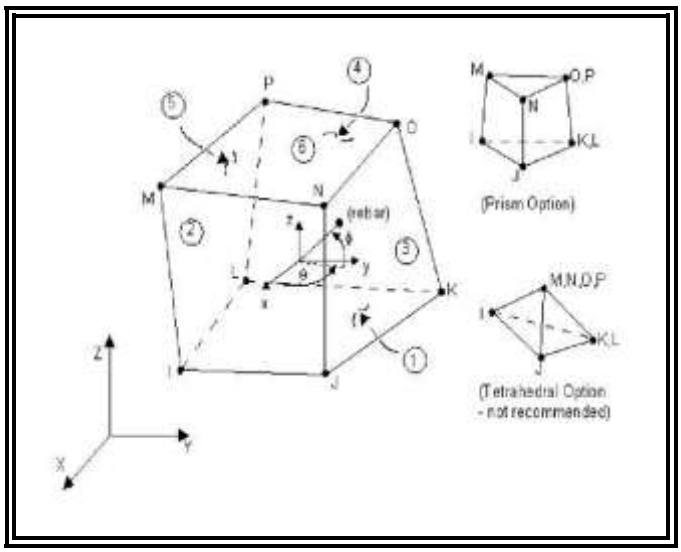


**Figure 1.** Solid65 element (ANSYS help, 2009).

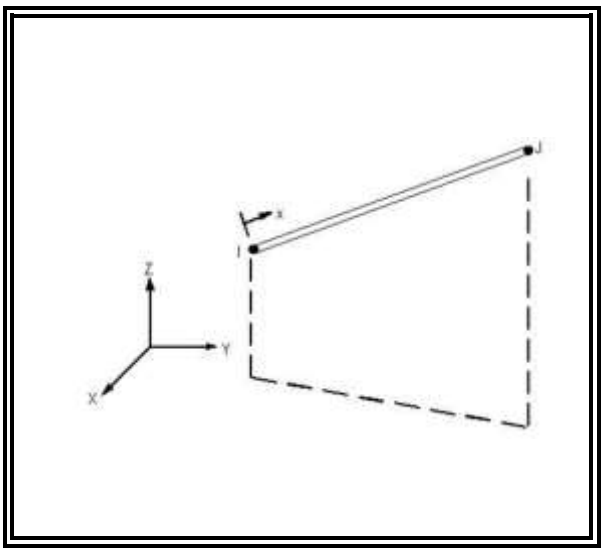

**Figure 2.** Link8 element (ANSYS help, 2009).

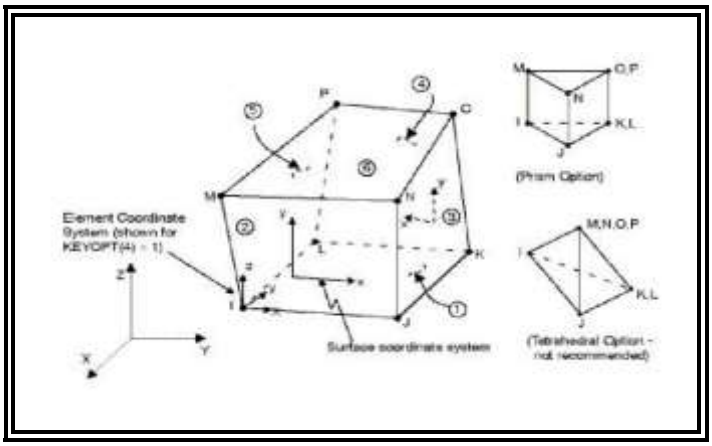


**Figure 3.** Solid45 element (ANSYS help, 2009).

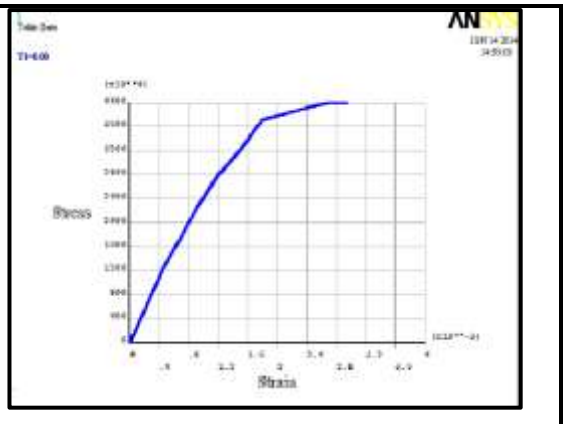

a- Uniaxial stress-strain curve of concrete.

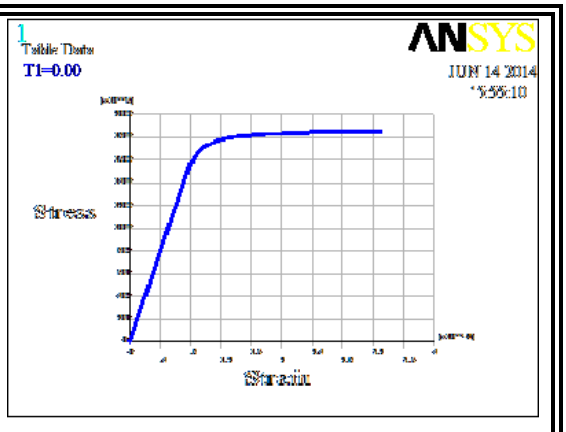


b- Stress-strain curve of 270 Ksi strand

**Figure 4.** Stress-strain curve for (a- concrete & b- strand).

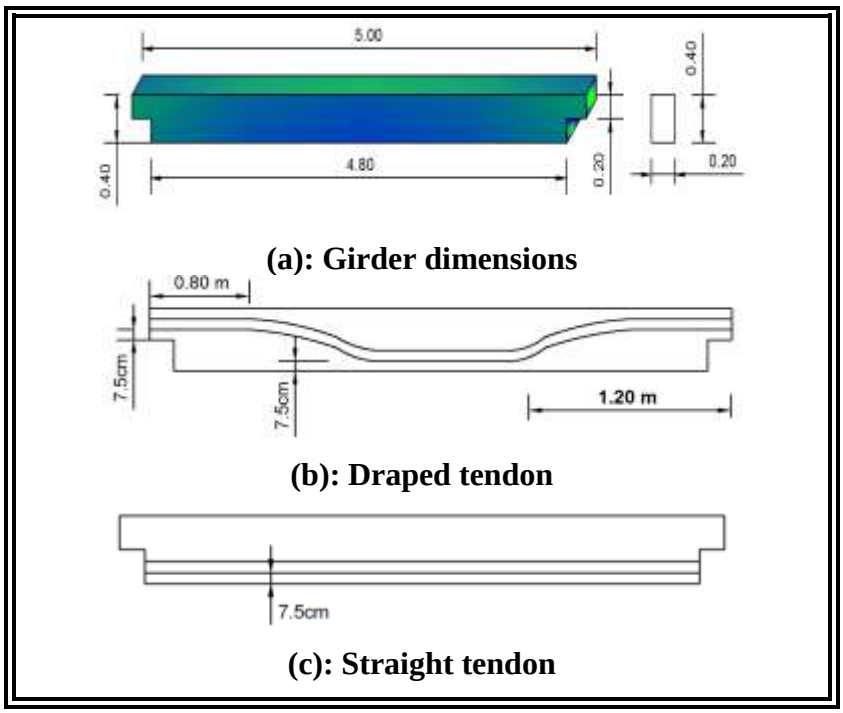


**Figure 5.** Geometric layout of the modeled girder (Mohammed, S. D., and Mahmoud, T. K., 2014).

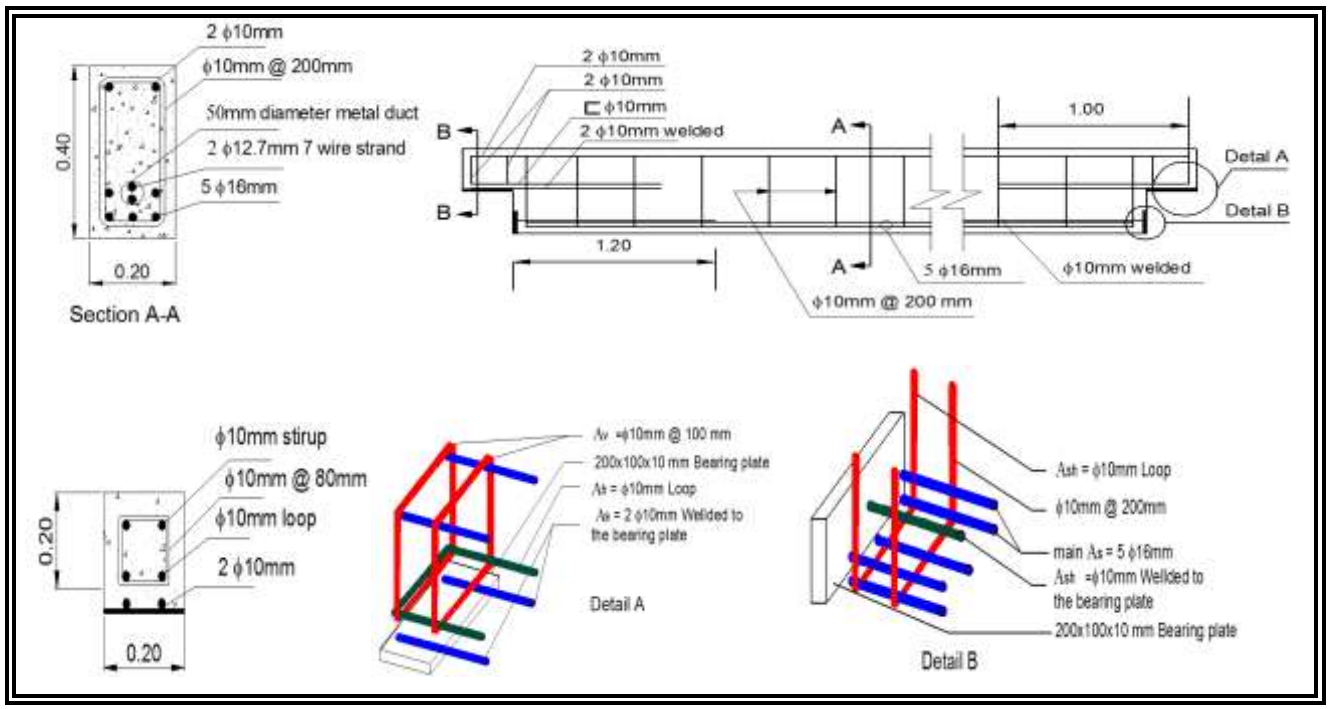


**Figure 6.** Details of the reinforcement (Mohammed, S. D., and Mahmoud, T. K., 2014).

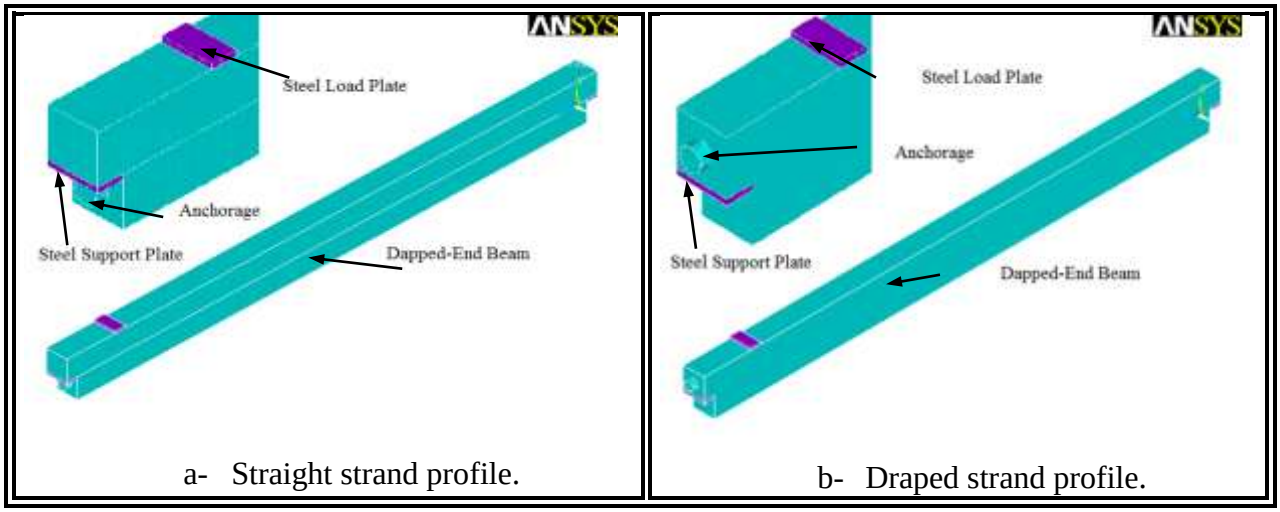


a- Straight strand profile. b- Draped strand profile.

**Figure 7.** Volumes of the modeled dapped-ends girder.

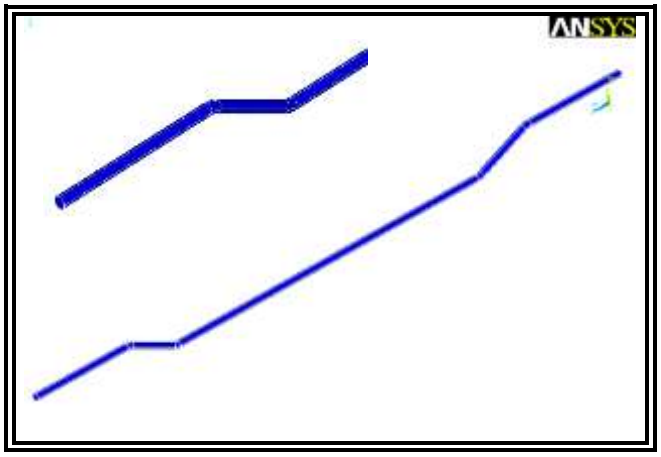


**Figure 8**. Volumes created for draped duct**.**

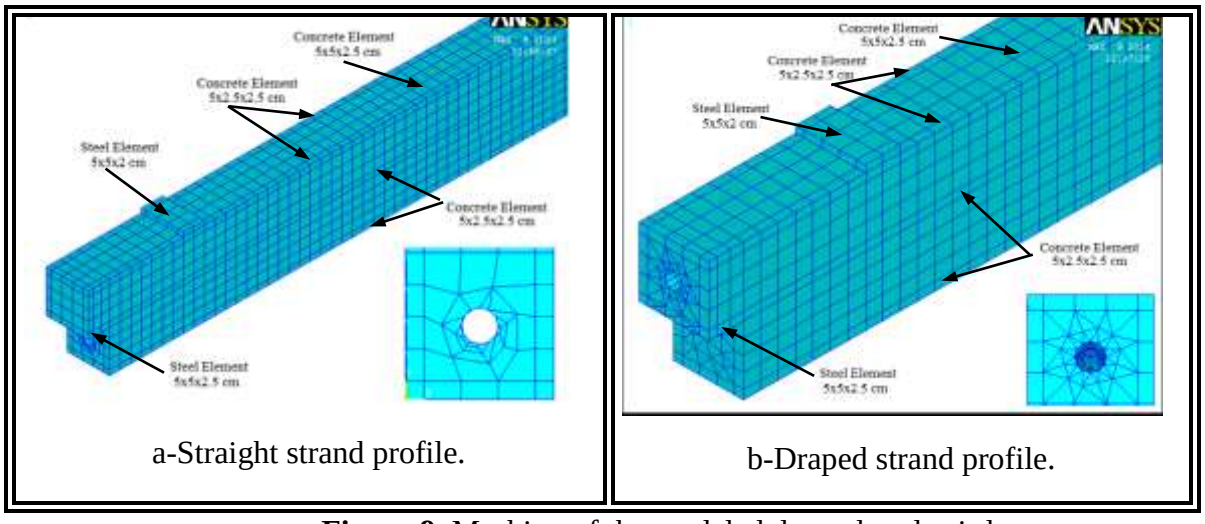


a-Straight strand profile. b-Draped strand profile.

**Figure 9**. Meshing of the modeled dapped-ends girder

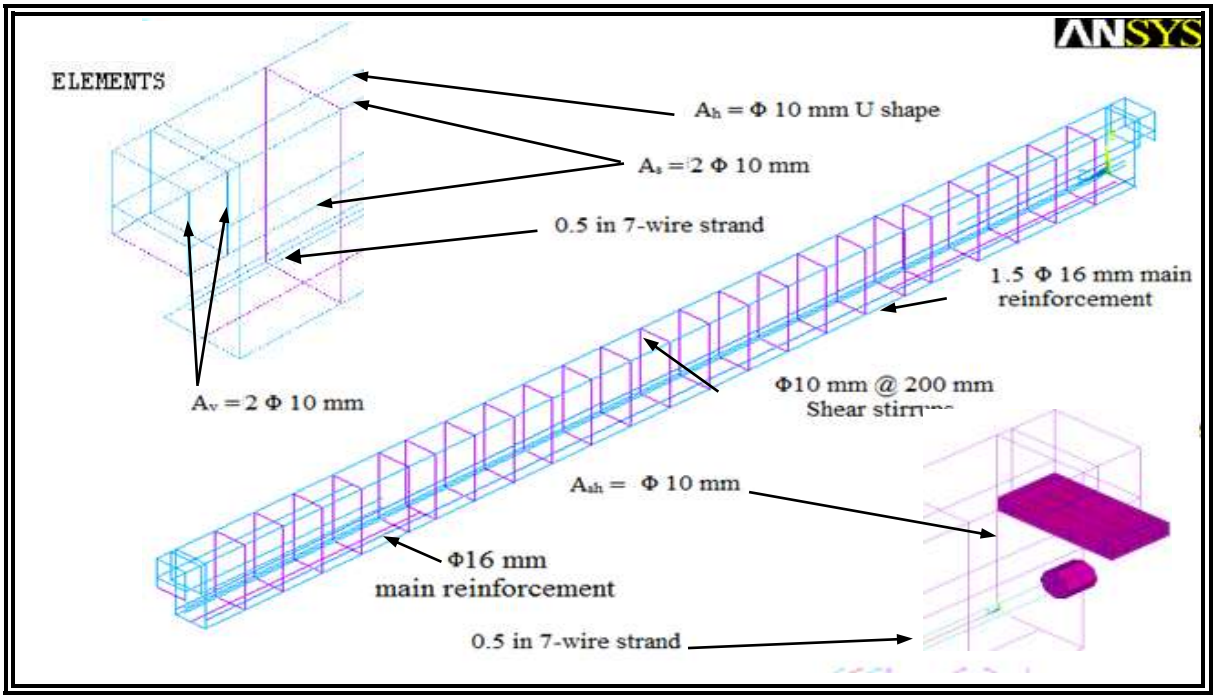


**Figure 10.** Reinforcement configuration for straight strand profile.

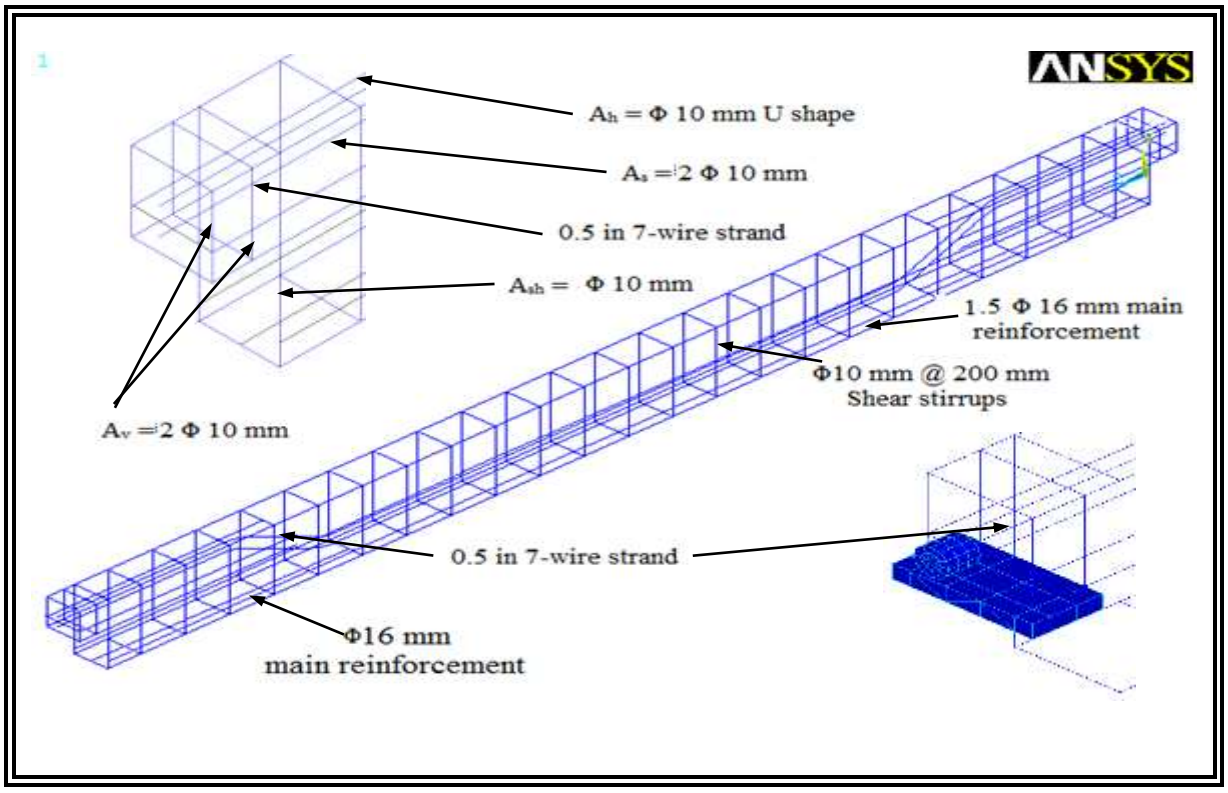


**Figure 11.** Reinforcement configuration for draped strand profile.

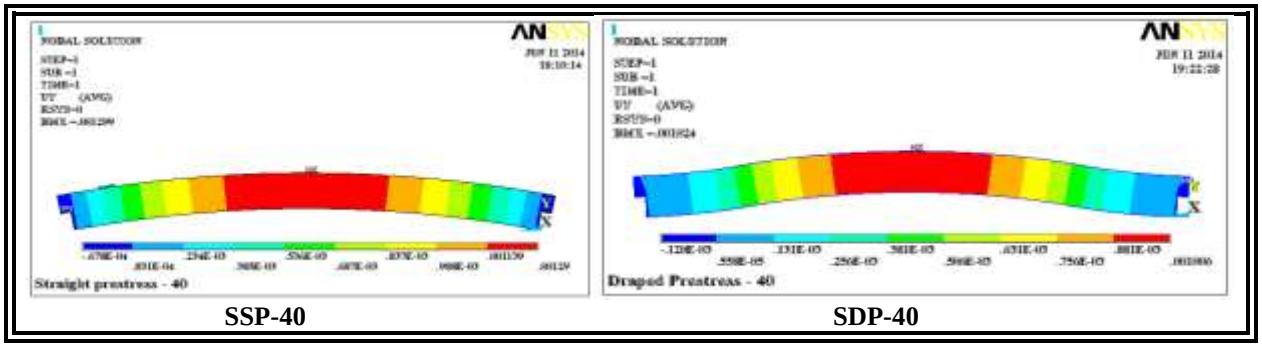


**Figure 12.** Contour of the pre-stress effect

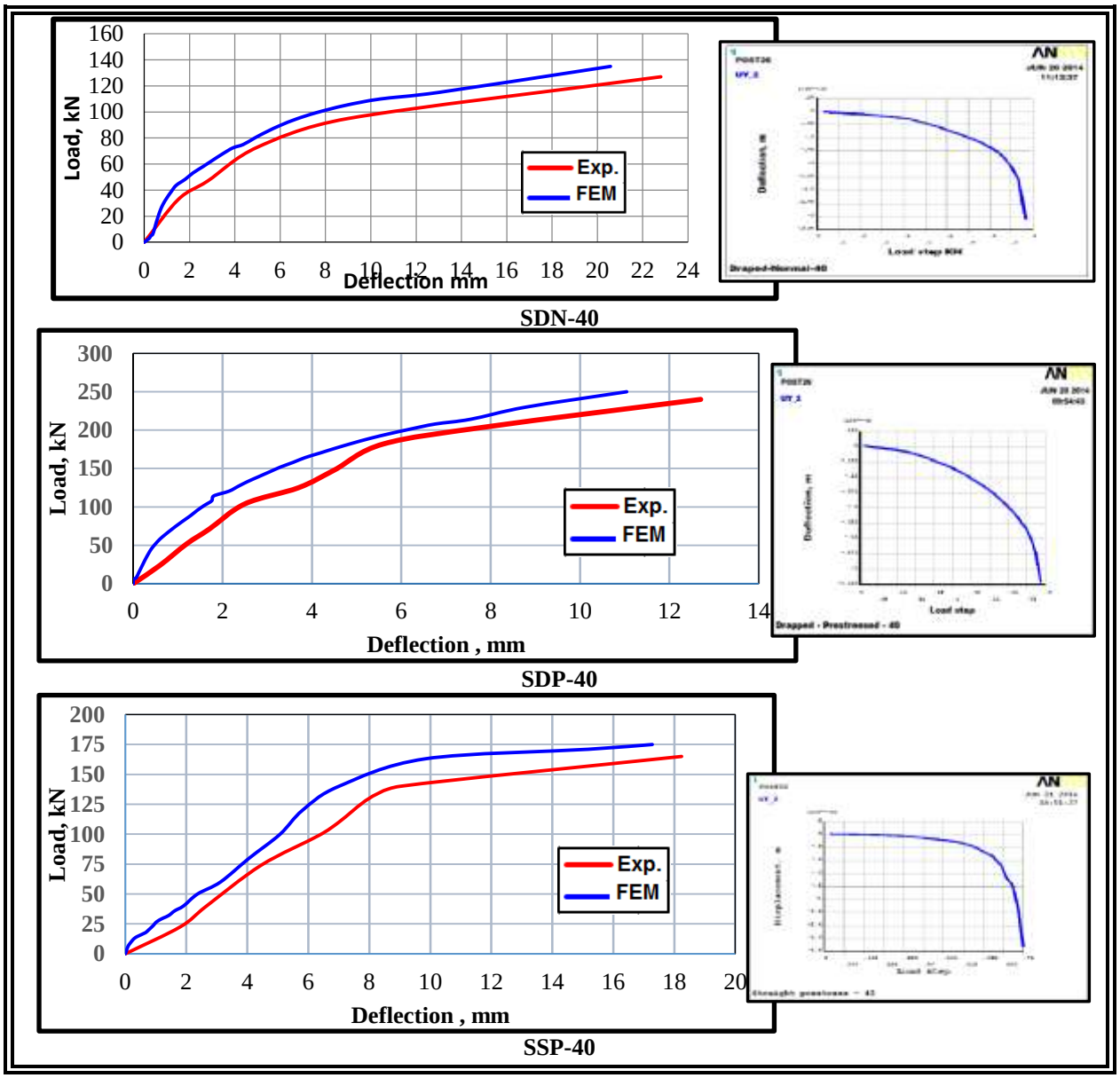


**Figure 13.** Comparison of load-deflection relation.

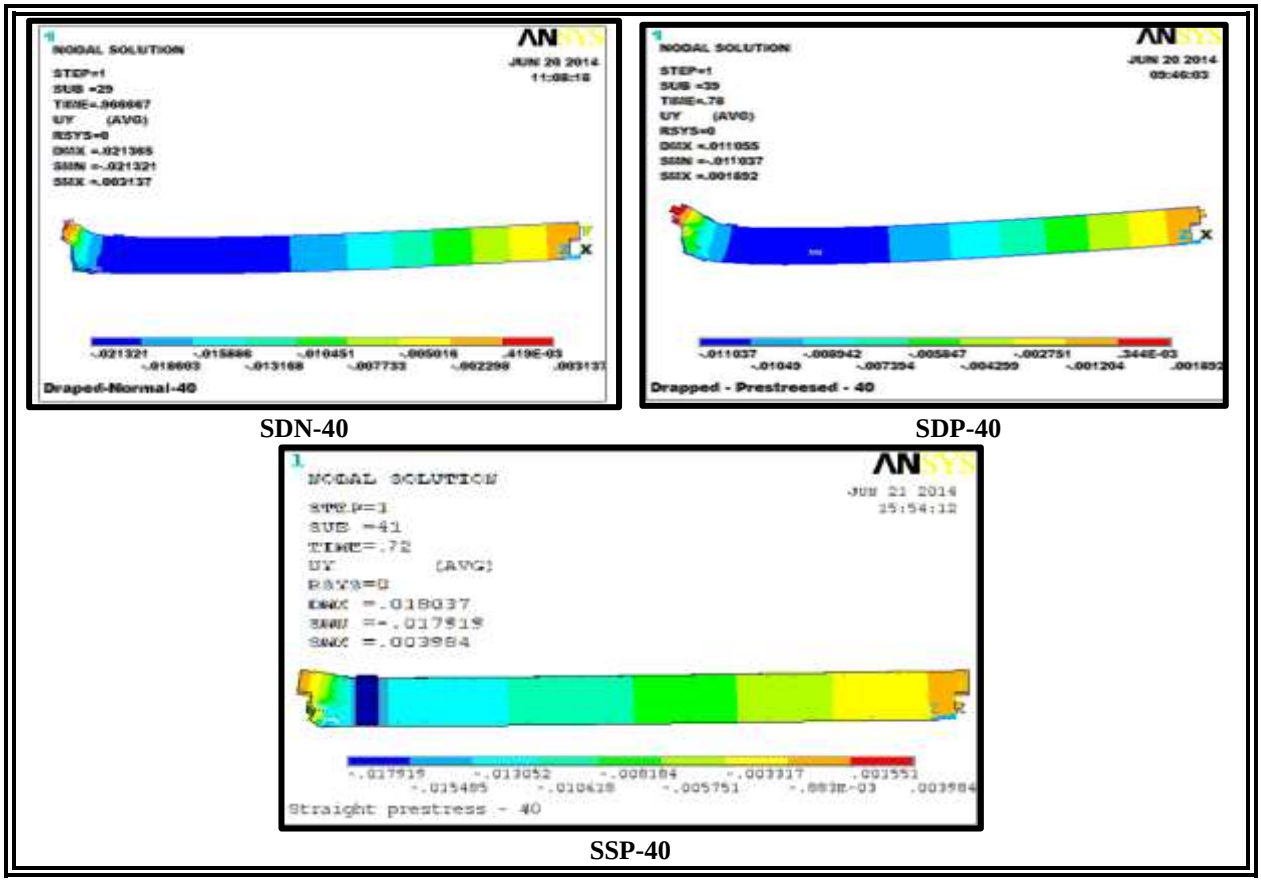


**SDN-40** **SDP-40**

**SSP-40**

**Figure 14.** Deflection contour at failure stage.

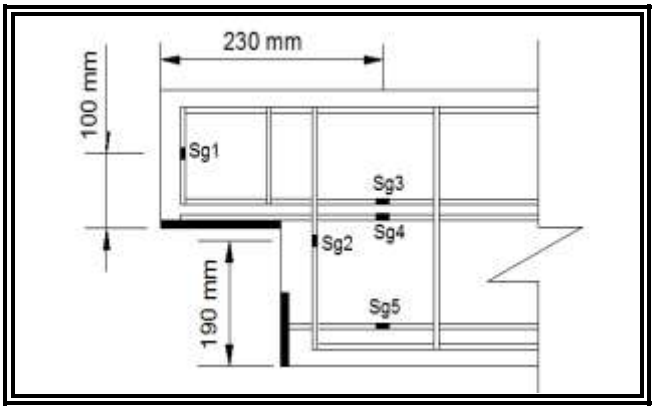


**Figure 15.** Adopted locations on the dapped-end reinforcements.

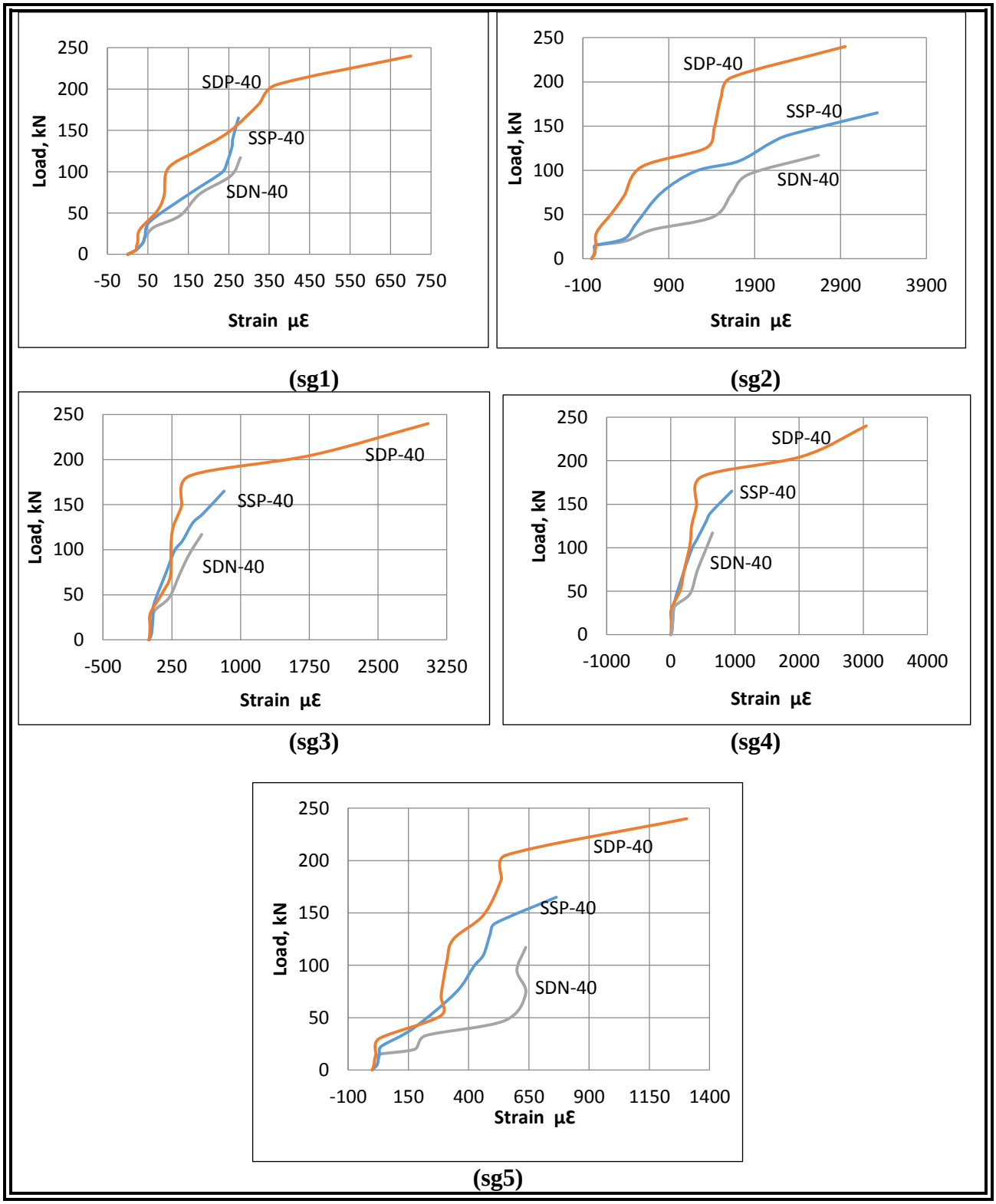


**Figure 16.** Load – strain curve at different locations.

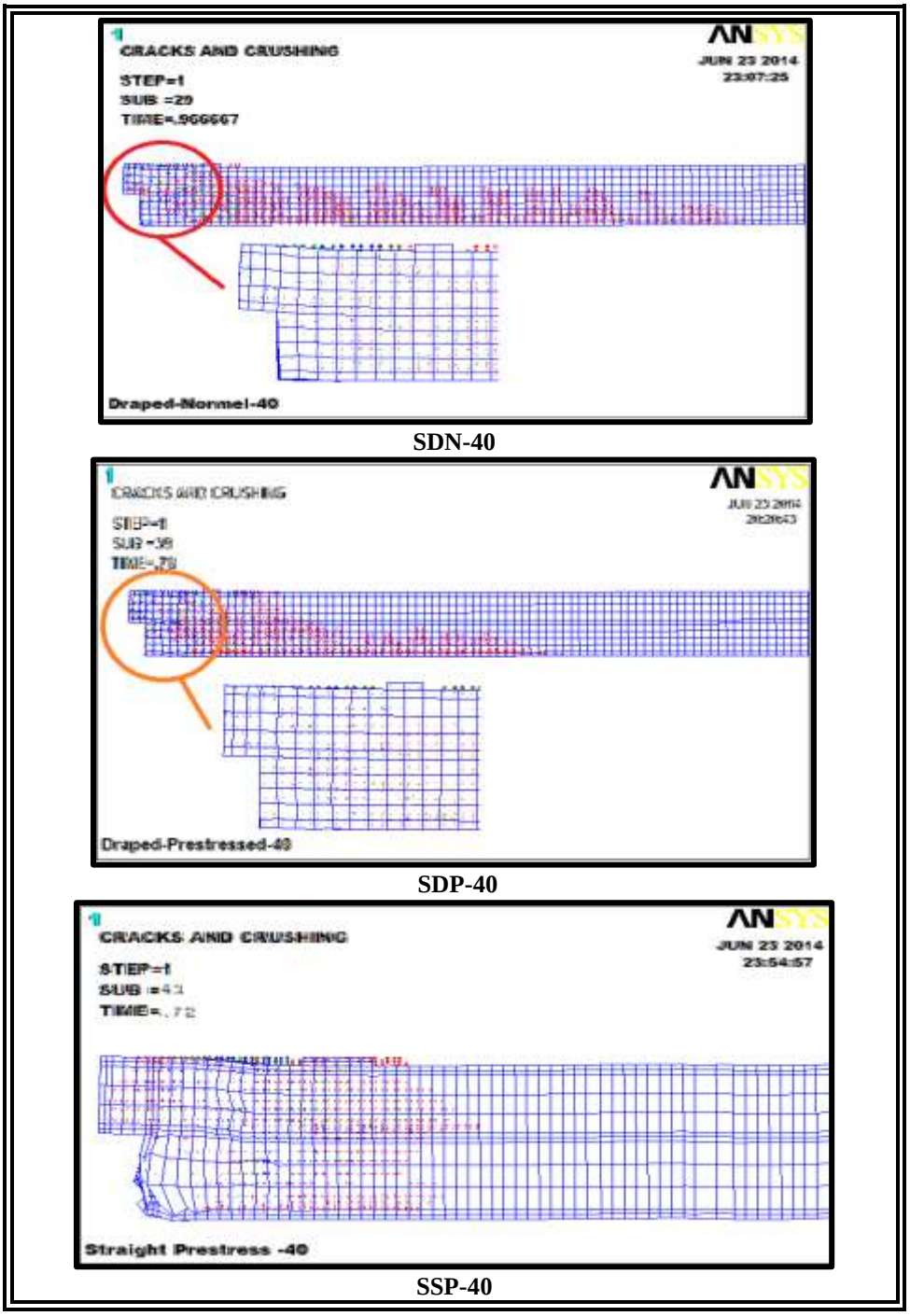


**Figure 17.** Crack pattern at failure stage.

**Table 1.** Material properties.

<table>
<tr><th>Material Model NO.</th><th>Element Type</th><th>Material Properties</th></tr>
<tr><td>1</td><td>Solid65</td><td>
<table>
<tr><th colspan="2">Linear Isotropic</th></tr>
<tr><td>EX</td><td>29725 MPa</td></tr>
<tr><td>PRXY</td><td>0.2</td></tr>
</table>
<table>
<tr><th>Density</th></tr>
<tr><td>2500 kg</td></tr>
</table>
<table>
<tr><th colspan="2">Multilinear Isotropic</th></tr>
<tr><td>Strain</td><td>Stress MPa</td></tr>
<tr><td>0.0004</td><td>12.00</td></tr>
<tr><td>0.0006</td><td>16.99</td></tr>
<tr><td>0.009</td><td>24.06</td></tr>
<tr><td>0.0012</td><td>29.76</td></tr>
<tr><td>0.00185</td><td>36.97</td></tr>
<tr><td>0.002</td><td>38.30</td></tr>
<tr><td>0.00269</td><td>39.98</td></tr>
</table>
<table>
<tr><th colspan="2">Concrete</th></tr>
<tr><td>ShrCf-Op</td><td>0.2</td></tr>
<tr><td>ShrCf-Cl</td><td>0.8</td></tr>
<tr><td>UnTensSt</td><td>4.0 MPa</td></tr>
<tr><td>UnCompSt</td><td>40 MPa</td></tr>
<tr><td>BiCompSt</td><td>0</td></tr>
<tr><td>HydroPrs</td><td>0</td></tr>
<tr><td>BiCompSt</td><td>0</td></tr>
<tr><td>UnTensSt</td><td>0</td></tr>
<tr><td>TenCrFac</td><td>0</td></tr>
</table>
</td></tr>
<tr><td>2</td><td>Link 8</td><td>
<table>
<tr><th colspan="2">Linear Isotropic</th></tr>
<tr><td>EX</td><td>200000 MPa</td></tr>
<tr><td>PRXY</td><td>0.3</td></tr>
</table>
<table>
<tr><th colspan="2">Bilinear Isotropic</th></tr>
<tr><td>Yield stress</td><td>630MPa</td></tr>
<tr><td>Tangent modulus</td><td>0</td></tr>
</table>
</td></tr>
<tr><td>3</td><td>Link 8</td><td>
<table>
<tr><th colspan="2">Linear Isotropic</th></tr>
<tr><td>EX</td><td>200000 MPa</td></tr>
<tr><td>PRXY</td><td>0.3</td></tr>
</table>
<table>
<tr><th colspan="2">Bilinear Isotropic</th></tr>
<tr><td>Yield stress</td><td>593MPa</td></tr>
<tr><td>Tangent modulus</td><td>0</td></tr>
</table>
</td></tr>
<tr><td>4</td><td>Solid 45</td><td>
<table>
<tr><th colspan="2">Linear Isotropic</th></tr>
<tr><td>EX</td><td>200000 MPa</td></tr>
<tr><td>PRXY</td><td>0.3</td></tr>
</table>
</td></tr>
</table>

**Table 2.** Details of the modeled girders.

| Girder No. | $f_{c'}$ (MPa) | Strand Path | Level of Prestress |
|---|---|---|---|
| SDN-40 | 40 | Draped | Not prestressed |
| SSP-40 | 40 | Straight | $0.62f_{pu}$ |
| SDP-40 | 40 | Draped | $0.62f_{pu}$ |

**Table 3.** Pre-stress effect.

| Status | Specimens | |
|---|---|---|
| | Canter line deflection at pre-stress stage , mm | |
| | SDP-40 | SSP-40 |
| Experimen | 0.91 | 1.25 |
| Calculated | -- | 1.31 |
| F.E. | 0.93 | 1.29 |

**Table 4.** Comparison of the failure load.

| Specimen | Failure Load, kN | | $\frac{(P_u)_{FE_u}}{(P_u)_{Exp}}$ |
|---|---|---|---|
| | $(P_u)_{FE}$ | $(P_u)_{Exp}$ | |
| SDN-40 | 135 | 122 | 1.11 |
| SDP-40 | 250 | 240 | 1.04 |
| SPP-40 | 175 | 165 | 1.06 |

.

# تاثير تعاقب دورات التسخين والتبريد وتأثير حجم النماذج على مقاومة إنضغاط الخرسانة المعرضة لدرجات حرارة عالية

**شامل عبد الرحيم سلمان**
**مدرس مساعد**
**معهد التكنولوجيا / بغداد**

**المستخلص**

تم في هذا البحث دراسة تأثير تعاقب دورات التسخين والتبريد على مقاومة إنضغاط الخرسانة عند تعرضها لدرجة حرارة 400 درجة مئوية ولمدة ساعة واحدة .

بينت النتائج ان النماذج التي تم تعريضها لدرجة حرارة عالية (400 درجة مئوية) ولمرة واحدة انخفضت قيمة مقاومة إنضغاطها بنسبة 32.5% عن النماذج المرجعية بينما كانت نسبة الانخفاض للنماذج التي تعاقبت دورات التسخين والتبريد عليها لعشرة دورات انخفضت مقاومة انضغاطها بـ 52.7% .

كما تم دراسة تأثير حجم النماذج الخرسانية على النسبة المئوية لأنخفاض مقاومة الأنضغاط عند تعرضها لدرجات حرارة عالية (250 , 500 , 750 درجة مئوية) لنماذج مكعبات خرسانية ذات طول اضلاع (100 , 150 , 200 ) ملم.

وبينت النتائج ان النسبة المئوية للأنخفاض في مقاومة انضغاط الخرسانة تزداد بزيادة درجات الحرارة المسلطة عليها الا إن نسبة الأنخفاض في المقاومة تقل كلما زادت احجام النماذج ولجميع درجات الحرارة التي تعرضت لها النماذج .

# The Effect of Recycled Heating and Cooling and The Effect of The Speciment Size on The Compressive Strength of Concrete Exposed To High Temperature

**SHAMIL ABDUL RAHEEM**

## ABSTRACT

In the present work effect of recycled heating and cooling on the values of concrete compressive strength due to high temperature of $400^0$C was studied.

The tests show that the percent of reduction in compressive strength of the samples which exposed to a temperature of $400^0$C for one cycle was 32.5%, while the reduction was 52.7% for the samples which were exposed to recycled heating and cooling of ten times .

Moreover a study of the effect of specimen sizes on the percentages of compressive strength reduction due to high temperatures (250, 500, $750^0$C) with the variation of cub's size (100, 150, 200 mm) was studied.

The tests show that the rate of reduction in compressive strength increases with increasing the exposed temperatures, but, the rate of reduction was decreased as the specimen size was increased.

**المقدمة**

تعتبر الخرسانة من أكثر المواد الانشائية استعمالاً في إنشاء المباني وغيرها لأبدائها قوة ومقاومة عالية للأحمال الشاقولية والجانبية وخاصةً المسلحة منها إضافةً الى ديمومتها (Durable) وسهولة تشكيلها (Fabrication) وهي تعتبر من المواد الرديئة للتوصيل الحراري مقارنة بغيرها كالحديد وكذلك تعتبر من المواد الغير قابلة للأشتعال . لكل هذه الأسباب تعتبر الخرسانة العادية والمسلحة افضل من بقية المواد الأنشائية في بناء هياكل الأبنية المرتفعة وفي الأنفاق وقواعد انطلاق المركبات الفضائية وغيرها .

على الرغم من ذلك فأن الحرائق الكبيرة والمستمرة لفترات طويلة (اكثر من ساعة واحدة) تعتبر من المشاكل الرئيسية التي تتعرض لها الأبنية الخرسانية والزيادة العظمى في هذه المشاكل بنقصان المقاومة تكون بدرجات الحرارة العالية بحدودها العليا مع طول زمن التعرض للحرائق .

كمثال على ذلك فأن احدى هذه الحوادث تمت في احد انفاق الجزائر حيث تصادف اصطدام قطارين يحوي احداها 750 متر مكعب من الوقود تم احتراقها مولدة درجة حرارة عالية وصلت الى 1200 درجة مئوية مما ادى الى دمار كبير في جسم النفق الخرساني ، والنفق لا يزال مغلق لحد الآن . (Toumi and Rasheidat, 2010)

من جانب اخر، فان كثير من الأبنية التي تعرضت الى احتراق شديد غير أن الخرسانة المسلحة لهياكل هذه الأبنية تم اصلاحها بدلاً من ازالتها . وقد تم وضع جداول من قبل احدى الجهات الهندسية المتخصصة في هذا المجال ( The Concrete Society, 1990 and Smart, 1999 ) يعين المهندسين على كيفية اصلاح او ازالة الاجزاء الخرسانية المعرضة للحريق اعتماداً على الهطول والتشققات والتقشر (Spalling) حيث قدمت جداول تعتمد على الفحص ومؤشرات الرؤيا الموقعية (Visual Indication) لتقدير وضع كل جزء من المبنى المعرض للأحتراق مقسماً الى خمسة درجات . حيث قدم لكل درجة طرق الأصلاح لها تبدأ من اصلاحات بسيطة الى اصلاح رئيسي . (Zween, 2008)

وفي دراسة بين الباحثون ان التغير في مقاومة انضغاط الخرسانة يلاحظ بدرجات الحرارة بين 200 – 250 درجة مئوية وفي درجات حرارة اعلى ما بين 500 – 550 درجة مئوية تكون فاعلة وذلك يعود بسبب بدأ تحلل هيدروكسيدات الكالسيوم (Calcium Hydroxide dehydration) ، اما بدرجة حرارة بحدود 750 درجة مئوية وما فوقها يبدأ الركام بتردي خواصه الفيزياوية (Physical Deteriorate of agg.) وبدرجات حرارة اعلى بحدود 1200 درجة مئوية تبدأ الخرسانة بالتفتت . كما بينوا ان ديمومة واداء (Durability and Performance) الخرسانة المعرضة للحريق تتأثر بنوع الأسمنت ونوع الركام الناعم والخشن والمضافات الأخرى الداخلة في تركيبها اضافةً الى نسبة الماء المستعمل . وقام الباحثون بناءا على ماسبق بدراسة استعمال احدى التقنيات الحديثة وهي اجهزة المسح الصوري (Image Scanning) حيث وجدوا من دراستهم امكانية استعمال هذه التقنية الحديثة في تقييم شدة الشقوق على سطح الخرسانة المعرضة للأحتراق ومعرفة امكانية اصلاحها او ازالتها بشكل كامل .(Toumi and Rasheidat, 2010)

يوجد عدد من الدراسات التي قام بها الباحثون لدراسة سلوك وتصرف الخرسانة عند تعرضها الى درجات حرارة مرتفعة ( من درجة حرارة المختبر الى ما فوق 1000 درجة مئوية) وقد بينوا ان الخرسانة تعتبر من المواد الضعيفة التوصيل الحراري وتبدي مقاومة عالية للانتقال الحراري ولكن بالرغم من ذلك فأن الحرارة الشديدة والسرعة العالية في ارتفاعها وتوقدها تؤدي لتغيرات حجمية كبيرة (Large Volume Change) بسبب التمدد الحراري (Thermal dilation) وكذلك التقلص الحراري (Thermal Shrinkage) ويعود ذلك بسبب إنتقال او ارتحال الرطوبة الداخلية في الخرسانة ( Moisture migration) اضافة الى التشظي او التقشر (Spalling) لسطح الخرسانة والذي يؤدي الى نقصان في المقطع

الخرساني بسبب الأجهادات الحرارية العالية (High Thermal Stress ) ونشوء الضغط الداخلي في الخرسانة (Pore Pressure Build up) كما ان الزيادة الحجمية الكبيرة (Large Volume Change) تؤدي لنشوء اجهادات وبالتالي تؤدي لتكون تشققات شعرية (Micro Cracking) وشروخ كبيرة والتي تؤدي في مرحلة ما الى فشل المنشأ الخرساني . (Zween, 2008)

وفي دراسة تم دراسة تأثير درجات الحرارة العالية على الخرسانة الخفيفة الوزن ((LWAC)) [ *حيث تم تعريفها حسب معهد الخرسانة الأمريكي " ACI 213" بأنها الخرسانة المكونة من ركام خفيف الوزن النوعي لها بين 1440 الى 1850 كغم / متر$^3$ ومقاومة إنضغاطها اعلى من (17.2 MPa)* ] حيث تبين ان مقاومتها للحرائق اكبر من الخرسانة العادية وهذا يعود الى أنخفاض توصيلها الحراري (Lower thermal Conductivity) اضافة لأنخفاض معامل التمدد الحراري لها (Lower Coefficient of thermal Expansion) مما يؤدي الى بطيء ارتفاع درجة حرارتها وانخفاض الأجهادات الناشئة تحت تأثير التقييدات الداخلية (Stress Restraint) . وقد قام الباحث بدراسة عدة متغيرات على الخرسانة الخفيفة الوزن وقد بين ان معدل التسخين العالي يؤدي الى انخفاض اكبر في الخواص الميكانيكية للخرسانة الخفيفة من معدل التسخين الواطيء حيث ان معدل التزايد الحراري الواطيء يؤدي الى تمدد حراري اقل . كما بينت النتائج ان الخرسانة الحاوية على السليكا مع نسبة ماء / اسمنت واطئة هي اكثر ميلاً للتشظي من تلك الحاوية على ماء / اسمنت اعلى . وان اضافة 0.25% بالحجم من الياف البولي بروبلين (Polypropylene) تبدو مناسبة لمنع التشظي بينما لم تمنع الياف الحديد تشظي الخرسانة حتى مع اضافة 1% بالحجم . ولكن تبين انه بأضافة الياف الحديد مع الياف البولي بروبلين ادت الى تحسن الخواص الميكانيكية للخرسانة المعرضة لدرجات حرارة عالية . (Zween, 2008)

وفي دراسة بين الباحثون ان الخرسانة المعرضة للحرائق قد تؤدي الى تفاعلات كيمياوية وخاصةً في تحلل مركبات هيدروكسيدات الكالسيوم $Ca(OH)_2$ والذي يؤدي في نقصان مقاومة إنضغاط الخرسانة . اي ان الخرسانة التي يدخل في انتاجها سمنت ذو نسبة هيدروكسيد الكالسيوم اقل تكون اكثر صموداً بوجه الحريق . (Alan, 2000)

وفي دراسة اخرى تم اختبار تأثير درجات الحرارة العالية على الخرسانة الحاوية على الياف الحديد لنوعين من الخرسانة العادية والعالية الأداء (High Performance Concrete) . وقد وجد ان الخرسانة العالية الأداء تتأثر سلباً بشكل اكبر من الخرسانة العادية عند تعرضها الى درجات حرارة عالية .

وقد وجد ايضاً انه بأضافة 1% من الياف الحديد (Steel Filer) فأن الخرسانة العالية الأداء اعطت مقاومة اكبر ضد التشقق من الخرسانة العادية عند تعرضهما الى درجات حرارة عالية . (Sri Ravindrarjah et al. 2002)

وفي بحث آخر بين الباحث ان هنالك نقصاً في البحوث حول الخرسانة الحاوية على الرماد المتطاير (Fly ash) والخرسانة الذاتية الرص (Self – consolidated Concrete) والخرسانة العالية الأداء .

وبين ايضاً ان إضافة الياف البولي بروبلين (Polypropylene Fiber) الى الخرسانة العالية الاداء تؤدي الى تحديد وتقليص اثر التشظي فيها (Spalling effect) . كما اشار الى امكانية تقوية الأعمدة الخرسانية المسلحة باستعمال انواع من الأطواق الحديدية (Bent ties) في مركز المقطع الخرساني . (Koudur, 2014)

وفي دراسة اخرى بين الباحث ان اضافة الياف البولي بروبلين الى الخرسانة العالية الاداء تؤدي الى زيادة مقاومتها عند تعرضها الى درجات حرارة عالية وتؤدي ايضاً الى نقصان في ظاهرة التشظي (Spalling Behaviors) ووجد ان الخرسانة الحاوية على نسبة سمنت اعلى تتأثر بالحرارة العالية بشكل اكبر كما بين انه كلما كانت الخرسانة جافة اكثر كلما كانت مقاومتها للحريق اكبر وقلت احتمالية تشظيها . (B. Toumi et al. 2009)

وفي دراسة تبين ان الخرسانة الحاوية على خبث الحديد (Steel Slag) عند تعرضها الى درجة حرارة 800 درجة مئوية اظهرت تمددات غير مستقرة ادت الى حدوث تشققات في الخرسانة مما ادى الى تردي اكبر في خواصها الميكانيكية وبين الباحث بأن اعادة تسخين الخبث قبل استعماله لدرجة حرارة 1000 درجة مئوية تؤدي الى ان تكون اكثر استقراراً . (Alexander et al. 2012)

وفي احدى الدراسات وجد الباحث ان الخرسانة العالية الأداء والتي يتم تبريدها بعد التسخين بواسطة الماء تتردى خواصها الميكانيكية بشكل اكبر منها عندما تبرد بشكل طبيعي الى درجة حرارة المختبر بنسبة 25% ، كما أظهرت النتائج ان الخرسانة التي تم غمرها بالماء لمدة 180 يوماً ثم تم تعريضها الى درجات حرارة عالية تكون نسبة الأنخفاض في مقاومتها اكبر من المعالجة بالماء لمدة 28 يوماً لذا يجب اخذ الأعتبار لهذا العامل عند تصميم الخرسانة العالية الاداء . (R. V. Balendran et al. 2003)

وفي دراسة اخرى تبين ان الفترة الزمنية لتسليط الحرارة على النماذج الخرسانية الخفيفة الوزن ليست مؤثرة كما تأثير درجة حرارة القصوى التي تصلها وبين كذلك انه كلما زادت نسبة الزجاج البركاني الخفيف (Pumic) بدلاً من الركام العادي قلت مقاومة الخرسانة . (A. Ferhat and Rustem, 2004)

وفي دراسة على تأثير درجات الحرارة العالية على الخرسانة الذاتية الرص (Self-Compacted Concrete) تبين ان مقاومة انضغاطها تنخفض بنسب اكبر منها للخرسانة العادية كما انها معرضة لظاهرة التشظي بشكل اكبر . (Kulkurni and S N patil, 2011)

وفي دراسة تبين ان استعمال الركام من بقايا الخرسانة (Recycled Course agg. From waste Concrete) وبنسب مختلفة عند تعرضها الى درجات حرارة عالية او عدم تعرضها تبدي في كلتا الحالتين خواص جيدة كما تبين ان اضافة نسب 10% من الرماد المتطاير (Fly Ash) بدلاً من الاسمنت تعطي تحسن اكبر في اداء الخرسانة مقارنتاً بنسبة 20%. كما تبين ان اضافة 10% من الرماد المتطاير الى الخرسانة بالركام المدور من بقايا خرسانة اخرى ادت الى تحسن خواصها . (Arundeb Gupta et al. 2012)

كما بين باحث اخر ان اضافة الألياف تحسن مقاومة الخرسانة لظاهرة التشظي عند تعرضها الى درجات حرارة عالية . كما بين ان هنالك نقصان في مقاومة الخرسانة عند تعرضها لدرجات حرارة عالية مع او بدون الألياف ولكن قوة المقاومة للنماذج في كلتا الحالتين كانت اكبر مع الألياف وبين ايضاً ان النماذج المبردة بالماء تكون مقاومتها اقل من التي تبرد بشكل طبيعي . (Rahol, 2014)

في دراسة اخرى بين الباحث ان هنالك ستة عوامل تؤثر على مقاومة الخرسانة العالية الاداء ( High Performance Concrete) عند تعرضها الى درجات حرارة عالية وهي:

- الرطوبة النسبية اثناء معالجة الخرسانة (Relative Humidity of Curing) .
- تسارع التسخين او ارتفاع درجة حرارة النموذج (Rate of Heating) .
- نسبة الماء الى الأسمنت .
- نوع الركام (لايمستون ، ركام خفيف الوزن او خليط من الركام العادي والخفيف)
- نسبة الياف البولي بروبلين ( Polypropylene fibers)

وقد قام الباحث بتعريض نماذج من الجسور (Beams) المسلحة والغير مسلحة الى درجات حرارة عالية وقد بين الباحث :

* ان جميع نماذج الجسور لم تنهار بسبب التشظي وذلك لوجود الياف البولي بروبلين .

* المعالجة بالماء (Curing) لم تؤثر على الجسور غير المسلحة بموضوع التشظي ولكنها كانت مؤثرة في نماذج الجسور المسلحة .

* سرعة زيادة درجات الحرارة (Heating rate) زادت من تشظي الجسور المسلحة والغير مسلحة .

* التحميل المسبق يقلل من تشظي الجسور غير المسلحة ولكن في الجسور المسلحة وجد انه غير ذا تأثير .

* نسبة الماء للاسمنت مساوياً لـ 0.35 كانت النسبة المؤثرة في حدوث ظاهرة التشظي عنها في النسب الاقل او الأكثر .

* نماذج الجسور الخرسانية المسلحة التي تم اعدادها في هذه الدراسة باستخدام ركام حجر الجير (Limestone) تعرضت لأنهيارات قاسية مقارنتا ببقية الجسور التي تم استخدام انواع اخرى من الركام في تكوينها عند تعرضها لدرجات حرارة عالية وقد اوصى الباحث بعدم استعمال الركام العادي وباستعمال (الياف البولي بروبلين) . كما اوضح ان الخرسانة الخفيفة جيدة لولا ان بعض الباحثين وجد استمرار التفجر المتشظي لها عند تعرضها للهب النيران . (Sullivan, 2001)

وفي بحث حول تأثير درجات الحرارة العالية على نوعين من حديد التسليح الأول حسب المواصفة ( ASTM – A36) والثاني على الحديد المسبق الجهد (Pre stressed Steel) (ASTM – A421) حيث تبين من نتائج الفحص ان الأنخفاض في الجهد المرن (yield stress) واقصى مقاومة (Ultimate Strength) كانت قليلة تحت درجة حرارة 371 درجة مئوية ولكن بأرتفاع درجات الحرارة فأن مقاومتها بدأت بالأنخفاض بشكل ملحوض ولجميع النماذج . (Kadhum, 2010)

إن جميع الدراسات اعلاه تعمل على القاء بعض الضوء لفهم سلوك وخواص الخرسانة عند تعرضها الى درجات حرارة عالية وهو يعتبر امر مهم للعمل على زيادة مقاومة الخرسانة ضد الحريق وتحسين التصميم الحراري (Fire Design) للأبنية الخرسانية وخاصةً الأجزاء الرئيسية مثل الأعمدة والتي تعتبر جزء رئيسي من الهياكل الخرسانية المسلحة لكونها تسند جميع الأجزاء الخارجية (Super Structure) وتنقل الأحمال الى القواعد او الأسس لذا اي انهيار يحدث لهذه الأعمدة وخاصةً الرئيسية منها تؤدي الى انهيار جزئي او كلي للبناء وربما بشكل تسلسلي (Chain action) .

إن هذا البحث يهدف لدراسة تعاقب تعرض المنشآت الخرسانية لدرجات حرارة عالية لعدة مرات عند درجة حرارة عالية بحدودها المتوسطة (400 م$^0$ ) وتأثير ذلك على مقاومة انضغاطها . ويهدف ايضاً لدراسة تأثير حجم او ابعاد النماذج الخرسانية المعرضة لدرجات الحرارة العالية على مقاومة انضغاطها .

## الجزء العملي

### المواد المستخدمة:

أ- **الأسمنت** : تم استخدام السمنت البورتلاندي الأعتيادي (OPC) ، (Type I) عراقي المنشأ ، المخزن بصورة جيدة للحفاظ عليه من تأثير الرطوبة والجدولان رقم (1) و (2) يبينان نتائج الفحوصات الفيزيائية والكيميائية للسمنت وفق المواصفات القياسية العراقية رقم 5 لسنة 1984

**ب- الركام الناعم** : تم استخدام رمل الأخيضر المطابق للمواصفات القياسية العراقية رقم 45 لسنة 1984 [16] بوزن نوعي 2.62 ومحتوى رطوبة 1.5% . جدول رقم (3) يبين التحليل المنخلي للرمل الناعم المستخدم في الخلطة الخرسانية وتبين ان الرمل يقع ضمن منطقة التدرج (3) .

**ج- الركام الخشن** : تم استخدام حصى نهري مطابق للمواصفات العراقية رقم 45 لسنة 1984 بوزن نوعي 2.64 ومحتوى رطوبة 0.45% ، ويبين الجدول (4) نتائج فحص التدرج للحصى .

**د- الماء** : تم استعمال الماء الصالح للشرب في الخلطة الخرسانية ، جدول رقم (5) يبين نتائج فحص الماء وفق المواصفات القياسية العراقية 1073 لسنة 1992 .

**تحضير النماذج الخرسانية**

تم خلط السمنت والرمل والحصى بنسبة خلط وزنية (1 : 2 : 4) وبنسبة (1 : 1.5 : 3) ونسبة ماء سمنت بحدود 0.55 وتم رصها ميكانيكيا في قوالب حديدية بأبعاد 100x100x100ملم و150x150x1500ملم و200x200x200ملم حسب المواصفات القياسية البريطانية BS 1991 part 116 – 8.3 . وتم إنضاجها بغمرها في الماء لغاية عمر 28 يوما ثم اخراجها من احواض الانضاج وتركها في الهواء الطلق لمدة 32 يوماً اخرى للحصول على جفاف شبه تام . ثم تجفف لمدة يوم في فرن تجفيف (بدرجة حرارة 105 م$^0$) لحين الوصول الى الوزن الثابت .

**الأختبارات والنتائج**

**الجزء الأول** : تم في هذا الجزء اختبار تأثير تعاقب حرق نماذج الخرسانة الأسمنتية وتبريدها الى درجة حرارة المختبر. حيث تم تحضير احد عشر مجموعة من المكعبات الخرسانية بابعاد 100x100x100 ملم وبنسب خلط وزنية 1 : 2 : 4 . تترك مجموعة واحدة ، ويتم ادخال العشرة مجاميع الباقية داخل فرن حراري ذا معدل تزايد حراري مقداره 10 درجات مؤية في الدقيقة. ثم يتم تسخينها الى درجة حرارة 400 م$^0$ وتترك عند هذه الدرجة لمدة ساعة ثم يطفىء الفرن لتعود جميع المجاميع الى درجة حرارة المختبر وتسحب اول مجموعة منها ثم يعاد تسخين بقية المجاميع الى نفس الدرجة السابقة ولمدة ساعة عند هذه الدرجة ثم يعاد تبريدها الى درجة حرارة المختبر وتسحب المجموعة الثانية للفحص وهكذا حتى المجموعة العاشرة .

بعد ذلك تم فحص جميع النماذج في جهاز فحص مقاومة الأنضغاط والجدول رقم (6) والشكل رقم (1) يبين قيم مقاومة الأنضغاط لكل مجموعة حسب عدد دورات التسخين واعادة التبريد والنسبة المئوية لأنخفاض مقاومة الأنخفاض مقارنة بالمجموعة الاولى (المرجعية) التي لم تعرض الى درجة حرارة عالية .

**الجزء الثاني** : تم في هذا الجزء اختبار تأثير ابعاد النماذج المعرضة لدرجات حرارة عالية على النسبة المئوية لأنخفاض مقاومة انضغاطها ، ولهذا الغرض تم اخذ ثلاث مجاميع بأبعاد مختلفة 100x100x100 ملم و 150x150x150 ملم و 200x200x200 ملم وبنسب خلط 1 : 1.5 : 3 وكل مجموعة تقسم الى اربعة مجاميع فرعية تعرض الى درجات حرارة 250 م$^0$ ، 500م$^0$ ، 750 م$^0$ على التوالي في افران حرارية ترفع درجات حرارتها الى هذه الدرجات حيث يثبت الفرن على هذه الدرجة لمدة ساعة واحدة لتماثل فعل الحرائق الغير مباشرة عليها وتترك المجموعة الرابعة لكل حجم بدون تسخين ثم تفحص هذه النماذج بجهاز فحص النماذج ومعرفة مقادير مقاومة الأنضغاط لكل مجموعة ولكل درجة حرارة والنتائج موضحة في الجدول رقم (7) والشكل رقم (2) ورقم (3) .

**مناقشة النتائج:**

**اولاً** : تأثير تعاقب دورات الحرق واعادة التبريد على مقاومة انضغاط الخرسانة :

أ- يلاحظ من الجدول رقم (6) والشكل رقم (1) انخفاض مقاومة انضغاط النماذج في الدورة الاولى من التسخين بنسبة 32.5% وهذا يعزى الى نتيجة التغير في الصفات الكيميافيزياوية (Physico – chemical) والذي يؤدي بدوره الى تغير خواص السمنت والركام اضافة الى التفاوت في مقادير التغيرات الحجمية (volume change) بين الركام والسمنت ، والذي يؤدي الى حدوث تشققات في السمنت والركام وبالتالي تردي خواصها.

ب- يلاحظ ايضاً ان الأنخفاض في مقاومة الأنضغاط للنماذج المعرضة للحرق بدرجة حرارة (400م$^0$) تتناسب طردياً مع تعاقب عدد دورات التسخين واعادة التبريد الى درجة حرارة المختبر .

ج- مقدار الانخفاض في مقاومة الأنضغاط بعد الدورة العاشرة من تسخين نفس النموذج وصل الى 52.7% . اي بنسبة زيادة عن الدورة الأولى بمقدار 28.4% وهذا يمكن ايعازه الى فعل مشابه لفعل اجهادات الـ (Fatigue) . حيث اظهرت الدراسات ان درجات الحرارة العالية تؤدي الى تغيرات حجمية تنتج بدورها اجهادات تؤدي الى حدوث تشققات شعرية (Micro cracking) وشروخ كبيرة (Large Fractures) ونتيجة لأعادة حرق هذه النماذج تبدأ الأجهادات بالتركز عند حافات التشققات والشروخ مما يؤدي الى زيادة اطوالها واتساعها وبالتالي زيادة في تردي خواص الخرسانة .

يتبين من ذلك ان الأبنية والأجزاء الخرسانية التي تتعاقب عليها دورات الحرارة والتبريد مثل الغرف الخرسانية الخاصة بحرق النفايات والمداخن الحرارية تكون عرضة لفقدان مقاومة جدرانها ربما بشكل مستمر كذالك الابنية التي تتعرض لأكثر من حريق عرضة للانهيار بشكل اكبر لذا يجب إتخاذ احتياطات اكبر وتقوية وتدعيم الأجزاء التي تعرضت لفعل الحريق (بشكل مباشر او غير مباشر) بشكل جيد ومتين .

**ثانياً** : تأثير ابعاد او حجم النماذج الخرسانية المعرضة لدرجات حرارة عليها على نسبة انخفاض مقاومة انضغاطها :

أ- يلاحظ من الجدول رقم (7) والشكل رقم (2) ان جميع النماذج للمجاميع (A , B , C) تزداد النسبة المئوية للأنخفاض في مقاومة انضغاطها بزيادة درجات الحرق في الفرن الحراري مقارنتاً بمثيلاتها التي فحصت بدون تعريضها الى درجات حرارة عالية وتصل مثلاً هذه النسبة عند درجة حرارة 750 م$^0$ الى (76% ، 71% ، 60%) على التوالي وهذا يعزى الى التغيرات المجهرية في التركيب البلوري للسمنت اضافة الى حدوث تشققات في حبيبات الركام الخشن والتفاوت في التغيرات الحجمية بين الركام والسمنت والذي يؤدي الى حدوث تشققات في السمنت او الى انفصالها عن الحصى .

ب- يلاحظ من الجدول رقم (7) ان مقاومة الأنضغاط للنماذج التي تم فحصها بدون تعرضها للحرق تقل بزيادة ابعاد (حجم) النماذج وهذا قد يعزى الى زيادة نسبة الفراغات والشقوق المجهرية التي تنتج نتيجة لأجهادات التقلص اثناء فترة التصلب اضافة الى نقصان درجة الحصر ( Confinement effect) .

ج- يلاحظ من الجدول رقم (7) والشكل (3) ان النسبة المئوية للأنخفاض في مقاومة انضغاط النماذج تقل بزيادة حجم النموذج ولجميع درجات الحرارة التي تم اختبار النماذج عليها . فمثلاً قلت نسبة الانخفاض في مقاومة الانضغاط عند درجات حرارة 250 و 500 $^0$ م بحدود 40% بين النماذج باحجام 100 ملم$^3$ والنماذج باحجام 200 ملم$^3$ و20% لنفس الاحجام عند درجة حرارة 750 م$^0$، وهذا قد يعزى بسبب زيادة عمق النموذج الخرساني حيث تعتبر الخرسانة مادة رديئة التوصيل الحراري نسبة لبقية المواد الأنشائية مثل الحديد .

د- يلاحظ ايضاً من الجدول رقم (7) انه كلما زادت ابعاد النماذج المعرضة لدرجات حرارة عالية فان قيمة حمل الفشل لها تكون اكبر من قيمة حمل الفشل للنماذج الاصغر والتي تم حرقها بدرجات حرارة اقل منها او بدرجة حرارة المختبر, فمثلا ان حمل الفشل للنماذج بابعاد 150 و200 ملم والتي تم حرقها بدرجات حرارة 500 م$^0$ و750 م$^0$ على التوالي كانت اكبر من حمل الفشل للنماذج بابعاد 100 ملم والتي تم فحصها بالضروف الاعتيادية ( درجة حرارة المختبر ) , على هاذا يمكن التنبوء بان اي زيادة في ابعاد االمقاطع الرئيسية للهياكل الخرسانية عن التصميم الأولي لها تعطيها مقاومة لا يستهان بها للصمود بوجه الحرائق او عند تعرضها لدرجات حرارة العالية وتسمح كذلك بمعالجتها بعد ازالة السطوح المهشمة بواسطة الراتنجات الحديثة (Resin Epoxy) الخاصة بالحرائق.

مما سبق اعلاه ينصح بأجراء دراسة مستفيضة على نماذج خرسانية يتم اعدادها بأبعاد مختلفة اكبر واصغر من 200 ملم$^3$ وذلك لمعرفة هل الزيادة في ابعاد النماذج الخرسانية تكون زيادة محددة ام نسبة مئوية من ابعاد النماذج للصمود بوجه الحرائق .

كما يوصى باعتماد حمل الفشل وليس اجهاد الفشل في الدراسات وذلك لتعرض النماذج الخرسانية للتشظي والتخصر نتيجة لتعرضها الى درجات حرارة عالية بسبب الحرائق والمؤدية الى عدم دقة النتائج المستحصلة لقيم الاجهادات.

**<u>الأستنتاجات</u>**

1- الأجزاء الخرسانية المعرضة لتعاقب دورات الحرارة العالية عليها نتيجة للحرائق او غيرها لأكثر من مرة مثل الغرف الخرسانية الخاصة بحرق النفايات والمداخن الحرارية وكذالك الابنية الحاوية على مواد سريعة الاشتعال والتي تتكرر فيها اشتعال الحرائق ، تنخفض مقاومة انضغاطها وصمودها ضد الحريق بشكل طردي مع تكرار تعرضها للحرارة حتى إن كان ذلك التعرض بدرجات حرارة عالية بحدودها المتوسطة (400 م$^0$) .

2- كلما كان ابعاد المقاطع في الهياكل الخرسانية اكبر كلما كان صمودها بوجه الحرائق اكبر حيث بينت نتائج هذا البحث ان نسبة الأنخفاض في مقاومة الأنضغاط للخرسانة المعرضة لدرجات حرارة عالية اقل كلما كانت ابعاد هذه المقاطع اكبر اي ان العلاقة عكسية بينهما . ويمكن التنبؤ بأن اي زيادة في ابعاد اجزاء الهياكل الخرسانية عن التصميم الأولي لها (اضافة الى الغطاء الخرساني لحديد التسليح ) تؤدي الى زيادة كبيرة في مقاومتها وصمودها ضد الحرائق.

**REFERENCE**


- Toumi and Musa Rasheidat, *Influence of high temperatures on surface cracking of concrete studied by Image Scanning Technique*, Jordan Journal of Civil Engineering, volume 4, No. 2, 2010.
- Zween , Ali Talib Jasim *Performance of light weight aggregate concrete in corpora ting fiber exposed to elevated temperature* PhD , Thesis , University of Technology , Iraq , pp. 6-12 , 2008 .
- ALAN LAU , "*Effect of high Temperature on normal strength concrete and high performance concrete containing steel fibers*" , the Hong Kong polytechnic university , 2000 .
- Sri Ravindrarjah , R. , Lopez , R. and Reslan , H. , "Effect of Elevated Temperature on the properties of High strength concrete containing cement supplementary materials" , *International conference on Durability of Building materials and components* , Brisbane , Australia , pp. 1-9, 17 – 20th March , 2002.
- Venkatesh kodur "*properties of concrete at elevated temperature*", Department of civil and Environmental Engineering, Michigan state University – 2014.
- B. Toumi , M . Resheidat , Z. Guemmadi and H. chabil , "*Coupled effect of high temperature and heating time on the residual strength of normal and high strength concrete*" , Jordan Journal of Civil Engineering, volume 3 , No.4 , 2009 .
- Alexander etal. "*Concrete Containing Steel Slag aggregate "Performance after high temperature Exposure"*, concrete repair, Rehabilitation 111, Netinger , 2012 .
- R.V. Balendran , T. Maqsood , A. Nadeem , " *Effect of cooling method on residual compressive strength of high strength concrete cured for 28 days and 180 days and heated to elevated temperatures*" , 26 th conference on our world in concrete and structures , Singapore , 2003 .
- A. Ferhat Bingol & Rustem GUL, "*Compressive strength of light weight aggregate concrete exposed to high temperature*", Indian Journal of Engineering & material science, vol. 11, pp.68 – 72, February, 2004.
- Prof. D. B. Kulkurni & Prof. Mrs. SN patil , "*Compressive study of effect of sustained high temperature on strength properties of self compacting concrete and ordinary conventional concrete* " , International Journal of engineering and technology , vol. 3 (2) , 106 – 118 , 2011 .
- Arundeb Gupta , Saroj Mandal and somnath Ghosh , " *Recycled Aggregate concrete exposed to elevated temperature* " , APPN Journal of engineering and Applied sciences , vol .7 , No.1 , 2012 .
- Rahol Sobhash patil , *" Effect of elevated temperature and type of cooling on M20 Grade concrete using Fibers "* , International Journal of science and research (IJSR) , vol.3 ISSve 2 , 2014 .
- Sullivan , "*Deterioration and spalling of high strength concrete under fire*" , HSE , offshore Technology Report , 2001 / 074 .
- Kadhum , Mohammed Mansour , *" Behavior of fire Exposed Reinforced concrete columns "* , PHD . Thesis civil engineering Department, university of Baghdad , Iraq , 2010 .
- Iraqi specification No. S. "Portland cement", 1984.
- Iraqi specification No.; 45, "Aggregate from natural sources for concrete and construction", 1984.

**جدول (1) نتائج الفحوصات للسمنت**

| نوع الفحص | النتائج | حدود المواصفة العراقية |
|---|---|---|
| وقت التماسك الابتدائي (دقيقة) | 82 | لا يقل عن 45 دقيقة |
| وقت التماسك النهائي (ساعة) | 5.3 | لا يزيد عن 10 ساعة |
| نعومة الأسمنت بطريقة بلين $m^2/Kg$ | 300 | لا يقل عن 230 |
| تحمل الأنضغاط بعمر 7 ايام MPa | 42.1 | لا يقل عن 23 MPa بعمر 7 أيام |
| الأستطالة % | 0.18 | لا يزيد عن 0.8% |

**جدول (2) نتائج الفحوصات الكيميائية للسمنت**

| المركب الكيميائي | الرمز الكيميائي | المحتوى (%) | حدود المواصفة العراقية |
|---|---|---|---|
| الكلس | CaO | 65.8 | - |
| السليكا | $SiO_2$ | 19.8 | - |
| الالومينا | $Al_2O_3$ | 4.77 | - |
| اوكسيد الحديد | $Fe_2O_3$ | 2.99 | - |
| المغنيسيا | MgO | 1.89 | لا يزيد عن 5% |
| الكبريتات | $SO_3$ | 2.6 | لا يزيد عن 2.8% |
| الفقدان في الحرق | L.D.I. | 3.8 | لا يزيد عن 4% |
| النواتج غير الذائبة | I.R. | 1.3 | لا يزيد عن 1.5% |
| معامل الأشباع بالكلس | L.S.F. | 1.02 | 0.66 – 1.02 |

جدول رقم (3) التحليل المنخلي للرمل

| قياس المنخل (mm) | النسبة المارة % | حدود المواصفة العراقية (منطقة التدرج 3) |
|---|---|---|
| 4.75 | 100 | 90 – 100 |
| 2.36 | 87 | 85 – 100 |
| 1.18 | 82 | 75 – 100 |
| 0.6 | 68 | 60 – 79 |
| 0.3 | 24 | 12 – 40 |
| 0.15 | 7 | 0 – 10 |
| 0.075 | 0 | 0 – 3 |

جدول (4) التحليل المنخلي للركام الخشن

| قياس المنخل (mm) | النسبة المارة % | حدود المواصفة العراقية |
|---|---|---|
| 14 | 100 | 90 – 100 |
| 9.5 | 60 | 50 – 85 |
| 4.75 | 10 | 0 – 10 |
| 2.36 | 0 | 0 – 5 |

جدول (5) فحوصات الماء

| الفحوصات المطلوبة | | حدود المواصفة ملغم / لتر |
|---|---|---|
| الكبريتات $SO_3$ | 135 | 1000 |
| الكلوريدات | 65 | 500 |
| الشوائب غير العضوية | 450 | مجموع الايونات لا يتجاوز 3000 ملغم / لتر |
| الشوائب العضوية | صالح للشرب | يجرى فحص المياه التي لها لون ورائحة ملحوظة |

جدول (6) نتائج مقاومة الأنضغاط للخرسانة المعرضة لتعاقب دورات التسخين والتبريد الى درجة حرارة $400\ C^0$

| المجموعة | عدد دورات التسخين الى درجة حرارة 400م$^0$ والتبريد لدرجة حرارة المختبر | مقاومة الأنضغاط نيوتن / مليمتر$^2$ | النسبة المئوية للانخفاض في مقاومة الأنضغاط |
|---|---|---|---|
| 1 | 0 | 24.3 | % 0 |
| 2 | 1 | 16.4 | % 32.5 |
| 3 | 2 | 15.9 | % 34.6 |
| 4 | 3 | 15.6 | % 35.8 |
| 5 | 4 | 15.47 | % 36.33 |
| 6 | 5 | 15.04 | % 38.00 |
| 7 | 6 | 14.17 | % 41.68 |
| 8 | 7 | 13.78 | % 43.30 |
| 9 | 8 | 13.20 | % 45.68 |
| 10 | 9 | 12.78 | % 47.41 |
| 11 | 10 | 11.50 | % 52.70 |

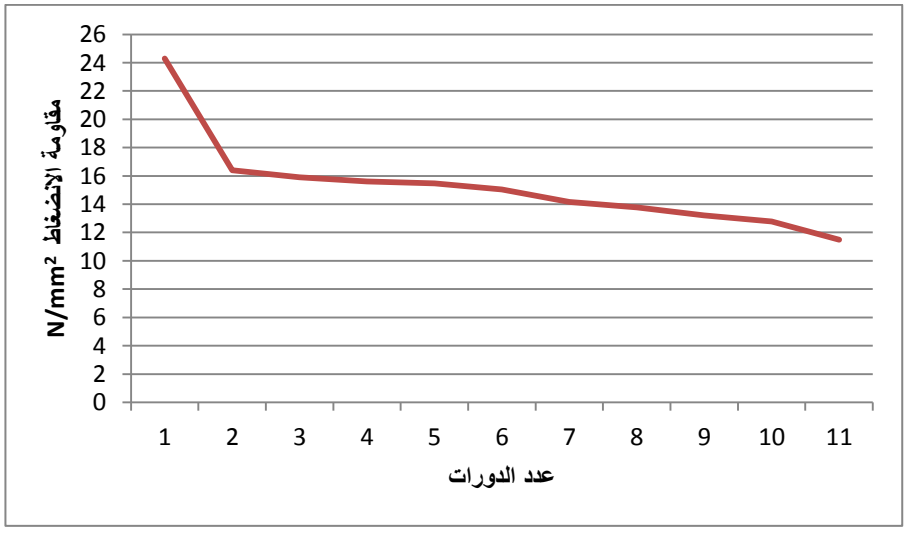


شكل (1) العلاقة بين مقاومة انضغاط النماذج وعدد دورات التسخين

**جدول رقم (7) نتائج الأختبارات على العينات بأحجام مختلفة**

| المجموعة ابعاد النموذج | مقاومة الأنضغاط بدرجة حرارة المختبر $25C^0$ N /$mm^2$ حمل الفشل | مقاومة الأنضغاط بدرجة حرارة $250C^0$ N /$mm^2$ حمل الفشل | النسبة المئوية للأنخفاض في مقاومة الأنضغاط بدرجة حرارة N/$mm^2$ $250C^0$ | مقاومة الأنضغاط بدرجة حرارة $500C^0$ N /$mm^2$ حمل الفشل | النسبة المئوية للأنخفاض في مقاومة الأنضغاط بدرجة حرارة N/$mm^2$ $500C^0$ | مقاومة الأنضغاط بدرجة حرارة $750C^0$ حمل الفشل | النسبة المئوية للأنخفاض في مقاومة الأنضغاط بدرجة حرارة N/$mm^2$ $750C^0$ |
|---|---|---|---|---|---|---|---|
| A 100x100x100mm | **320 KN** 32 | **248 KN** 24.8 | 22.5 % | **151 KN** 15.10 | 52.8% | **77 KN** 7.7 | 76% |
| B 150x150x150mm | **641 KN** 28.5 | **517 KN** 23.0 | 19% | **378 KN** 16.80 | 41% | **187 KN** 8.3 | 71% |
| C 200x200x200mm | **1040 KN** 26.0 | **904 KN** 22.6 | 13% | **708 KN** 17.70 | 32% | **416 KN** 10.4 | 60% |

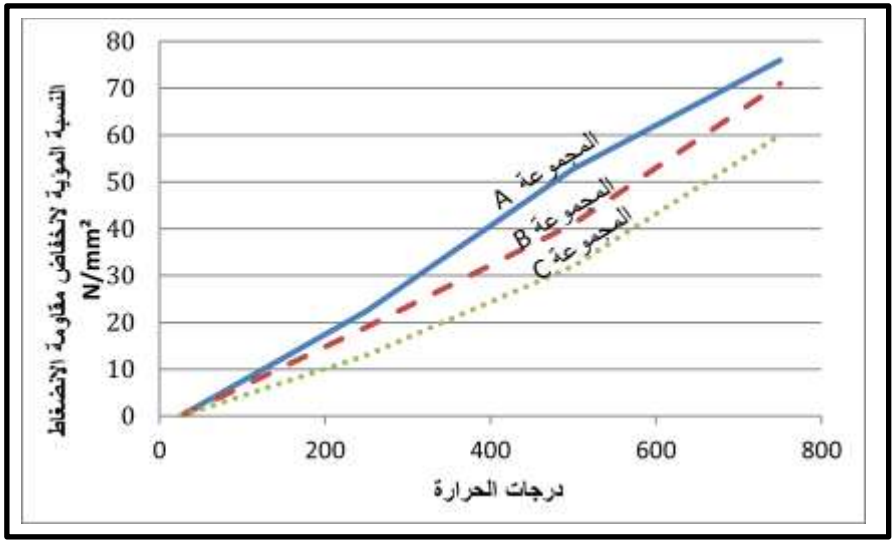


شكل (2) : العلاقة بين النسبة المئوية لأنخفاض مقاومة الانضغاط ودرجات الحرارة للنماذج حسب احجامها

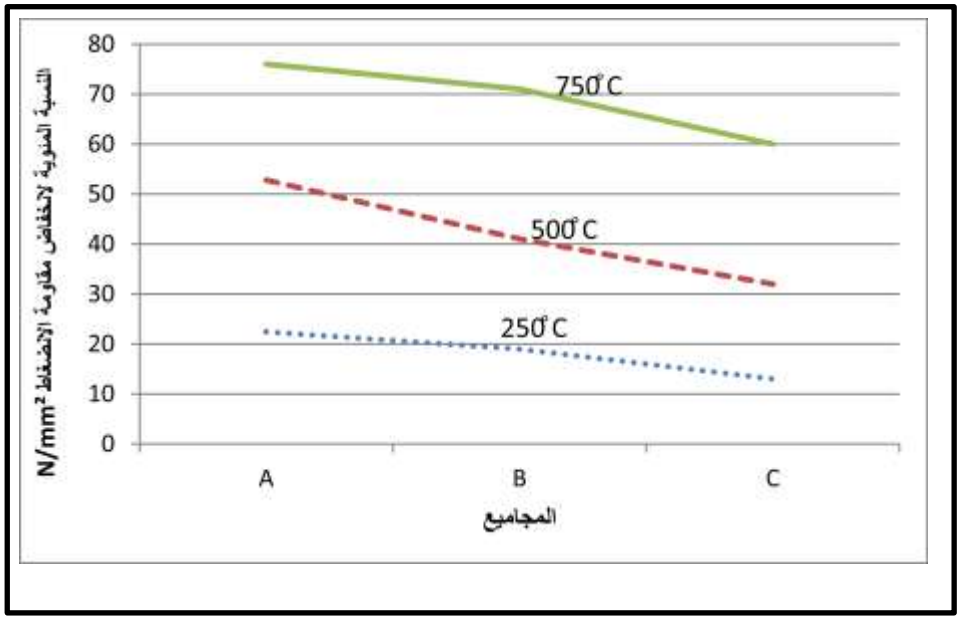


شكل (3):العلاقة بين النسبة المئوية لأنخفاض مقاومة الانضغاط وحجم النماذج حسب درجات الحرارة المسلطة

# Studying the Utility of Using Reed and Sawdust as Waste Materials to Produce Cementitious Building Units

**Prof .Dr. Shakir Ahmed Salih**

Department of Building and construction Engineering
College of Engineering
University of Technology
Email: professorshakir@uotechnology.edu.iq

**Eng. Aseel Mahmood Kzar**

Department of Civil Engineering
College of Engineering
Baghdad University
Email: aseelkzar_89@yahoo.com

## ABSTRACT

In this research, the possibility of using waste wooden materials (reed and sawdust) was studied to produce sustainable and thermal insulation lightweight building units , which has economic and environmental advantages. This study is intended to produce light weight building units with low thermal conductivity, so it can be used as partitions to improve the thermal insulation in buildings. Waste wooden materials were used as a partial replacement of natural sand, in different percentages (10, 20, 30, and 40) % . The mix proportions were (1:2.5) (cement: fine aggregate) with w/c of 0.4. The values of 28 days oven dry density ranged between (2060-1693) kg/m$^3$.The thermal conductivity decreased from (0.745 to 0.222) W/m. K .The percentages of decrease in 28 days compressive strength were (30.8, 36.8, 50 and 56.4) % .The flexural strength increased at low replacement of reed and sawdust content, and then it decreases with the increase of reed and sawdust content. At the end of the work, building units were produced from selected mix (natural sand with 30 % reed and sawdust) (MS30) .Two types of brick units were produced; the first type without coating reed or sawdust and the second type was coated with bituminous emulsion. The coating with bituminous emulsion increased the compressive by about (20.3) % and the water absorption was reduced by about (30.4) %. Efflorescence was almost negligible for both types of bricks.

**Key words:** reed, sawdust , thermal conductivity, cementitious building units

# دراسة إمكانية الاستفادة من استخدام القصب ونشارة الخشب كمخلفات لانتاج وحدات بنائية

**أ .د . شاكر احمد صالح**
قسم البناء والانشاءات
كلية الهندسة / الجامعة التكنولوجية

**م .اسيل محمود كزار**
قسم الهندسة المدنية
جامعة بغداد /كلية الهندسة

## الخلاصة

تم في هذا البحث دراسة إمكانية الاستفادة من المخلفات الخشبية (قصب ونشارة الخشب) لانتاج وحدات بنائية مستدامة وعازلة للحرارة وخفيفة الوزن والتي لها العديد من الفوائد الاقتصادية والبيئية. هذه الدراسة تهدف إلى إنتاج وحدات بنائية خفيفة الوزن مع توصيل حراري واطئ لكي يتم استخدامها في القواطع لتحسين العزل الحراري للابنية. تم استخدام المخلفات الخشبية كتعويض جزئي من الركام الناعم وبنسب مختلفة (10, 20 , 30 , 40 ) % .حيث تم استخدام نسب خلط (2.5:1) ( سمنت : الركام الناعم ) و نسبة ماء الى السمنت 0.4. قيم الكثافة المجففة بالفرن بعمر 28 يوم تراوحت بين (2060-1693) كغم /م$^3$.

إستخدام القصب والنشارة ساهم في تقليل الموصولية الحرارية وبذلك زيادة العزل الحراري بصورة جيدة فقد تناقصت الموصولية الحرارية من ( 0.745 الى 0.222 ) واط / م. كلفن . النقصان في مقاومة الانضغاط بعمر 28 يوم كان (30, 36, 50, 56 )% . قيم معاير الكسر زادت عند نسب الاستبدال الواطئة للقصب ونشارة الخشب ومن ثم بدأت بالتناقص مع زيادة محتوى النشارة والقصب. في نهاية العمل تم إنتاج وحدات بنائية من خلطات مختارة وهي ( الرمل الطبيعي مع نسبة 30 % قصب ونشارة ) , تم إنتاج نوعين من الطابوق النوع الاول بدون طلاء القصب او النشارة بمادة مانعة للرطوبة والنوع الثاني تم طلاء القصب والنشاره بمادة مانعه للرطوبه وهي مستحلب قيري . استخدام المستحلب القيري ادى إلى زيادة مقاومة الانضغاط بمقدار 20.3 % وقلل الامتصاص بمقدار 30.4 % , أما التزهر فقد كان شبة معدوم لكلا النوعين من الطابوق.

**الكلمات الرئيسية** : قصب , نشارة خشب , موصولية حرارية , وحدات بنائية رابطة

## 1. INTRODUCTION

Iraq is located in the semitropical region which dominated by the semi-desert climate, where the summer season continuous for long period. Sun shines for more than 12 hours / day, which has a significant impact on the buildings. Temperature differences between the inside and the outside of the building are very high. Therefore the need for using air – conditioning became necessary to obtain the suitable temperature inside the building. Air – conditioners represent a fundamental load on the consumed electrical power ; statistics indicate that using air-conditioners represent (70%) of the entire electric power consumed ,**Al-Hadithi,1975 and ESCAWA , 2005.**The acceleration of social and urban renaissance in Iraq led to an increase in the number of houses built ; they increased in Baghdad city over the last three decades from 352870 in (1977) to 611022 in( 2007) the ratio of increment was 73.2 % , while in whole Iraq , they increased from 470942 to 2391262 for the same period and the increment ratio was 62.6 %.This led to increasing the amount of produced energy to each person from 403.8 kw – hour /person in (1977) to 1115 kw- hour/ person in(2007),**Central Bureau of Statistic, 2007**. In 2014, there is a continues increase in buildings with time, which will have a great effect on economy. For reducing the load on electrical power generation, should taking into the account using thermal insulator materials inside the building. These materials have a low thermal conductivity to reduce the amount of heat passes through ceilings and Walls. This Keeps the building in suitable Temperature, without the need of using air – conditioning for a long period, **Rofa, 2011**. Many countries edited codes to make the use of thermal insulation mandatory in buildings. It was noticed from the previous researches that using thermal insulation in building reduces the consumed electricity by (30 – 40) %. Thermal insulation in buildings can be achieved by using materials with thermal insulation characteristics which include low density and high porosity.

The main criterion for the selection of thermal insulation materials is to have a low thermal conductivity, in addition to other properties such as their durability and endurance; it also prefers to have the capacity to absorb the sounds and vibrations

**Taoukil et al, 2011,** studied the thermal properties of a concrete lightened by wood aggregates from waste products of the carpentry work .They made a comparison between the properties of concretes lightened by sawdust and by wood shavings. They found that at equal mass percentage of wood aggregates, the concretes made from shavings present better thermal insulation than those obtained from sawdust.

**Dawood, 2010,** investigated the thermal conductivity of sawdust of different densities, (100,150,200,250) kg/m$^3$ without using a binder, then he studied the same densities of sawdust with binder (white glue) at different ratios (10, 25, 40) % from the weight of sample for each density. He found that the lowest thermal conductivity was 0.18W/m.K at a density of (100 kg/m$^3$) without a binder. While the highest value of thermal conductivity was 0.285 W/m.K at a density of (250kg/m$^3$) with 40% binder.

**Saaed, 2013,** treated sawdust before being used as an aggregate for making sawdust concrete. The treatment included boiling the sawdust in water containing hydrated lime in order to dissolve all soluble organic components. He used waterproofing materials to reduce water absorption of sawdust. Two types of waterproofing materials were used (cutback asphalt and classic varnish). The properties of sawdust concrete were highly improved; the increase of compressive strength was up to 50% for Moderate sawdust ratios. Flexural strength also increased; water absorption and thermal conductivity were highly reduced.

**Al-Ubaidi, 2002,** studied the properties of reed in concrete; she used two types of reeds (shredded reed of 4 cm length and sliced reed of 2 cm length) as coarse aggregate in different percentages (10, 20, 30 and 40) % by volume of total mix. The properties of 4 cm length shredded reed show better results than 2 cm length sliced reed .The 28 days air density was between (1360-1890)kg/m$^3$ for the 4cm shredded reed, while for 2 cm sliced reed ,the density was between(1302-1850)kg/m$^3$. Using reed as a coarse aggregate in concrete reduces the 28-days compressive strength from 24 to 0.4 MPa for shredded reed and 11.7 to 0.16 MPa for sliced reed. The thermal conductivity values were between (1.36-0.765) W/m.K for shredded reed and between (1.05-0.57) W/m.K for sliced reed.

**Adullatif, 2009**, investigated the durability of reed in cement media; he used (epoxy, SBR, PVD and liquid mastic) coatings to reduce the absorption of water and (sodium chloride, sodium sulfates and sodium nitrite) to reduce the alkaline of concrete. He found that epoxy paint is the best coating ; it reduced the absorption from 70 % to 26 % , while the liquid mastic reduced it by 30 % the reduction in SBR and PVA were (46.23, 52.15 ), respectively. The results of splitting and modulus of elasticity after immersion in lime for 90 days indicates that epoxy coating gives the highest splitting strength , but not higher than the reference mix (reed without coating and chemical treatment ); the results also indicate that the treatment with sodium chloride is better than sodium nitrite and sodium sulfate.

## 2. MATERIALS

The materials used in this research are:

### 2.1 Cement

Ordinary Portland cement produced by Mass cement Factory was used in this work. It was stored in a dry and shaded place to avoid exposure to the atmospheric conditions like humidity. The chemical properties of the cement are shown in **Tables 1**; results show that the adopted cement conforms to the Iraqi specification **No.5/1984.**

### 2.2 Natural Sand

Natural sand from Al – Ekhadir region was used through this work. The grading , physical and chemical properties. **Table 2& 3** show the grading, chemical and physical properties of sand indicate that the used sand conforms to the Iraqi specification **No.45/1984.**

### 2.3 Sawdust

Sawdust was used as a partial replacement of fine aggregate to offer thermal insulation. It was brought from carpentry workshop, as shown in **Fig. 1.**

### 2.4 Reed

Local reeds from different river banks in Baghdad region are used in this work as shown in **Fig.2.** The reed crushed by a small hammer and cut with scissors to small particles as shown in **Fig. 3.**

### 2.5 High Range Water Reducers Admixtures

The superplactizer used was Top Flow (SP 603), (**Type F)**. It is a liquid admixture without any chloride content, basically consists of (Naphthalene Sulphonate ) with other admixtures to produce high strength concrete , the products is designed to reduce the quantity of water without affecting on the initial setting time of the mix.

## 3. PRETREATMENT OF REED AND SAWDSUT

The pretreatment procedures for reed and sawdust used in this study and which are also used by other studies:

1- The reed and sawdust was washed under running water, to remove the barks and ash.

2- The reed or sawdust was soaked in boiling water; lime was added to the boiling water of about 20 % from the weight of reed or sawdust for an hour to reduce the harmful soluble carbohydrates, tannins, waxes and resins in wood.

3- The reed or sawdust removed from the boiling water and exposed to the atmosphere for 2 days to be air dried.

4- Before using the reed or sawdust, it was soaked in water with salt of about 10 gm/L, to protect the reed and sawdust from fungi.

## 4. THE EXPERIMENTAL PROGRAM

The experimental program consists of using reference mix of proportion (1:2.5) by weight (cement: fine aggregate), the cement used was about 550 kg/m$^3$ and sawdust and reed were used together in different percentages (10,20, 30 and 40) % as a partial replacement from the volume of fine aggregate. The (w/c) ratio is adjusted to produce mixes with a flow of 100$\pm$10 mm, several trail mixes were done in order to determine the suitable dosage of superplacrizer for each mix to maintain the determined flow. The details of mix designations are shown in **Table 4.** All the tests were done at University of Baghdad laboratory, expect the thermal conductivity test was done at Building Research Directorate / Ministry of Science and Technology.

### 4.1. Mixing Procedure

According to **ASTM 305-99**, the following sequences used for mixing sand and fine brick aggregate mortars:

1- Reed and sawdust were added gradually to the fine aggregate and mixed together properly until they formerly distributed through the fine aggregate.

2- Cement was mixed with the fine aggregate until they are thoroughly blended.

3- The superplacticizer was added to the mixing water, and squeezed in the graduated cylinder to ensure that the superplactizer spread homogeneously through water.
4- The water and superplactizer was added to the mass and mix until the mixture is homogenous in appearance and has the desired consistency.

### 4.2. Casting and Compaction

After mixing, the mix was poured immediately into the molds by means of scoop, and was compacted in one layer by vibrating table. The top surface was trowelled to obtain smooth surface.

### 4.3. Curing

After casting, the specimens were covered by nylon sheets to prevent the evaporation of water from the surface for (24±2) hours. After that period, the specimens were demolded and cured in water until the age of testing. All specimens were cured in water until the age of testing except the length change specimens were cured in water for seven days and then they were kept in a dry place inside the laboratory. The laboratory temperature was about 25-30 $^0$C.

### 4.4 Hardened Tests

#### 4.4.1 28 Days Oven Dry Density

The oven dry density was conducted in accordance with **B.S EN12390-7: 2009,** on (50 mm) cubes. The specimens were cured until the age of 28 days. After that, the specimens were dried in ventilated oven at 105 ± 5 $^0$C until constant mass is achieved. Then the specimen was cool near room temperature. The density is calculated as follows:

**Ƥ = m / v**
Where:
Ƥ: oven dry density (kg/m$^3$).
m:the mass of oven dry specimen (kg).
v: the volume of specimen calculated from its dimensions (m$^3$).

#### 4.4.2 Compressive Strength Test

Compressive strength test was conducted on a (50) mm cubes according to **ASTM C 109C 109/C 109M – 02, by** using 650 KN capacity, digital testing Machine. The test was conducted at ages of (7, 28 and 90) days .The average of three specimens were adopted at each age. The compressive strength computed as follows:
Fcu = P / A
Where
Fcu : compressive strength (N/mm$^2$).
P: The applied load (N).
A: The surface area of the cube (mm).

#### 4.4.3 Flexural Strength Test

The flexural strength was conducted by using (160x40x40) mm prisms according to **ASTM C 348-02**.The prisms were subjected to single point loading. The specimens were tested at ages of

(7, 28 and 90) days. The average of three specimens was tested at each age. The flexural strength was tested by using 650 KN capacity tester machine. The following equation was used to estimate the flexural strength, where the failure occurred in the middle point:

$Sf = 0.0028p$

Where:

SF: flexural strength, MPa.

P: total maximum load, N.

### 4.4.4 Thermal Conductivity Test

The thermal conductivity conducted using wood moulds of (300x300x50) mm was tested in accordance with **ASTM C177.**The type of thermal conductivity apparatus is (Linseis HFM 300) It is made in Germany and is shown in figure (3.10) .It is used to measure the thermal conductivity and overall coefficient of heat transfer (U-value). The test sample is placed between plates, operating the apparatus until the thermal equilibrium happens. The time taken to reach the thermal equilibrium depends on the type of material, thickness and the temperature difference between the upper and lower plate. The specimens should be completely dry.

## 5. RESULTS AND DISSCUSIONS

### 5.1 The 28 Days Oven Dry Density

The 28 days oven dry densities of natural sand mixes are shown in **Table 5** and **Fig. 4.**The results indicate that the 28 days oven dry densities decrease with the increase in reed and sawdust content. This is due to low density, and high porosity of reed and sawdust; this will contribute in producing air voids inside the structure of the matrix, and hence reducing the density. At 28, days the oven dry density for sand mixes ranged between (1976 – 1693) $kg/m^3$ for (10, 20, 30 and 40) % of reed and sawdust content respectively, and 2060 $kg/m^3$ for the reference mix. The percentages of decrease in unit weight compared with reference mix were (4.07, 7.57, 11.4 and 17.8) %, respectively.

### 5.2 Compressive Strength

The compressive strength test results of natural sand mixes are shown in **Table 6** .The compressive strength of all cubic specimens decreases with the increase in sawdust and reed content. This is due to the inclusion of reed and sawdust to the matrix, which considered weak when compared with natural sand aggregates. The strength development with time of natural sand mixes are shown in **Fig. 5**. **Fig. 6** shows a relationship between the 28 days compressive strength and oven dry density for sand mixes. It is indicated that the density is a major factor affecting on compressive strength.

### 5.3 Flexural Strength

The flexural strength test results are shown in **Table 7** .The results show an increase in flexural strength for (MS10, MS20) mixes by about (26, 30) %, respectively compared with the reference

mix. Then the flexural strength decrease with the increase of reed and sawdust content for (MS30, MS40) mixes. **Fig. 7** shows the effect of reed and sawdust content on the 28 days flexural strength. The decrease in flexural strength with the increase in reed and sawdust content it is attributed to the increase of air voids content and is due to non homogeneity of the matrix; also the cement paste – aggregate bond becomes weaker. The development of flexural strength with time is shown in **Fig. 8.** Most of the flexural strength is gained at 28 days then the rate of increment decreases with time. This is because of the rate of hydration and the properties of reed and sawdust, which are affected when exposed to water for long period.

### 5.4 Thermal Conductivity

The main purpose for producing such a type of light weight mortar is to improve the thermal insulation. **Table 8** and **Fig. 9** show the thermal conductivity test results .it is found that when reed and sawdust content increases, the thermal conductivity decreases compared with the reference mix and hence the thermal insulation is improved. Reed and sawdust are classified as fibrous insulating materials; they have a high porosity, which can be considered as hollow bodies filled with gases that can resist the heat flow. They have good thermal insulation and characterized by their lightness. The range of thermal conductivity for natural sand mixes at the sawdust content %, by volume) respectively, compared with 0.745 for reference age of 28 days is between (0.222-0.524) W/m.K for 10% to 40% (reed and sawdust content %, by volume).

### 5.5 Thermal Insulation Building Units

From the previous discussion of the results, it is intended to select the suitable mixes to produce building units. They can be used in multiple applications, due to their low weight and good thermal insulation, such as boards, panels and building units.

Several considerations were taken when choosing the optimization mix, such as the thermal conductivity and compressive strength. It was decided to select MS30 mixes to produce bricks. **Table 9** summarizes the tests results of bricks units for MS30 mix. The produced products with dimensions of (240x120x55) mm as shown in **Fig. 10.**

#### 5.5.1 Test Results for Thermal Insulating Bricks

##### 5.5.1.1 Compressive Strength

**Table 9** shows the compressive strength results of bricks. The compressive strength for MS30 without coating was (19.3) MPa. The compressive strength with coating was (24.1) MPa According to IQS 25 /1988 the two types of bricks can be classified as (class A) brick.

##### 5.5.1.2 Water Absorption

The results for water absorption are listed in **Table 9** .Reed and sawdust has high water absorption. According to IQS 25/1988[13], the max water absorption is 24 %. The absorption is reduced by coating the sawdust and reed with bituminous emulsion. For bricks made with natural sand without coating the absorption was 16.4%, while with coating it was 11.6% .The reduction in absorption is 29.2%.

#### 5.5.1.3 Efflorescence

**Table 9** shows that bricks made with sand were with almost negligible efflorescence, while the building units made with fine brick aggregate were with very light efflorescence of 5% from the total area of faces of bricks .

## 6. CONCLUSIONS

**1-** It is possible to produce aggregate from reed and sawdust of different grading to be used in producing lightweight mortar. Local waste materials such as reed and sawdust can be used in construction after pretreatment. The reusing of waste materials in concrete helps in reducing the disposing of waste materials, and thus will preserve the environment.

**2-**The inclusion of sawdust and reed in mortar decreased the compressive strength significantly. The percentage of decrease at 28 days was (30.8, 36.8, 50 and 56.4) % for (10, 20, 30 and 40) % reed and sawdust content as a replacement by volume of natural sand, respectively.

**3-**The flexural strength increased for 10 and 20 % reed and sawdust content while using higher percentages of replacement (30 and 40) % sawdust and reed content causes a reduction in flexural strength up to (8.3, 23.4) %.

**4-** The addition of reed and sawdust reduced the thermal conductivity of the mixes by about (0.524, 0.410, 0.334 and 0.222) W/m.K compared with (0.745) W/m.K the thermal conductivity of reference mix of natural sand mixes.

**5-** Two types of bricks (240x120x50) mm without bituminous emulsion coating and with coating were produced. The compressive strength of natural sand mixes with and without coating were (24.1, 19.2) MPa, respectively. It can be concluded that using recycled materials (reed, sawdust) provide good thermal insulation and could be used as building units to construct partitions in framed structure.

## REFERNCES


- Al- Ubaidi, Z., 2002, *Use of Reed as Concrete Aggregate to Produce Light Weight Concrete* , M.Sc. dissertation, Department of Civil Engineering, the University of Al- Mustansiriya.
- ASTM C 109/C 109M – 02, *Standard Test Method for Compressive Strength of Hydraulic Cement Mortars (Using 2-in. or [50-mm] Cube Specimens)*.
- ASTM C 348 – 02, *Standard Test Method for Flexural Strength of Hydraulic-Cement Mortars.*
- ASTM C177-04, *Standard Test Method for Steady-State Heat Flux Measurements and Thermal Transmission Properties by Means of the Guarded –Hot-Plate Apparatus*.
- 
- BS EN 12390-7: 2009, Methods for Determination of Density of Hardened Concrete.
- Saeed, H.H., 2013, *Pretreatment of Sawdust for Producing Sawdust Concrete*, Engineering & Technical Journal, Vol.31, No.3, PP. 541-549.

- Taoukil, D., El-bouardi,A., Ezbakhe, H., and Ajzoul , T., 2011,*Thermal Proprieties of Concrete Lightened by Wood Aggregates*, Research Journal of Applied Sciences, Engineering and Technology , PP113-116.

- عبد الاله الحديثي,1975, *حسابات الاشعه الشمسيه على سطوح الابنية* , تقرير من منشورات مركز بحوث البناء – مجلس البحث العلمي العراقي.

- د. عادل محمود عبد اللطيف,2009,*تحسين ديمومة القصب في الوسط السمنت*, مجلة جامعة كربلاء العلمية, المجلد 7, العدد1.

- اللجنة الاقتصادية والاجتماعية لغربي اسيا, ملامح قطريه واقليميه لمؤشرات التنمية المستدامة لقطاعات مختارة في منطقة الاسكوا / قطاع الطاقة, نيويورك, الامم المتحدة, 21 كانون الاول 2005.

- الجهاز المركزي الاحصائي – المجموعة الاحصائيه السنويه / للسنوات 1977,2007 وزارة التخطيط والتعاون الانمائي / العراق .
- فاروق موسى روفا, 2011, *تأثير إضافة حبيبات عازلة الحرارة إلى الخرسانة المستخدمة في البناء على الموصلية الحرارية ومقاومة الانضغاط* , مجلة التقني ,العدد 24 ,ص 2 .

- المجموعة الاحصائيه لمنطقة اللجنة الاقتصادية والاجتماعية لغربي اسيا- العدد 25 .

- هيثم كامل داود,2010 " دراسة عملية لحساب الموصوليه الحرارية لنشارة الخشب", مجلة الهندسه والتنميه, المجلد 14, العدد 1.
- م ق ع1984/5,السمنت البورتلاندي,الجهاز المركزي للتقييس والسيطرة النوعية,العراق.

- م م ق ع 1984/45, ركام المصادر الطبيعية المستعمل في الخرسانة والبناء,الجهاز المركزي للتقييس والسيطرة النوعية,العراق.

- م ق ع 25 / 1988 الطابوق المصنوع من الطين , الجهاز المركزي للتقييس والسيطرة النوعية.

**Table 1.** Chemical composition and main compounds of ordinary Portland cement used in this research.

| Oxide composition | Abbreviation | Content % | Limits of Iraqi specification No.5/1984 |
|---|---|---|---|
| Lime | CaO | 61 | - |
| silica | $SiO_2$ | 19.84 | - |
| Alumina | $Al_2O_3$ | 5.28 | - |
| Iron oxide | $Fe_2O_3$ | 4.2 | - |
| Magnesia | MgO | 2.48 | 5.0% max |
| Sulfate | $SO_3$ | 2.49 | 2.8% max if C3A > 5 |
| Loss on ignition | L.O.I | 3.8 | 4 % max |
| Insoluble residue | I.R | 1.13 | 1.5 % max |
| Lime saturation factor | L.S.F | 0.92 | 0.66-1.02 |
| **Main compounds (Bogue's equations).** | | | |
| Triccalcium silicate | $C_3S$ | 48.97 | - |
| Dicalcium silicate | $C_2S$ | 20.01 | - |
| Tricalcium aluminate | $C_3A$ | 6.88 | - |
| Tetracalcium Alumino -ferrite | $C_4AF$ | 12.78 | - |

**Table 2.** Sieve analysis of natural sand.

| Sieve size (mm) | Cumulative passing % | Limits of Iraqi specification No.45/1984 (cumulative passing %( zone 2) |
|---|---|---|
| 10 | 100 | 100 |
| 4.75 | 94 | 90-100 |
| 2.36 | 79.4 | 75-100 |
| 1.18 | 65.4 | 55-90 |
| 0.6 | 51.5 | 35-59 |
| 0.3 | 19 | 8-30 |
| 0.15 | 3.7 | 0-10 |

**Table 3.** Physical and chemical properties of natural sand.

| **Properties** | **Test results** | **Limits of Iraqi specification No.45/1984** |
|---|---|---|
| Specific gravity | 2.7 | - |
| Absorption % | 1.66 | - |
| Dry rodded unit weight kg/m$^3$ | 1550 | - |
| Fineness modulus | 2.81 | - |
| sulfate content | 0.25 | 0.5 (max value) |

**Table 4.** Details of mix designation of sand mixes.

| Series No | Details | Mix designation | Reed and sawdust content as a partial replacement of natural sand, by volume % | HRWRA % by weight of cement | Cement Kg/m$^3$ | Natural sand Kg/m$^3$ |
|---|---|---|---|---|---|---|
| 1 | Natural Sand mixes | MS0 | - | 1 | 550 | 1375 |
| 2 | | MS10 | 5reed+5sawdust | 1 | 550 | 1239 |
| 3 | | MS20 | 10 reed+10 sawdust | 1.2 | 550 | 1101 |
| 4 | | MS30 | 15 reed+15 sawdust | 1.35 | 550 | 964 |
| 5 | | MS40 | 20 reed+20 sawdust | 1.4 | 550 | 826 |

**Table 5.** The 28 days oven dry density for reference mix and various types of mixes.

| Details | Mix designation | Reed and sawdust content % | Fresh density kg/m$^3$ | 28 days oven dry density kg/m$^3$ |
|---|---|---|---|---|
| Natural Sand mixes | MS0 | - | 2242 | 2060 |
| | MS10 | 5 reed+5 sawdust | 2218 | 1976 |
| | MS20 | 10 reed+10 sawdust | 2186 | 1904 |
| | MS30 | 15 reed+15 sawdust | 2140 | 1824 |
| | MS40 | 20 reed +20 sawdust | 2090 | 1693 |

**Table 6.** Compressive strength test results for reference mixes and various types of mixes**.**

| Details | Mix designation | Reed and sawdust content % | Compressive strength MPa At different ages | | |
|---|---|---|---|---|---|
| | | | 7days | 28days | 90days |
| Sand mixes | MS0 | - | 32.02 | 40.00 | 45.00 |
| | MS10 | 5 reed+5 sawdust | 21.12 | 27.68 | 35.13 |
| | MS20 | 10 reed+10 sawdust | 16.12 | 25.28 | 31.66 |
| | MS30 | 15 reed+15 sawdust | 13.96 | 20.84 | 29.5 |
| | MS40 | 20 reed +20 sawdust | 11.62 | 17.44 | 25.76 |

**Table 7.** Flexural strength test results of reference mixes and various types of mixes.

| Details | Mix designation | Reed and sawdust content % | Flexural strength MPa at different ages | | |
|---|---|---|---|---|---|
| | | | 7days | 28days | 90days |
| Sand mixes | MS0 | - | 4..05 | 4.32 | 4.97 |
| | MS10 | 5 reed+5 sawdust | 4.13 | 5.21 | 5.52 |
| | MS20 | 10 reed+10 sawdust | 5.10 | 5.44 | 5.96 |
| | MS30 | 15 reed+15 sawdust | 3.24 | 3.96 | 4.36 |
| | MS40 | 20 reed +20 sawdust | 2.88 | 3.50 | 3.85 |

**Table 8.** The Thermal conductivity test results and 28 days oven dry density of reference mixes and various types of mixes.

| Details | Mix designation | Reed and sawdust content % | 28 days oven dry density kg/m$^3$ | Thermal conductivity W/m.K |
|---|---|---|---|---|
| Natural Sand mixes | MS0 | - | 2060 | 0.745 |
| | MS10 | 5 reed+5 sawdust | 1976 | 0.524 |
| | MS20 | 10 reed+10 sawdust | 1904 | 0.410 |
| | MS30 | 15 reed+15 sawdust | 1824 | 0.334 |
| | MS40 | 20 reed +20 sawdust | 1704 | 0.222 |

**Table 9.** The mechanical and physical properties of building units.

| Test | MS30 without coating | MS30 with coating | LIMITS OF IQS 25 /1988 | | | |
|---|---|---|---|---|---|---|
| | | | Limitations for 10 bricks | | Limitations for one brick | |
| | | | Class A | Class B | Class A | Class B |
| Average compressive strength (MPa) | 19.6 | 24.1 | Min 18 | Min 13 | Min 16 | Min 11 |
| Average absorption | 16.4 | 11.4 | Max 20 % | Max 24 % | Max 22 % | Max 26 % |
| Efflorescence | Very light | Very light | Class A : Light<br>Class B : Moderate | | | |

**Figure 1.** Sawdust particles.

**Figure 2.** Reed.

**Figure 3.** Reed particles.

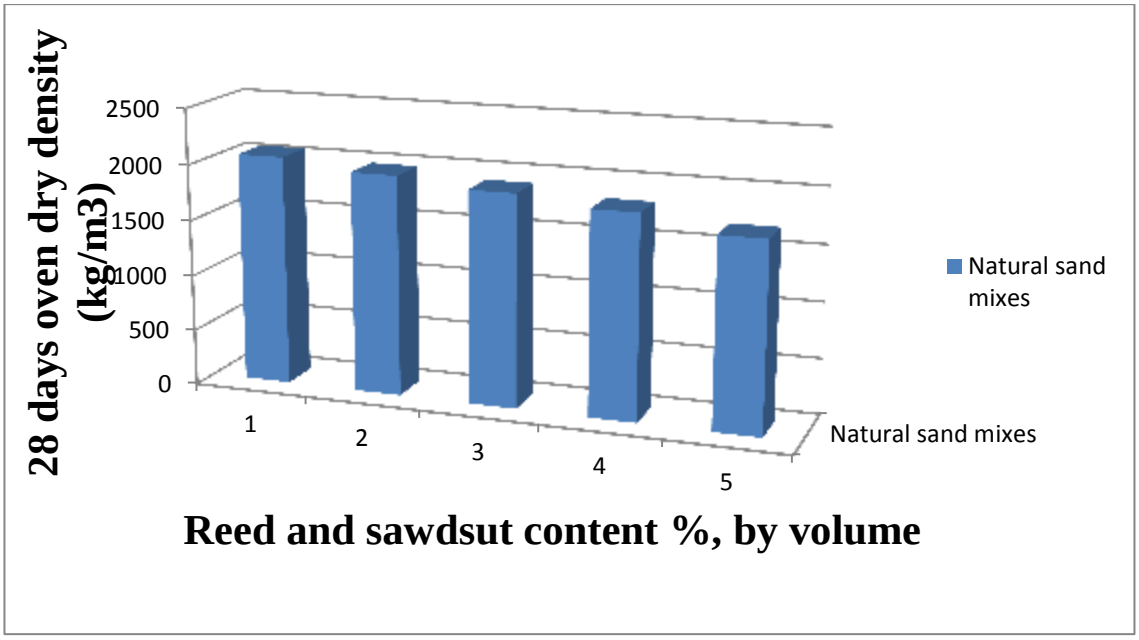


**Figure 4.** The 28 days oven dry density of natural sand mixes with various percentages of replacement of reed and sawdust.

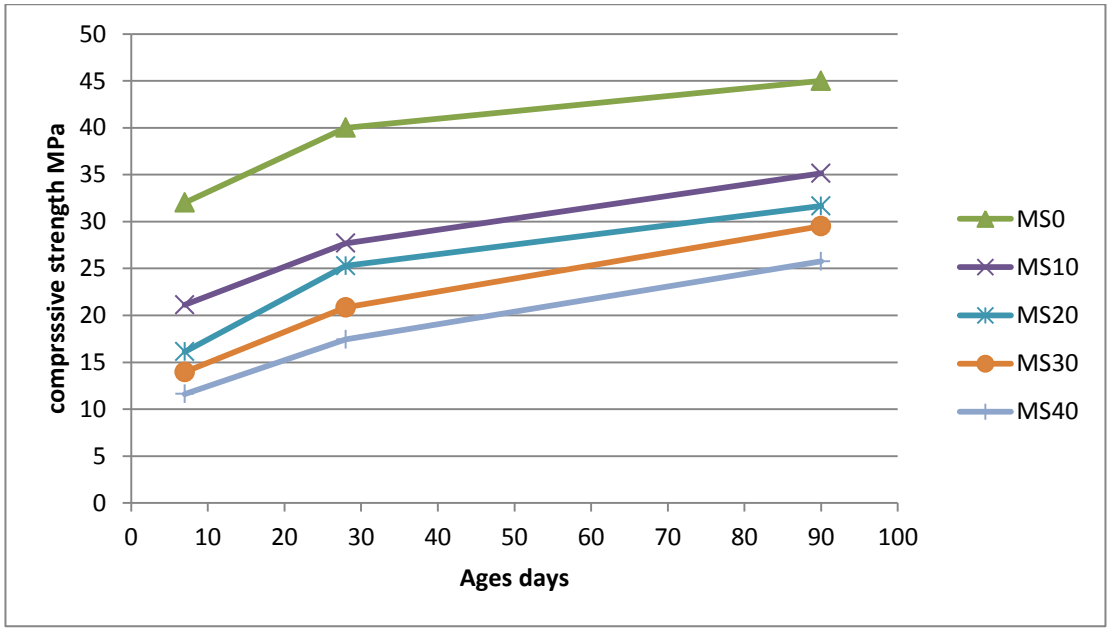


**Figure 5.**Effect of reed and sawdust content on the compressive strength of natural sand mixes at different ages.

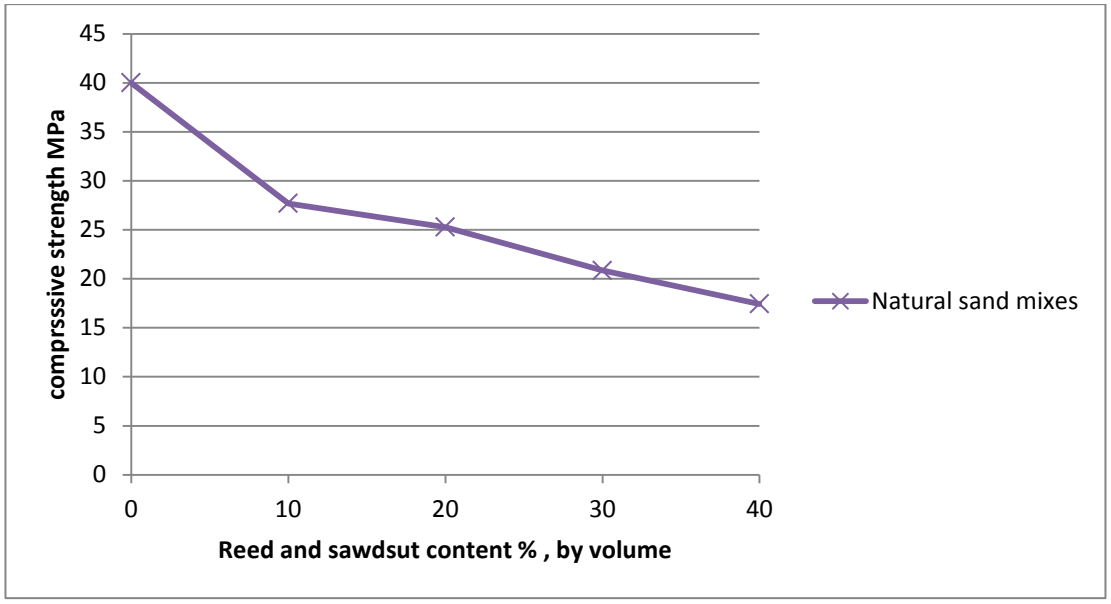


**Figure 6.** Effect of various percentages of reed and sawdust content on the 28 days compressive strength.

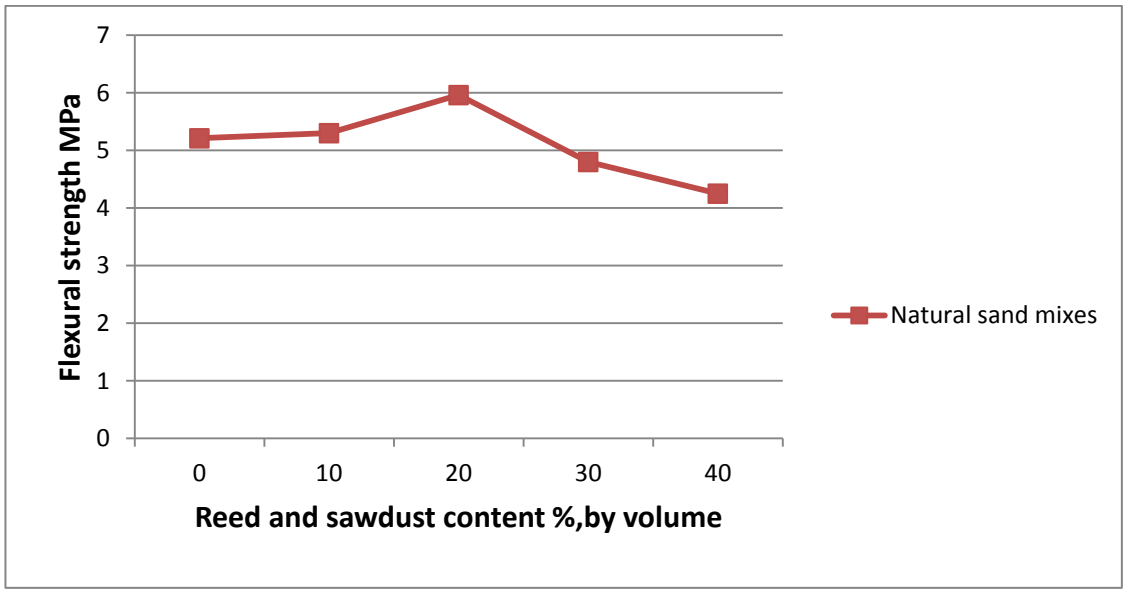


**Figure 7.** Effect of various percentages of reed and sawdust content on the 28 days flexural strength.

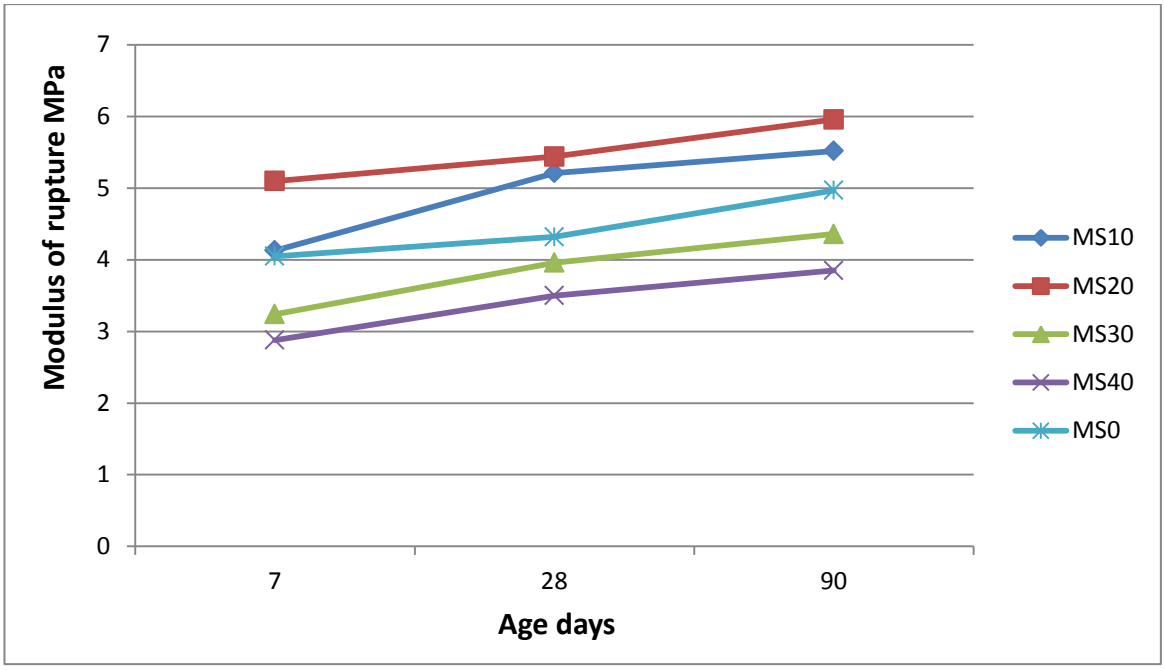


**Figure 8.** Relationship between the age of test and the flexural strength of natural sand mixes.

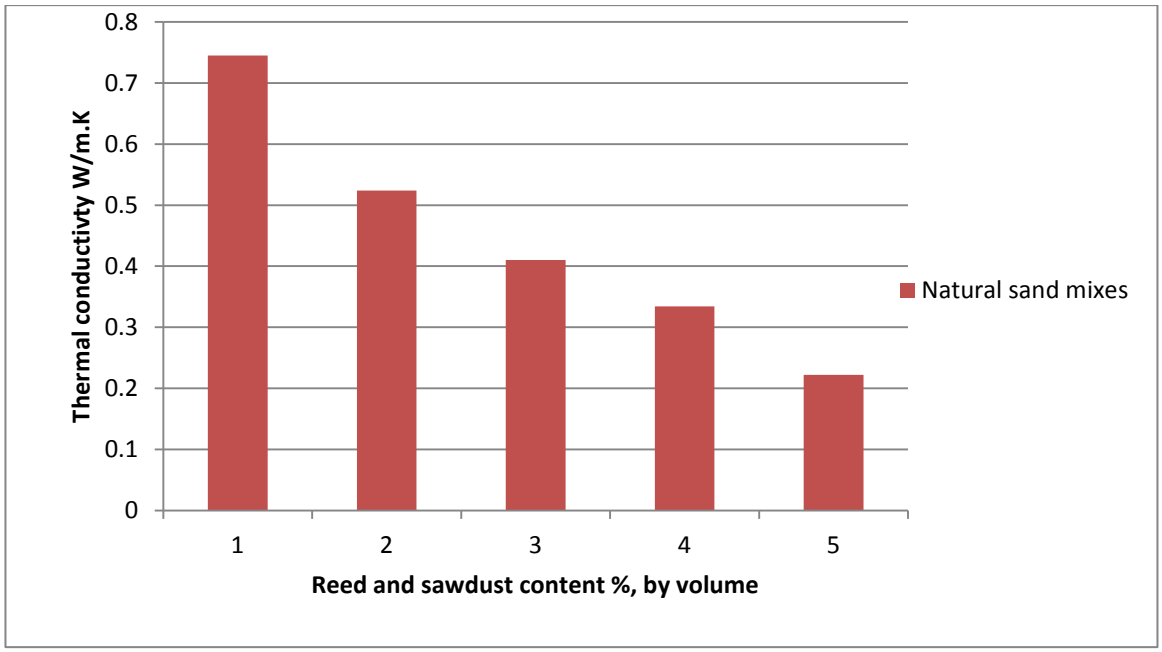


**Figure 9.**Effect of various reed and sawdust content on the thermal conductivity of natural sand mixes.

**Figure 10.** Brick units.

# Predicting Crop Coefficient Values of Cucumber (Cucumis sativus) inside Greenhouse

Ahmed Abied Hamaza
Graduate Student
College of Engineering
University of Baghdad
E-mail:albabele.ahmed@yahoo.com

Asst. Prof. Sabah Anwer Almasraf
Department of Water Resources Engineering
College of Engineering
University of Baghdad
E-mail: Sabah_dawood@yahoo.com

## ABSTRACT

The objective of the study was to predict crop coefficient ($K_c$) values for cucumber inside the greenhouse during the growing season 2014, using watermarks gypsum blocks and atmometer apparatus during the growing stages and to compare the predicted values of the crop coefficient with different methods and approaches. The study was conducted in the greenhouses field within Al-Mahawil Township, 70 km south of Baghdad, Iraq. The watermarks soil water sensors and atmometer apparatus were used to measure crop evapotranspiration and reference evapotranspiration on daily basis, respectively. The comparison and the statistical analysis between the calculated $K_c$ in this study and values obtained from greenhouse gave a good agreement. The root mean square difference (RMSD) and relative error (RE) gave an average value of: 0.065 mm/day and 9%, respectively. While, the comparison between the predicted $K_c$ values and approaches developed by FAO (modified) and Ministry of Water Resources of Iraq gave less agreement. The values of RMSD and RE gave an average value of: 0.188 mm/day, 27%, and 0.17 mm/day and 26.8%, respectively. The method used by FAO and Ministry of Water Resources of Iraq was conducted on basis of using modified empirical equation suggested by FAO-56.

**Key words:** crop coefficient, evapotranspiration, water sensor, atmometer.

# أستنباط معامل الخيار(Cucumissativus) داخل البيوت الخضراء

**أحمد عبيد حمزة**
طالب ماجستير / قسم هندسة الموارد المائية
كلية الهندسة- جامعة بغداد

**أ.م صباح أنور داود المصرف**
قسم هندسة الموارد المائية
كلية الهندسة/ جامعة بغداد

## الخلاصة

يهدف هذا البحث الى أستنباط معامل نبات الخيار داخل البيوت الخضراءللموسم الزراعي 2014 بأستخدام متحسسات الجبس وجهاز الاتموميتر خلال مراحل نمو النبات, ومقارنة القيم المستنبطة لمعامل نبات الخيار مع القيم المستنبطة من طرق واساليب مختلفة. تمت الدراسة داخل بيوت خضراء مغطاة في حقل ضمن منطقة المحاويل التي تبعد 70 كم جنوب بغداد- العراق. أستخدمت متحسسات الرطوبة الجبسية وجهاز الاتموميتر لقياس الاستهلاك المائي للنبات والاستهلاك المائي الكامن بشكل يومي على التوالي. أظهرت نتائج المقارنة والتحليل الاحصائي بين قيم معامل النبات المستنبطة في هذه الدراسة مع قيم لطريقة أجريت داخل البيوت الخضراء بتوافق جيد, اذ كان معدل الجذر ألتربيعي للفرق والخطأ النسبي :0.065 ملم/يوم و 9% على التوالي. بينما كانت نتائج المقارنة بين القيم المستنبطة من الدراسة الحالية والقيم المعدلة من منظمة الفاو و وزارة الموارد

المائية في العراق اقل توافقا. كان معدل الجذر التربيعي للفرق والخطأ النسبي :0.188 ملم/يوم و 27% و 0.173 ملم/يوم و 26.8% على التوالي, اذ تم أحتساب قيم معامل النبات اعتمادا على المعادلة الوضعية المقترحة من قبل منظمة الفاو (التقرير 56).

**الكلمات الرئيسية**: معامل النبات, الاستهلاك المائي, متحسسات الرطوبة, الاتموميتر

## 1. INTRODUCTION

The plastic covering utilized on greenhouses significantly changes the radiation balance relative to the external environment, because of the attenuation of the incident solar radiation, resulting in a reduction of the internal radiation balance and, consequently, affecting evapotranspiration ,**Sentelhas, 2001**. The difference between internal and external evapotranspiration varies according to meteorological conditions, usually evapotranspiration inside greenhouses around 60 to 80% of that verified outside , **Montero, et al., 1985 ,Rosenberg, et al., 1985 and Hashem, et al., 2011** studied the effect of polyethylene sheet white, and black net of greenhouse covers, and 80%, 100%, and 120% of potential evapotranspiration (as an irrigation levels), estimated according to class A pan equation on plant growth and crop yield of cucumber. The results showed that white net greenhouse cover optimized growth and yield of cucumber plant. Estimating crop evapotranspiration for specific crops is important for irrigation scheduling and agricultural water management ,**Irmak and Martin, 2005** and **Fernandes, et al., 2003** estimated and compared $ET_o$ by different methods inside and outside a greenhouse. They used A class pan (CAPi), a reduced pan (RPi), and an atmometer (Ai) installed inside a greenhouse, and another class A pan (CAPo) installed outside. $ET_o$ estimates, obtained by CAPi, RPi, and Ai were 56%, 69% and 63% of those estimated by CAPo, respectively. A simple linear regression showed the level of significance coefficients R = 0.94 for the RPi and the CAPi, R = 0.91 for the Ai and the CAPi, R = 0.70 for the CAPi and the CAPo, R = 0.66 for the RPi and the CAPo, and R = 0.62 for the Ai and the CAPo. It is possible to use reduced pans or atmometers to estimate the $ET_o$ inside the greenhouse. **Mujahed, 2007**, in his work measured evapotranspiration and weather parameters for cucumber grown in a greenhouse during the growing season. A model was developed that correlated simple weather data to evapotranspiration for cucumber under greenhouse conditions. **Abedi- Koupai, et al., 2009**, used climate data for calculating evapotranspiration inside greenhouse from indirect methods. They used artificial neural networks (ANNs) to estimate daily grass reference evapotranspiration ($ET_o$) and compared the performance of ANNs with the conventional methods: Penman, Penman-Monteith, Stanghellini and Fynn. Meteorological variables including air temperature, solar radiation, wind speed, and relative humidity were considered daily. The results showed that ANNs, Penman, and P-M models were overestimated ETo, while the Fynn and Stanghellini models underestimated $ET_o$. Crop water requirements, also called crop evapotranspiration, are usually represented as $ET_c$. As $ET_c$ varies with plant development stage and weather conditions, both the amount and timing of irrigation are important. The water

balance method of irrigation scheduling is one method of estimating the required amount and timing of irrigation for crops **, British Colombia, 2001** and **Allen, et al., 1998** suggested an empirical equation to adjust the crop coefficient values when air velocity is about 2 m/s and the minimum relative humidity is approximately 45%. Crop coefficient values recommended by FAO for different crops and tress are values under typical irrigation management and soil wetting conditions. Crop evapotranspiration can be observed and measured by monitoring soil moisture content, when no rainfall and irrigation were added to the soil. Soil water status can be measured directly with sensors such as watermark sensors. **Balnco** and **Folegatti, 2003**, predicted crop coefficient values for the cucumber inside a greenhouse during winter-spring season in Brazil. Crop was irrigated with water of three different levels of salinity. The average value of crop coefficient for initial, development, mid-season and late of season was: 0.16, 0.89, 1.4 and 0.6, respectively. **Fathalian** and **Emamzadei, 2013** calculated the evapotranspiration and crop coefficient of greenhouse cucumber by installing two microlysimeters for growing cucumber and grass. Daily evapotranspiration rate of both plants was measured by weighing method. Also, by using meteorological data, recorded inside the greenhouse, $ET_o$ was calculated by using Penman-Monteith equation. They concluded that $K_c$ for cucumber in a greenhouse was 0.14 for initial stage of growth, 0.78 in the development stage, 1.37 in the middle stage, and 0.86 in the last stage. **Fakhri, 2014** predicted crop coefficient values for eggplant and maize in open field based on daily basis using watermark sensors, measuring crop evapotranspiration, and atmometers measuring reference evapotranspiration. The objective of this study was to predict crop coefficient values for the cucumber crop inside the greenhouses through the growing stages. Comparison was conducted between the predicted crop coefficient values with different approaches and models.

## 2. MATERIALS AND METHODS

### 2.1 Location of the Greenhouses Field Study

The research field for this study is located within AL-Mahawil Township, 70 km south of Baghdad. The greenhouse field is located at latitude: 32° 76' N, longitude: 44° 59' E, altitude: 27 m. **Fig. 1** shows a Google map for the greenhouses field site location. The main source of water is from a water pond charged continuously from a local stream from Al- Mahawil River. Three soil samples were taken from two locations in the greenhouse field of cucumber and at layers 0-20 cm, 20- 40 cm and 40- 60 cm. Analyses of soil samples were conducted in the laboratories of the College of Agriculture-University of Babylon. The goal of the analysis was to identify the physical characteristics of the soil in order to determine soil texture and physical properties of the soil which included bulk density, soil texture, field capacity, and permanent wilting point. The soil texture type of the two greenhouse fields is classified as loam soil.

### 2.2 Devices and Equipment

The followings are specifications and description of devices and equipment used in the field work.

#### 2.2.1 Atmometer apparatus

An atmometer, the brand name (ETgage), has gained increasing popularity. It is one of the alternative tools that can be used to measure the amount of water evaporated to the atmosphere from a wet, porous ceramic surface. The atmometer consists of a canvas-covered ceramic evaporation plate mounted on a distilled water reservoir. The reservoir capacity is 300 mm as water depth. The fabric covering creates a diffusion barrier (resistance) that controls the evaporation rate and ranging from 112–294 s/m similar to that found in healthy leaves in a well-watered plant community. The green canvas cover that surrounds the ceramic plate mimics the crop albedo so that solar radiation absorption by the ETgage will be similar to the solar radiation received at the crop canopy. In theory, the diffusion barrier of the canvas cover and the stomata resistance of healthy, actively growing, green, and well- watered grass vegetation is assumed to be similar. In the ETgage system, water is provided to the ceramic cup by suction through a glass or plastic supply tube and check valve consisting of a diaphragm mounted in a section of silicon tubing attached at the lower end of the glass supply tube. The ETgage reservoir is ventilated by two holes (1.5 mm diameter) drilled at the upper end of the clear polyvinyl chloride pipe. Distilled water is always used in the ETgage reservoir to prevent accumulation of solutes in and on the plate that can reduce the porosity of the plate and affects the evaporation rate. A sight glass on the water reservoir allows the water level in the reservoir to be read manually. The ETgage is easy to install and requires little maintenance which is typically mounted on a wooden post and to be above the top level of the crop as shown in **Fig. 2**. It should not be installed near tall trees, buildings, or tall crops that may prevent full exposure of the gage to prevailing winds and other environmental factors affecting evapotranspiration.

#### 2.2.2 Watermarks soil water sensor

Watermark sensors are widely available and have a number of favorable technical characteristics for on farm use, due to its low cost, ease of installation, and durability. These sensors typically require site calibration of the threshold soil-moisture content to which the soil will be allowed to dry before irrigation will be permitted. The patented watermark sensor is a solid-state electrical resistance sensing device that is used to measure soil water tension. This type of sensor consists of two electrodes embedded in a reference matrix material, which is confined within a corrosion-proof and highly permeable case (unit range from (0-wet- to 200 cb-dry). The matrix material includes gypsum to buffer against the effects of salts and fertilizer, but these sensors do not dissolve like gypsum block sensors. Soil moisture is constantly absorbed or released from the sensor as the surrounding soil moisture conditions change. As the soil moisture changes, the sensor moisture reacts as reflected by the change in electrical resistance between the electrodes. Granular matrix sensors operate on the same electrical resistance principle as gypsum

blocks. As the moisture level increases, conductivity increases, and the sensor is calibrated to output the moisture level in terms of soil tension, **McCready, et al., 2009**. Total of three watermark sensors were used in the field area within the root zone of cucumber crop at depths equal 15, 30 and 40 cm.

**2.3 Description of the Greenhouse**

In this study two greenhouses were used each was 56 m long, 9 m wide and 3 m high (or an area of about 500 $m^2$). They were covered by 100 μm transparent polyethylene film treated against ultraviolet radiation. The greenhouse was without heating nor air ventilation. The greenhouse was classified as low technology greenhouse. Trickle irrigation system has been used in the two greenhouses, which was a perfect method for water application and simple in scheduling the irrigation water at low cost. **Fig.3** shows the layout of the greenhouse. The system consists of five double irrigation lines of 55 m long (each). Each line consists of two drip tapes, the distance between two drip tapes 0.3 m (T-Tape). Trickle drip tape contains 500 dripper points along its total length. The dripper points were spaced 0.1 m apart. The discharge of each dripper point was 17 $cm^3$/min. Cucumber crops (*Cucumis sativus*) were planted at a spacing of 0.3-0.4 m and the planted points form rows running parallel to the lines. The irrigation date and duration were scheduled by agricultural advisor responsible for managing the greenhouses. In other words, the greenhouse conditions were uncontrolled in the study. However, in each irrigation process, date, flow rate from the dipper, and time of the irrigation were recorded when possible.

## 3. CALCULATION AND PROCEDURES

Modified or predicted crop coefficient values for the cucumber crop were calculated from water consumption by dividing daily measured crop evapotranspiration ($ET_c$) by reference evapotranspiration ($ET_o$) which is measured from the atmometer as follows **, Allen, et al., 1998.**

$$K_c = \frac{ET_c}{ET_o} \quad (1)$$

where:

$K_c$ = estimated or predicated crop coefficient,
$ET_c$ = crop evapotranspiration (mm/day), and
$ET_o$ = reference evapotranspiration (mm/day).

The crop evapotranspiration ($ET_c$) was calculated from the following water balance equation:

$$IR - DP - R - ET_c = \Delta\theta \quad (2)$$

where:

$\Delta\theta$ = change in soil water content in two consecutive days (mm),
IR = irrigation water depth (mm),
DP = deep percolation (mm), and
R = surface runoff (mm).

The water content in the effective root zone was estimated by using watermarks sensors readings throughout the growing season of the cucumber. The water balance equation was applied when there is no irrigation, so Eq. (2) becomes:

$$ET_c = \Delta\theta \quad (3)$$

Daily values of reference evapotranspiration ($ET_o$) were calculated on the basis of atmometer readings which equal to the difference between two consecutive readings (mm/day). The crop coefficient value for the cucumber was predicted for each growing stage which are: initial, development, mid of season, and harvest time or end of season, starting from the date of planting till the harvest time. The growing stages (initial, development, mid of season, and late of season) of the cucumber were based on the observation of the crops development in the greenhouses which was similar to the study conducted by Ministry of Water Resources **, Ministry of Water Resources-Iraq, 2014**. The time period of each growing stage was identified depending on an estimation of the percentage of the period length of the cucumber crop stage starting from the planting date till the harvest date, as shown in **Table 1**.

### 3.1 Statistical Analysis Methods

Comparison between predicted $K_c$, local, and international values were conducted on daily basis, monthly, and growing stages. The following parameters were used:

$$RMSD = \sqrt{\frac{1}{n}\sum_{i=1}^{n}(yi - xi)^2} \quad (4)$$

$$RE = \frac{RMSD}{xav} * 100 \quad (5)$$

where:

RMSD = root mean square difference (with its optimal value equal to zero),
n = number of observations,
yi = predicted crop coefficient,
xi = local or FAO crop coefficient,
xav = average value of crop coefficient (from local or FAO values), and
RE = relative error (%).

## 4. RESULTS AND DISCUSSIONS

Daily and average values of the predicted crop coefficients ($K_c$) for the cucumber crop throughout the growing stages were plotted as shown in **Fig. 4**. The average value of $K_c$ in the initial stage was about 0.16. The development stage started with an average value of 0.87 and

reached a value of 1.23, which was represented the mid-season stage. At the end of the mid-season and beginning of late season, the crop coefficient value decreased to an average value of 0.87 at the end of the late of season. The crop coefficient values suggested by FAO **,Allen, et al., 1998** for cucumber crop were for open field conditions and expected for sub-humid climatic conditions. Additionally, $K_c$ suggested by FAO were for typical irrigation management and soil wetting conditions and where the wind velocity equal to 2 m/s and minimum relative humidity equal to 45%. For $K_c$ values more or less than the assumed values for wind speed and relative humidity. FAO suggested an empirical formula to be used to correct the $K_c$ values for initial, mid, and late of season and as follows:

$$FAO_{modified} = FAO_{value} + \left(0.04(U_2 - 2) - 0.004\,(RH_{min} - 45)\right) * \left(\frac{H}{3}\right)^{0.3} \quad (6)$$

where:
$RH_{min}$= min. relative humidity (%),
$U_2$ = wind speed at 2 m height (m/s), and
H = crop's height (m).

Daily wind speed and minimum relative humidity values were measured inside the greenhouse. The predicted crop coefficient values of the cucumber in the case study were compared with different approaches and models inside the greenhouse. **Table 2** shows the $K_c$ values predicted in the case study, **FAO** (modified) using Eq. 6, **Fathalian** and **Emamzadei, 2013**, and Ministry of Water Resources **, Ministry of Water Resources Iraq, 2014**. The summary of the statistical analyses for the comparison between the predicted $K_c$ and different approaches and models for cucumber inside greenhouses are shown in **Tables 3**, **4**, **and 5.** The values of RMSD and RE for the comparison between predicted and different approaches for the $K_c$ values showed that the approach developed by **Fathalian** and **Emamzadei, 2013** gave an agreement as a first approach with the predicted $K_c$ in the case study for all growing stages. While, the $K_c$ values developed by Ministry of Water Resources-Iraq **,Ministry of Water Resources, 2014,** agreed with the predicted $K_c$ except for the initial stage. Statistical analyses for RMSD and RE showed that $K_c$ values recommended by FAO **, Allen, et al, 1998** rank the third. Moreover, the statistical analyses showed that the adjusted values of $K_c$ by FAO and even by the Ministry of Water Resources – Iraq were unsatisfactory for the following reasons:

- Low technology of the greenhouses where there were no ventilation, air exchange, and uncontrolled temperature, effect the adjustment of $K_c$ values.
- Water management and method of applying water.
- Height and density of crop.
- Number and surface area of the crop's leaf.
- Starting time of the growing season.
- Crop's height and if the crop was vertically supported or grows on the ground surface.

**Fig. 5** shows a comparison among the crop coefficient values for the cucumber for different models inside the greenhouses for the growing stages.

## 5. CONCLUSIONS

The calculated $K_c$ values and the values estimated by **Fathalian** and **Emamzadei, 2013** agreed well. The statistical analyses using RMSD and RE gave an average value of: 0.065, 9%, respectively. While, the comparison between the predicted $K_c$ values and approaches developed by FAO (modified) and Ministry of Water Resources of Iraq **,Ministry of Water Resources – Iraq, 2014,** gave an fair agreement. Values of RMSD and RE gave an average value of: 0.188, 27%, and 0.17 and 26.8%, respectively. Where the methods used by FAO and Ministry of Water Resources of Iraq was conducted on basis of using Eq. (6), **Allen, et al., 1998**, and measuring weather parameters inside the greenhouses. Accurate values of the crop coefficient could be obtained from the ratio of crop evapotranspiration and reference evapotranspiration. The trend and variation of the crop coefficient for cucumber inside and outside greenhouses is affected by many factors due to followings: type of technology used inside greenhouse, type of the greenhouse's shaded cover, type of crop (height, density, leaf area), and irrigation management.

## REFERENCES


- Abedi-Koupai, J., Amiri, M. J., and Eslamian, S. S., 2009, *Comparison of Artificial Neural Network and Physically Based Models for Estimating of Reference Evapotranspiration in Greenhouse,* Australian Journal of Basic and Applied Sience, Vol.3, No. 3, PP.2528-2535.
- Allen, R.G., L.S., Pereira, D. R., and Smith, M., 1998, *Crop Evapotranspiration-Guidelines for Computing Crop Water Requirements*, FAO Irrigation and Drainage Paper 56.Food and Agriculture Organization. Rome, Italy.
- Balnco, F. F., and Folegatti, M. V., 2003, *Evapotranspiration and Crop Coefficient of Cucumber in Greenhouse*, RevistaBrasileira de Engenharia Agricola, Vol. 2, No.2.
- British Colombia, 2001, *Crop Coefficients for Use in Irrigation Scheduling*, Factsheet, Order no. 577.100-S.
- Fakhri, E. H., 2014, *Evaluation of Atmometer (Evapotranspiration Gage) Under Iraqi Conditions"*, M.Sc. Thesis, Department of Water Resources Engineering, College of Engineering, University of Baghdad.160 P.
- Fathalian, F. and Emamzadei, M. R., 2013, *Determination of Evapotranspiration and Crop Coefficient of Cucumber by Using Microlysimeter in Greenhouse Conditions,* Journal of Science at Technology Greenhouse Culture, Vol. 3, No.12, Iran.

- Fernandes, C., Eduardo, J., and Comos de Araujo, J. A., 2003, *Reference Evapotranspiration Estimation inside Greenhouses*, Scientia Agricola, Vo. 60, No. 3, PP.591-594.
- Hashem, A. F., Medany, M. A., Abd El-Moniem, and E.M., Abdullah, M. M. F., 2011, *Influence of Greenhouse Cover on Potential Evapotranspiration and Cucumber Water Requirements*, Annals of Agricultural Science 56, PP. 49-55.
- Irmak, S. and Martin, J. D., 2005, *Using Modified Atmometers (ETgage®) for Irrigation Management*, Irrigation Engineering, Irrigation Operations and Management, University of Nebraska-Lincoln. U.S.A.
- McCready, M. S., Dukes, M. D., and Miller, G. L., 2009, *Water Conservation Potential of Intelligent Irrigation Controllers on St. Augustine Grass*, Agric. Water Manage, Vol. 96, PP. 1623-1632.
- Montero, J. I., Castilla, N. G. de Rave E., and Bretones, F., 1985, *Climate Under Plastic in the Almeria*, Acta Horiculturae, No.170, PP.227-234.
- Mujahed, A. F. 2007, *Estimation of Crop Water Requirement for Cucumber Grown in Green House*, M.Sc. thesis , Hebron University, College of Graduate Studies and Academic Research.
- Rosenberg, N. J., Mckenney, M. S., and Martin, P., 1985, *Evapotranspiration in a Greenhouse-Warmed World, a Review and a Simulation*, Agricultural and Forest Metrology, Vol. 47, PP.303-320.
- Sentelhas P. C., 2001, *A Grometorelogia Aplica du a Irrigacao in Miranda*, J. H. Pires, R. C. de M. Irrigacao, Piracicaba, Funep, PP.63-120.


**NOMENCLATURE**

DP = deep percolation (mm).
$ET_c$= crop evapotranspiration, mm/day.
$ET_o$= reference evapotranspiration, mm/day.
H = crop' height (m).
IR = irrigation water depth (mm).
Kc = crop coefficient.
n = number of observations.
R = surface runoff (mm).
RE = relative error (%).
$RH_{min}$= min. relative humidity (%).
RMSD = root mean square difference.
$U_2$ = wind speed at 2 m height (m/s).
xav = average value of crop coefficient.
xi = value of crop coefficient.
yi = predicted crop coefficient.
$\Delta\theta$ = change in soil water content in two consecutive days (mm).

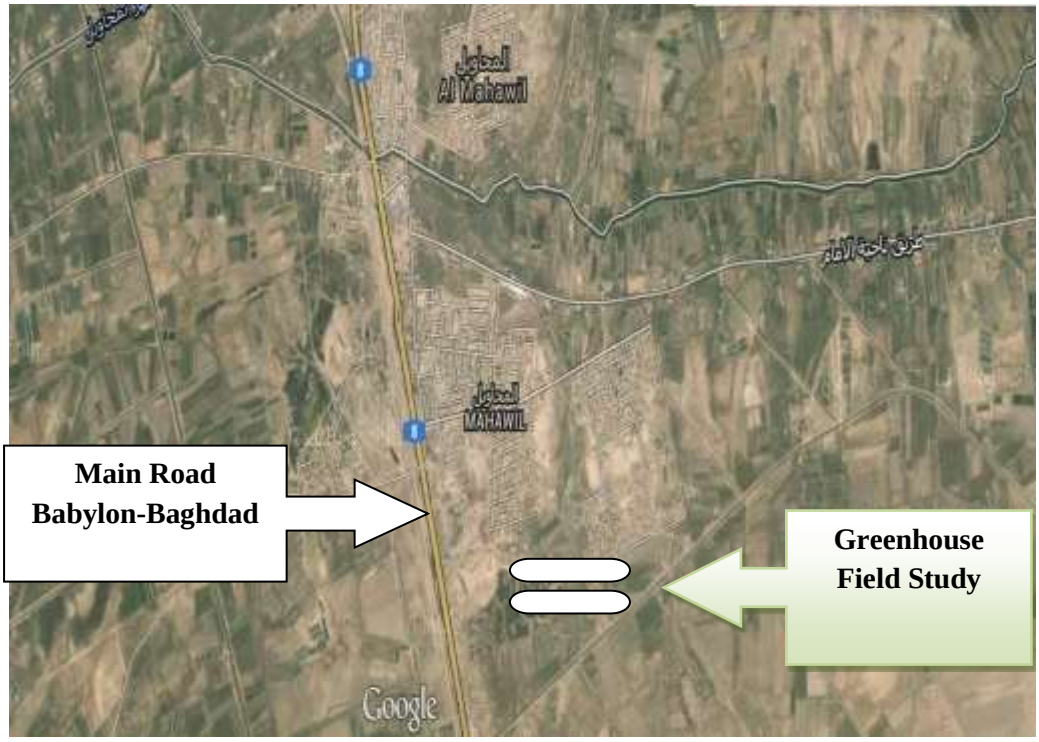


**Figure 1.** Google map for the research site work.

**Figure 2.** Location of the atmometer apparatus in the cucumber's greenhouse.

**Figure 3.** Layout of the greenhouse.

**Table1.** Estimation of the period and percentage of the growing stage of cucumber.

| Stage and period | Initial | Development | Mid-season | Late season |
|---|---|---|---|---|
| Growing stage (%) | 19 | 27 | 38 | 16 |
| Stage period (day) | 21 | 31 | 43 | 18 |

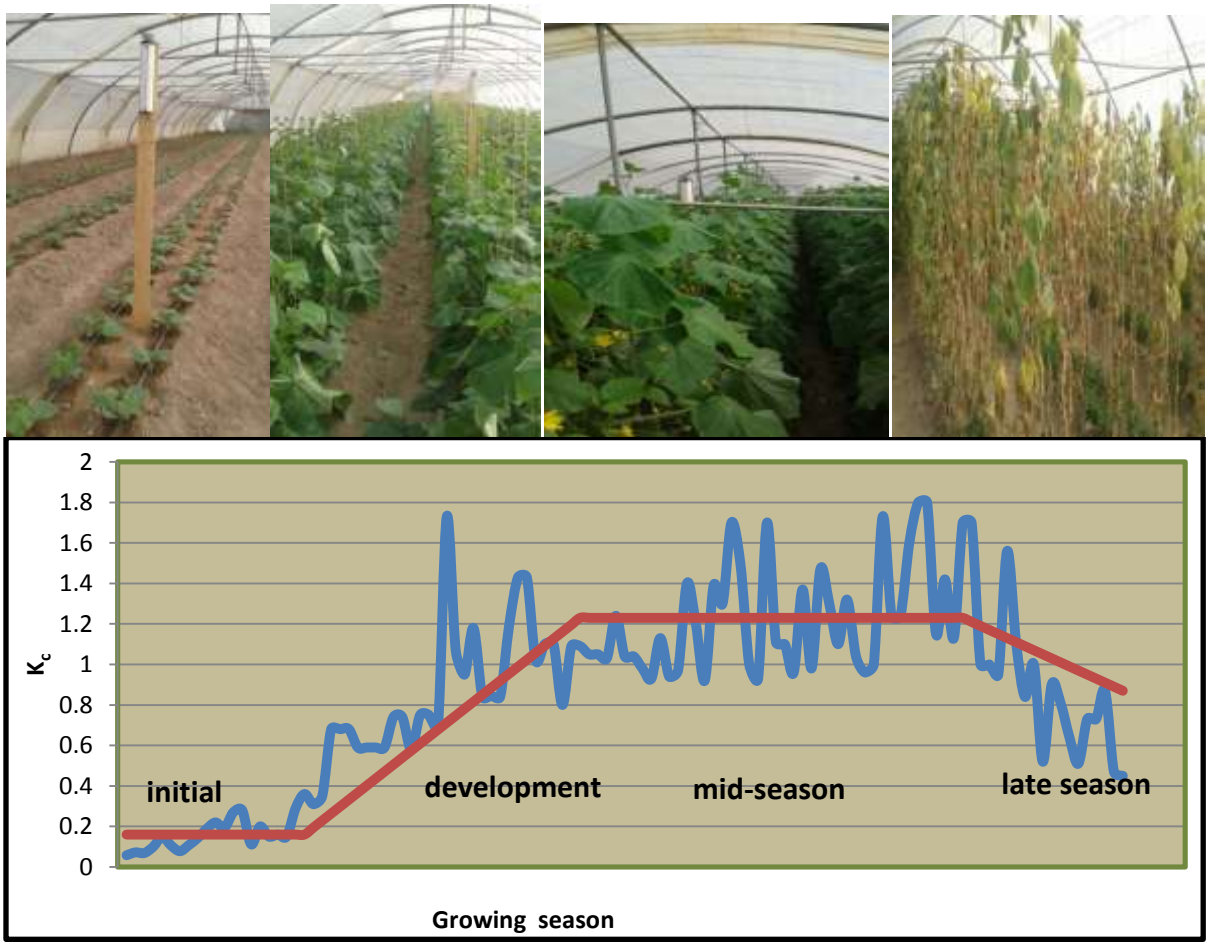


**Figure 4.** Daily and average values of the cucumber's crop coefficient throughout the growing season, 2014.

**Table2.**Crop coefficient values of the cucumber inside the greenhouse as predicted in the case study, Fathalian and Emmazadei, Ministry of water Resources and FAO (modified).

| Approach and model | Growing season -$K_C$ | | | |
|---|---|---|---|---|
| | Initial | Development | Mid-season | Late-season |
| Case study | 0.16 | 0.87 | 1.23 | 0.87 |
| Fathalian,and Emamzadei (2013) | 0.14 | 0.78 | 1.37 | 0.86 |
| Ministry of Water Resources- Iraq ,2014 | 0.45 | 0.75 | 0.98 | 0.85 |
| FAO (modified) | 0.15 | 0.6 | 0.97 | 0.66 |

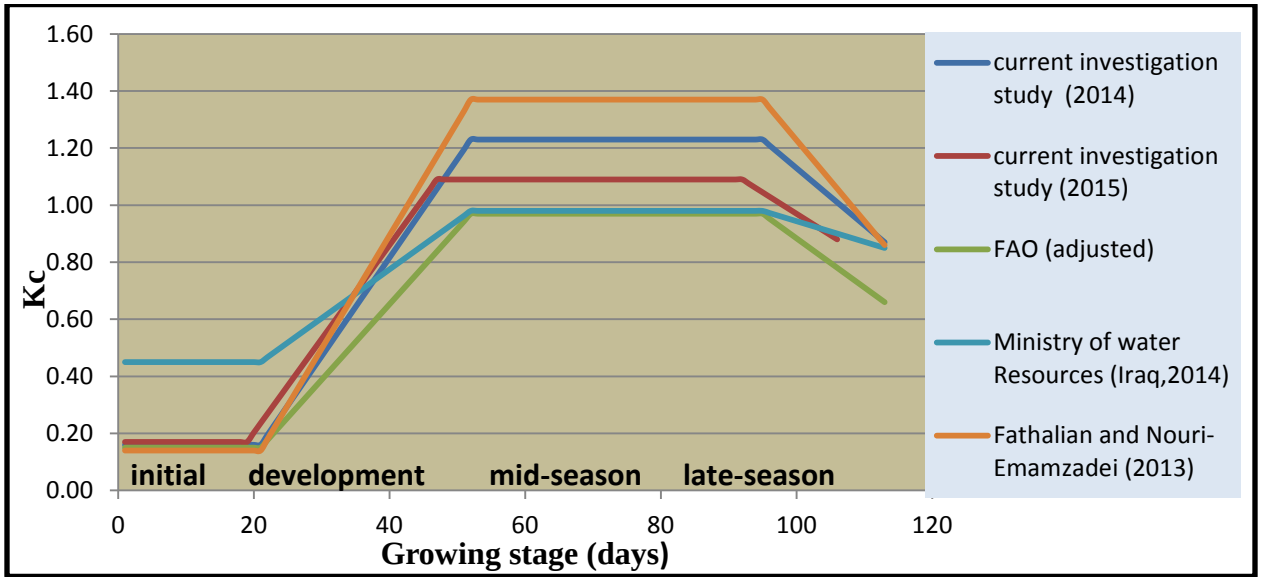


**Figure 5.** Comparison of the crop coefficient values for the cucumber inside greenhouse.

**Table 3.** Root mean square difference and relative error between predicted $K_c$ and the FAO (modified) values.

| Growing stage | RMSD | RE (%) |
|---|---|---|
| Initial | 0.01 | 6 |
| Development | 0.27 | 45 |
| Mid of season | 0.26 | 26 |
| Late of season | 0.21 | 31 |
| Average | 0.188 | 27 |

**Table 4.** Root mean square difference and relative error between predicting $K_c$ and the values from **Ministry of Water Resources- Iraq, 2014**.

| Growing stage | RMSD | RE (%) |
|---|---|---|
| Initial | 0.29 | 64 |
| Development | 0.12 | 16 |
| Mid of season | 0.25 | 25 |
| Late of season | 0.02 | 2 |
| Average | 0.17 | 26.8 |

**Table 5**. Root mean square difference and relative error between predicting $K_c$ and from **Fathalian** and **Emamzadei, 2013**.

| Growing stage | RMSD | RE (%) |
|---|---|---|
| Initial | 0.02 | 14 |
| Development | 0.09 | 11 |
| Mid of season | 0.14 | 10 |
| Late of season | 0.01 | 1 |
| Average | 0.065 | 9 |

# Modeling and Optimization the Influence of $CO_2$-MAG Welding Parameters on the Weld Joint Shape Factors

**Dr. Samir Ali Amin Alrabii**
Assistant Professor
Department of Mechanical Engineering
University of Technology
(alrabiee2002@yahoo.com)

**TarekM. A. Al**
Assistant Lecturer
Department of Applied Sciences
University of Technology
(tarekza@yahoo.com)

## ABSTRACT

This paper represents an experimentalattempt to predict the influence of CO2-MAG welding variables on the shape factors of the weld joint geometry. Theinput variables were welding arc voltage, wire feeding speed and gas flow rate to investigate their effects on the shape factorsof the weld joint geometry in terms of weld joint dimensions (bead width, reinforcement height, and penetration). Design of experiment with response surface methodology technique was employed to buildmathematical models for shape factors in terms of the input welding variables. Thepredicted models were found quadratic type and statistically checked by ANOVA analysis for adequacy purpose. Also, numerical and graphical optimizations were carried out to determine the optimum values for all responses and input variables. The optimum values of the voltage, wire feeding speed, gas flow rate, WPSF, and WRFF are (20 Volt), (153 cm/min), (10 L/min), (5.222), and (3.970), respectively. And, a good agreement was found between the experimental and predicted results. The weld joint efficiency was found (73%) at the optimum conditions.

**Keywords**:bead dimensions, WPSF, WRFF, CO2-MAG welding, joint efficiency.

## نمذجة وامثلية تأثير متغيرات لحام القوس المعدني بغاز $CO_2$ على عوامل شكل وصلة اللحام

**د. سمير علي أمين الربيعي**
أستاذ مساعد
قسم الهندسة الميكانيكية
الجامعة التكنولوجية

**طارق محمد علي علي**
مدرس مساعد
قسم العلوم التطبيقية
الجامعة التكنولوجية

**الخلاصة**

يمثل هذا البحث محاولة عملية لتنبأ تأثير متغيرات لحام القوس المعدني بغاز ($CO_2$) على عوامل الشكل الهندسي لوصلة اللحام. المتغيرات الداخلة هي طاقة القوس وسرعة تغذية سلك اللحام ومعدل جريان الغاز لبحث تأثيراتها على عوامل الشكل الهندسي لوصلة اللحامبدلالة أبعاد وصلة اللحام (عرض درزة اللحام وارتفاع التقوية والنفاذية) . تم تطبيق تقنية تصميم التجارب مع طريقة الاستجابة السطحية لبناء نماذج رياضية لعوامل الشكل بدلالة متغيرات اللحام الداخلة. وجدت نماذج التنبوء بالنوع التربيعي ودققت أحصائيا" بتحليل التباين (ANOVA) لغرض الملائمة. أجريت أيضا" الامثلية العددية والبيانية لآيجاد القيم المثلى لجميع الاستجابات والمتغيرات الداخلة. والقييم المثلى هي (20) فولت ، (153) سم / دقيقة سرعة تغذية السلك ، (10) لتر / دقيقة معدل جريان الغاز ، (5.222) معامل شكل نفاذية اللحام و (3.970) معامل شكل تقوية اللحام. ووجد توافق جيد بين النتائج العملية والنظرية. ووجدت كفاءة وصلة اللحام (73%) عند الظروف المثلى..

## 1. INTRODUCTION

MAG stands for metal-active-gas arc welding. This is a variation of MIG welding, in which identical equipment is used, but the inert gas is replaced by carbon dioxide, which is chemically active, **Patel, and Patel, 2014**.CO2-MAG is a process in which the source of heat is an arc format between the consumable metal electrode and the work piece, and the arc and the molten puddle are protected from contamination by the atmosphere (i.e., oxygen and nitrogen) with an externally supplied gaseous shield of carbon dioxide or argon-carbon dioxide mixture. All the major commercial metals can be welded by this process, including carbon steels, low alloy and high alloy steels, stainless, aluminum, and copper titanium, zirconium and nickel alloys, **Jadeja, and Patel, 2013**. With CO2 shielding, the electrode tip is not heated directly by the arc plasma but by the arc heat conducted through the molten drop. The molten drop grows in size andfinally detaches by short circuiting or gravity, **Singla, et al., 2010**. During the investigation by **Boiko and Avisans, 2013**, it was revealed that different shielding gas gives different influence on the welding process, welding joint quality and also on the welding costs. CO2 shielding provides deeper penetration, **Reddy, 2012**.

In the automated applications, a precise means of selection of the process variables and control of weld bead shape has become essential, because the mechanical strength of weldis influenced not only by the composition of the metal, but also by the weld bead shape, **Hould, 1989**.Also, the weld pool geometry plays an important role in determining the mechanical and corrosion properties of the weld, **Dasgupta, and Mukherjee, 2013**. Also, optimization of the process variables to control and obtain the required shape and quality of weld joint is possible with these expressions. The quality of the weld joints depends on the bead geometry and shape factors. The weld joint is specified by the bead width, height of reinforcement, depth of penetration, weld reinforcement form factor (WRFF) and weld penetration shape factor (WPSF). **Figure 1** shows the transverse cross section of a weld bead geometry. WPSF and WRFF are also called as coefficients of internal shape and external shape, respectively. The ratio of bead width to penetration and bead width to reinforcement are termed as Weld Penetration Shape Factor and Weld Reinforcement Form Factor, respectively.

Nowadays, DOE has been more widely used in quality control, manufacturing, and system engineering disciplines for design or development of a new product and redesign of an existing product **DeVor et al., 1992**. Due to the highly competitive global industry, companies need to understand the impact of both operational and environmental variables and their interactions on system or product performance. Therefore, mathematical model–based optimization employing DOE is a powerful design technique for use by system analysts, engineers, and designers. Compared to many methods, DOE is a more efficient method among optimization models in terms of number of required experiments. Its applications and computations are also more time efficient **Antony, 2003**. Normally the use of DOE technique is combined with RSM and ANOVA statistical tests. In the present work, DOE software version 8 was used. The most popular designs within RSM designs are the central composite design (CCD) and Box-Behnken design. In the present work, the central composite design (CCD) was used in the RSM technique (**Benyounis, and Olabi, 2005**).

Many researchers have been previously carried out by using CO2-MAG welding processes considering mainly the effect of process variables on the structure and mechanical properties. In addition, most studies have attempted to model the directed measured bead width, bead height and bead penetration only, regardless of the important shape relations of the weld bead. But, some important shape relations, such as weld reinforcement form factor (WRFF) and weld penetration shape factor (WPSF) have significant impact on the quality of weld. However, there is few works (**Gunaraj and Murugan, 1999; Kumar, 2011**) have focused on studying the influence of process variables on WPSF and WRSF using the Design of Experiment (DOE) and Response Surface Methodology (RSM) technique for predicting, modeling and optimization purposes for CO2-MAG welding.

Therefore, the aim of this paper is to investigate experimentally the effect of input welding variables of CO2-MAG welding process (arc voltage, wire feeding speed and gas flow rate) on the weld joint shape factors (WPSF and WRFF) obtained by the measurements of bead width, height of reinforcement and depth of penetration through experiments based on the DOE design matrix. The analysis of variance (ANOVA) technique was adopted to check the level and degree of the direct or interactive effect of the input variables on these factors. RSM was applied to derive mathematical models, and the predicted equations were used to represent graphically the effects of process variables on the shape factor responses. No much work so far has been performed which considers the three process variables used in this study using DOE and RSM approach.

## 2. EXPERIMENTAL PROCEDURE

### 2.1 Material Verification

Low carbon steel material type AISI 1010 in form of plate with 5 mm thickness in the hot rolled condition was used in this work to prepare specimens for welding tests. The chemical analysis for this material was carried out, and the results are presented in Table 1. Also, three samples from this material were then prepared for tensile tests according to ASTM-E8 standard. The mechanical properties of this steel were obtained and the resulted data are given in Table 2, showing the average of three readings for three tested samples**.** These tables verify that the used material is in conformity with the standard base metal, **ASM, 1992**.

### 5.2 Specimens Preparation for Welding Tests

Specimens were then prepared from low carbon steel material type AISI 1010 with dimensions of 50 mm× 25 mm×5 mm to be welded in a closed butt weld joint design by CO2-MAG process. These specimens were then cleaned by a wire brush to remove the oxide layers and any surface defects.

### 2.3 Welding Variables

The effective selected input factors of CO2- MAG welding in this work were welding speed, arc voltage and wire feeding speed in two levels, as shown in Table 3. These parameters were used based on the ability of welding machine and experimental skill of the welder operator.

### 2.4 Welding Procedure

The machine employed for welding experimentation was 'INVERTER CO2 MAG - BEAM-350' in Korean-Iraqi Vocational Training Center in Baghdad. The welding wire type 'AWS ER70S-6'1.2 mm diameter in form of rod was used for welding specimens. $CO_2$-MAG welding tests were conducted for twenty samples using the welding factors mentioned above and depending on the design matrix established by Design of Experiment software, as given in Table 4.These tests were conducted randomly according the design matrix made by DOE program to prevent any systematic error.

### 2.5 Measurements of Weld Joint Dimensions and Shape Factors Calculations

After welding, transverse sections of the weld joints were cut from the middle portions of specimens. The specimens were prepared by grinding and polishing methods. The properly polished specimens were etched with a 2% Nital solution for about 30 seconds for measurements purpose. For each sectioned specimen, the important dimensions of the weld joints were measured by using a digital caliper. The average measurements of bead width, reinforcement height and depth of penetration were recorded to calculate the average weld penetration shape factor (WPSF) and average weld reinforcement form factor (WRFF) using the following equations, **Bahrami, et al., 2010**:

$$WPSF = \frac{W}{P} \quad (1)$$

Where, W = Width of the bead (mm).
P= Depth of penetration (mm).

$$WRFF = \frac{W}{R} \quad (2)$$

Where, R = Height of reinforcement (mm).

The results of calculations of shape factors as responses together with the input welding variables are listed in Table 4. With the help of these calculated responses, models were developed.

## 3. RESULTS AND DISCUSSION

The response surface methodology was employed using the Design of Expert software 'version 8' to determine the following predicted models for the shape factors of the weld joint geometry in terms of arc voltage, wire feeding speed and gas flow rate:

### 3.1 Mathematical Model of Weld Penetration Shape Factor (WPSF)

For the weld penetration shape factor (WPSF), the analysis of variance (ANOVA) was established by DOE software version 8, as shown in Table 5, illustrating that the input parameters individually (A and B), the interaction of wire feeding speed and gas flow rate (BC) and the quadratic terms of voltage ($A^2$) and wire feeding speed ($B^2$) are all statistically significant and have the greatest influence on the weld penetration shape factor response (WPSF) according to

their P-values (< 0.05). This table also depicts that the gas flow rate (C) has no significant effect on WPSF, since its P-value (>0.05).The lack of fit test indicates a good model, since it is insignificant with P-value greater than 0.05. So, this analysis indicates that this model is significant at 95% confidence. In addition, this model showed a good agreement between the predicted and actual values for weld penetration shape factor WPSF, as shown in **Fig.2**. Therefore, the final predicted equation for the WPSF in terms of the coded input factors is:

$$WPSF = +5.03 + 0.68 * A + 0.20 * B - 0.063 * C + 0.83 * B * C - 0.23 * A^2 - 0.33 * B^2 \quad (3)$$

And, the final equation in terms of actual factors is:

$$WPSF = -86.99497 + 9.74713 * Voltage - 8.34643E\text{-}004 * Wire\ feeding\ speed - 2.51597 * Gas\ flow\ rate + 0.016563 * Wire\ feeding\ speed * Gas\ flow\ rate - 0.22678 * Voltage^2 - 5.22843E\text{-}004 * Wire\ feeding\ speed^2 \quad (4)$$

**Figure 3** shows the interaction effect of wire feeding speed and gas flow rate on WPSF at 20 v voltage. It is evident from this figure that WPSF increases for all values of wire feeding speed, while it decreases with increasing gas flow rate. This is due to fact that WPSF= W/P, where W increases with increase of wire feeding speed, whereas P decreases with increasing gas flow rate. Thus, wire feeding speed has a positive effect on WPSF, while gas flow rate has a negative effect on WPSF.

The statistical properties of this model were diagnosed, and it was found that the residuals that falling on a straight line implying errors are normally distributed, as shown in **Fig.4**. Additionally, the residuals versus predicted actual for WPSF data revealed no obvious pattern or unusual structure, as shown in **Fig.5**.

The perturbation of the predicted WPSF response resulted by varying only one parameter at a time from the center point of the investigated region is shown in **Fig.6**. It can be seen that increasing the voltage and wire feeding speed generally increases the WPSF, since these input parameters increased the fusion effect of the weld joint, which resulted in the increase of bead width. While, the gas flow rate had a very little effect on WPSF.

Due to no statistical problems found, the response surface plot was generated in terms of 2D surface plot as shown in **Figs.7**, depicting WPSF as a function of voltage and wire feeding speed at various gas flow rate10 L/min. This figure indicates that both voltage and wire feeding speed have greater influence on increasing WPSF. This is possibly due to increase of molten material accumulated in the weld joint caused by higher voltage and wire feeding speed. Also, this is more likely ascribed to the increased chemical reaction of $CO_2$ with the accumulated molten material in the weld joint.

**Figures 8** shows the 3D surface plot for WPSF as a function of voltage and wire feeding speed at 10 L/min gas flow rate, showing the similar behavior as mentioned above; higher WPSF occurred at higher values of voltage and wire feeding speed.

### 3.2 Mathematical Model of Weld Reinforcement Form Factor (WRFF)

Similarly, the analysis of variance (ANOVA) for RSM reduced quadratic model was determined for the weld reinforcement form factor (WRFF) given in Table 6. The results in this table show

that the voltage (A), wire feeding speed (B) and their squared terms ($A^2$ and $B^2$ ) are statistically significant, since their P-values were very small (< 0.5).While, the gas flow rate term (C) has no influence on the weld joint, since it is not seen in this analysis (model).Moreover, this table also reveals that the lack of fit is insignificant (P-value > 0.05), indicating that this model is adequate and significant at 95% confidence. So, the final predicted equation for the WRFF in terms of the coded input factors is:

$$WRFF = + 3.90 + 0.12 * A + 0.68 * B - 0.55 * A^2 - 0.29 * B^2 \quad (5)$$

And, the final equation in terms of actual factors:

$$WRFF = - 231.85179 + 21.99545 * Voltage + 0.16738 * Wire\ feeding\ speed - 0.54684 * Voltage^2 - 4.67743E\text{-}004 * Wire\ feeding\ speed^2 \quad (6)$$

The adequacy of this model was checked to examine the predicted model. Two types of model diagnostics, the normal probability plot and the residuals versus the actual values plot, were used for verification, as shown in **Figs. 9 and 10** for WRFF, respectively. It can be observed from these plots that there was no violation of the normality assumption, since the normal probability plot followed a straight line pattern, the residual was normally distributed, and as long as the residuals versus the predicted values show no unusual pattern and no outliers. Also, this model shows a good agreement between the predicted and actual values for WRFF, as depicted in **Fig.11**. The perturbation plot of the predicted responses caused by changing only one factor at a time from the center point of the experimental region is shown in **Fig. 12.** This figure indicates that, individually, the wire feeding speed has greater effect than the voltage on WRFF, since WRFF first increased and then decreased with increasing the voltage. This is more probably because of increasing wire feeding speed resulted in an increase in the bead with, leading to more accumulation of molten material due to more thermal effect and less chemical affinity of the $CO_2$gas with the weld joint material. Also, the decrease of WRFF at higher values of voltage is more likely due to the increase of reinforcement height that resulted from less bead penetration depth.

Because of no statistical problem with the model, **Fig. 13**shows the 2D contour plot for WRFF as a function of voltage and wire feeding speed at gas flow rate of 10 L/min. This figure exhibits that WRFF increases with increasing both voltage and wire feeding speed up to (20 volt) due to their combined effect by increasing the bead width. Whereas, **Figs. 14** depicts the 3D surface plot for the WRFF at gas flow rate 10 L/min. It can be noted from this figure that increasing both voltage and wire feeding speed increases the WRFF due to the increase of quantity of the molten material that resulted by the increase of bead width and thermal effect.

### 3.3 NUMERICAL OPTIMIZATION

The numerical optimization is provided by the Design of Experiment software to find out the optimum combinations of parameters in order to fulfill the requirements as desired. Therefore, this software was used for optimizing WPSF and WRFF; based on the data from the predicted models as a function of three factors: arc voltage, wire feeding speed and gas flow rate.

Table 7 shows constrains of each variable for numerical optimization of the WPSF and WRFF. According to this table, one possible run fulfilled the specified constrains to obtain the optimum

values for WPSF and WRFF and desirability, as listed in Table 8. It can be noted that this run gave a desirability of 0.849 with the optimum values of the voltage (20 volt), wire feeding speed (153 cm/min), and gas flow rate (10 L/min). **Figures 15-17** manifest the 3D surface plots for desirability, optimum value of WPSF (5.222)and optimum value of WRFF (3.970), respectively as a function of voltage and wire feeding speed at 10 L/min gas flow rate.

### 3.4. GRAPHICAL OPTIMIZATION

**Figure 18** depicts the overlay plot produced by the graphical optimization in DOE. In this figure, the regions not meeting the required variables are shaded out, leaving an operating window or "sweet spot". This means that the shaded area on the graphical optimization plot do not meet the selection criteria, and the clear 'window' shows where one can set the variables to satisfy the requirements for both responses. The flag is planted at the optimum values of welding variables and responses.

### 3.5. EFFICIENCY OF THE WELD JOINT

In order to obtain the efficiency of the weld joint obtained by $CO_2$-MAG welding of low carbon steel AISI 1010, three tensile samples were first welded with the optimum welding condition given in Table 8 and then tensile tested to determine the ultimate tensile strength of the weld joint. The average tensile strength was found to be 285 MPa. Therefore, the efficiency of the weld joint was calculated to be 73% according to the joint efficiency definition which is the ratio of the tensile strength of the weld joint to the tensile strength of the base metal (Table 2). This result indicates the importance of using $CO_2$-MAG welding process and its effectiveness and suitability for welding steel AISI 1010 from strength point of view.

## 4. CONCLUSIONS

1. Regarding the WPSF, a quadratic model was obtained by DOE with RSM technique for the optimum WPSF response in terms of input welding parameters. This model indicated that the arc voltage and wire feeding speed are largely effective on WPSF, while the gas flow rate is not influential.
2. The interaction effect in WPSF model indicated that the wire feeding speed has a positive influence on WPSF response, while the gas flow rate has a negative effect on WPSF.
3. Concerning the WRFF, a quadratic model was obtained for the optimum WRFF response in terms of input welding parameters. This model shows that the wire feeding speed has greater impact than voltage on WRFF, whereas the gas flow rate was found not effective.
4. By numerical optimization, the optimum values of the voltage, wire feeding speed, gas flow rate, WPSF,WRFF and desirability are (20 Volt), (153 cm/min), (10 L/min), (5.222), (3.970) and (0.849), respectively.
5. The overlay plot produced by the graphical optimization is very useful to show the window of operability, where the requirements simultaneously meet the critical properties.
6. Using $CO_2$-MAG welding process is importantly effective and suitable for welding steel AISI 1010 from the strength point of view (with 73% joint efficiency).
7. DOE with RSM was found a useful tool for predicting the responses in MAG-$CO_2$ welding technique for any given input parameters.

## REFERENCES


- Antony, J., 2003, *Design of Experiments for Engineers and Scientists* ISBN: 0750647094, Elsevier Science and Technology Books.
- ASM Materials Engineering Dictionary,1992, Edited by Joseph R. Davis, *Table 13 on Page 13*, ASM International.
- Benyounis, K. Y., and Olabi, A. G., 2005, *Effect of Laser-Welding Parameters on the Heat input and Weld-Bead Profile*, Journal of Materials Processing Technology, Vol. 164-165, PP. 978-985.
- Boiko, I., and Avisans, D., 2013, *Study of Shielding Gases for MAG*, Materials Physics and Mechanics, 16, PP. 126-134.
- Dasgupta, E. B., and Mukherjee, S., 2013, *Optimization of Weld Bead Parameters of Nickel Based Overlay Deposited By Plasma Transferred Arc Surfacing*, International Journal of Modern Engineering Research (IJMER), Vol.3, Issue.3, PP. 1330-1335.
- DeVor, R. E., Chang, T–h., and Sutherland, J. W., 1992, *Statistical Quality Design and Control — Contemporary Concepts and Methods*, New Jersey: Prentice–Hall, Inc., PP. 542–562.
- Gunaraj,V., and Murugan, N., 1999, *Application of Response Surface Methodology for Predicting Weld Bead Quality in SAW of pipes*, Journal of Materials Processing Technology, Vol. 88, PP. 266-275.
- Hould, C. P. T., 1989, *Submerged Arc Welding*, Second Edition, Abington Publishing, Cambridge, England.
- Jadeja D. V., and Patel, S. P., 2013, *A Review on Parametric Optimization by Factorial Design Approach of Mag-$CO_2$ Welding Process*, International Journal of Engineering Research and Applications (IJERA), Vol. 3, Issue 2, PP. 420-424.
- Kumar, V., 2011, *Modeling of Weld Bead Geometry and Shape Relationships in Submerged Arc Welding using Developed Fluxes*, Jordan Journal of Mechanical and Industrial Engineering, Vol. 5, No. 5, PP. 461-470.
- Patel, P. D., and Patel, S. P., 2014, *Prediction of Weld Strength of Metal Active Gas (MAG) Welding Using Artificial Neural Network*, International Journal of Engineering Research and Applications (IJERA), Vol. 1, Issue 1, PP. 036-044.
- Reddy, A. C., 2012, *Studies on the Effects of Oxidation and Its Repression in MAG Welding Process*, International Journal of Advanced Research in Engineering and Technology (IJARET), Vol. 3, No.1, PP. 48-54.
- Singla M., Singh, D., and Deepak, D., 2010, *Parametric Optimization of Gas Metal Arc Welding Processes by Using Factorial Design Approach*, Journal of Minerals and Materials Characterization and Engineering, Vol. 9, No.4, PP. 353-363.
- **www.efunda.com**, *Mechanical Properties of steel AISI 1010*.

**Table 1.** Chemical Composition for used LCS with standard type (wt%).

| Material | C | Si | Mn | P | S | Cr | Mo | Ni | V | Fe |
|---|---|---|---|---|---|---|---|---|---|---|
| Experimental | 0.13 | 0.01 | 0.450 | 0.003 | 0.003 | 0.001 | 0.002 | 0.043 | 0.001 | Bal. |
| Standard Steel AISI 1010 [ASM, 1992] | 0.08 – 0.13 | 0.1 max | 0.3 - 0.6 | 0.04 max | 0.05 max | -- | -- | -- | -- | Bal. |

**Table 2.** Mechanical properties for used LCS with standard type

| Material | Yield strength (MPa) | Tensile strength (MPa) | Reduction in Area (%) |
|---|---|---|---|
| Experimental | 262 | 391 | 42 |
| Standard steel 1010 [www.efunda.com] | 305 | 365 | 40 |

**Table 3.** Levels of input parameters used with respective coding.

| Input parameter | Unit | Low Level - 1 | High Level + 1 | -alpha | +alpha |
|---|---|---|---|---|---|
| Voltage | volt | 19 | 21 | 18 | 22 |
| Wire feeding speed | cm/min | 125 | 175 | 100 | 200 |
| Gas flow rate | L/min | 8 | 12 | 5 | 14 |

**Table 4.** Design matrix for input factors and experimental values of output (responses)

| Std | Run No. | Type of point | Voltage (volt) | Wire feeding speed (cm/min) | Gas flow rate (L/min) | WPSF | WRFF |
|---|---|---|---|---|---|---|---|
| 1 | 12 | Factorial | 19 | 125 | 8 | 4.404 | 2.530 |
| 2 | 7 | Factorial | 21 | 125 | 8 | 5.921 | 2.500 |
| 3 | 8 | Factorial | 19 | 175 | 8 | 3.100 | 3.500 |
| 4 | 1 | Factorial | 21 | 175 | 8 | 4.600 | 3.800 |
| 5 | 14 | Factorial | 19 | 125 | 12 | 2.900 | 2.200 |
| 6 | 4 | Factorial | 21 | 125 | 12 | 3.900 | 2.400 |
| 7 | 16 | Factorial | 19 | 175 | 12 | 4.700 | 3.600 |
| 8 | 18 | Factorial | 21 | 175 | 12 | 6.100 | 3.900 |
| 9 | 9 | Axial | 18 | 150 | 10 | 2.800 | 1.500 |
| 10 | 15 | Axial | 22 | 150 | 10 | 5.500 | 2.000 |
| 11 | 6 | Axial | 20 | 100 | 10 | 3.300 | 1.400 |
| 12 | 2 | Axial | 20 | 200 | 10 | 4.200 | 4.136 |
| 13 | 19 | Axial | 20 | 150 | 6 | 5.293 | 4.000 |
| 14 | 10 | Axial | 20 | 150 | 14 | 5.000 | 4.050 |
| 15 | 3 | Center | 20 | 150 | 10 | 5.300 | 4.050 |
| 16 | 11 | Center | 20 | 150 | 10 | 4.963 | 3.800 |
| 17 | 17 | Center | 20 | 150 | 10 | 5.200 | 3.715 |
| 18 | 5 | Center | 20 | 150 | 10 | 5.100 | 3.900 |
| 19 | 13 | Center | 20 | 150 | 10 | 4.700 | 4.100 |
| 20 | 20 | Center | 20 | 150 | 10 | 4.800 | 3.750 |

**Table 5.** Analysis of variance (ANOVA) for response surface reduced quadratic model (WPSF).

| Source | Sum of squares | df | Mean square | F value | p-value Prob > F |
|---|---|---|---|---|---|
| Model | 17.09 | 6 | 2.85 | 90.74 | < 0.0001 significant |
| A-Voltage | 7.31 | 1 | 7.31 | 233.05 | < 0.0001 |
| B-Wire feeding speed | 0.63 | 1 | 0.63 | 20.08 | 0.0006 |
| C-Gas flow rate | 0.064 | 1 | 0.064 | 2.04 | 0.1772 |
| BC | 5.49 | 1 | 5.49 | 174.84 | < 0.0001 |
| $A^2$ | 1.36 | 1 | 1.36 | 43.19 | < 0.0001 |
| $B^2$ | 2.81 | 1 | 2.81 | 89.68 | < 0.0001 |
| Residual | 0.41 | 13 | 0.031 | | |
| Lack of Fit | 0.14 | 8 | 0.017 | 0.32 | 0.9276 not significant |
| Purr Error | 0.27 | 5 | 0.054 | | |
| Core Total | 17.49 | 19 | | | |
| Std. Dev. = 0.18 | | | R-Squared = 0.9767 | | |
| Mean = 4.59 | | | Adj R-Squared = 0.9659 | | |
| C.V. % = 3.86 | | | Pred R-Squared = 0.9580 | | |
| PRESS = 0.73 | | | Adeq Precision = 32.493 | | |

**Table 6.** Analysis of variance (ANOVA) for response surface reduced quadratic model (WRFF)

| Source | Sum of squares | df | Mean square | F value | p-value Prob > F |
|---|---|---|---|---|---|
| Model | 16.48 | 4 | 4.12 | 295.50 | < 0.0001 significant |
| A-Voltage | 0.24 | 1 | 0.24 | 17.04 | 0.0009 |
| B-Wire feeding speed | 7.32 | 1 | 7.32 | 524.97 | < 0.0001 |
| $A^2$ | 7.88 | 1 | 7.88 | 565.18 | < 0.0001 |
| $B^2$ | 2.25 | 1 | 2.25 | 161.52 | < 0.0001 |
| Residual | 0.21 | 15 | 0.014 | | |
| Lack of Fit | 0.081 | 10 | 8.113E-003 | 0.32 | 0.9425 not significant |
| Purr Error | 0.13 | 5 | 0.026 | | |
| Core Total | 16.69 | 19 | | | |
| Std. Dev. = 0.12 | | | R-Squared = 0.9875 | | |
| Mean = 3.23 | | | Adj R-Squared = 0.9841 | | |
| C.V. % = 3.65 | | | Pred R-Squared = 0.9812 | | |
| PRESS = 0.31 | | | Adeq Precision = 45.824 | | |

**Table 7.** Constrains used for the numerical optimization.

| Name | Goal | Lower Limit | Upper Limit | Lower Weight | Upper Weight | Importance |
|---|---|---|---|---|---|---|
| A:Voltage | is in range | 19 | 21 | 1 | 1 | 3 |
| B:Wire feeding speed | is in range | 125 | 175 | 1 | 1 | 3 |
| C:Gas flow rate | is in range | 8 | 12 | 1 | 1 | 3 |
| Welding velocity | minimize | 64.66 | 125 | 1 | 1 | 3 |
| Arc energy | maximize | 230 | 1800 | 1 | 1 | 3 |
| WPSF | maximize | 2.8 | 6.1 | 1 | 1 | 3 |
| WRSF | maximize | 1.4 | 4.136 | 1 | 1 | 3 |

**Table 8.** Optimum solution of the desirability .

| Numer | Voltage | Wire feeding speed | Gas flow rate | WPSF | WRFF | Desirability |
|---|---|---|---|---|---|---|
| 1 | 20 | 153 | 10 | 5.222 | 3.970 | 0.849 Selected |

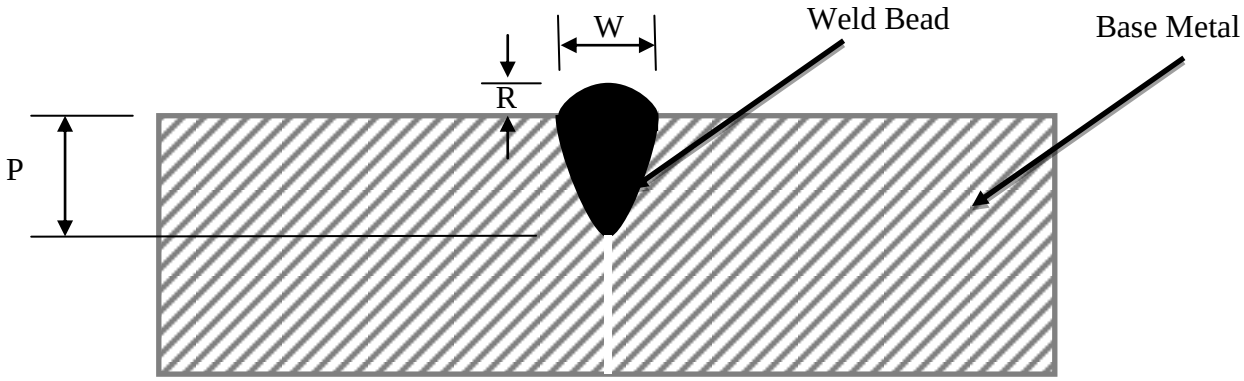


**Figure 1.** Weld bead geometry.

(P: Penetration, W: Bead Width, R: Bead Reinforcement)

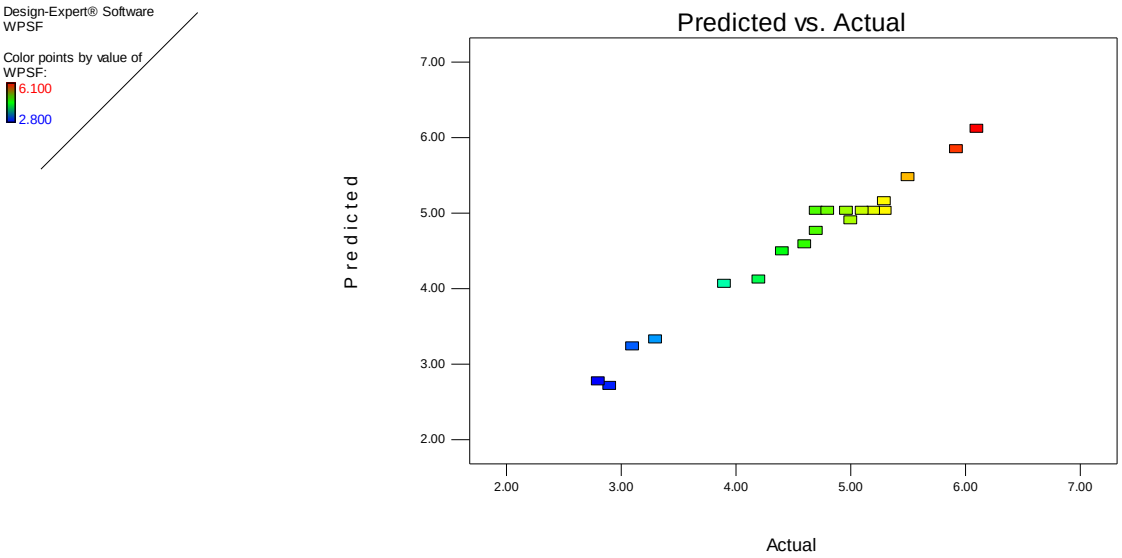


**Figure 2.** Predicted versus actual WPSF data.

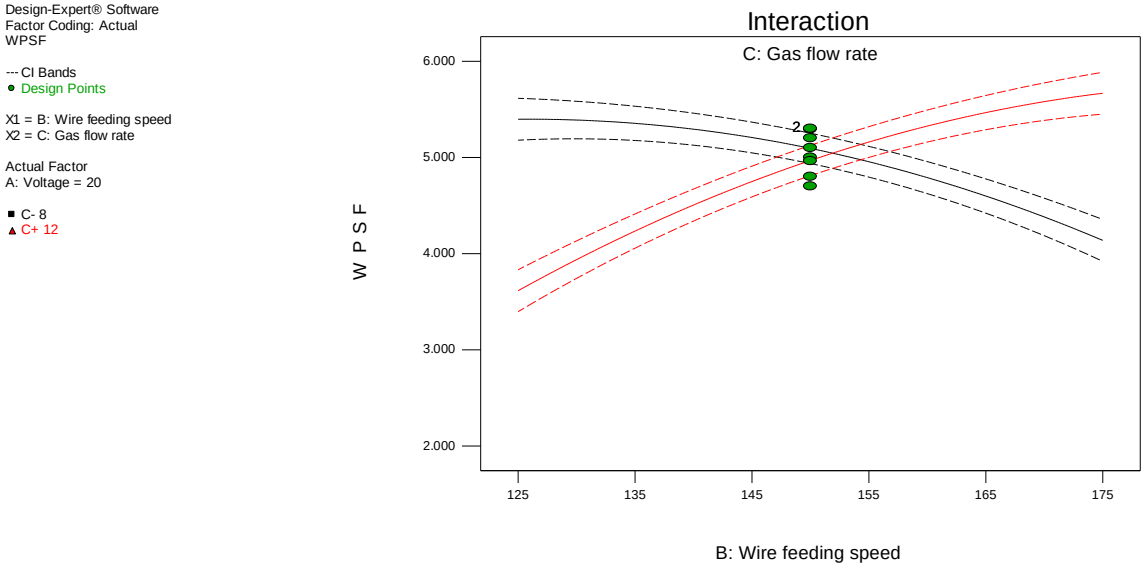


**Figure 3.** Effect of interaction of wire feeding speed and gas flow rate on WPSF.

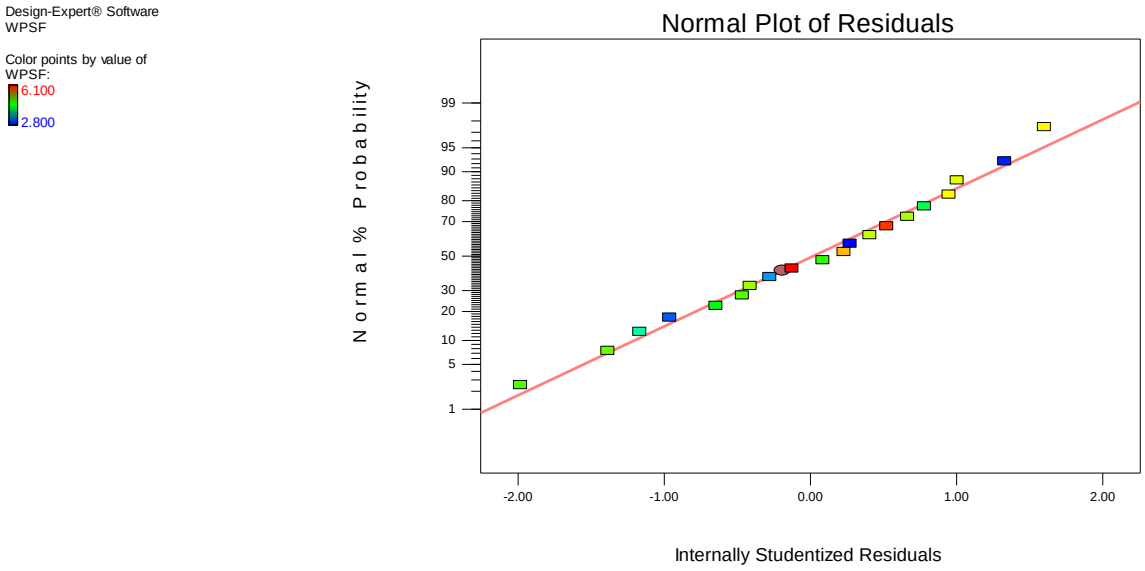


**Figure 4.** Normal probability plot of residuals for WPSF data.

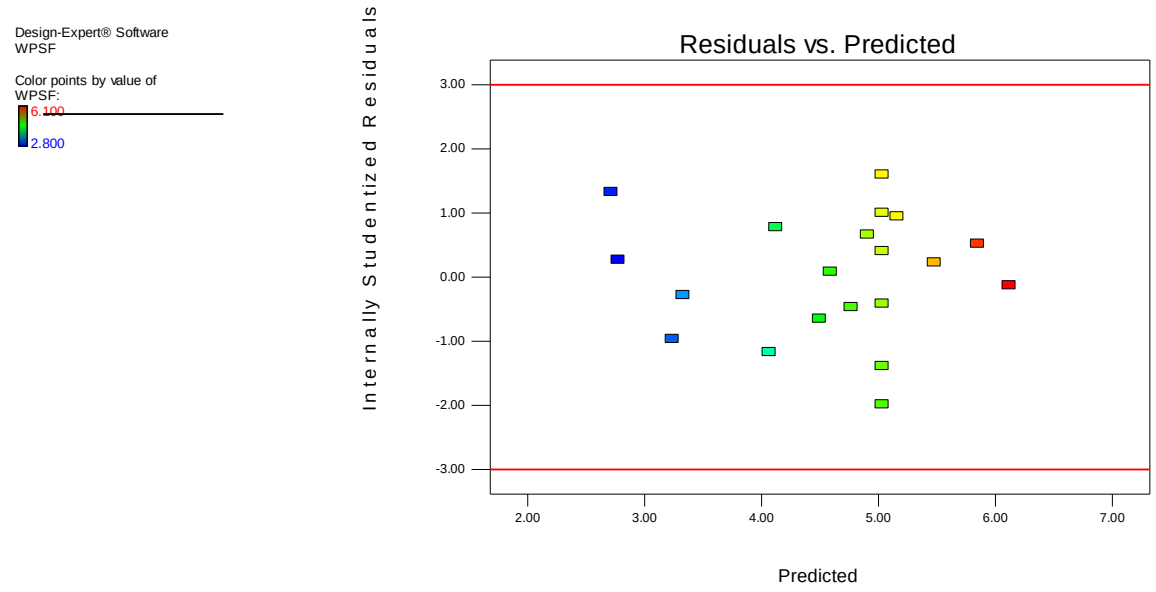


**Figure 5. Residuals versus predicted WPSF data.**

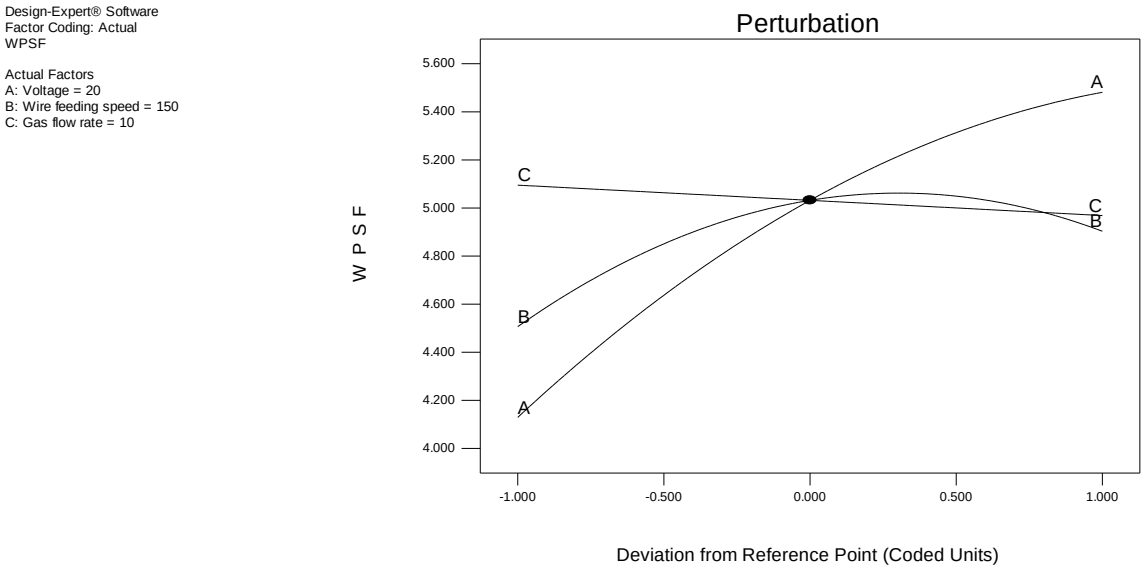


**Figure 6.** Perturbation of WPSF on wire feeding speed and gas flow rate.

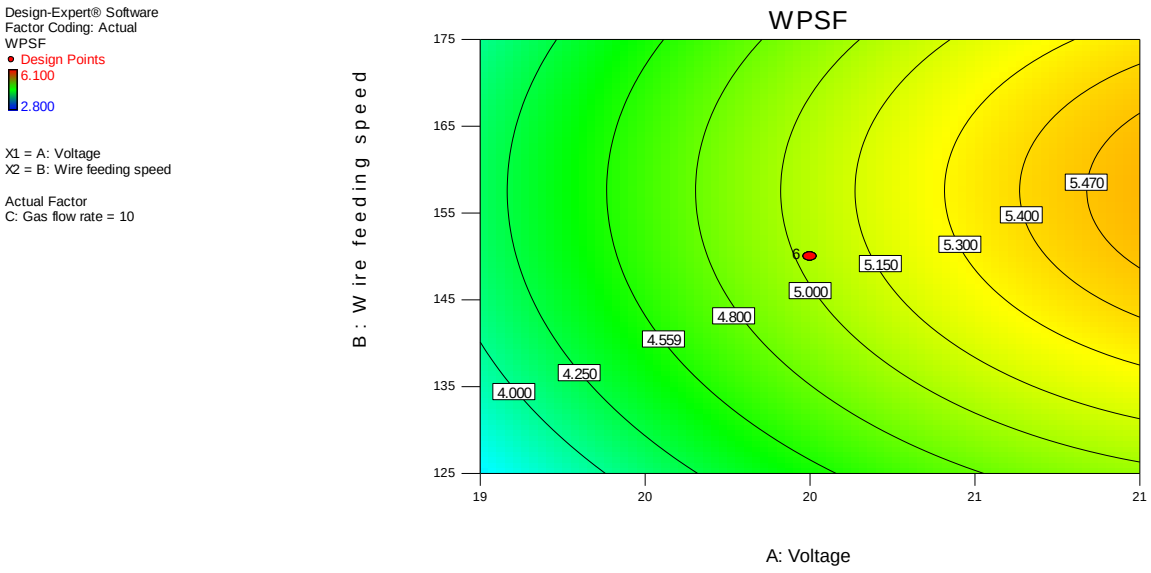


**Figure 7.** Contour graph WPSF as a function of voltage and wire feeding speed gas flow rate 10 L/min.

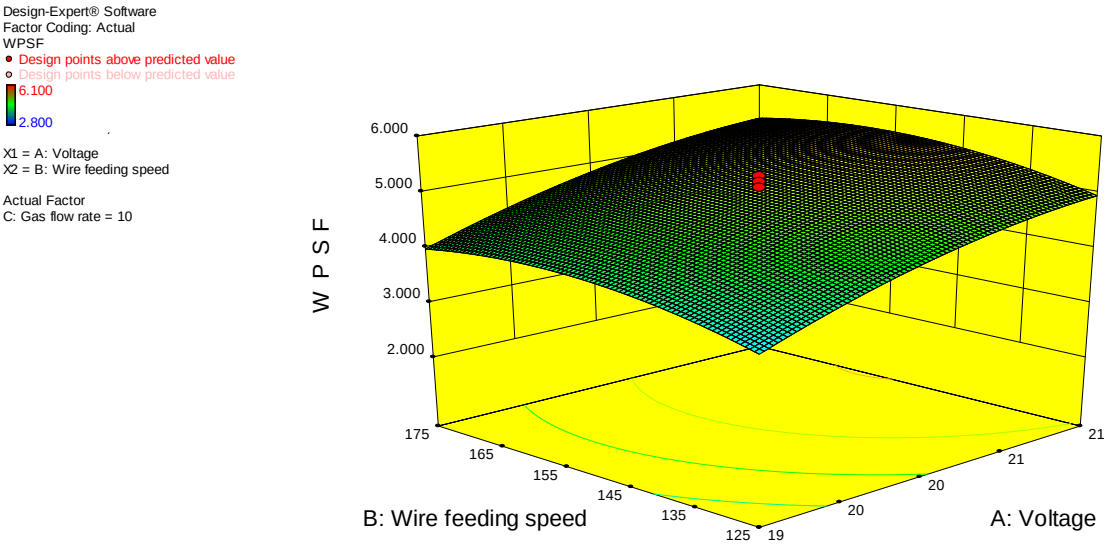


**Figure 8.** 3D graph of WPSF as a function of voltage and wire feeding speed at gas flow rate 10 L/min.

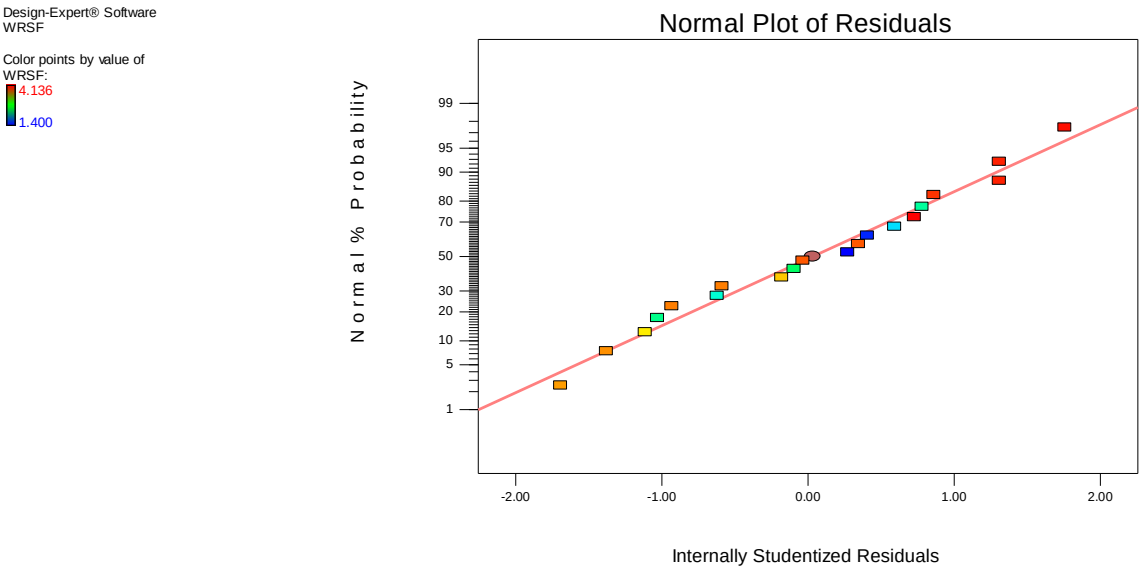


**Figure 9.** Normal probability plot of residuals for WRFF data.

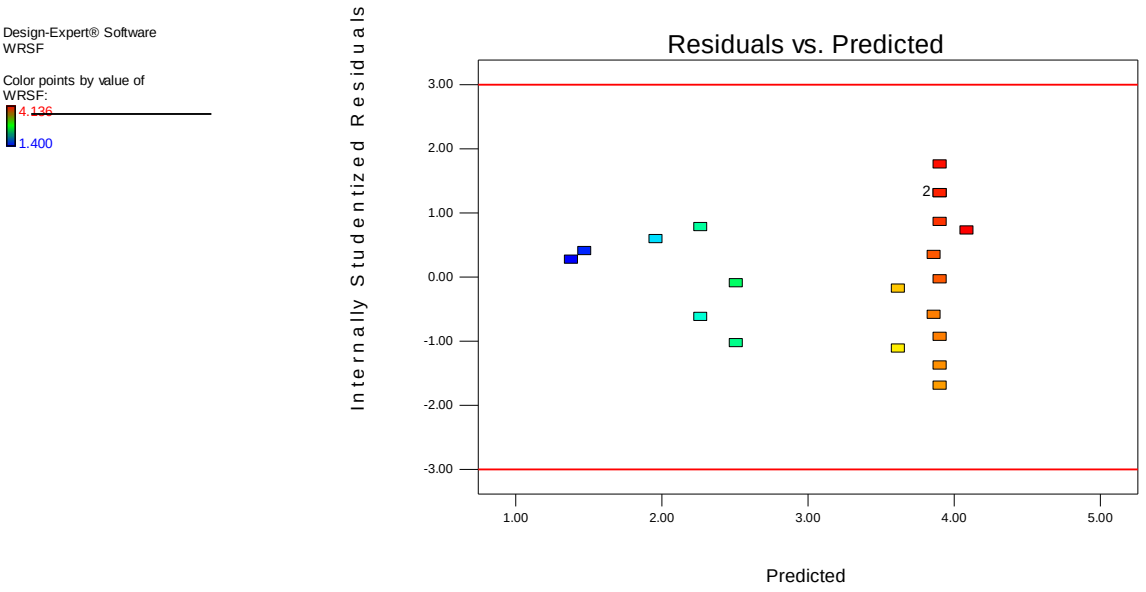


**Figure 10.** Residuals versus predicted WRFF data.

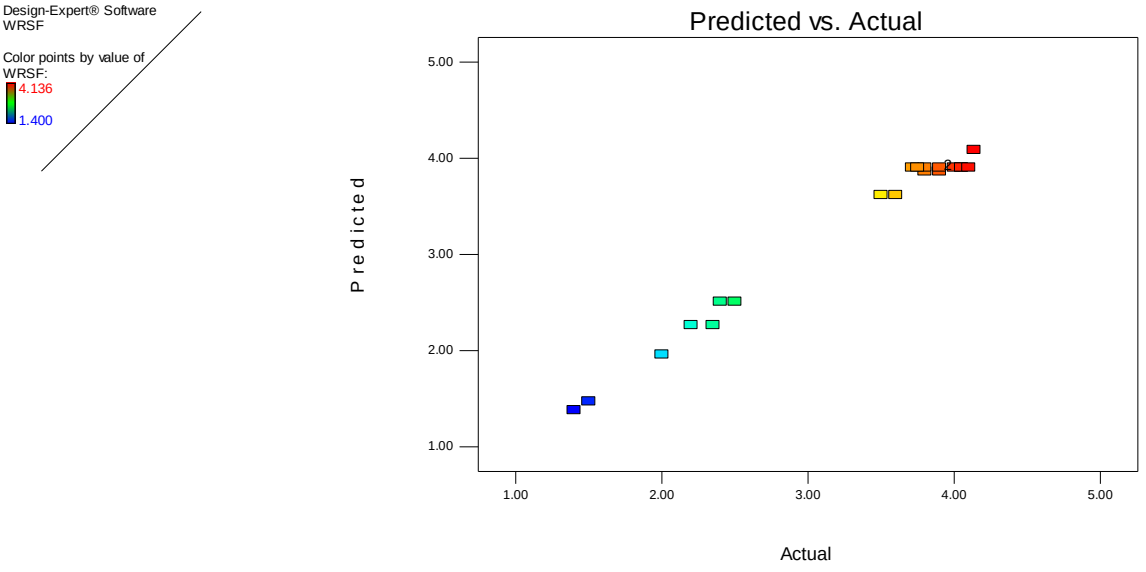


**Figure 11.** Predicted versus actual WRFF data.

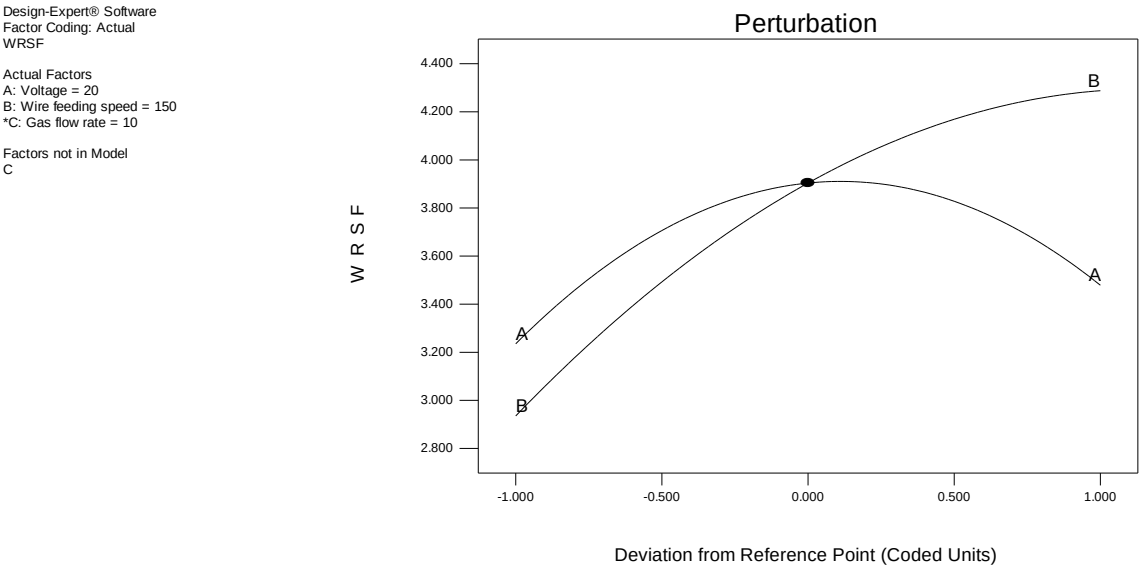


**Figure 12.** Perturbation of WRFF on wire feeding speed and gas flow rate.

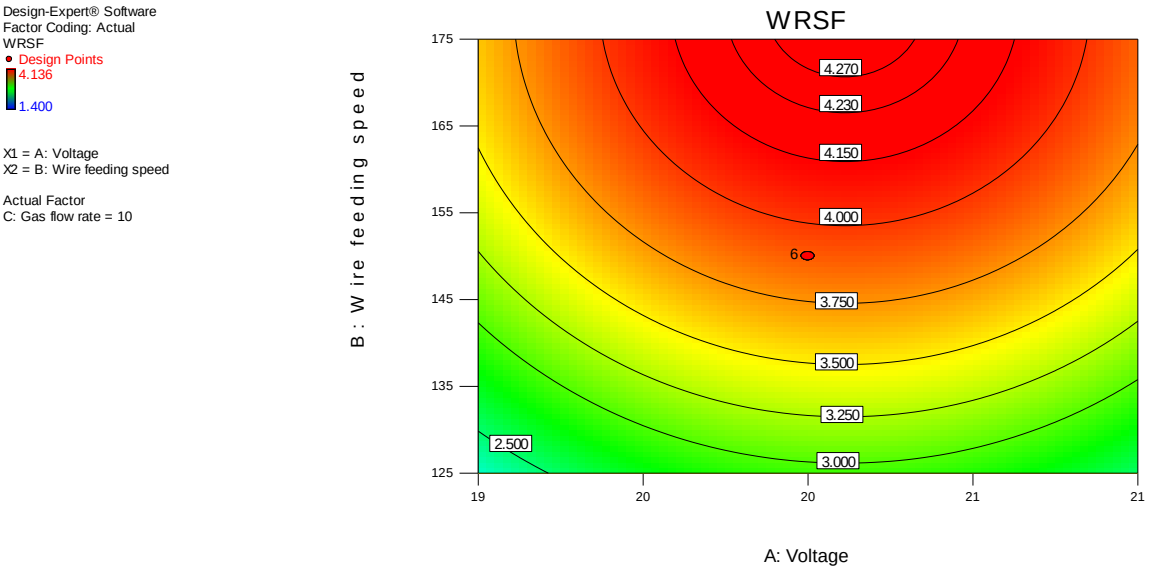


**Figure 13.** Contour graph of WRFF (or WRSF)welding velocity as a function of voltage and wire feeding speed gas flow rate 10 L/min.

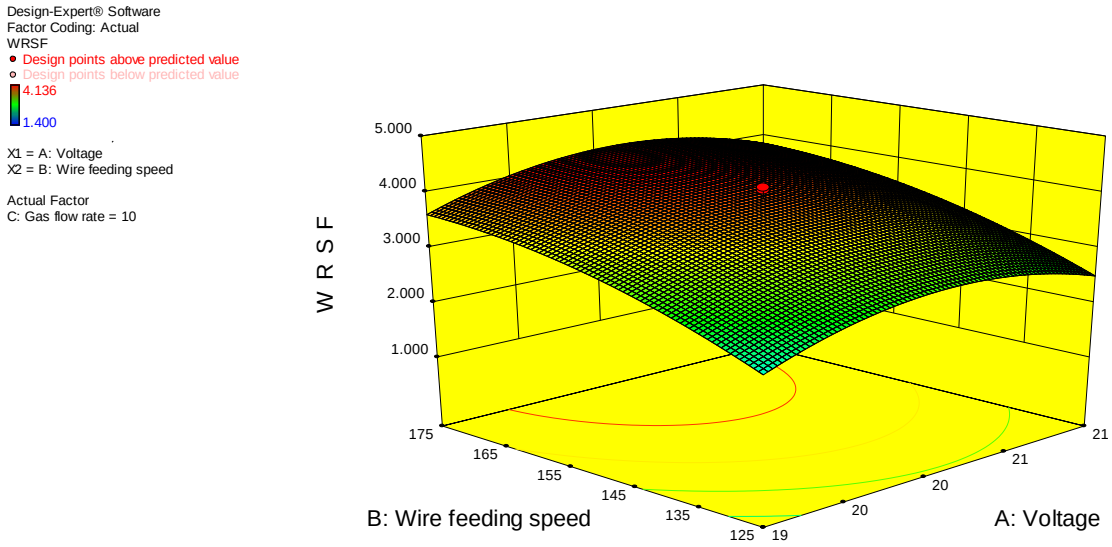


**Figure14.** 3D graph of WRFF as a function of voltage and wire feeding speed at gas flow rate 10 L/min.

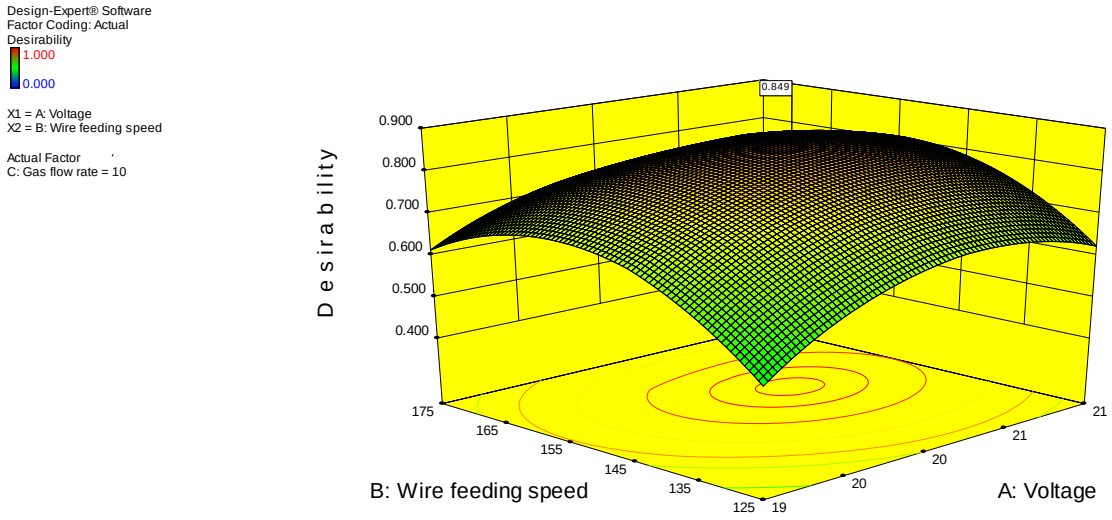


**Figure 15.** 3D graph for desirability as a function of voltage and wire feeding speed at gas flow rate 10 L/min.

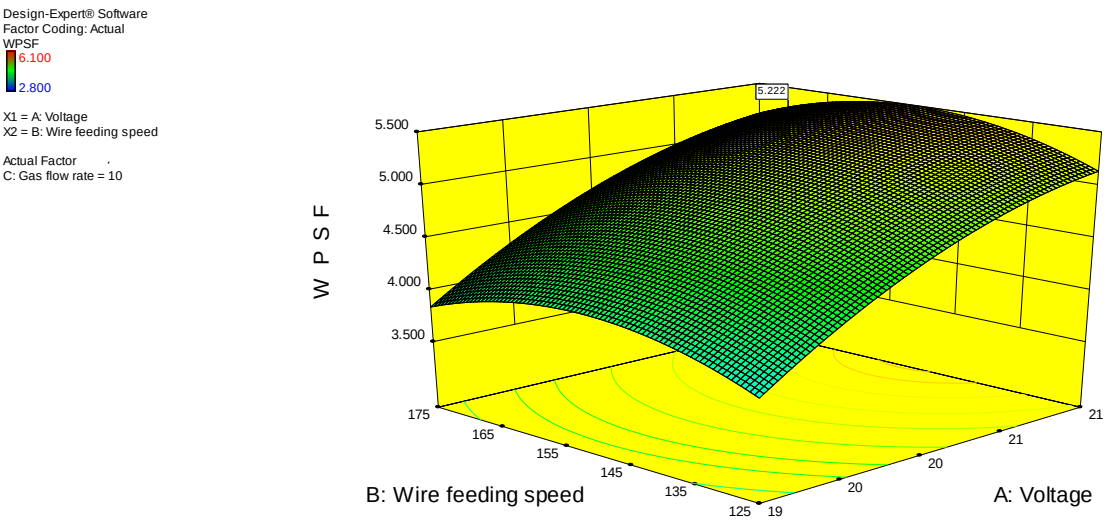


**Figure 16.** The optimum value for WPSF at 10 /min gas flow rate.

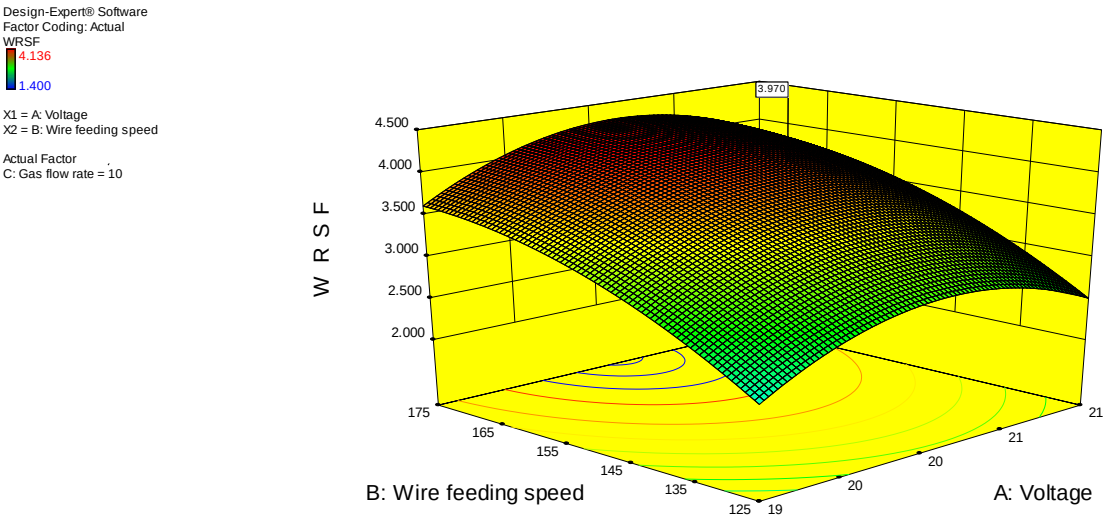


**Figure 17.** The optimum value for WRFF at 10 L/min gas flow rate.

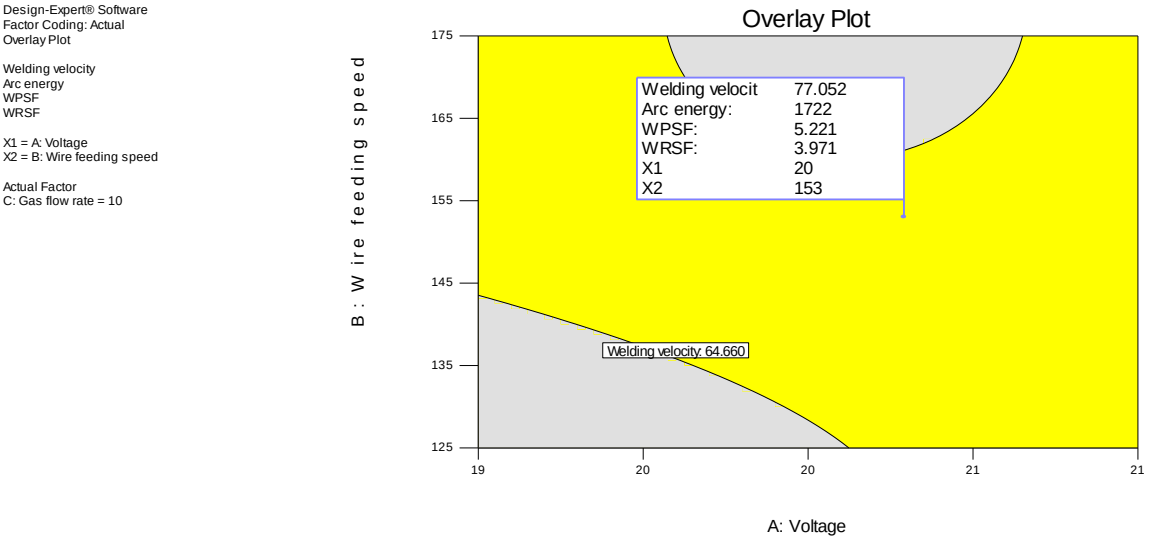


**Figure 18.** Overlay plot produced by numerical optimization showing the region of optimal welding variables at 10 L/min gas flow rate.

# Wear Rate and Hardness of Boride Low Carbon Steel

**Jabbar Hussein Mohmmed**
Assistant Lecturer
Material Engineering Department-University of Technology
jabbaraljanaby@yahoo.com

## ABSTRACT

There are no single materials which can withstand all the extreme operating conditions in modern technology. Protection of the metals from hostile environments has therefore become a technical and economic necessity.
In this work, for enhancing their wear-resistance, boride layers were deposited on the surface of low carbon steel by a pack cementation method at 850 °C for (2, 4, and 6) h using vacuum furnace. The boronizing process was achieved using different concentration of boron source (20, 25, and 30) % wt. into coating mixture to optimize the best conditions which ensure the higher properties with lower time. The coating was characteristic by X ray diffraction (XRD), and it is confirmed the presence of ($Fe_2B$) and (FeB) in the coating. The wear rate, hardness and thickness of the boride layers were measured, and it was observed that they effected by concentration of boron and time holding of boronizing process. Experimental results show that the higher properties of coating layer were obtained with 30% wt. of boron concentration and 4 h time holding.
**Keyword:** boronizing, diffusion coating. Wear rate.

# معدل البلى والصلادة للفولاذ الواطئ الكاربون المبورن

**جبار حسين محمد**
مدرس مساعد
قسم هندسة المواد-الجامعة التكنولوجية

## الخلاصة

لا توجد مادة مفردة ممكن ان تتحمل ظروف التشغيل القاسية في التكنلوجيا الحديثة. لذلك, حماية المعدن من المحيط القاسي اصبح ضرورة تقنية واقتصادية. في هذا العمل، ولتحسين مقاومتها للبلى، تم ترسيب طبقات من البوريد على سطح الفولاذ المنخفض الكاربون باستخدام طريقة السمنتة الصلبة عند درجة حرارة 850ْم ولازمان (2، 4، و6) ساعات باستخدام فرن مفرغ. تم اجراء عملية البورنة باستخدام تراكيز مختلفة لمصدر البورون (20، 25، و30) % من الوزن داخل خليط الطلاء للحصول على أفضل القيم لأفضل ظروف للحصول على أعلى خواص بأقل زمن. تم توصيف الطلاء باستخدام حيود الاشعة السينية وقد اثبتت وجود طوري ($Fe_2B$) و(FeB) في الطلاء. تم قياس معدل البلى، الصلادة، وسمك طبقة البوريد، وقد لوحظ تأثرها بتركيز البورون وزمن الابقاء لعملية البورنة. اثبتت النتائج العملية ان افضل خواص ممكن الحصول عليها عند الطلاء ب 30 % من الوزن تركيز البورون مع زمن ابقاء 4 ساعات.

**كلمات رئيسية:** البورنة، الطلاءات الانتشارية، معدل البلى.

## 1. INTRODUCTION

Poor wear resistance still the main problem of steel alloys used in application involve aggressive conditions and elevated temperature like turbine and power plant applications.

In recent years, many studies on the enhancing of mechanical properties of materials have been carried out. From these researches, it was found that the large improvement in surface properties can be achieved by applied surface treatment on engineering materials, **Calika, et al, 2008**. Therefore, the use of surface coatings opens up the possibility for material designs in which the specific properties are located where they are most needed. A number of coating systems are known ranging from metallic or polymeric to oxide based ceramics. Among them diffusion based coatings (pack cementation) have additional advantages of high wear resistance, high temperature stability and superior mechanical, **Kayacan, et al, 2010.**

Boronizing is a thermochemical surface-hardening process. It's similar to other surface hardening treatments, such as carburization and nitriding. In boronizing treatment the surface of material was enriched by diffusing boron atoms into the surface at high temperatures, **Dong, et al, 2009**.

Industrial boronizing can be applied to most ferrous steels such as structural steels, tool steel, and carbon steel as well as to austenitic stainless steels. Thus, boronizing has long been used to improve the surface properties of valves, burner nozzle, etc. in the utility industry as boride layers have a high hardness, oxidation resistance, strong indicator of wear resistance and fracture strength.

Several researches were accomplished in this field. **Calika, et al, 2008**, investigated some mechanical properties of borided and unborided four types of steels. Boronizing of steels was performed by powder pack method at 1210$^{\circ}$C. **Kayacan, et al, 2010**, investigated the diffusion mechanism of the boronizing process of AISI 1040. While, **Pazarlıoglu et al, 2012**, studied niobium boride layers deposited on the surface of AISI 1010 steel.

The most of the previous studies (**Gatea, and Abbas, 2009, and Al-Azawi, 2005**) carried out the diffusion coatings in pack process in the range of 1000-1200$^{\circ}$C. It was found that the pack mass was sintered, and stuck to the samples so that it was very difficult to remove the contaminations from the pack. The samples were very much distorted and the grain size of the core increased due to high temperature and prolonged heat treatment.

In this study, the pack cementation process was achieved in relatively low temperature (850) $^{\circ}$C to avoid sintering of the pack and adhesion of material to the samples surface. The coating diffusion employed in this work was boronizing coating.

The aim of this research is to the optimum conditions which brought the higher surface properties (hardness and wear). The resultant coatings were characteristic by X-ray diffraction to identify the formed phases. The effects of boron concentration and holding time of boronizing process were also studied.

## 2. EXPERIMENTAL WORK

### 2.1 Material Selection and Sample preparation

The substrate material used in this study was low carbon steel. Low carbon steel is widely used in different areas of machine constructions. The chemical composition of material used in this work was given in **Table 1**. Before the boronizing, round samples were cut into proper

dimensions for each test, and ground up to 600 grid emery paper and then washed ultrasonically for 15 min in ethyl alcohol.

### 2.2 Coating Process

Boronizing process was performed using a fluoride-activated powder pack cementation method. The boronizing media were composed of different concentration of $B_4C$ (20, 25, and 30) %wt., 5% wt.KBF4 and remaining was $SiO_2$. In this boronizing media, $B_4C$ serves as the source of boron, $SiO_2$ as the diluent, and KBF4 as the active agent.

Simple steps was involved to achieve the boronizing process as following: all the media powders were mixed in a polyurethane jar for 6 h, using porcelain balls as the mixing medium; low carbon steel specimens were buried in the powders and packed into a rectangular stainless steel retort (25 cm length, 15 cm width and 8 cm), which was then placed in a horizontal tube vacuum furnace (**Fig. 1**) at 850°C. The heating rate for all runs was 10 °C/min. the varying soaking time (2, 4, and 6) h was used to get the lower time possible to achieve the higher properties. After treatment, the samples were cooled to room temperature in the furnace. Nine runs were repeated in each treatment condition. **Fig. 2(a & b)** illustrates the boronized and un-boronized samples respectively. All experimental work was carried out in metallurgy laboratory in material engineering department in university of technology.

### 2.3 Inspection and Testing

#### 2.3.1 Characterization of boronizing coatings

After the boronizing treatment, the thickness of the resultant coating was measured by an eddy current based thickness measuring instrument with ND-2 type probe, suitable for ferrous and non-ferrous alloys.

Phase analysis of the boronizing coatings was identified utilizing X-ray diffraction analysis (Philips PLO1840 X-ray diffractometer in 2θ ranging between 20˚ to 90˚ using Cu Kα radiation).

#### 2.3.2 Microhardness measurement

The hardness of the specimens was measured with a Vickers micro-hardometer model (HVS-1000). The hardness tests were performed under an indentation load of 100 N with a dwelling time of 20 s. In order to obtain reliable statistical data, analysis points were spaced so as to eliminate the effect of neighboring indentations, and the hardness was evaluated by taking five indentations on each specimen and averaging of only three middle values**.**

#### 2.3.3 Wear test

Wear tests were performed according to the ASTM G99 for wear testing with a pin-on-disk apparatus. The wear rate of the materials were determine at a load of 10N, rotating speed of 2cm/sec, sliding distance of 50m using a pin-on-disk tribometer.

Specimens were weighed on an electrical balance with an accuracy of 0.1 mg before and after wear testing. Then, the wear rate expressed in (gm/cm) is calculated as follows:

$$W.R = \frac{\Delta w}{S} \quad (1)$$

Where: $W.R$: wear rate in (gm/cm), $\Delta w$: weight loss in (gm), $S$: sliding distance in (cm).

All of the tests were conducted at ambient atmospheric condition at room temperature (25)˚C. Lubrication is not applied to avoid the complication of terbo-chemical effects.

## 3. Results and Discussion

### 3.1 Thickness Measurement

Thickness of boride samples was in general increases with increasing the concentration of boron and time of treatment. The results presented in **Fig. 3**. Boronizing is diffusion process and obeyed the diffusion laws which are agreement with the result of increasing the thickness coating with increasing the exposure time to high temperatures.

Coating thickness of the boride specimens was in range of (0.25-0.135μm). Thinner layers of coating were favored in practical application because it can be helped to reduce the defects of the like porosity or micro-cracks.

### 3.2 X-ray Diffraction

The coating has been characterized by X-ray diffraction. It was observed that the main phases formed on the coating layers were $Fe_2B$, and only a small amount of FeB. The XRD patterns also reveal that the increasing of soaking time led to increase the amount of FeB.

Furthermore, the results indicates that the boron concentration has no much effect on the formed phases, only on intensity of $Fe_2B$ peak, which become more intensive as boron concentration increases. The X-ray diffraction patterns for 30% $B_4C$ boride samples treated at different time holding are shown in **Fig 4**.

### 3.3 Micro-hardness

The results of microhardness for un-boronized and boronized samples are shown in **Fig. 5**. It can be found from this Figure that the microhardness values of all boronizing coatings are much higher than that of the substrate, i.e. 151 HV.

It is also observed that the value of microhardness was enhanced strongly with increase the boron concentration and time of treatment. This improvement can be explained by the fact that the diffusion of boron atoms into substrate arise with increasing the period of exposing to higher temperature. These atoms produced in deformation of crystal lattice of substrate leading to generate of internal stresses. These stresses act as obstacle to motion the dislocation resulting in increasing the hardness values. However, during boronizing for longer than 4 h, the micro hardness shows to decrease slightly with increasing time. This phenomenon might be attributed to the formation of a great number of micro-cracks in the coatings when the treatment was carried out for long duration at high temperature. Also, this reduction in microhardness value may be caused by the phase transformation and changes in crystalline structure. Recrystallization, grain growth and change the microstructure make the metal softer. The similar observation was found by **Dong, et al, 2009**.

### 3.4 Wear Test

**Fig. 6** illustrate the wear rate results. In order to find the differences in wear behavior, through their different wear mechanisms, the unboronized specimen was also examined. It is can be clearly observed that the wear rates of the boronized specimens were much lower compared with those of the unboronized specimen under the employed loads. Moreover, the wear resistance of the boronized layer increases with the increase of boron concentration from 20 to 30 % wt. The percentage of improvement in wear resistance of boronized samples varied depending on boron concentration and time of treatment.

The maximum improvement percentage was brought with boron concentration 30% and holding time 4 h. It is obvious that the wear resistance increases with the increase of the surface micro hardness. Hard and complex phases especially the phase ($Fe_2B$) is responsible for the excellent wear resistance property of the boronized samples.

The results of this study suggest that there is an inverse relationship between the hardness and wear rate. The harder materials revealed more wear resistance as shown in **Fig 7**. Although similar results have been reported by **Borgioli et al, 2005**,and **Hamood, Abd Al- khalaq F., 2012**, several studies have found no correlation between hardness and wear due to the complexity of wear process [**Seghi, et al, 1991, Yap, et al, 1997, Mandikos, et al, 2001, and Mair, et al, 1996**].

In other hand, the results can be explained according to wear mechanism. The wear mechanism for the un-boronized specimens takes place mainly through scratch and plastic deformation. On the contrast, the boronized specimens the wear mechanism are mainly characterized by scuffing and brittle micro-fracture.

## 4. CONCLUSION

The following conclusions may be drawn from the results obtained in this work:

- The boronizing coatings were successfully applied by a simple pack cementation process onto already prepared low carbon steel samples.
- The proposed coatings were applied at a relatively low temperature 850˚C, leading to less cost and energy consumption during application the coating.
- increasing the time soaking led to increase the amount of phase FeB formed in resultant coatings, while that the boron concentration has no much effect on the formed phases, only on intensity of $Fe_2B$ peak.
- Boronizing coating improves the micro-hardness value and wear resistance of the resultant coatings in all cases.
- The optimum conditions which brought the higher enhancement of micro-hardness value and wear resistance were at 30% wt of $B_4C$ with 4 h soaking time.

## REFERENCES


- Al-Azawi, Sabah Noori, 2005, "Modification of 304 Steel Surface Properties after Diffusion Coatings", Master Thesis, University of Technology.

- Borgioli F., Galvanetto E., Iozzelli F., and Pradelli G., 2005, "Improvement of wear resistance of Ti–6Al–4V alloy by means of thermal oxidation, *"Materials Letters*, vol. 59, No. 17, pp. 2159– 2162.

- Calika, O. Sahinb, Ucar, N., 2009, "Mechanical Properties of Boronized AISI 316, AISI 1040, AISI 1045 and AISI 4140 Steels", ACTA PHYSICA POLONICA A, Vol. 115, No.3.

- Dong, X., Huang, J. Hu, Wang, Z., Gao, H., Guo, R., Z., 2009, "Microstructure and Properties of Boronizing Layer of Fe-based Powder Metallurgy Compacts Prepared by Boronizing and Sintering Simultaneously", Science of Sintering, Vol. 41, pp. 199-207.

- Gatea, Jawad Badr, and Abbass, Muna khedier, 2009, " Effect of Pack Cementation Coating on Hot Corrosion Resistance of Low Alloy Steel", Engineering & Technology Journal, Vol. 27, No. 2, pp.332-347.

- Hamood, Abd Al- khalaq F., 2012, " Using of Pulsed Nd-Yag Laser in the Treatment of Thermal Spray by Aluminum and Diffusion Coating Phases of Low Alloy Steel", Engineering & Technology Journal, Vol. 27, No. 2. pp. 222-237.

- Kayacan, O., Sahin, S., Tastan, F., 2010, "A Study for Boronizing Process Within NonextensiveThermostatistics ", Mathematical and Computational Applications, Vol. 15, No. 1, pp. 14-24.

- Mair L. H., Stolarski T. A., Vowles R. W., and Lloyd C. H., 1996, "Wear: mechanisms, manifestations and measurement. Report of a workshop," *Journal of Dentistry*, vol. 24, no. 1–2, pp.141-148.

- Mandikos M. N., McGivney G. P., Davis E., Bush P. J., and Carter J. M., 2001, "A comparison of the wear resistance and hardness of indirect composite resins," *Journal of Prosthetic Dentistry*, vol. 85, no. 4, pp. 386–395.

- Pazarlıoglu, S. Serdar, Ozkan Kon, Şaduman Şen, Ugur Şen, 2012, "Niobium boride coating on the surface of AISI 1010 by a duplex treatment", Usak University Journal of Material Sciences, Vol. 2, pp. 199 – 204.

- Seghi R. R., Rosenstiel S. F., and Bauer P., "Abrasion of human enamel by different dental ceramics in vitro," *Journal of Dental Research*, vol. 70, no. 3, pp. 221–225, 1991.

- Yap A. U. J., Teoh S. H., Hastings G. W., and Lu C. S., 1997, "Comparative wear ranking of dental restorative materials utilizing different wear simulation modes," *Journal of Oral Rehabilitation*, vol. 24, no. 8, pp. 574–580.

**Table 1 chemical composition of metal substrates.**

| Element | C | Mn | Fe | Si | Mo | Cu | Ti | V | P |
|---|---|---|---|---|---|---|---|---|---|
| Low carbon steel (wt%) | 0.18 | 0.8 | 98.45 | <0.05 | 0.4 | <0.05 | <0.05 | <0.05 | <0.05 |
| Standard (DIN LW) | 0.17-0.22 | 0.6-0.9 | 98.40 | 0.04-1 | 0.4-0.5 | ..... | ..... | ..... | <=0.035 |

**Figure 1.** Vacuum furnace

**Figure 2. (**a) Boronized and (b) un-boronized samples.

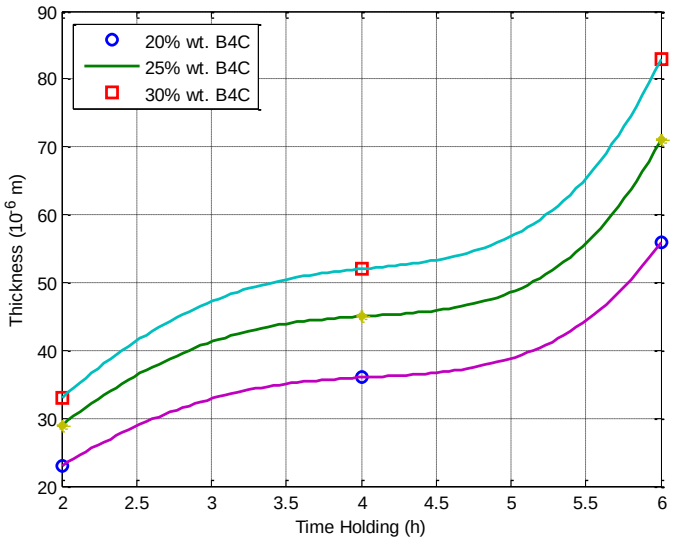


**Figure 3.** Variation of layer thickness as a function of boronizing time and $B_4C$ concentration.

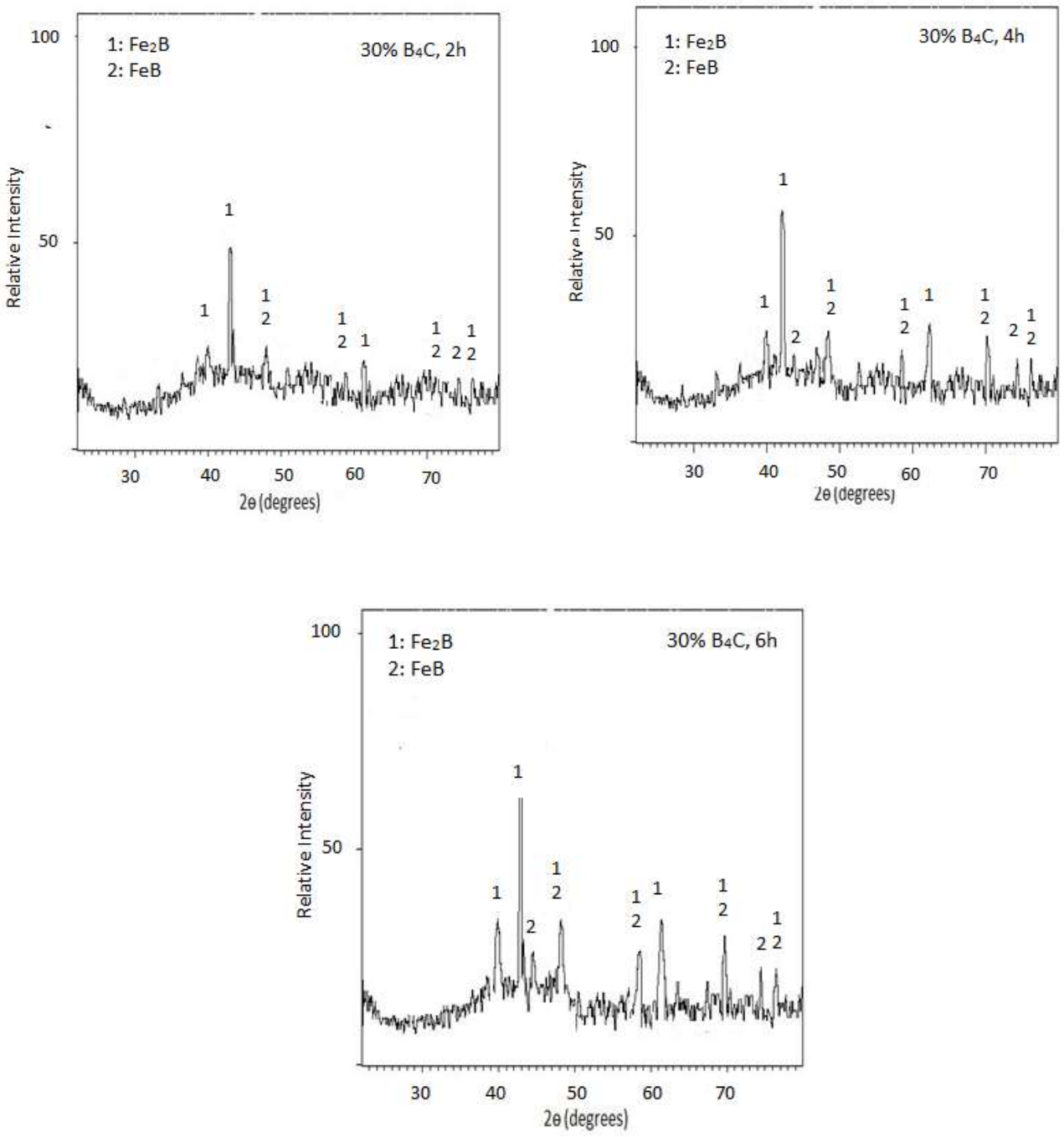


**Figure 4.** X-ray diffraction patterns of boronized samplesat 30% $B_4C$ for different time treatment:2h,4h, and 6h.

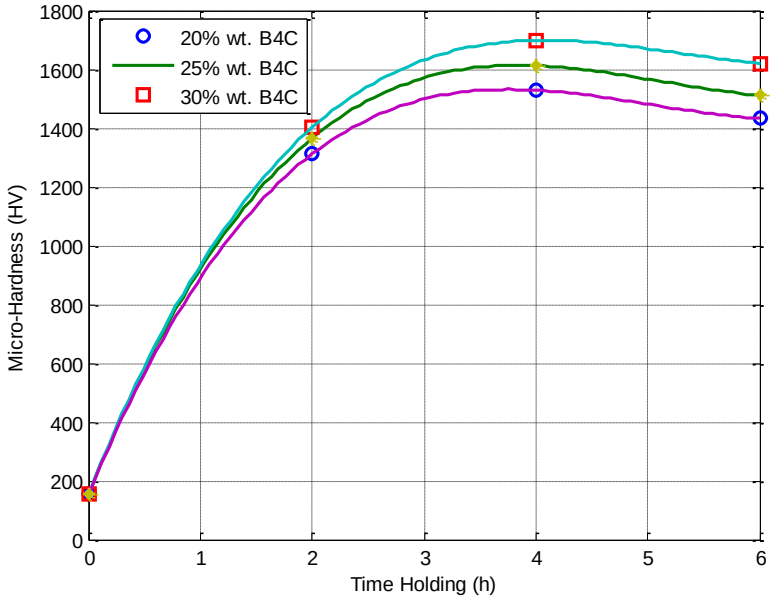


**Figure 5.** The micro-hardness variation of boronized samples at different time treatment and $B_4C$ concentration.

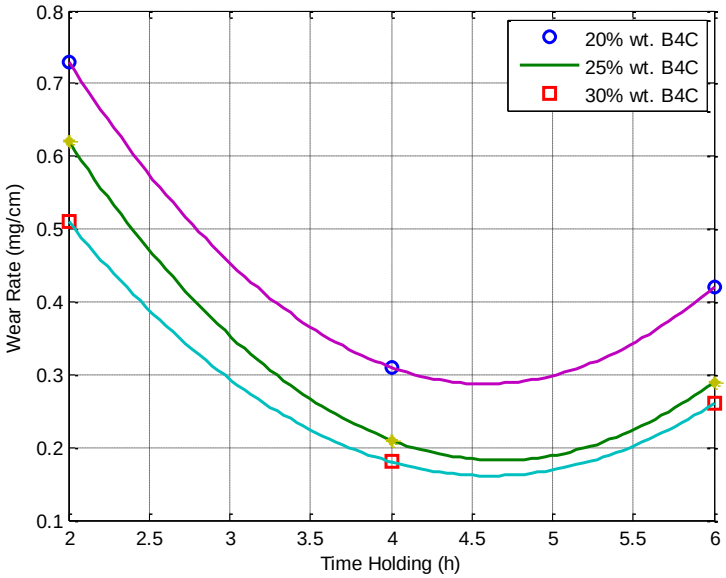


**Figure 6.** Variation of wear rate to time holding for the boronized samples at different $B_4C$ concentration.

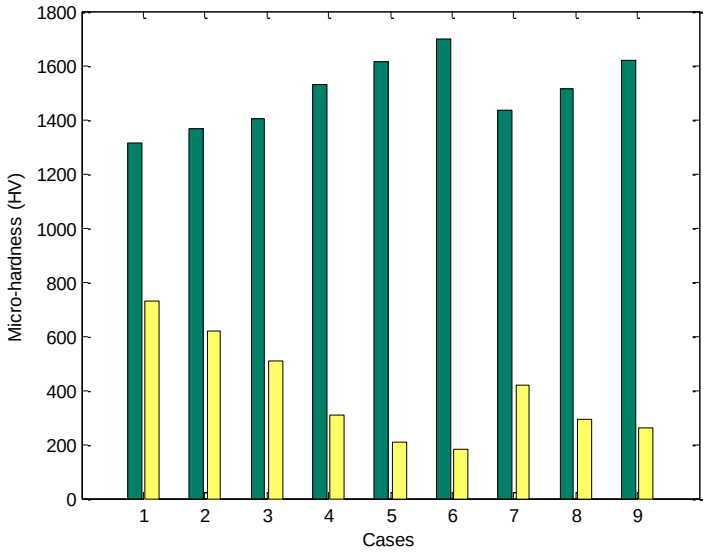


**Figure 7.** Microhardness (HV) and wear rate boronized samples.

# Numerical Simulation of Natural Convection Heat Transfer from Interrupted Rectangular Fins

**Dr. Ali A. F. Al- Hamadani**
Lecturer
Department of Mechanical Engineering
College of Engineering -University of Wasit
Email: alirudhaengmec@ uowasit.edu.iq

**Dr. Abbas Jassim Jubear**
Lecturer
Department of Mechanical Engineering
College of Engineering-University of Wasit
Email: a.aljassanai@uowasit.edu.iq

## ABSTRACT

Numerical simulations have been investigated to study the external free convective heat transfer from a vertically rectangular interrupted fin arrays. The continuity, Naver-Stockes and energy equations have been solved for steady-state, incompressible, two dimensional, laminar with Boussiuesq approximation by Fluent 15 software. The performance of interrupted fins was evaluated to gain the optimum ratio of interrupted length to fin length ($\gamma_{opt}$). The different geometric parameters of project are assumed such as ratio of interrupted length to the fin length and the ratio of thickness to the fin length at different temperature. Results show the employment of fin interruption technique for resetting the boundary layer, which was causing reduced in thermal resistance. It was also concluded heat flux and heat transfer coefficient direct proportional with the temperature difference. Another significant parameter is the value of $\gamma$ which has most advantageous at equal or less 25 after that there is not any significant on the value of Nu. The enhancing of thermal performance of the fin and the reduction of the weight of it as a result of adding interruption to a vertical fin.

**Key words:** fins; heat transfer; interrupted fins; natural convection.

## نمذجة رقمية لانتقال الحرارة بالحمل الحر من خلال زعانف غير متصلة مستطيلة المقطع

**د. علي عبد الرضا فرحان**
مدرس
قسم الهندسة الميكانيكية
كلية الهندسة-جامعة واسط

**د. عباس جاسم جبير**
مدرس
قسم الهندسة الميكانيكية
كلية الهندسة-جامعة واسط

**الخلاصة**

تم اجراء محاكات عددية على انتقال الحارة بالحمل الحر من خلال جدار احادي عمودي ذو زعانف غير متصلة مستطيلة المقطع. تم حل معادلات الاستمرارية،Naveries-Stokes والطاقة باستخدام برنامج Fluent15. لدراسة وحساب أداء الزعانف المنفصلة والحصول على أفضل نسبة بين الطول المتقطع الى الطول الزعنفة. تم أستخدام نموذج مستقر ، ثنائي الأبعاد لا أنضغاطي حيث تم حل المعادلات الحاكمة باستخدام نموذج Boussiuesq. خلال هذه الدراسة تم فرض عدد من المتغيرات الهندسية المختلفة مثل النسبة بين طول المتقطع الى طول الزعنفة، وسمك الزعنفة الى طولها عند درجات حرارة مختلفة. ان من أبرز النتائج التي تم التوصل اليها، ان استخدام الزعانف المتقطعة يعمل على حصول تقطيع في الطبقة المتاخمة الحرارية المتكونة على الزعانف والذي يعمل على تقليل المقاومة الحرارية. وجد ان الفيض الحراري ومعامل أنتقال الحرارة يتناسب مع الفرق في درجات الحرارة. وجد ايضا ان من اهم المتغيرات المؤثرة الاخرى هي قيمة $\gamma$ حيث تكون ذو ناثير فعال على قيمة عدد Nu عندما $\gamma \leq 25$. اما بعد هذه القيمة فان تأثيرها قليل. ان الزعانف الغير متصلة مستطيلة المقطع تزيد من الاداء الحراري وكذلك تعمل على تقليل وزن المصدر مما يؤدي الى تقليل كلفة التصنيع.

**الكلمات الرئيسية**: زعانف, انتقال الحرارة , الزعانف المقطعة , الحمل الحر

## 1. INTRODUCTION

Natural convection phenomena in enclosures is essential for reliable performance of high power density electronics. Buoyancy driven flows have many applications in a widely preferred phenomena for it. The Natural convection is one method of rejected heat, which little expensive, discreet and most dependable. The heat generated in electronics devices can be controlled by using Fin. In the design of efficient cooling system generally 55% of failure mechanisms in electronic devices are related to thermal effects. **Mostafaviet et al., 2013,** Presented compact relationship for the Nusselt number based on geometrical parameters for interrupted fins. A two-dimensional numerical model for investigation of fin interruption effects by using COMSOL Multiphysics software. The results show that interrupted fins enhance the thermal performance of the heat sink and reduce the weight of it. **Pathaket et al., 2013,**studied numerically using FLUENT 6.3, it was concerned with heated wall from the rectangular shape with a finned base plate to simulate the behavior of air under natural convection. It investigated different fin length and spacing. It concluded the fin number (i.e., decreasing fin spacing S/H) significant on the Nu. This value of Nu reaches a high value at certain values of (S/H) and with extra increased the number of fins, Nu starts to reduction.

**Edlabadkaret et al., 2008,** Submitted a numerical analysis using Computational Fluid Dynamics (CFD) software, FLUENT, for free convection together to a vertical heated plate in ambient air temperature. It was observed that among the three V-type partition plates, subjected to computational analysis, 900 V-partition plate gave the maximum heat transfer enhancement at 12% and 15.27% for vertical and horizontal partition plate respectively. **Wankar, and Taji, 2012**, developed experimental setup to study the effect of free convection on rectangular fin model. The experimental parameters of this study were fin spacing, height and heater input. The wide range of length and spacing was tested with temperature difference. The study concluded that the Natural convection manner enhanced the transfer of heat with fin spacing 9-11 mm. It is noticed experimentally that the values of Nusselt based on ambient or Nusselt based on base where reached maximum value 7.86 and 58.35 respectively. Further, both Nusselt enhanced 81% and 27% respectively. **Sukumar R. S. et al., 2013,** Studied different models which icontained continuous, interrupted and interrupted fins with holes by using CFD simulation models. The study concluded that the interrupted fins are efficient than continuous, also find the better performance when used interrupted fins with hole as a result make reduction of fin's weight.

## 2. PROBLEM STATEMENT

A schematic of the considered heatsink geometry with interrupted rectangular is shown in Fig. 1. The growth of boundary layer already started when the wall is heated immediately, at the surface of the adjoining fins. At the long channel the boundary layer is continuously especially when the fins/channels are sufficiently long creating fully developed channel flow. **Bejan**, **1984**, Interrupted fins dislocate the thermal boundary layer growth, maintaining a thermally developing flow system, which result a higher natural heat transfer coefficient.

In this study the Fluent software **ANSYS Fluent** has been implemented to investigate the performance of 2-D interrupted fins and the effects of fin interruption, then finding of an optimum fin interruption to fin length ratio and fin length to fin thickness. It started by using the existing analytical models **Bar-Cohen and Rohsenow, 1984**, and **Tamayol et al., 2011** .The idea is to decouple the effect of fin spacing from the fin interruption. In the present study, it has been used the optimum fin spacing value of 9.5 mm according to Rosenhow-Bar-Cohen model, **Bar-Cohen and Rohsenow, 1984**.

## 3. NUMERICAL ANALYSIS

Advanced solver technology provides fast, accurate CFD results, flexible moving and deforming meshes, and superior parallel scalability. Computational Fluid Dynamics (CFD) procedures solve all the interacting governing equations in a coupled manner, albeit in a finite framework. With a careful use of CFD, its results could be used to validate those of the theoretical models, at least qualitatively.

### 3-1 Modelling in GAMBIT

For the simulation part, the model is designed by using GAMBIT 2.4.6 for this configuration. This software is provided with the advanced geometry and meshing tools. The functions of GAMBIT are design the two dimensional (2-D), setup the boundary condition for each edge and faces, and provide the meshing analysis for each configuration. The data are for heat sinks with fin length of L = 1400 mm and fin spacing of S = 9.5 mm. The interrupted fins have been modeled with the various values of $\zeta$ which represents the ratio of the fin length $l$, to the fin thickness t, ($\zeta$ = 5, 7.5,10 and 15) and with various values of $\gamma$ which represent the ratio of the interrupted length, G to the fin length, $l$, ($\gamma$ =5, 10 and 30) as shown in **Fig.1**.

The numerical examination of the flow behavior of air under the steady state condition has been studied at both the inlet and outlet of interrupted fins. The fluid flow calculation has been simulated using FLUENT software. The buoyancy driven flow in the system was assumed to be laminar based on previous studies. The boundary condition of model is defined the situation occur at the surface condition in term of friction. Meanwhile, defining the meshing is vital in order to discrete each part to certain section for more accuracy FLUENT's analysis. It is important to define model, meshing, and boundary conditions before running into FLUENT. The suitable boundary conditions are needed for a successful computational work. After creating a geometry which have one surface defined the specify boundary types of heat sink, the fin length such as the isothermal wall , while the entry and exit zones type is Inlet and Outlet-Pressure boundary and interruption length is symmetry as shown in **Fig.2**.The surface was meshed for the heat sink using a Quad element of Pave schema type in the space interval size (0.001) chosen as shown in **Fig.3**, the Gambit grid generator used approximately (0.5) million computational cells for different cases. No-slip condition is applied for velocity and temperature on the walls.

### 3-2 Simulation with FLUENT

FLUENT solves the governing integral equations for the conservation of mass, momentum, energy. There are two processors used to solve the flow and heat transfer equations. The first

preprocessor is the program structure which creates the geometry and grid by using GAMBIT. The second post processor is solving Navier-Stokes equations which include continuity, momentum and energy. **Bocu and Altac, 2011.**
The set of conservation equations are:
Mass conversion equation

$$\nabla . V = 0 \quad (1)$$

Momentum.

$$(V.\nabla)V = -\frac{1}{\rho}\nabla P + v\nabla^2 V + g\,\beta(T - T_o)j \quad (2)$$

Energy.

$$(V.\nabla)T = \alpha\,\nabla^2 \mathrm{T} \quad (3)$$

The analysis is carried using laminar flow. The effect of density variation with temperature estimated by Boussinesq approximation. In the current study there are different wall temperatures of (20 ,30 ,40 ,50 ,60 and 100 ºC) will be used. The interruption region used the symmetry boundary condition when there is no heat flux in the direction normal to the fin surfaces. The pressure inlet and outlet boundary condition are applied to the channel inlet and out let which define at inlet and outlet as static/gauge pressure boundary. ‘‘A no-slip isothermal solid surface is considered for the walls. **Fig. 2**, shows the numerical simulation of the domain considered, along with the chosen boundary conditions for continuous and interrupted fins’’. The initially condition for second order is used in this study.

## 4. SIMULATION RESULTS

### 4-1 Validation of the Present Work

The present numerical simulation results have been validated with **Mostafavi, G. 2012**. In **Fig.4,** it can be seen that there is a good agreement between our numerical simulation results with the correlation equation of it and the error is not more than 6%.

### 4-2 The Variation of Heat Sink on Temperature and Velocity Distribution.

A single channel has been chosen to show the effect of interrupted length on the temperature and velocity distribution. **Figs. 5. to 8.** show the temperature and velocity distribution contours. The effect of interruption length on the thermal boundary layer could be noticeably observed. The figures show also the effect of repeated interruption on temperature distribution and restore the thermal boundary layer in the channel. The repeated resetting is lead to delay the flow to get the fully-developed condition.
The development of flow in the channel can be seen through a largamente regions. The flow in the lower, middle and top regions is non uniform developing flow due to discontinuous of the thermal boundary layer. The velocity increases as the channel height increase due to the buoyancy effect.

### 4-3 The Variation of the Interruption Length

The effect of important parameters on heat transfer from interrupted rectangular fins has been investigated. The effect of the fin length *l* and fin interruption length G on Nusselt number is shown in **Figs. 9 to 14.** It is clear that the relation between $\xi$ and the Nusselt number was directly proportion. Which is meaning the heat transfer coefficient improved. These Figures prevail if the fin length is constant, and G is variable, it can conclude that the Nusselt number increases. Another significant parameter the value of $\gamma$ which is most advantageous when $\gamma \leq 25$ after that not any significant on the value of Nusselt number.

### 4-4 The Variation of Temperature Difference

The relation between Nusselt number and $\gamma$ with different temperatures (different heat fluxes) can be seen in **Figs. 15. to 18.** The result shows the Nusselt number has increased when the $\gamma$ and temperature of fins wall was increased. In another word when the heat flux increases the heat transfer coefficient enhanced. Therefore the increasing of fin interrupted length causes an increase in the heat flux due to butter interruption in the thermal boundary layer, as well as the number of interruption length.

### 4-5 The Effect of Different Temperature on Heat Flux and Heat Transfer Coefficient

The numerical simulation result of the heat flux from heat sink with interrupted fins as a function of different wall temperatures are shown in **Figs. 19. to 22**. As it was expected the heat flux improves as $\gamma$ increases (i.e., as G increases). The increasing of heat flux due to enhance interruption in thermal boundary layer. It is clear from **Figs. 23. to 26** depict the relation between different temperature and heat transfer coefficient with different $\gamma$. This show that the heat transfer coefficient enhances as the different temperature and $\gamma$ increase. Further the effect of different temperatures have not significant on the heat transfer coefficient when the temperature is greater than 70 $^{o}$C in all cases. That means the interruption length leads to a higher thermal performance due to the fact that interrupted fins dissipation the thermal boundary layer growth, thus, leads to a higher natural heat transfer coefficient.

## 5- CONCLUSIONS

Numerical studies have been performed for free convective heat transfer from installed interrupted rectangular fins in order to find the relation between heat sink with different parameters (such as fin length and interrupted length) and heat transfer coefficient. The following conclusion can be considered as follows:

- The most significant component of the current study is the strength of character of the effect of interruption length in natural convection fin. The purpose of employment the fin interruption technique for resetting the boundary layer, which was causing reduced in thermal resistance.

- The increasing the fin interruption length and the number of interruptions cause an increasing in the heat flux which is a result of the frequent resets imposed on to the thermal boundary layer, in other word "better" interruption occurs in the thermal boundary layer.
- In this study the optimum ratio of interrupted length to fin length ($\gamma_{opt}$) is a function of surface temperature, for different length ( 12.5 mm<$l$<37.5 mm), as follows.

$$\gamma_{opt} = \left(\frac{G}{l}\right)_{opt} = C\left(\frac{T_w - T_{amb}}{T_{amb}}\right)^n$$

Where C = 11 and n = -2.18

- The heat flux, and the heat transfer coefficient are direct proportion with the temperature difference. Another significant parameter the value of $\gamma$ which is most advantageous ≤ 25 after that there is not any significant on the value of Nusselt number.

## REFERENCES


- Bejan A., 1984, *Convection Heat Transfer*, Wiley, New York.
- ANSYS Fluent (ver. 15) *Computational Fluid Dynamics Softrware, ANSYS*, Inc. Academic.
- Bar-Cohen and Rohsenow, *Thermally Optimum Spacing of Vertical, Natural Convection Cooled, Parallel Plates,*1984, J. Heat Transfer Vol. 106,pp-116-124.
- Mostafavi G., 2012, *Natural Convective Heat Transfer from Interrupted Rectangular Fins*, Thesis in Master of Applied Science, School of Engineering Science Faculty of Applied Sciences, Simon Fraser University Fall.
- Mostafavi Golnoosh, Mehran Ahmadi and Majid Bahrami,2013, *Effect of Fin Interruptions on Natural Convection Heat Transfer from A rectangular Interrupted Single-Wall*, International Technical Conference and Exhibition on Packaging and Integration of Electronic and Photonic Microsystems InterPACK2013 Burlingame, CA, USA.
- Pathak, M. K., Mer, K. K. S. and Pawan K. P., 2013, *Numerical Analysis of Natural Convection in Rectangular Enclosure with Heated Finned Base Plate*, IJRMET Vol. 3, Issue 2,pp-64-67.
- Edlabadkar, R. L., N. K. Sane and Parishwad, G.V., 2008, *Computational Analysis of Natural Convection with single V-Type Partition Plate*, 5th European Thermal-Sciences Conference, The Netherlands.

- Tamayol, F. McGregor, E. Demian, E. Trandafir, P. Bowler and M. Bahrami, 2011, *Assessment of Thermal Performance of Electronic Enclosures with Rectangular Fins: A passive thermal solution*," in ASME pacific rim technical conference and exhibition on packaging and Integration of electronic and photonic systems, Portland, Oregon, USA,.

- Sukumar, R. Sam, G. Sriharsha, S. Bala Arun, P. Dilip kumar, Ch. Sanyasi Naidu,2013 *,Modelling And Analysis of Heat Sink with Rectangular Fins Having Through Holes,*International Journal of Engineering Research and Applications (IJERA) ISSN: 2248-9622 www.ijera.com, Vol. 3, Issue 2, March -April 2013, pp.1557-1561.

- Vinod M. Wankar and S.G. Taji, 2012, *Experimental Investigation of Flow Pattern on Rectangular Fin Arrays under Natural Convection*, International Journal of Modern Engineering Research (IJMER), Vol.2, Issue.6, pp-4572-4576.

- Z. Bocu, Z. Altac, 2011, *Laminar Natural Convection Heat Transfer and Air Flow in Three-Dimensional Rectangular Enclosures with Pin Arrays Attached to Hot Wall*", Applied Thermal Engineering, 31, , pp. 3189-3195.


## NOMENCLUTER

| Symbol | Description | Unit |
|---|---|---|
| G | interrupted length | m |
| g | gravitational acceleration, | $m/s^2$ |
| h | heat transfer coefficient | $W/m^2k$ |
| j | unit vector in y-direction | |
| L | total length | m |
| *l* | fin length | m |
| Nu | nusselt number | |
| P | pressure | $N/m^2$ |
| S | fin spacing | m |
| T | temperature | C° |
| V | velocity | m/s |
| α | thermal diffusivity | |

| | | |
|---|---|---|
| β | thermal expansion coefficient | $K^{-1}$ |
| ∇ | divergence | |
| γ | ratio of the interrupted length, G to the fin length, *l* | |
| ζ | the ratio of the fin length *l*, to the fin thickness t | |
| ν | kinematic viscosity | $m^2/s$ |
| ρ | fluid density | kg/m3 |
| C , n | constant | |

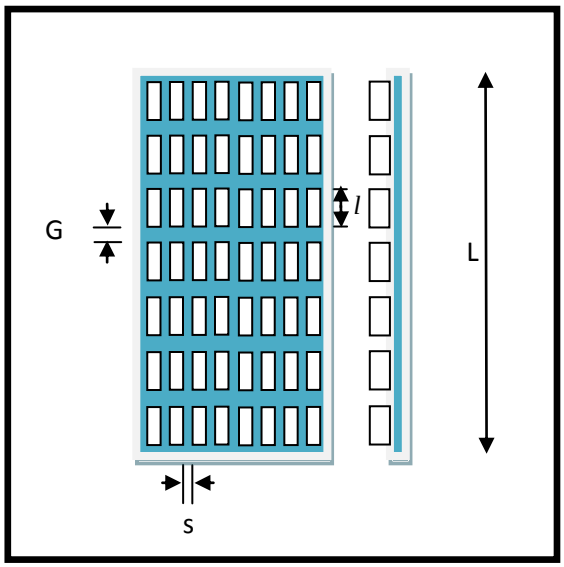


**Figure 1.** Schematic of the considered heatsink geometry interrupted rectangular.

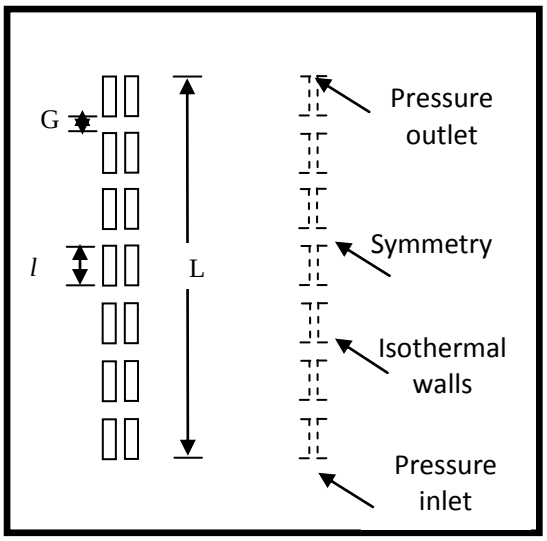


**Figure 2.** Schematic of the numerical domain of interrupted fins and boundary conditions.

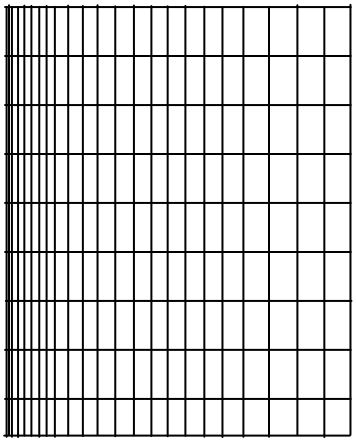

**Figure 3.** Grid used in the model .

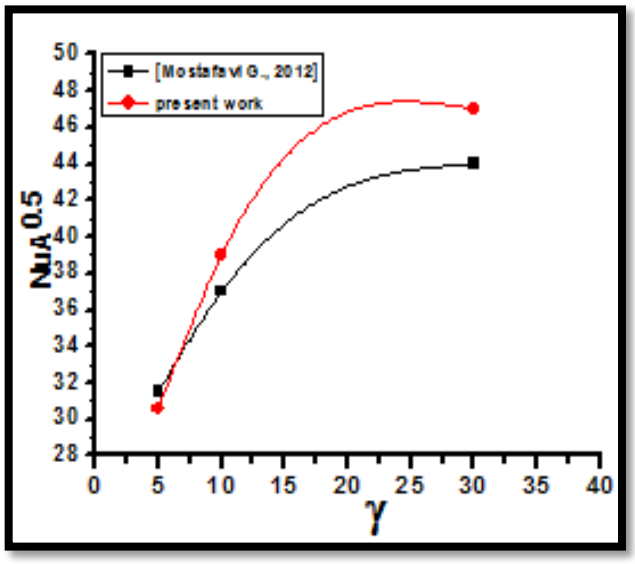


**Figure 4.** Validation of computational analysis graph.

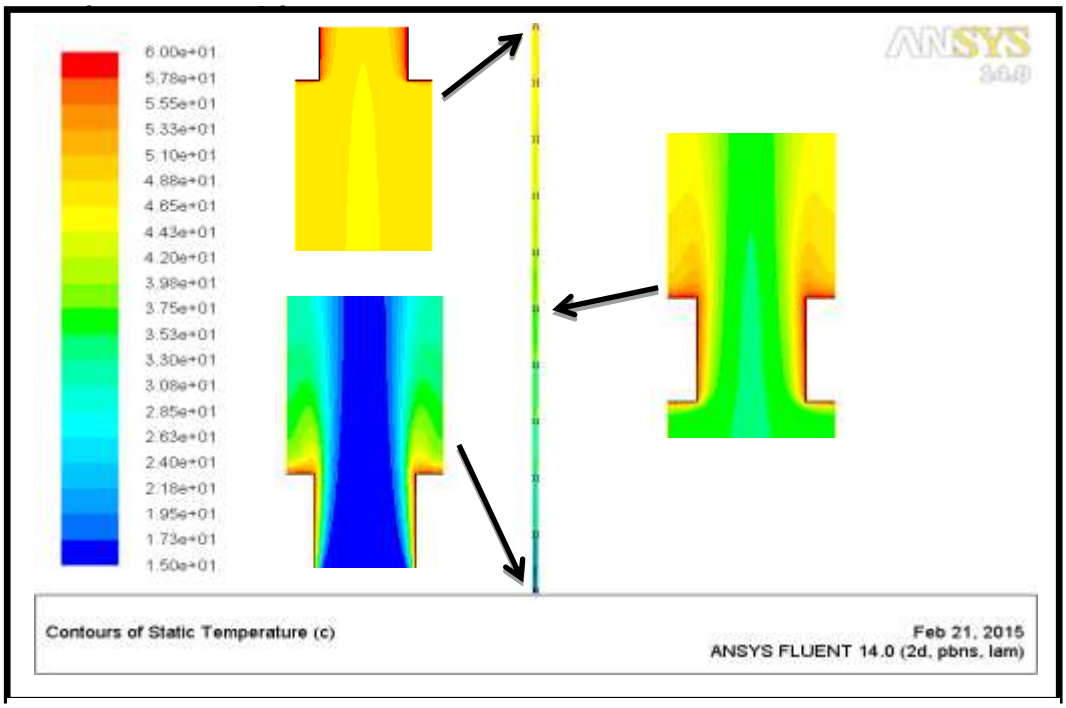


**Figure 5.** Temperature distribution contours of the inturrputed fins for $\zeta$=5 and $\gamma$=10 with isothermal temperature = 60 $^{o}$C.

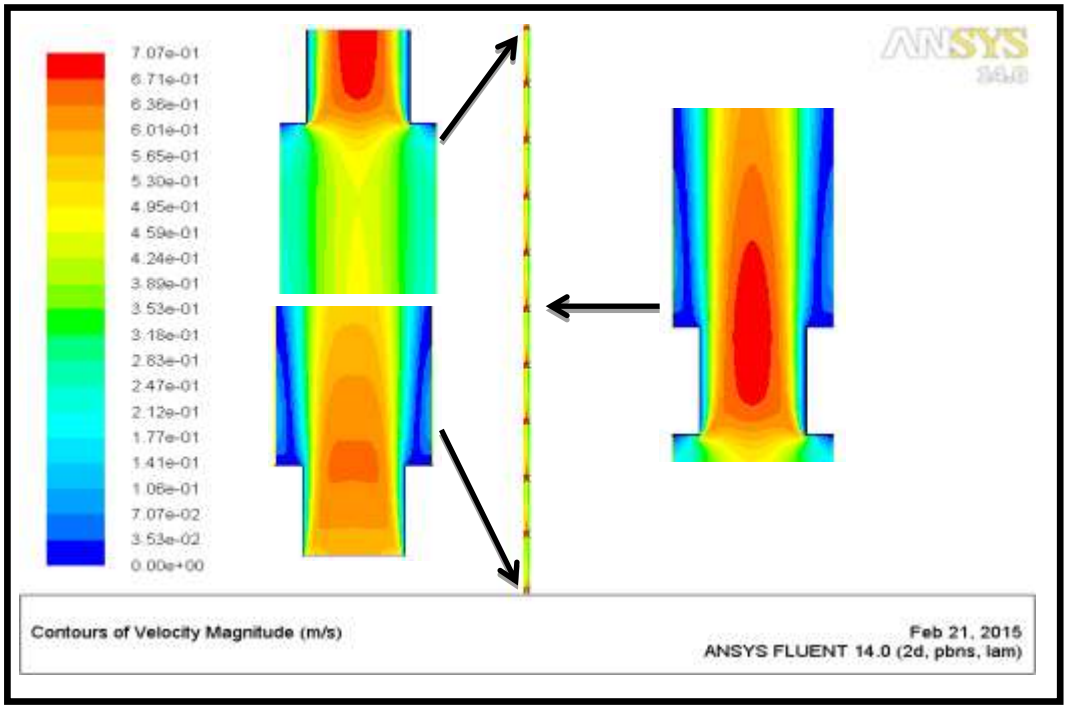


**Figure 6.** Velocity distribution contours of the interrupted fins for $\zeta$=5 and $\gamma$=10 with isothermal temperature = 60 $^{o}$C.

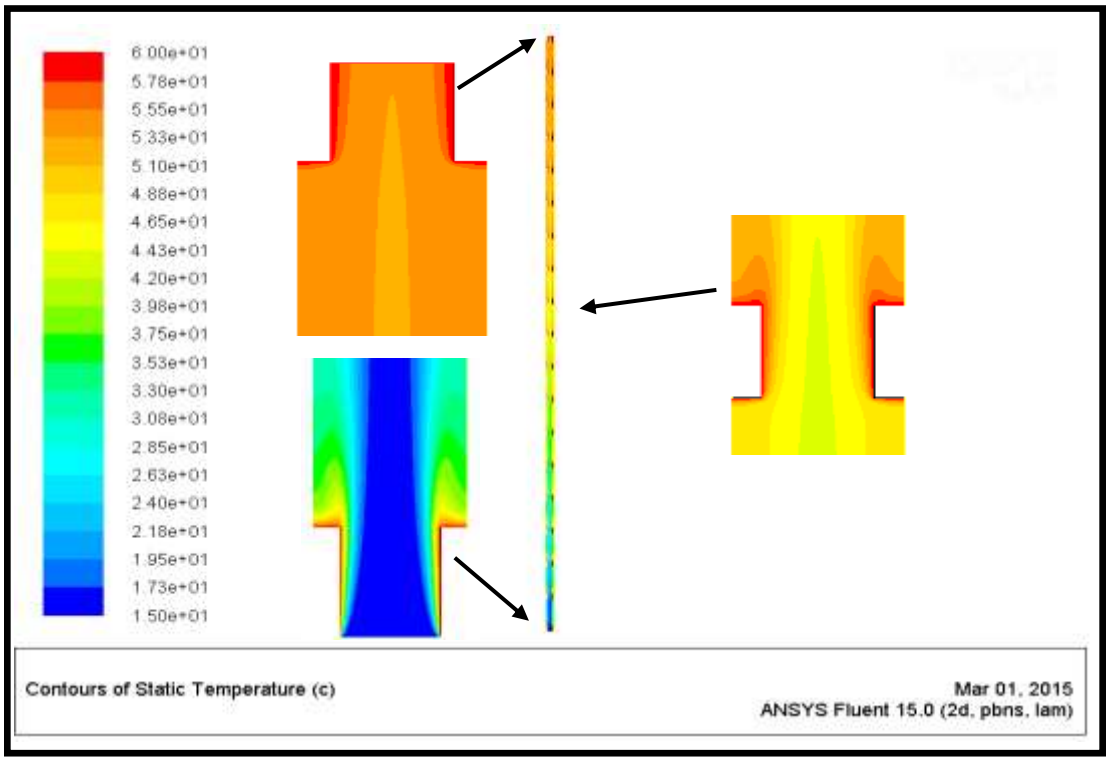


**Figure 7.** Temperature distribution contours of the interrupted fins for $\zeta$=5 and $\gamma$=5 with isothermal temperature = 60 $^{o}$C.

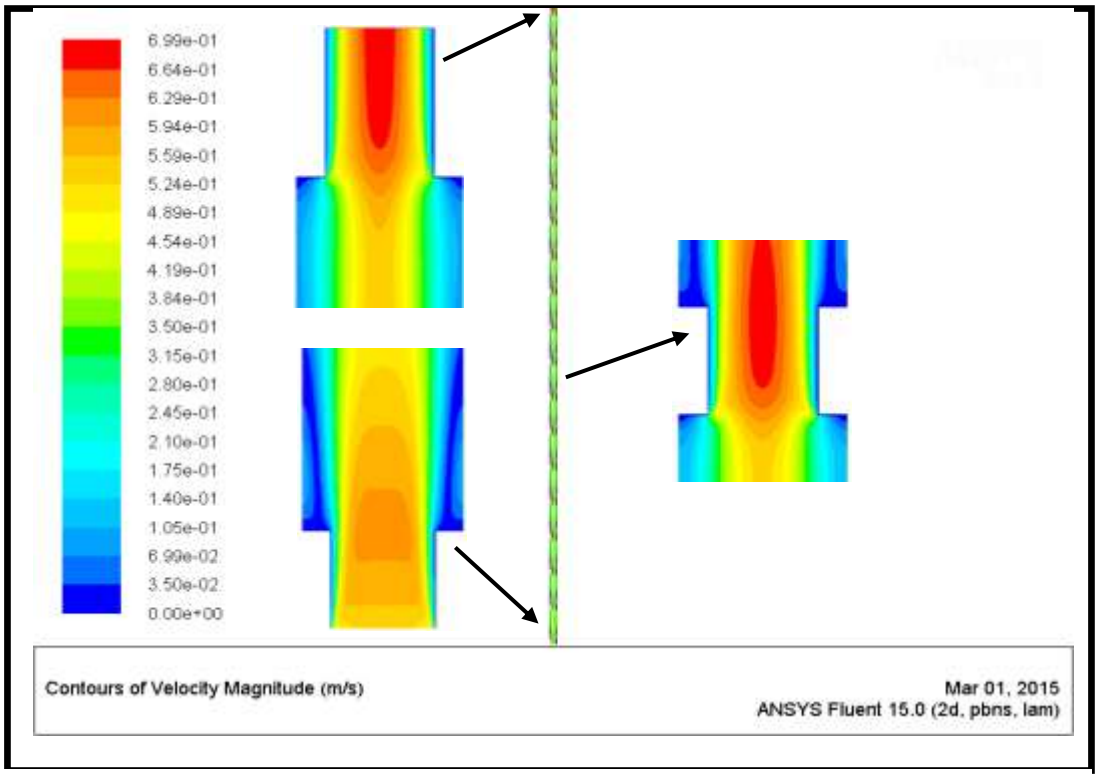


**Figure 8.** Velocity distribution contours of the interrupted fins for $\zeta$=5 and $\gamma$=10 with isothermal temperature = 60 $^{o}$C

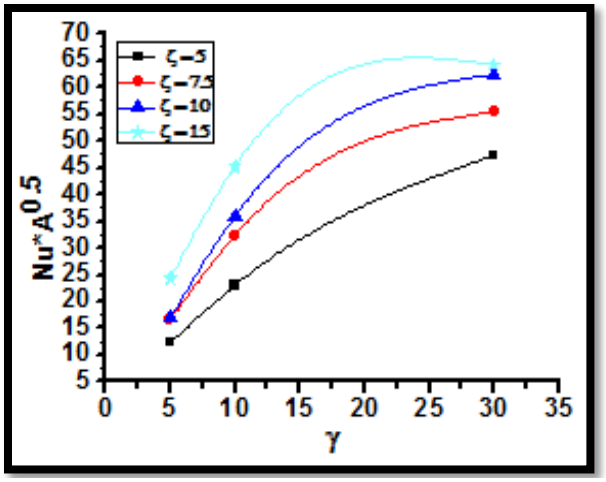


**Figure 9.** The effect of interruption length on Nu. With different $\zeta = l/t$ at T=20 $^{o}$C.

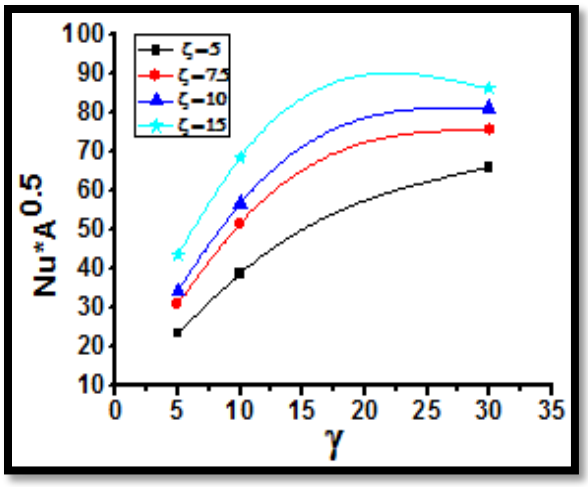


**Figure 10.** The effect of interruption length on Nu. With different $\zeta = l/t$ at T=30 $^{o}$C.

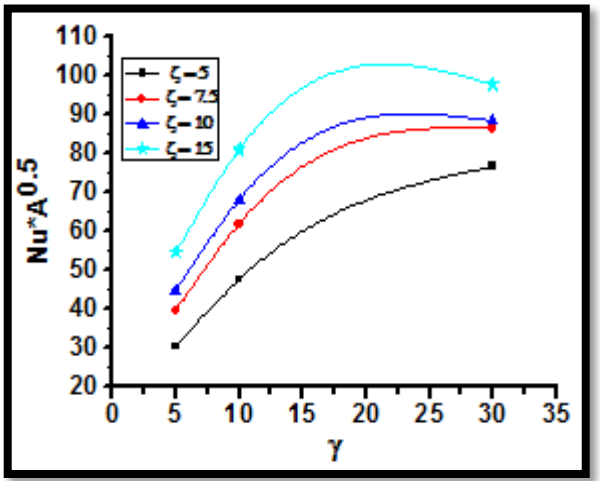


**Figure 11.** The effect of interruption length on Nu. With different $\zeta = l/t$ at T=40 $^{o}$C.

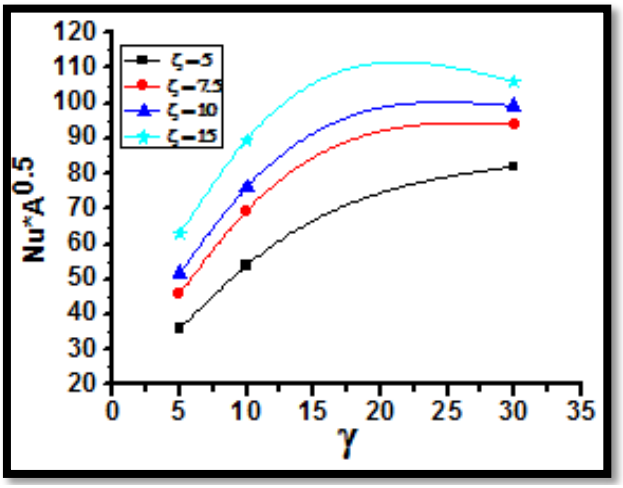


**Figure 12.** The effect of interruption length on Nu. With different $\zeta = l/t$ at T=50 $^{o}$C.

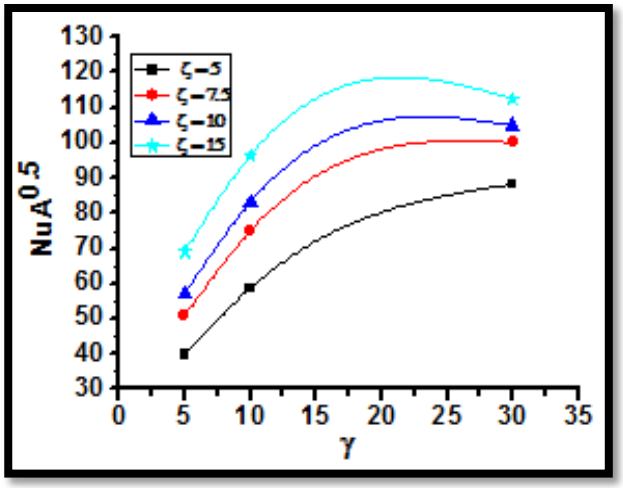


**Figure 13.** The effect of interruption length on Nu. With different $\zeta = l/t$ at T=60 $^{o}$C.

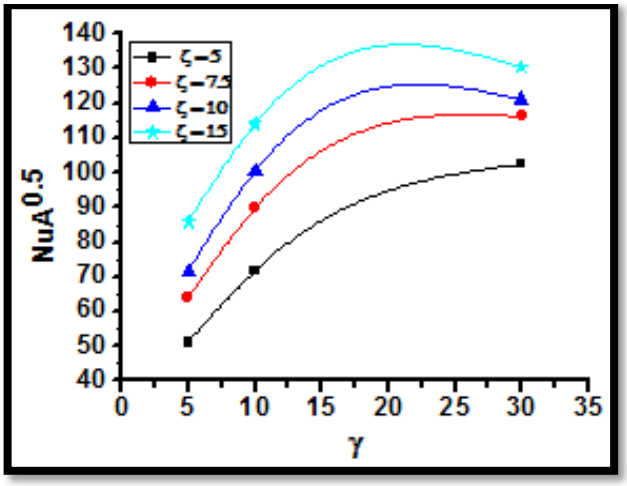


**Figure 14.** The effect of interruption length on Nu. With different $\zeta = l/t$ at T=100 $^{o}$C.

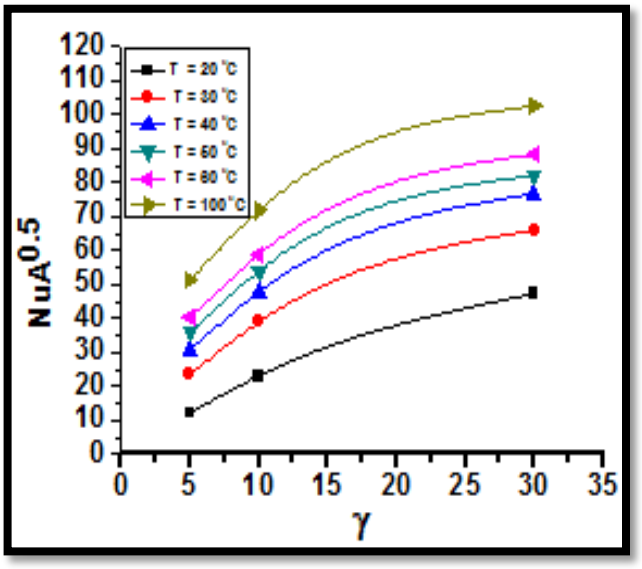


**Figure 15.** The effect of interruption length on Nu. With different temperature at $\zeta = 5$.

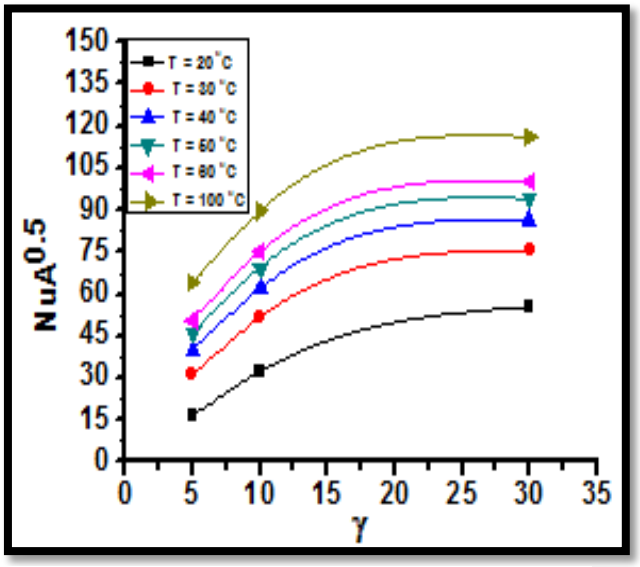


**Figure 16.** The effect of interruption length on Nu. With different temperature at $\zeta = 7.5$.

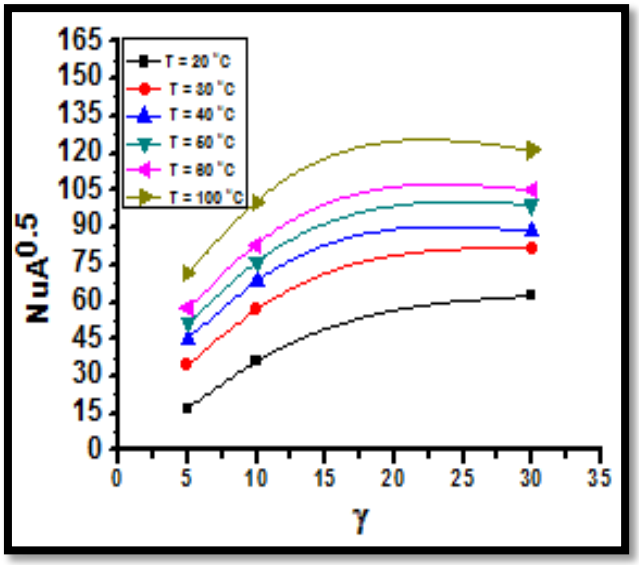


**Figure 17.** The effect of interruption length on Nu. With different temperature at $\zeta = 10$.

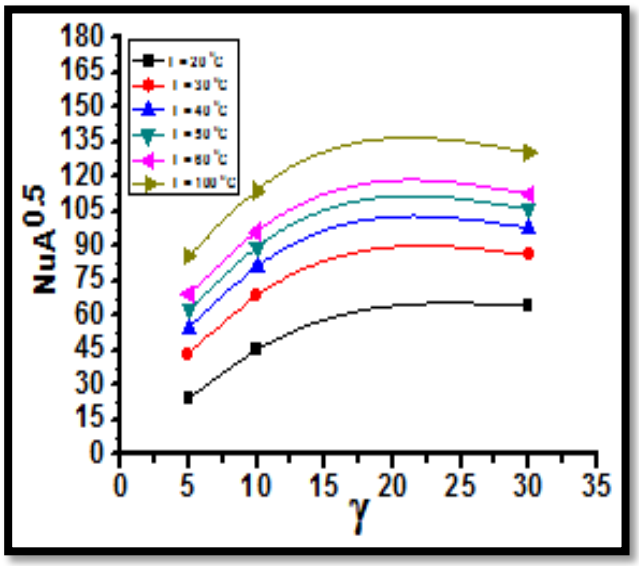


**Figure 18.** The effect of interruption length on Nu. With different temperature at $\zeta = 15$.

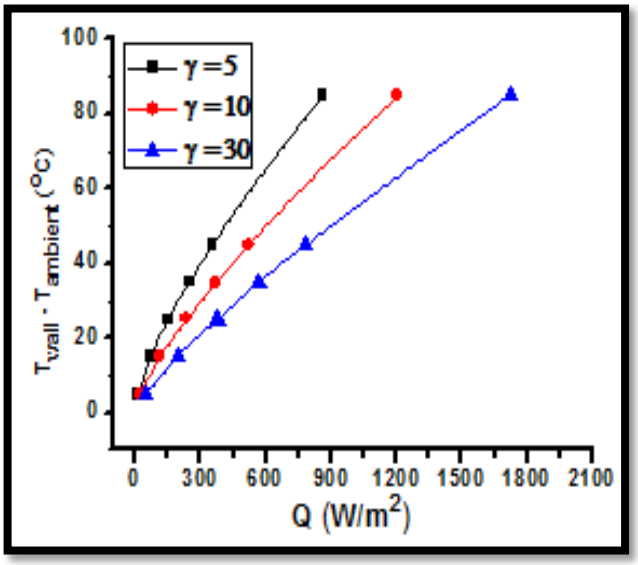


**Figure 19.** The effect of heat sink on heat flux with different $\gamma$ at $\xi$ =5.

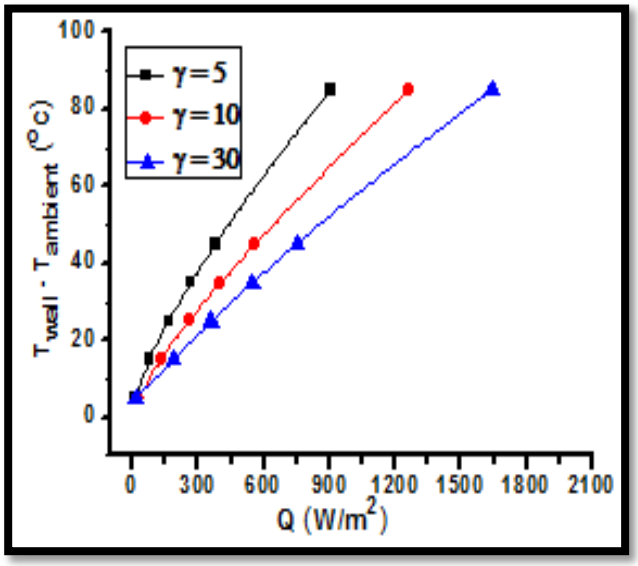


**Figure 20.** The effect of heat sink on heat flux with different $\gamma$ at $\xi$ =7.5.

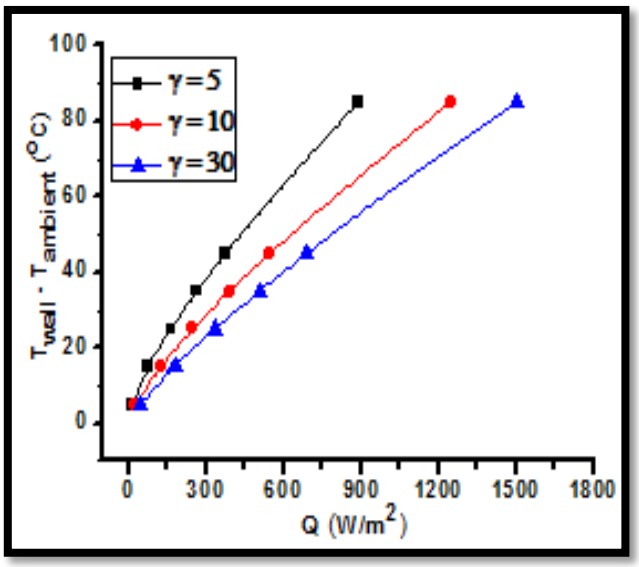


**Figure 21.** The effect of heat sink on heat flux with different $\gamma$ at $\xi$ =10.

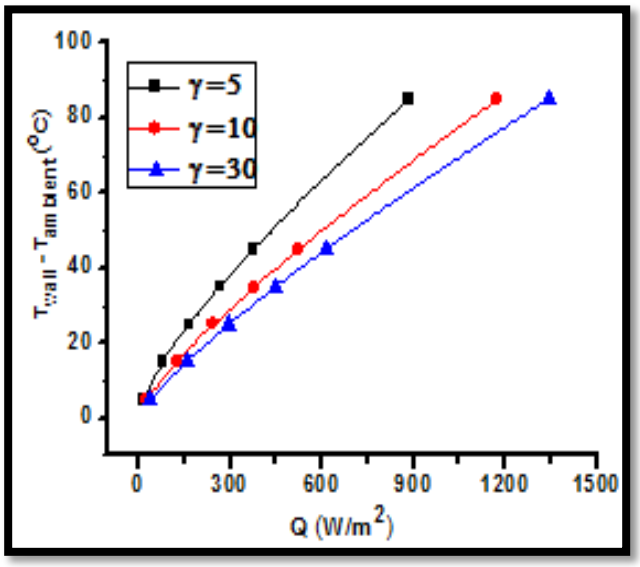


**Figure 22.** The effect of heat sink on heat flux with different $\gamma$ at $\xi$ =15.

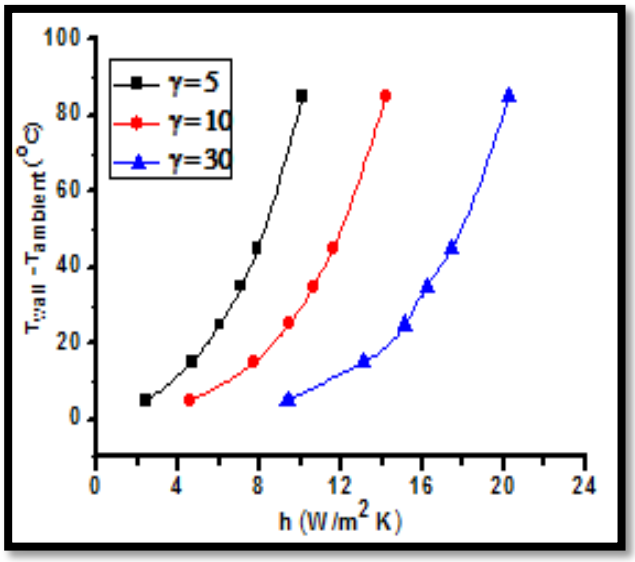


**Figure 23.** The effect of heat sink on heat transfer coefficient with different $\gamma$ at $\xi$=5

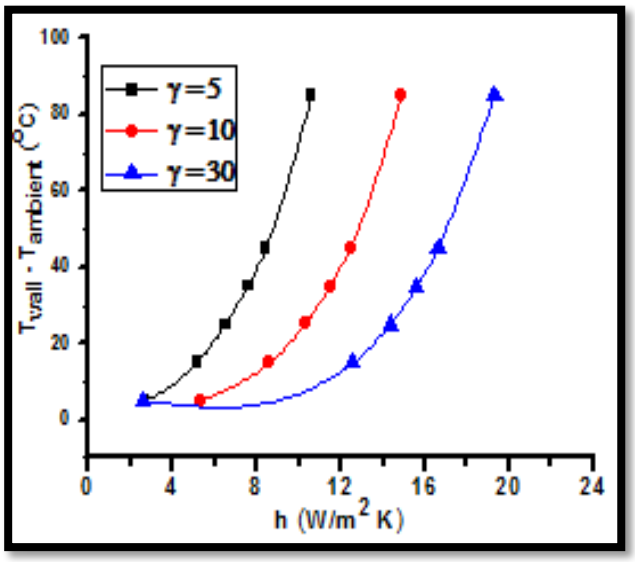


**Figure 24**. The effect of heat sink on heat transfer coefficient with different $\gamma$ at $\xi$ =7.5.

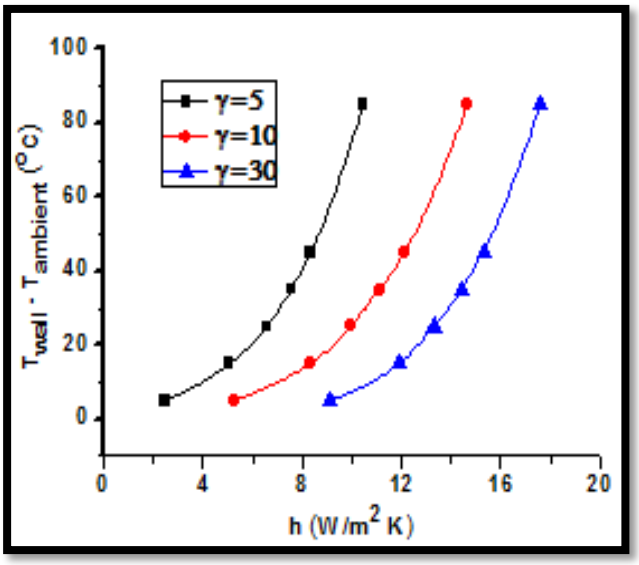


**Figure 25.** The effect of heat sink on heat transfer coefficient with different $\gamma$ at $\xi$ = 5

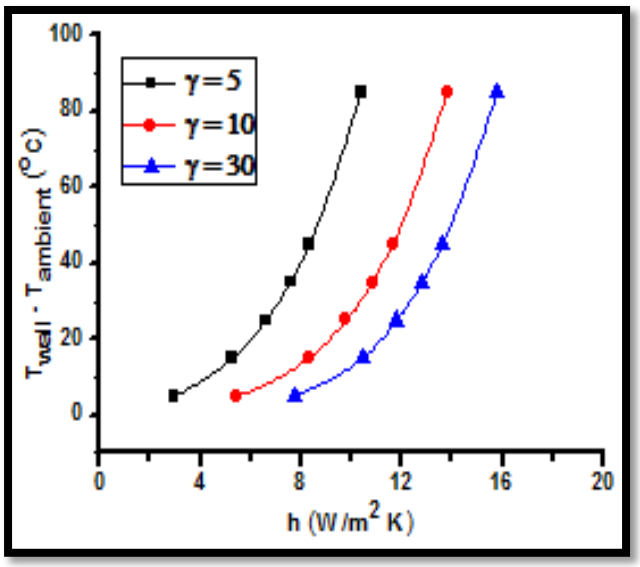


**Figure 26.** The effect of heat sink on heat transfer coefficient with different$\gamma$at $\xi$ =7.5.

# Quality Assurance for Iraqi Bottled Water Specifications

**Dr. May George Kassir**
Asst. Prof.
Production Engineering and Metallurgy / University of Technology
Email: may_kassir@yahoo.com

**Dr. Lamyaa Mohammed D.**
Prof.
Production Engineering and Metallurgy / University of Technology
Email:lamya_alkazaai@yahoo.com

**Fatin Fuad**
Asst. Lect.
Production Engineering and Metallurgy / University of Technology
Email:fatinfuad_87@yahoo.com

## ABSTRACT

In this research the specifications of Iraqi drinking bottled water brands are investigated throughout the comparison between local brands, Saudi Arabia and the World Health Organization (WHO) for bottled water standard specifications. These specifications were also compared to that of Iraqi Tap Water standards. To reveal variations in the specifications for Iraqi bottled water, and above mentioned standards some quality control tools are conducted for more than 33% of different bottled water brands (of different origins such as spring, purified,..etc) in Iraq by investigating the selected quality parameters registered on their marketing labels. Results employing Minitab software (ver. 16) to generate X bar, and Pareto chart. It was found from X bar charts that the quality parameters of some drinking bottled water brands are not within Iraqi standards set by the "Central Agency for Standardization and Quality Control" such as pH values, Fe, Na, and Mg concentrations.

While the comparison of previously mentioned standard specifications through radar chart many important issues are detected such as the absence of lower limits the whole bottled water quality parameters such as for Na and Mg also the radar chart shows that Iraqi bottled and tap water specifications are almost equal in their quality values. Also the same chart pictured the limited range of Iraqi specifications compared to that of Saudi Arabia, and WHO and the need to introduce other water specifications such as K, Na, etc. This confirms the need to improve Iraqi bottled water specifications since it was introduced on 2000.

These results also highlighted the weakness of quality assurance activities since only 33 % of the investigated companies registered the whole water quality specifications as shown in Pareto chart. Other companies do not register any quality characteristics. Also certain companies should be stopped due to non-conforming specifications, yet these companies are still producing and selling their products in the local market. Quality assurance requires continually monitor the reliability (accuracy and precision processes) of Iraqi drinking bottled water companies to match the Iraqi Specification Standards, and those companies should continually approve "How good (accurate and precise) is their product( water quality) produced?".

**Key words:** quality assurance, Iraqi bottled water, labels, tap water, specifications, WHO, control chart, radar chart. Pareto chart.

# ضمان نوعية مواصفات المياه العراقية المعبأة بالقناني

**د. مي جورج امين**
استاذ مساعد
هندسة الانتاج والمعادن / الجامعة التكنولوجية

**د. لمياء محمد داود**
استاذ
هندسة الانتاج والمعادن / الجامعة التكنولوجية

**فاتن فؤاد عبد الرزاق**
مدرس مساعد
هندسة الانتاج والمعادن / الجامعة التكنولوجية

**الخلاصة**

تم في هذا البحث التحقق من مواصفات مياه الشرب المعبأة بالقناني اعتماداً على البيانات المسجلة على الملصق التعريفي لشركات محلية والمقارنة بينها وبين المواصفات العراقية القياسية والمواصفة السعودية , و المواصفة القياسية لمنظمة الصحة العالمية للمياه المعبأه بالقناني . كما تمت مقارنة هذه المواصفات مع المواصفات العراقية القياسية لماء الشرب من الحنفية. لغرض استعراض التباين في المواصفات العراقية والمواصفات المذكوره اعلاه لاكثر من 33 % من الشركات المحلية المنتجة للمياه المعبأة بالقناني (من مصادر مختلفة مثلا ينابيع , مياه منقاة, ....الخ) استخدم بعض ادوات السيطرة النوعية ومخطط الرادار للمقارنة بين مختلف الخواص النوعية المنتخبة لمنتوجات تلك الشركات كما مثبت على ملصقاتها التجارية. تم استخدام برنامج ميني تاب (أصدار 16) لغرض توليد كل من لوحة السيطرة للمتوسط لمختلف الخواص النوعية و لمخطط باريتو. وجد من لوحة السيطرة للمتوسط ان بعض الخواص النوعية لبعض العلامات التجارية للمياه المعبأة ليست ضمن المواصفات العراقية المعدة من قبل" الجهاز المركزي للتقييس والسيطرة النوعية " كما في قيمة الدالة الحامضية وتراكيز كل من ( الحديد و المغنيسيوم و الصوديوم ). بينما اظهر مخطط الرادار وعبرالمقارنة بين المواصفات القياسية المذكورة انفاً عدة مؤشرات اهمها خلو المواصفة العراقية للحدود الدنيا لاي خاصية من الخواص القياسية للمياة المعبأة والذي من المهم ادراجه في المواصفة كما في الحدود الدنيا لمادتي الصوديوم و المغنيسيوم . كما اظهرت نتائج نفس المخطط التقارب الشديد بين مواصفات مياه الشرب من الحنفية والمياه المعبأة . وايضاً اظهرت النتائج محدودية المواصفات العراقية المدرجة مقارنة مع المواصفة السعودية ومواصفة منظمة الصحة العالمية من حيث خلوها من بعض المواصفات المتعلقة بتركيز البوتاسيوم و الصوديوم وغيرها مما يشير الى ضرورة تطوير المواصفة العراقية كونها اصدار عام 2000.

كما بينت نتائج البحث ضعف اجراءات ضمان النوعية حيث اظهر مخطط باريتو ان 33% فقط من الشركات قيد البحث قد سجلت كل مواصفات المياه اما بقية الشركات فلم تدرج في ملصقها التعريفي اي مواصفة. كذلك ضرورة تعليق انتاج بعض الشركات المنتجة للمياه المعبأة بسبب عدم مطابقة مواصفات منتوجها مع المواصفات القياسية العراقية علما ان هذه الشركات مستمرة بالانتاج وتزود السوق المحلية بمنتجاتها. ان ضمان النوعية يتطلب عملية مراقبة مستمرة لموثوقية (دقة وضبط العمليات) للشركات العراقية المنتجة للمياه المعبأة بالقناني للمواصفات العراقية القياسية, وعلى الشركات ان تثبت باستمرار كم هي دقيقة ومضبوطة منتجاتها (نوعية المياه) المنتجة.

**الكلمات الرئيسية** : ضمان النوعية, المياه العراقية المعبأة ,الملصق التجاري , مياه الحنفية , المواصفات, منظمة الصحة العالمية, لوحة السيطرة للمتوسط , مخطط الرادار , مخطط باريتو.

## 1- INTRODUCTION

Although Iraq has two major rivers as natural water sources, these sources are generally polluted, biologically and chemically as a result of lack in appropriate systems for safe disposal of sewage, wastewater, industrial, agricultural and medical waste. Water treatment plants, pumping stations and water networks suffered from lack of maintenance resulting breakdown ,**Stars Orbit Consultants and Management Development, 2010**. In general, the quality of water is equally important as its quantity therefore; water quality is considered as the factor to judge environment changes which are strongly associated with social and economic development ,**Toma, et al., 2013**. Bottled water can be defined as any potable water that is manufactured, distributed or offered for sale, sealed in food-grade bottles or other sanitary container and intended for human consumption Sources of water in bottled water may be springs, wells, or other approved sources, the water inside these bottles may be distilled, Carbonated, Ozonized or filtered ,**Toma, et al., 2013 and Alabdula'aly, and Khan, 1999**.

In developing countries about 1.8 million people, mostly children, die every year as a result of water related diseases. Tap water may be harmful to human health due to contamination with microbes. Tap water quality may change as a result of exposure to the surrounding environment as open tanks or in pipes throughout distances before reaching the consumers ,**1991 , والعزاوي ,المفرجي and Fadhel, 2010**. The most important characteristic of bottled water over tap water is the quality, especially in terms of taste and regularity. Therefore, bottled drinking water is one of the most important sources of drinking water not only in Iraq, but also in the entire world ,**World Health Organization (WHO), 2004**. Bottled water industry is one of the most thriving industries, in Iraq and worldwide. It is the fastest growing drink choice where water consumption worldwide is increased by average 10% annually, therefore, became the most dynamic sector of all food and beverage industries due to accessibility, relatively low cost, better taste, and lower level of impurities , **Saravanan and Nagarajan, 2013, and 2008 رزوقي والراوي** . The bottled drinking water industry in Iraq represents 54% over other food industries, more than 100 factories are registered (excluding the northern government) these factories produce about 160 Million $m^3$/yr. The factories authorized in Iraqi were 10 factories until the end of 2006; currently 234 factories are under construction distributed on the different Iraqi governorates. This increase is driven by decrease in tap water quality, the lack of control that offers high risk practices that contribute in environmental degradation, contamination of natural water resources, and the percentage of failure to conform health requirements to Iraqi Standard Specifications released on (2000) , **2010 , العزاوي واخرون**. Baghdad and other governorates are the most affected areas knowing that the highest production rates of bottled water factories is also in Baghdad about 11 Million $m^3$/yr ,**المديرية العامة للتنمية الصناعية**.

In this research quality control tools is conducted for more than 33% of different bottled water brands in Iraq by investigating the quality parameters registered on their marketing labels. Since quality reported in different bottled water labels should continually be assured so that companies could answer to the question "How good" (accurate and precise) they are ,**U.S. Environmental Protection Agency Office of Research and Development, 1979**. The collected data are analyzed and compared to Iraqi, Saudi Arabia, and World Health Organization (WHO) Standards so as to investigate differences in quality characteristic. Also to inform consumers that are not involved in the operations of this product quality as it is the goal of quality assurance activities. In the next paragraph literature survey is conducted to prevail Iraqi and international interest in bottled water quality followed by analysis of results and discussion. Finally conclusions are presumed and stated.

## 2- LITERATURE SURVEY

The attention of many researchers is directed towards drinking bottled water quality as they studied water specifications from different aspect such as chemical, biological, etc. **Ahmed, and Bajahlan, 2009**. compared the quality of drinking bottled water with tap water; the results showed that there were no significant differences in the quality of tap water and drinking bottled water in Saudi Arabia. Their physicochemical analysis showed the persistent quality of tap water. Based on hardness analysis, bottled and tap water are categorized as soft water.

**Matloob, 2011**, evaluated Fluoride content of tap and drinking bottled water currently consumed in Babel governorate in Iraq to determine whether Fluoride intakes by Iraqi consumers fell within the recommended Iraqi ranges. It was found that the level of Fluoride is far below the level recommended by World Health Organization (WHO) and that of Iraqi tap water specifications.

**Semerjian, 2011**, collected 32 different bottled water brands, analyzed them into various physicochemical levels then compared results with Lebanese institution standards for bottled water, where many characteristics are investigated, yet the majority that met different bottled water standards for physicochemical parameters.

**Abdulraheem, et al., 2012**, focused on measurements and comparison of bacterial concentration of endotoxin in variety samples for tap water and bottled water in Kuwait using the Limulus Amoebocyte lysate test. Researchers proved that drinking bottled water has less endotoxin compared to that of tap water.

**Queiroz, et al., 2012**, presented data from two Canadian newspapers of national circulation, for tap water and bottled water. The researchers used quantitative and qualitative data for their analysis. They observed that the selected print media presented wide range of news reports that provide the reader with thoughts on the current situation of water supply quality in Canada. The media has been supportive to consumers with important advices to reduce health threats.

## 3 - QUALITY CONTROL TOOLS

Seven basic tools of quality is a designation of statistical techniques identified as being most helpful in troubleshooting issues related to quality. These tools can be used to solve the majority of quality-related issues. The seven tools are ;(Cause-and-effect diagram, Check sheet, Control charts, Histogram, Pareto chart, Scatter diagram and flow chart) ,**Montgomery, 2005, Kaoru, 1985, Masaaki, 1986 and Juran , 1951**.

In this research, control (X-bar) and Pareto charts were employed while Radar chart is used to show the range and differences among the Iraq Specification and other standards.

Quality control and quality assurance differs in their prime goal since, the prime purpose of quality control is to serve those who are directly responsible for conducting operations and help in regulating current operations. While quality assurance primary purpose is to serve those who are not directly responsible for conducting operations but who need to know (consumers) ,**Kazemzadeh, et al., 2013**.

In general, control chart is used to distinguish between variations in process resulted from common and that special causes. Every process has variations; this could be special cause variation. Other variations are simply the result of numerous, ever-present differences in the process ,**Miller and Freund, 1985 and Walkenbach, 2003**. Control chart (X-bar) to build need three principals lines are; the upper line ($UCL_X$ ) as the upper control limit and the lower line ($LCL_X$) as the lower control

the center line ($CL_X$ ) arithmetic mean ($\overline{X}$) limit, calculated according to equations below ,**Miller and Freund, 1985**.

$$CL_X = \frac{1}{n}\sum_{i=1}^{n} \bar{X}_i \quad (1)$$

$$\mathrm{UCL_X} = \mathrm{CL_X} + \frac{3\bar{R}}{d_2\sqrt{n}} \quad (2)$$

$$\mathrm{LCL_X} = \mathrm{CL_X} - \frac{3\bar{R}}{d_2\sqrt{n}} \quad (3)$$

Where; ($CL_X$) is the arithmetic mean of the measurements for
*X 1….n* denotes the number of samples.

If a point lies within UCL, LCL, then the process is deemed to be under control. Otherwise, a point plotted outside the control limits can be regarded as evidence representing that the process is out of control. The performance of a control chart, especially X-bar chart, is usually evaluated under the assumption that there are no errors in estimating the process standard deviation used to determine the control limits (this is, of course, not always the case in practice) ,**Saravanan and Nagarajan, 2013 and Miller and Freund, 1985**.

Pareto charts could be in both bars and line graph, where individual values are represented in descending order by bars, and the cumulative total is represented by the line. The vertical axis is the frequency of occurrence, while the vertical axis is the cumulative percentage of the total number of defect occurrences ,**Kaoru, 1985 and Masaaki, 1986**.

Although Radar chart is not one of the seven quality control tools but it represents an effective graphical diagram of displaying multivariate data in the form of a two-dimensional chart for many quantitative variables represented on the axis starting from the same point. The application of radar charts is the control of quality improvement to display the performance metrics of any ongoing program ,**Walkenbach, 2003**.

## 4- EXPERIMENTAL PROCEDURE

In this study thirty five different types of Iraqi drinking bottled water labels are collected, three samples of each label is collected and the sample size is of (500ml/volume). These samples are of different Iraqi resources (springs, drinking water and purified bottled water), from different Iraqi governments. The specifications registered on the labels by the manufacturers are different, and quality parameters may vary such as for (pH, TDS, Ca, Na, Mg, K, Fe, Cl, and F) depending on the origin of the water and the manufacturing company purification processes. The previous nine parameters were chosen because they mostly exist in this study. The parameter value is compared first with Iraqi standard specifications set by the "Central Organization for Standardization and Quality Control" ,**Juran , 1951** then with other standard specifications. Results are generated employing Minitab software (Ver. 16) to generate X-bar, and Pareto chart.

## 5- DATA ANALYSIS, AND DISCUSSION

Each brand is given a specific number instead of the company trade name, as shown in **Table 1.** considering that No. 1 to No. 14 represent bottled from northern Iraq (are spring water), from No.15 to 35 are for other Iraqi governorate (drinking water). The specifications of the collected samples are listed in **Table1,** where some factories are not committed to set all the quality characteristics. Some factories set most of the quality characteristic such as in northern Iraq form {No.1 to No.14}.Other characteristics that are not stated since water origin is spring water from **Table 2** it could be noticed that there is no significant differences between Iraqi tap, and bottled water specifications this requires essential developments in bottled water specifications since consumers are currently paying more for almost the same water quality. Also bottled water specifications were released more than one decade ago on (2000) hence, updating these standards for such important industry is crucial as it is related to everyday use and human health.

To verify and compare Iraqi bottled water specifications with that of drinking water and tap water standards. Also Saudi and WHO standards are listed in **Table 2.**This table shows that Iraqi specification ,**Stars Orbit Consultants and Management Development, 2010,العزاوي واخرون and المواصفة القياسية العراقية لمياه الشرب رقم(417) , 2001, 2010** . are less restricted (wide range of values as in Mg and Ca values). Sometimes these specifications are far behind these standards as in TDS values, other quality characteristics values are not even included as in Na, or K values. As a result, these characteristic should be introduced and reviewed continuously to reduce the gap between other standards and that of Iraqi standards. It's worth mentioning that Saudi Arabia specifications' , **الهيئة العربية السعودية للمواصفات والمقاييس, 1997, كامل, 2002**. is one of Iraqi specifications references, yet Iraqi specifications are still behind their reference values. On comparison with WHO specifications ,**World Health Organization (WHO), 2004, and Darapu, and et al., 2011**. the values of Iraqi standards for (Ca, Fe, Cl) are on its maximum acceptable values to WHO standards as could be noticed from **Table 2.**

All samples had expire date of one year from production date (that should be included also in the specifications). From **Table 1** and **Fig. 1** it could be noticed that most of the investigated companies (35) does not classify more than (33%) Iraqi bottled water required characteristics {No. 1937/ (2000)}.Only (28 %) of the investigated bottled water factories registered all specifications that are declared in Iraqi bottled water specifications (2000). Also (40%) of the investigated companies in this research do not register (50%) of the Iraqi specification. While for company No. (27). No specific characteristic of the nine characteristics is registered, and this company still selling in the local market.

Pareto chart shows the accumulative specifications that are not registered for the collected Iraqi samples **Fig.1** where the horizontal axis represents the not registered characteristics on the water bottle label, and the vertical axis presents the number of companies investigated in this study. The above mentioned percentages could be observed clearly in this Pareto chart **Fig. 1.**

**Fig.2** presents comparison between (Iraqi, Saudi Arabia and Worldwide) Standards, Radar chart is conducted to reveal the range for each specification value, and the full view of each standards in graphical comparison between (Iraqi, Saudi Arabia and Worldwide). From **Fig. 2** and **Table 2** it could be noticed the absence of minimum limit values for Iraqi tap water standards. Since only the maximum values for each quality is stated, consequently updating this standards is essential. Also the limited range of coverage for Iraqi bottled water specifications in both aspects of values and existing characteristics, compared to the wide range covered especially by World health

organization standards. This means that Iraqi Specifications should be developed to enhance water specifications and update the standard periodically for this important industry that is related to everyday use and human health. These not including characteristics should be introduced and reviewed continuously to improve these characteristic also to reduce the gap between other standards and that of Iraqi standards.

Detailed notes and results of specifications for selected parameters are shown below as control charts for nine different water in **Figs. 3** to **11** {knowing that the red line indicates to the upper and lower control limits and the green line indicates to center line or means} generated employing Minitab software (Ver. 16).

- **pH**

pH is a measure of the activity of Hydrogen ions (H+) in a solution therefore, solution is either acidic (pH less than 7) or alkaline (pH greater than 7), pure water of pH very close to 7 ,**http://www.engineeringtoolbox.com/food-ph-d_403.html**. pH value according to Iraqi Standards for drinking bottled water ranges (6.5 – 8.5), but for WHO Specifications pH ranges (6.5 – 8.5) and their values do not exceed the allowable limits, as shown in **Fig.3** from this control chart it was found that company No. (18) does not reach the minimum limit (almost acidic). While for companies No. (26 and 30) pH values are not verified in their labels although it is basic and important characteristics.

- **Total Dissolved Solids (TDS)**

This quality characteristic is not included in Iraqi standard specification yet, although it is an important quality characteristic parameter. Yet it could be noticed from **Fig.4** that (50 %) of Iraqi companies tested in this study haven included the (TDS) values in their labels. Total dissolved solid (TDS) describe the inorganic salts and small amounts of organic matter present in water. The presence of dissolved solids in water may affect its taste. The estimated taste levels of TDS found as excellent (less than 300 mg/l), good between (300 and 600 mg/l) fair, between (600 and 900 mg/l); poor, between (900 and 1200 mg/l) and unacceptable (greater than 1200 mg/l).Water with extremely low concentrations of TDS may also be unacceptable because of its flat, insipid taste ,**Gray, 2008, Total dissolved solids in Drinking-water, 2003**. As a benchmark for assessment and verification X-bar chart for this investigated characteristic employ Saudi Arabia standard specification of bottled water as shown in **Fig. 4** where the minimum TDS value is (100) and the maximum value is (700).

- **Calcium (Ca)**

Calcium is one of the important elements to human body essential to embryonic stages of growth, pregnancy and lactation, as well as its importance in the formation of bones and teeth, blood clotting, and the work of the nervous system ,**Gray, 2008**. From control chart **Fig. 5** it could be noticed that all the investigated companies haven't exceed Iraqi standard specification limits that is equal to (75.0 mg/l). Ca value for WHO specifications is (0.10 mg/l). It could be noticed from **Fig. 5** for companies' No. (22 and 24) hadn't inscribed Ca content in their labels. Whilst for companies No. (13 and 21) Ca value is out of control limits. Therefore, better quality control, inspection and quality assurance to such factories' specification is mandatory.

- **Sodium (Na)**

Sodium value must be kept at minimum values because death of babies may occur, drinking formula feeds made up with high-Sodium mineral waters, so exploit the water with lowest Sodium content you can get. The taste sill for sodium in water depends on the associated anion and the temperature of the solution ,**Gray, 2008**. Na values are also not set in Iraqi standards neither in Saudi Arabia standards, but the minimum value for WHO standards is (0.20 mg/l) and the maximum limit is not recorded since less is better. Certain Iraqi companies didn't exceed the minimum limit, while for companies No. (17 and 23) their values are out of control limit. Whilst (25 %) of companies haven't include Na in their specification labels. as shown in control chart **Fig. 6.**

- **Magnesium (Mg)**

Along with Calcium, Magnesium is a major constituent of water hardness and a major dietary requirement for human. Levels are generally low in bottled water, although there are except ions ,**Gray, 2008**. Mg value in Iraqi standards is (30.0 mg/l).From control chart **Fig. 7** It could be noticed that for companies No. (7, and 17) exceed Iraqi limits while for two companies No. (27, and 35) haven't mention the Mg content in their labels, while company No. (17) Mg value is out of control as shown in **Fig. 7**

- **Potassium (K):**

It is an essential element the body finds it hard to deal with excess Potassium, resulting in kidney stress and possible kidney failure. Although Potassium is not considered to be toxic, long-term exposure to high Potassium concentrations should be avoided ,**Gray, 2008**. Iraqi and Saudi standards haven't included K values, but world health organization sets only the minimum value of K as (0.10 mg/l). This value is used on employing the control chart as shown in **Fig. 8.** Some Iraqi companies haven't exceed the minimum value, for company No.(20) K value is out of control as shown in **Fig. 8**

- **Iron (Fe)**

Iron is an essential and is very unlikely to cause a threat to health at the concentrations occasion ally recorded in water supplies. It is undesirable in excessive amounts and can cause number of problems. Iron encourages the development of a microbial slime comprised of iron bacteria on piped surfaces that can affect flow and cause consumer complaints. Iron also causes staining of laundry and discoloration of vegetables such as potatoes and parsnips during cooking. More importantly, Iron has a fairly low taste threshold for such a common element, giving the water strong unpleasant bitter taste that may spoils most beverages made from tap water , **Gray, 2008**. Control chart **Fig. 9** shows the companies under this study are within control limits of Fe values except for company No. (17) exceeded the upper control limit of Iraqi specifications (0.3 mg/l) {Fe value for this company is (22 mg/l)}.While (85 %) companies haven't register or evaluate an important content (Fe) in their specifications, as shown in **Fig. 9**

- **Chloride (Cl)**

Chloride is not dangerous at the concentrations found in bottled waters. It has a taste threshold of about (200 mg/l), but levels are generally much lower than this in mineral waters. If bottled water is to be used for making up drinks such as tea, coffee and fruit juice, then the lower the Cl is the better

,**Gray, 2008**. Control chart **Fig. 10** shows that Iraqi companies of bottled water hadn't exceeded Iraqi or World standards for Cl concentration. The range of Cl in Iraqi and World standards Specification is (0.10 – 250) mg/l. Control chart showed that Cl values of companies No. (17, 19, and 23) are out of control as shown in **Fig. 10**

- **Fluoride (F)**

If consumers are going to use bottled water as a complete replacement for tap water, for both drinking and cooking, then the F level must be (1.0 mg/ l) or less to avoid dental Fluorosis and other associated problems ,**Gray, 2008**. The studies show that drinking water containing (1.0 mg/l) Fluoride concentration helps to reduce the incidence of tooth decay by 65% for the children aged between (12-15) years ,**Fadhel,2010**. Iraqi specification did not include F concentration therefore, Saudi Standards are taken as a benchmark of (0.6 – 1.0) mg/l. Control chart showed that the whole investigated companies are within control limits as shown in **Fig.11** Also all Iraqi these companies haven't exceeded the WHO specifications. According to control chart **Fig. 11** (60 %) of the investigated companies haven't included the F specification label.

## 6. ANALYSIS OF QUALITY ASSURANCE ACTIVITIES

Quality assurance necessitates continuous monitoring processes to presents product (bottled water) with accurate and precise recorded results which are the quality characteristics claimed on the bottles (products) of these companies where:

- Some of the investigated companies have the same symbol (same specifications in the logo) such as companies (No.1, No.2, No.11, No.12), (No.3, No.9), (No.5, No.6) (No.22, No.24) and (No.29, No.33) or three different products (labels) such as company No.32. Others claim that the product is according to standards other than Iraqi standards as in company No.27 that did not register specific characteristic its register the minimum and maximum values as discussed earlier. On the other hand company No. 32 is promoting for their product depending on certain characteristics (low Sodium) that is not even included in Iraqi bottled water standards. Therefore, the quality should be assured so as the legal consequences could be enforced and activated.
- Although the water expire date is essential and it is one of the required characteristics to be registered on labels according to Iraqi standards, but none of the investigated companies(for 35 different Iraqi factories) fix the expired date on their labels rather fix the duration of use as one year.

## 7- CONCLUSIONS

Water issues are important for life and human health, this study highlighted the following conclusions are deduced:-

i. Plants in northern Iraq committed to recording water specifications on their labels more than other governorates in Iraq; this is due strict monitoring and demanding for control there.
ii. The expired date for all samples is one year as recorded by the manufacturer's note. It is within Iraqi specifications requirements and must be recorded on the labels too.
iii. It was found that some companies produces the same bottled water specifications under to different brands(trademarks){(No.1,No.2,No.11,No.12)},{(No.3,No.9)},{(No.5,No.6)},{(No.22,No.2

4)}and{(No.29,No.33) }, and one company produce its product brand with four different colors (No. 32).

iv. It was found that some companies misleading the consumers by labeling wrong data, use inappropriate or the same logo for different water sources when promoting their product.

v. Iraqi bottled water specifications need to introduce new and important quality parameters that are introduced Saudi standards such as (TDS, F) and WHO standards such as (Na, K) and to continual updating is needed towards reducing the gaps between them and those international standards.

## 8. RECOMMENDATIONS

i. Most of companies under study did not conform Iraqi specifications therefore; governmental quality control, quality assurance on this industry factory is required.

ii. Need of better control on manufacturing plants since most of the used bottled water lack in writing complete required information of Iraqi standards.

iii. Some manufacturing companies should be stopped since their water

iv. Characteristics are not registered either because they are not quantifying them or there is no quality control department in these companies.

v. Other sources of water: natural mineral, spring, etc. must be tested periodically to license them.

## REFERENCES


- Abdulraheem A., Mustafa S., Al-Saffar N. and Shahjahan M., 2012, *Detection of Bacterial Endotoxin in Drinking Tap and Bottled Water In Kuwait*, Environ Monit Assess 184:7323–7328, /IVSL.

- Ahmad, M., and Bajahlan, A. S., 2009, *Quality Comparison of Tap Water vs. Bottled Water in the Industrial City of Yanbu (Saudi Arabia)*, Environ Monit Assess 159:1–14, / IVSL.

- Alabdula'aly, A. I. and Khan, M. A., 1999 *Chemical Composition of Bottled Water in Saudi Arabia*, Environmental Monitoring and Assessment 54: 173–189, /IVSL.

- Available at http://www.engineeringtoolbox.com/food-ph-d_403.html

- Darapu, Er. S. S. K., SudhakarEr. B., Krishna K. S. R., Rao P. V., and Sekhar M. C., 2011 *Determining Water Quality Index for the Evaluation of Water Quality of River*, International Journal of Engineering Research and Applications (IJERA) Vol. 1, Issue 2, pp.174-182 .

- Fadhel A. M., 2010, *The Quality of Drinking Water Bottled Domestic and Important in Iraq*, Uruk Journal of Scientific Research, volume III, No.2, April.

- Gray N. F., 2008, *Drinking Water Quality*, Cambridge University Press2nd edition, Pages (191, 210, 426, 427).
- Juran, J. M., 1951, *Quality Control Handbook*, New York, New York: McGraw-Hill,.
- Kaoru, I., 1985, *What Is Total Quality Control? The Japanese Way*, (1 ed.), Englewood Cliffs, New Jersey/USA: Prentice-Hall, .
- Kazemzadeh, R. B., Karbasian, M., Babakhani, M. A., 2013, *An EWMA Chart with Variable Sampling Intervals for Monitoring The Process Mean"*, International Journal Advanced Manufacturing Technology, No.66, PP.125-139.
- Masaaki I., 1986, *Kaizen (Ky'zen), the Key to Japan's Competitive Success* (1 ed.), New York/USA: Random House,.
- Matloob, M. H., 2011,*"Fluoride Concentration of Drinking Water in Babil-Iraq"*, Journal of Applied Science 11(18): 3315-3321, /IVSL.
- Miller, I., Freund, J.E., 1985, *Probability and Statistics for Engineers*, 3rd edition., Prentice Hall, Englewood, Cliffs.
- Montgomery, D., 2005, *Introduction to Statistical Quality Control*. Hoboken, New Jersey/USA: John Wiley & Sons, Inc.
- Queiroz, J. T. M., Rosenberg, M. W., Heller, L., Zhouri, A. L. M. and Silva, S. R., 2012 *News about Tap and Bottled Water: Can This Influence People's Choices?* , Journal of Environmental Protection, 3, 324-333,/IVSL.
- Saravanan, A. and Nagarajan, P., 2013, *Implementation of Quality Control Charts in Bottle Manufacturing Industry*, International Journal of Engineering Science and Technology (IJEST), 0975-5462 Vol. 5 No.02 February, /IVSL.
- Semerjian, L. A., 2011, *Quality Assessment of Various Bottled Waters Marketed in Lebanon*, Environ Monit Assess ,172:275–285, / IVSL.
- Stars Orbit Consultants and Management Development, 2010, *Water Quality Control and Surveillance in Iraq (Phase Two) (E3-11)*, World Health Organization (WHO), May.
- Toma, J. J., Hanna N. S., and Mohammed, B. A., 2013, *Effect of Storage Condition on Some Bottled Water Quality in Erbil City, Kurdistan Region Iraq*, International Journal of Software and Web Sciences (IJSWS), 12-339.
- Total dissolved solids in Drinking-water, 2003, *Guidelines for drinking-water quality*, 2nd ed. Vol. 2, WHO, Geneva, Available at http://www.who.int/water_sanitation_health/dwq/chemicals/tds.pdf

- U.S. Environmental Protection Agency Office of Research and Development, 1979, *Handbook for Analytical Quality Control in Water and Waste water Laboratories*, March, Cincinnati, OHIO, USA.

- Walkenbach, J., 2003, *Excel Charts*, Wiley Publishing Inc., Indianapolis, Indiana.

- World Health Organization (WHO), 2004, *Water, Sanitation and Hygiene Links to Health Available* at:www.who.int/water_sanitation-health/publications/facts2004/en/index.html.

- www.minitab.com.

- رزوقي سراب محمد, الراوي محمد عمار, 2008, *" دراسة واقع صناعة مياه الشرب المعبأة في العراق بين الاعوام 1995-2008"*, المؤتمر العملي الاول الصحة العامة استثمار لحياة افضل, وزارة الصحة.

- العزاوي أثير سايب, الجواهري حلا فائز , الطائي وميض عادل, السلطاني ضرغام علي, 2010, *"دراسة فيزيائية وكيميائية للمياه المعدنية العراقية والعالمية المتوافرة في الاسواق المحلية"*, مجلة جامعة بابل / العلوم الصرفة والتطبيقية / العدد (5) / المجلد (18).

- كامل وليد بن محمد,2002, *"جودة مياه الشرب المعبأة المحلية والمستوردة في المملكة العربية السعودية"*, مجلة جامعة الملك عبد العزيز للعلوم الهندسية, م 14, ع 2 , ص ص 81-104.

- المديرية العامة للتنمية الصناعية http://www.gdid.gov.iq/index.php?name=Pages&op=page&pid=141

- المفرجي, طالب كاظم و العزاوي ,شذى سلمان, 1991, *"علم الاحياء المجهرية للتربة والمياه : الجزء العملي"* وزارة العالي والبحث العلمي, جامعة بغداد, دار الحكمة للطباعة والنشر, بغداد 459 التعليم .

- المواصفة القياسية العراقية لمياه الشرب رقم(417) / الجهاز المركزي للتقييس والسيطرة النوعية (م.ق.ع /2001/417)

- الهيئة العربية السعودية للمواصفات والمقاييس, 1997, المواصفة القياسية رقم 1984/409:مياه الشرب المعبأة, الرياض, المملكة العربية السعودية.

**Table 1.** Iraqi bottled water specifications of brands according to their labels.

| Quality Parameters | | | | | | | | | |
|---|---|---|---|---|---|---|---|---|---|
| **Company No.** | **pH** | **TDS** | **Ca** | **Na** | **Mg** | **K** | **Fe** | **Cl** | **F** |
| 1 | 7.2 | **N.A** | 24.2 | **N.A** | 4.4 | **N.A** | **N.A** | 11.5 | 0.03 |
| 2 | 7.2 | **N.A** | 24.2 | **N.A** | 4.4 | **N.A** | **N.A** | 11.5 | 0.03 |
| 3 | 7.2 | 120 | 22 | 2.2 | 5 | 0.2 | **N.A** | 4.1 | 0.7 |
| 4 | 7.8 | **N.A** | 26 | **N.A** | 7.5 | **N.A** | **N.A** | **N.A** | **N.A** |
| 5 | 7.38 | **N.A** | 28 | 2.91 | 3.4 | **N.A** | 0.003 | 1.4 | **N.A** |
| 6 | 7.38 | **N.A** | 28 | 2.91 | 3.4 | **N.A** | 0.003 | 1.4 | **N.A** |
| 7 | 7.48 | **N.A** | 16.74 | 2.76 | 42.44 | 1.17 | **N.A** | 5.27 | 0.19 |
| 8 | 7.48 | 257 | 25.65 | 0.4 | 7.05 | 0.2 | **N.A** | 4.9 | **N.A** |
| 9 | 7.2 | 120 | 22 | 2.2 | 5 | 0.2 | **N.A** | 4.1 | 0.7 |
| 10 | 7.3 | 125 | 34.2 | 7 | 11 | 1 | **N.A** | 11 | **N.A** |
| 11 | 7.2 | **N.A** | 24.2 | **N.A** | 4.4 | **N.A** | **N.A** | 11.5 | 0.03 |
| 12 | 7.2 | **N.A** | 24.2 | **N.A** | 4.4 | **N.A** | **N.A** | 11.5 | 0.03 |
| 13 | 7.9 | **N.A** | 52 | **N.A** | 9 | **N.A** | **N.A** | **N.A** | 0.32 |
| 14 | 7.2 | 124 | 27 | 1.1 | 8 | 0.5 | **N.A** | **N.A** | **N.A** |
| 15 | 7 | 110 | 0.5 | 16 | 13 | 1 | **N.A** | **N.A** | **N.A** |
| 16 | 7.2 | **N.A** | 10 | 9 | 12 | 6.2 | **N.A** | 20 | 0.7 |
| 17 | 8.2 | 150 | 3.5 | 50 | 125 | **N.A** | 22 | 40 | **N.A** |
| 18 | 6.08 | **N.A** | 8.64 | **N.A** | 5.40 | 2.36 | **N.A** | **N.A** | **N.A** |
| 19 | 7.2 | 150 | 3.6 | 21 | 10 | 1 | **N.A** | 50.2 | 0.02 |
| 20 | 7.5 | 180 | 19 | 13 | 11 | 15 | **N.A** | **N.A** | **N.A** |
| 21 | 7.3 | **N.A** | 64 | 11 | 22.08 | 2 | **N.A** | 4 | **N.A** |
| 22 | 7 | 110 | **N.A** | 16 | 1.3 | 1 | **N.A** | **N.A** | **N.A** |
| 23 | 7 | 170 | 16 | 44 | 11.7 | 1.5 | **N.A** | 59 | **N.A** |
| 24 | 7 | 110 | **N.A** | 16 | 13 | 1 | **N.A** | **N.A** | **N.A** |
| 25 | 7.4 | 180 | 33 | 2.3 | 16 | 0.3 | 0.01 | 7 | 0.1 |
| 26 | **N.A** | 110 | 5 | 16 | 13 | 1 | 0.01 | 27.5 | 1 |
| 27 | 7.5 | 30 | 15 | 10 | **N.A** | 5 | **N.A** | 10 | **N.A** |
| 28 | 7.5 | 120 | 24 | 21.9 | 7 | 1.06 | **N.A** | 14 | **N.A** |
| 29 | 7.4 | **N.A** | 22 | **N.A** | 10 | 0.3 | **N.A** | 7 | **N.A** |
| 30 | **N.A** | 80 | 15 | 13 | 4 | 0.9 | 0.02 | 14 | 0.9 |
| 31 | 7.9 | 130 | 31.3 | 3.5 | 5.2 | 0.5 | **N.A** | 5.1 | 0.01 |
| 32 | 7.2 | 101 | 12 | 11 | 3 | 0.6 | **N.A** | 25 | 1 |
| 33 | 7.4 | **N.A** | 22 | **N.A** | 10 | 0.3 | **N.A** | 7 | **N.A** |
| 34 | 7.3 | 190 | 20 | 5 | 2.4 | 0.4 | **N.A** | **N.A** | **N.A** |
| 35 | 7.6 | 30 | 15 | 10 | **N.A** | 5 | **N.A** | 10 | **N.A** |

**N.A: Not Available Values**

**Table 2 .** Comparison between Iraqi bottled water and other standards.

| Standards | | | | |
|---|---|---|---|---|
| **Specifications/units** | **Iraqi Standards** | | **Saudi Arabia Bottled Water Standards** | **WHO Bottled Water Standards** |
| | **Tap Water** | **Bottled Water** | | |
| pH | 6.5-8.5 | 6.5-8.5 | 6.5-8.5 | 6.5-8.5 |
| TDS (mg/l) | 1000 | N.A | 100-700 | 1-500 |
| Ca (mg/l) | 50 | 75 | 75 | 0.1-75 |
| Na (mg/l) | 200 | N.A | N.A | 0.20 |
| Mg (mg/l) | 50 | 30 | 30 | 0.10 |
| K (mg/l) | N.A | N.A | N.A | 0.10 |
| Fe (mg/l) | 0.3 | 0.3 | 0.3 | 0.01-0.3 |
| Cl (mg/l) | 250 | 250 | 250 | 0.1-250 |
| F (mg/l) | 1 | N.A | 0.6-1 | 0.1-2 |

**N.A: Not Available Values**

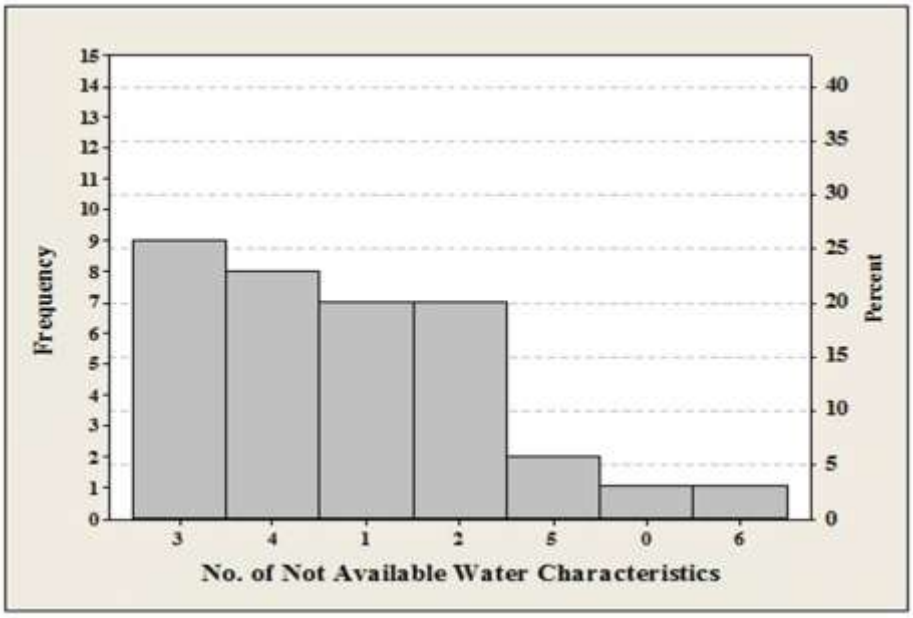


**Figure 1.**Pareto chart of Iraqi bottled water specifications.

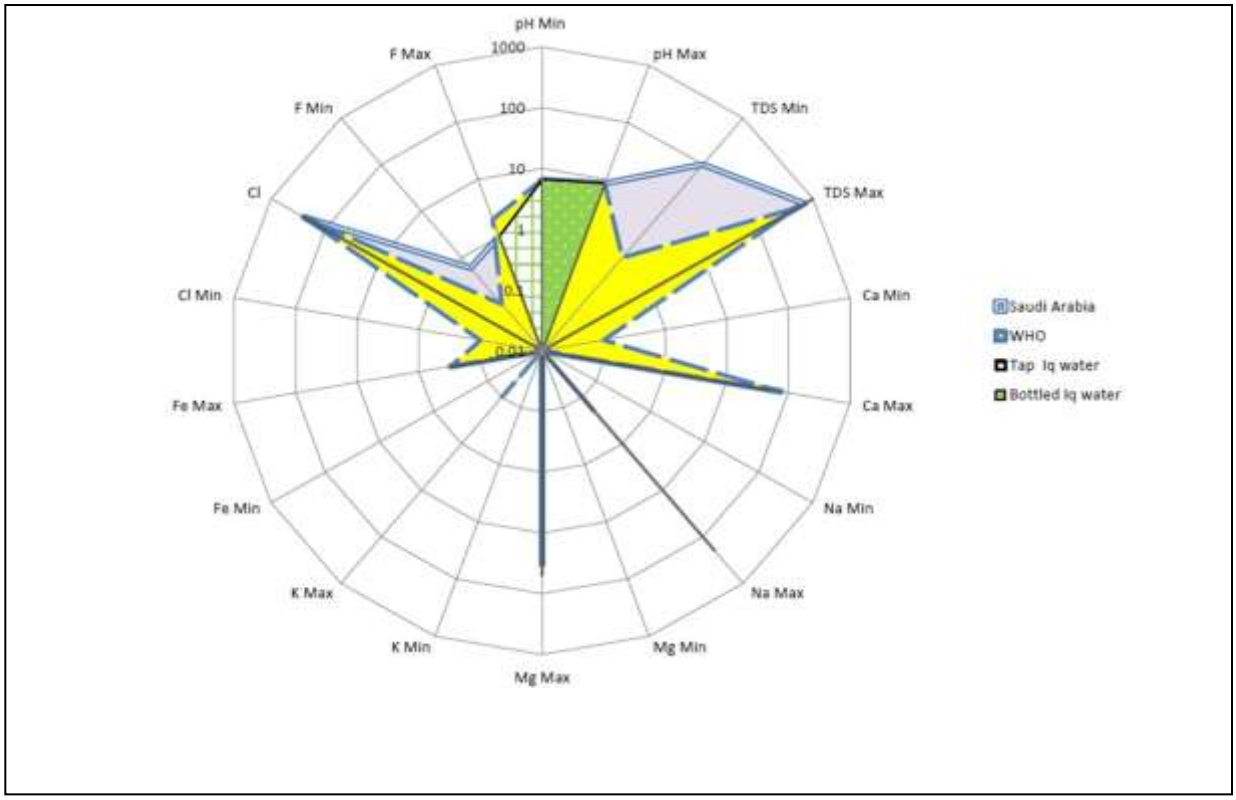


**Figure 2.** Radar chart of {Iraqi, Saudi Arabia, and WHO} bottled water specifications.

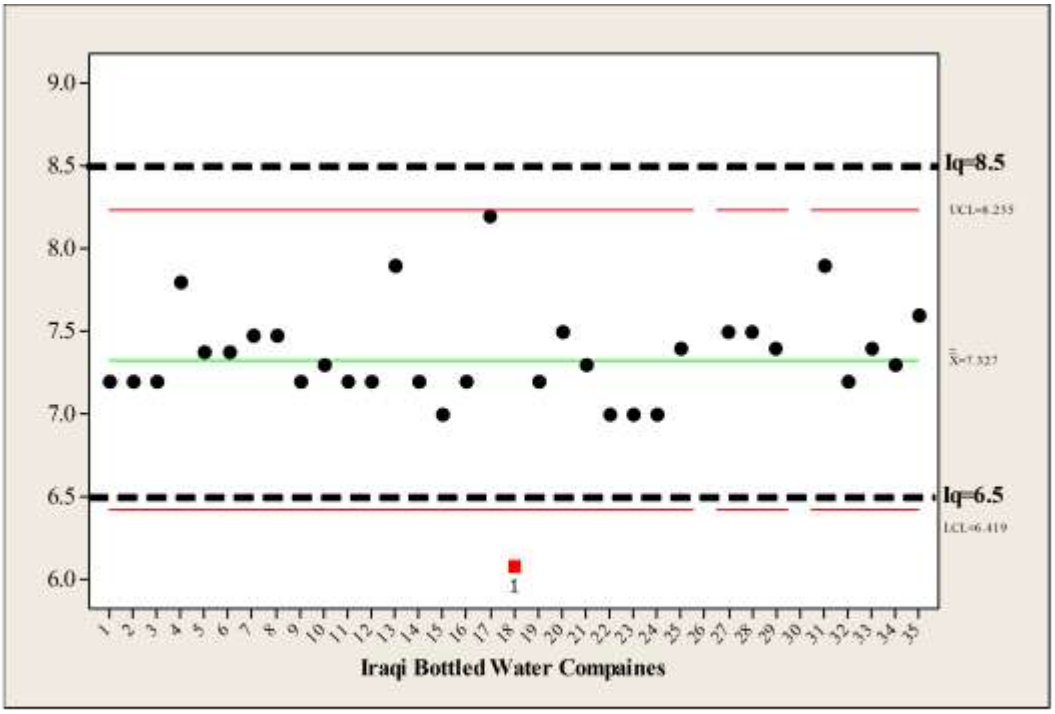


**Figure 3.** X-bar of pH values in bottled water companies.

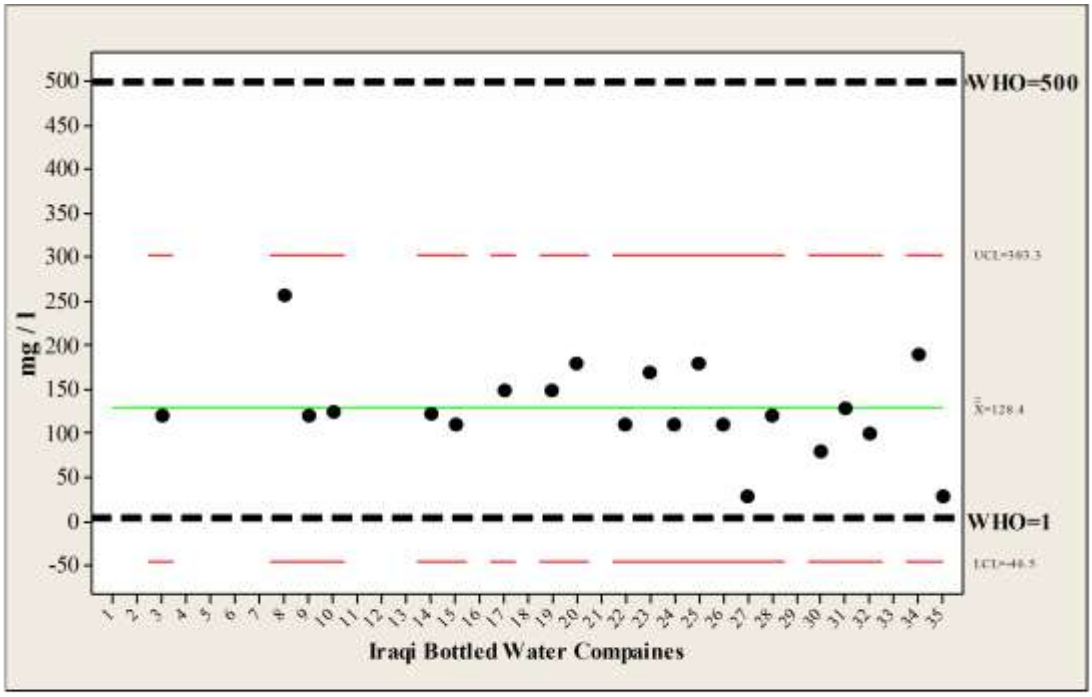


**Figure 4.** X-bar of TDS concentration in bottled water companies.

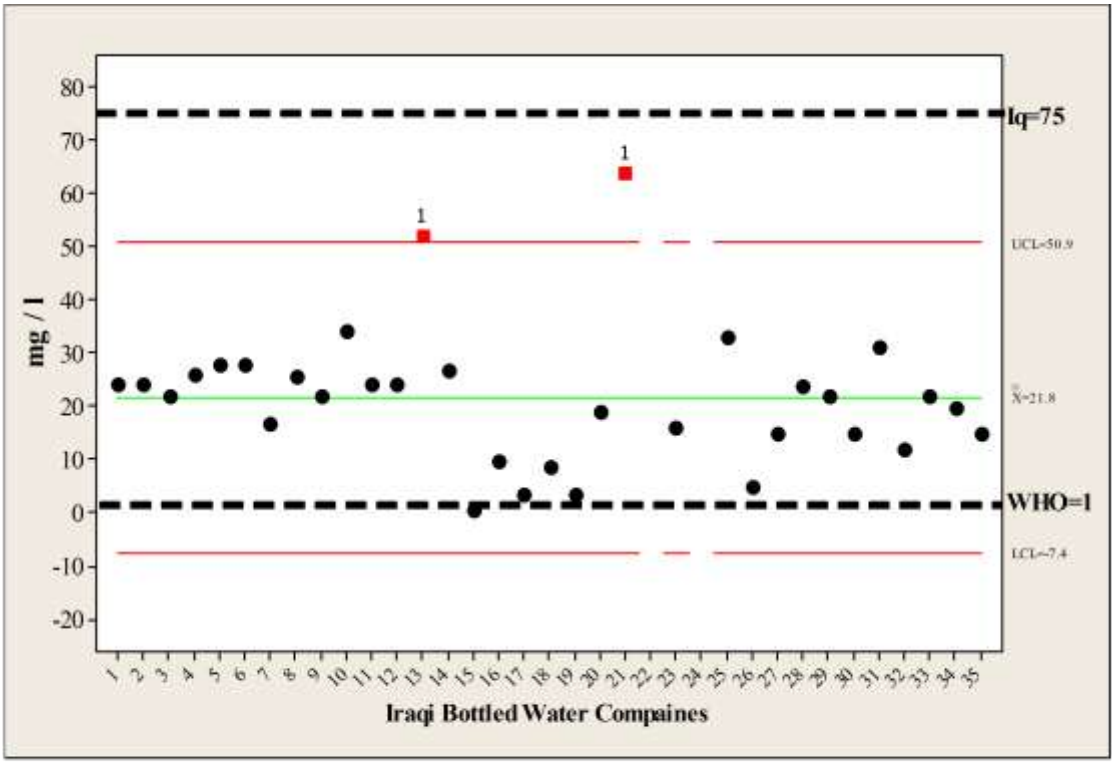


**Figure 5.** X-bar of Ca concentration in bottled water companies.

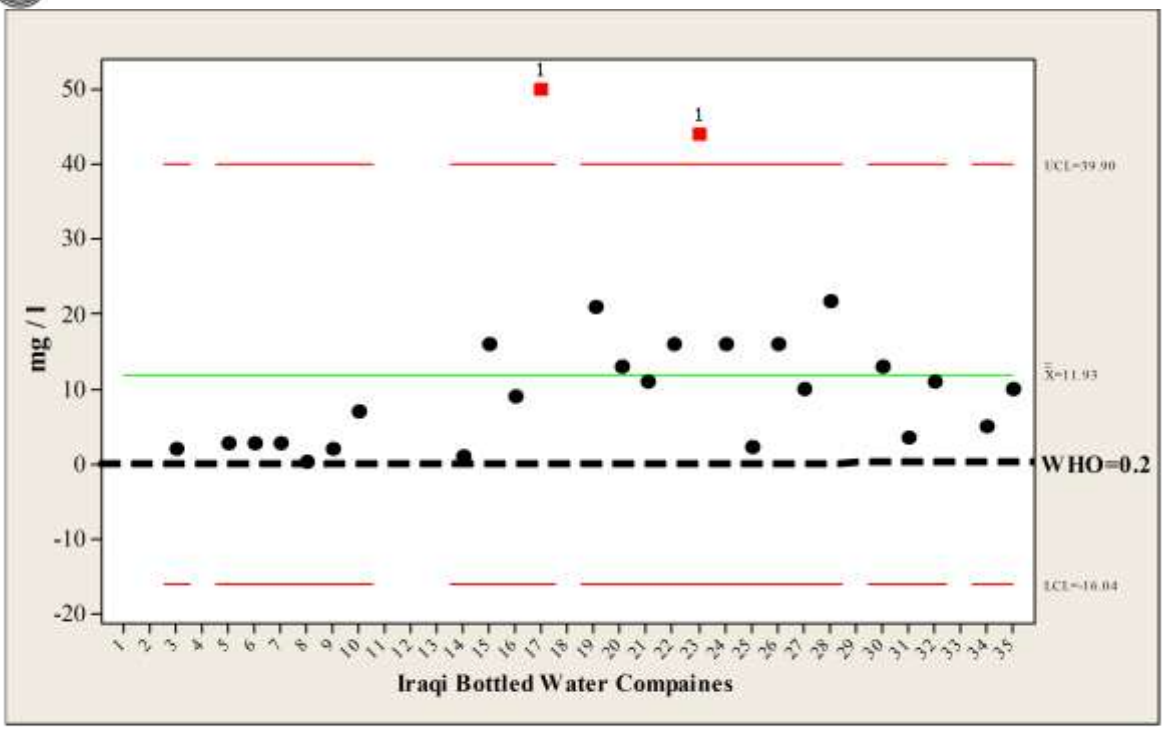


**Figure 6.** X-bar of Na concentration in bottled water companies.

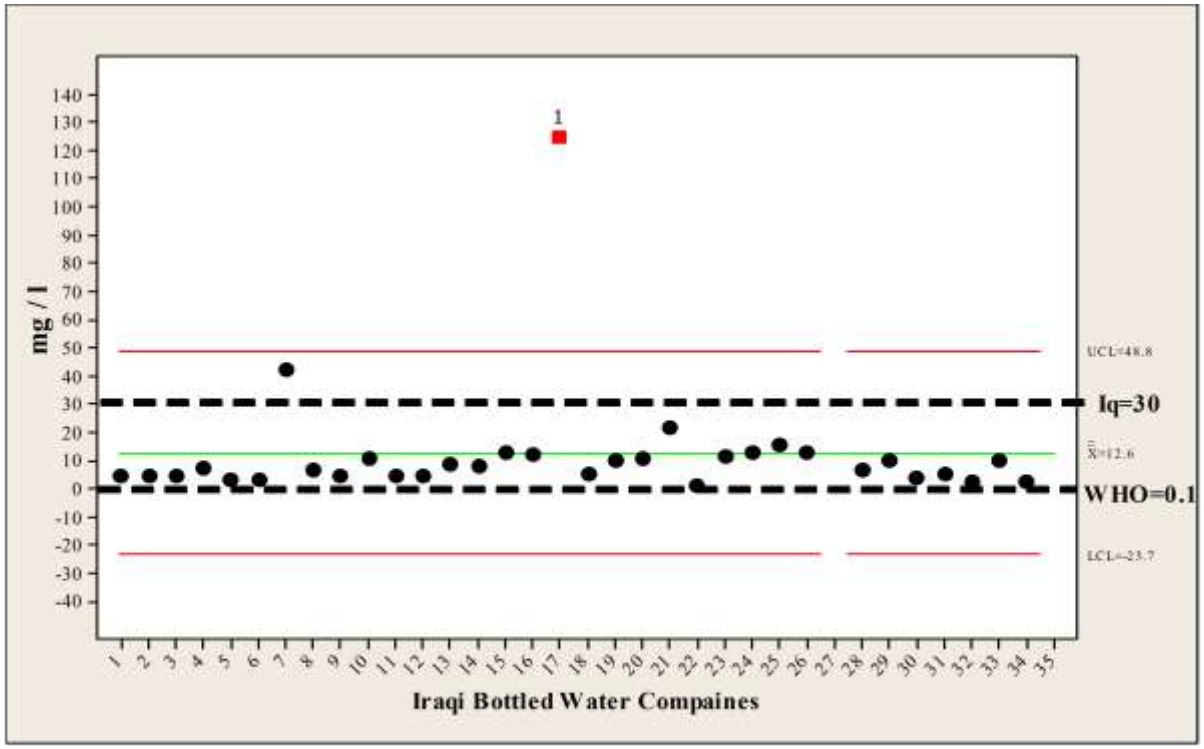


**Figure 7.** X-bar of Mg concentration in bottled water companies.

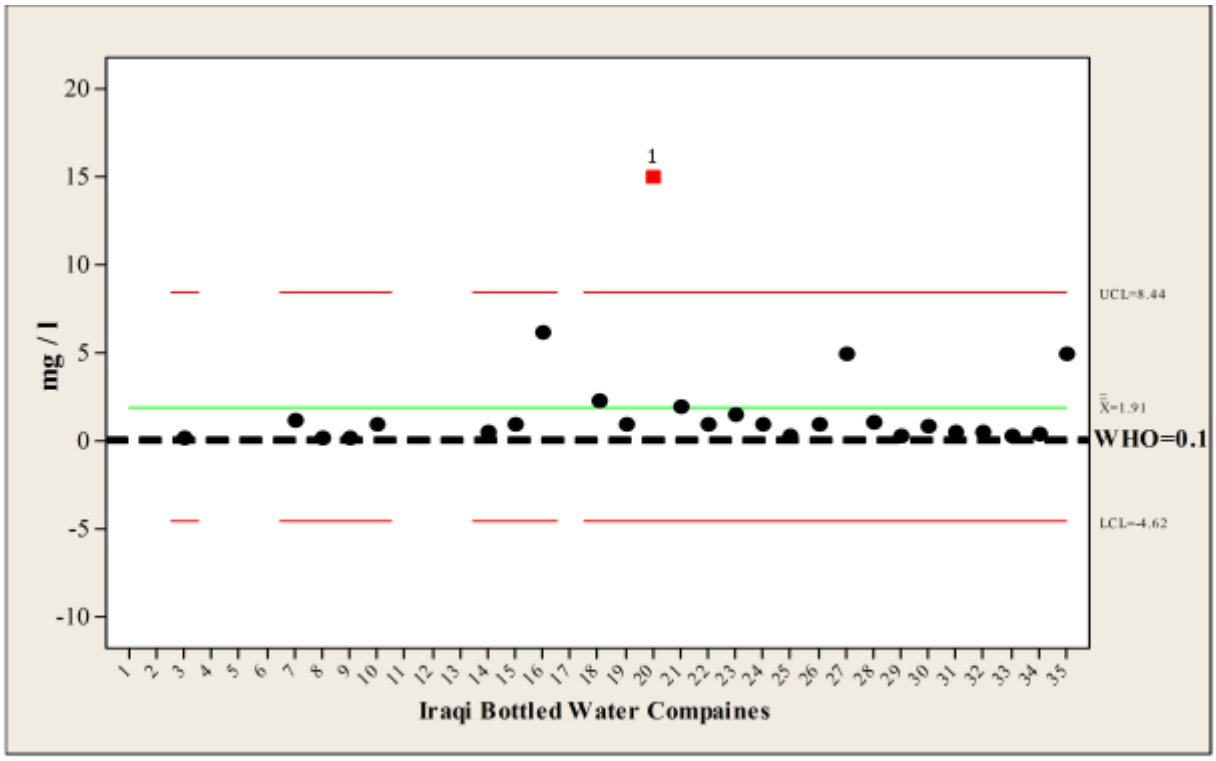


**Figure 8.** X-bar of K concentration in bottled water companies.

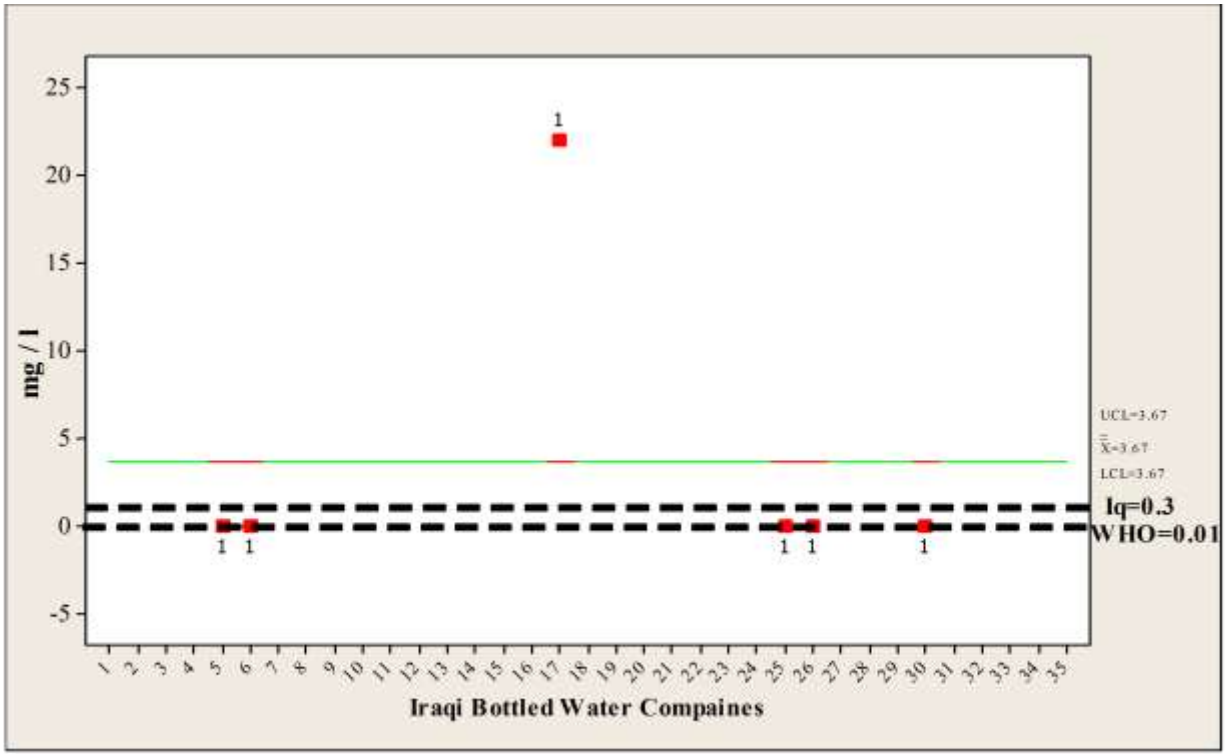


**Figure 9.** X-bar of Fe concentration in bottled water companies.

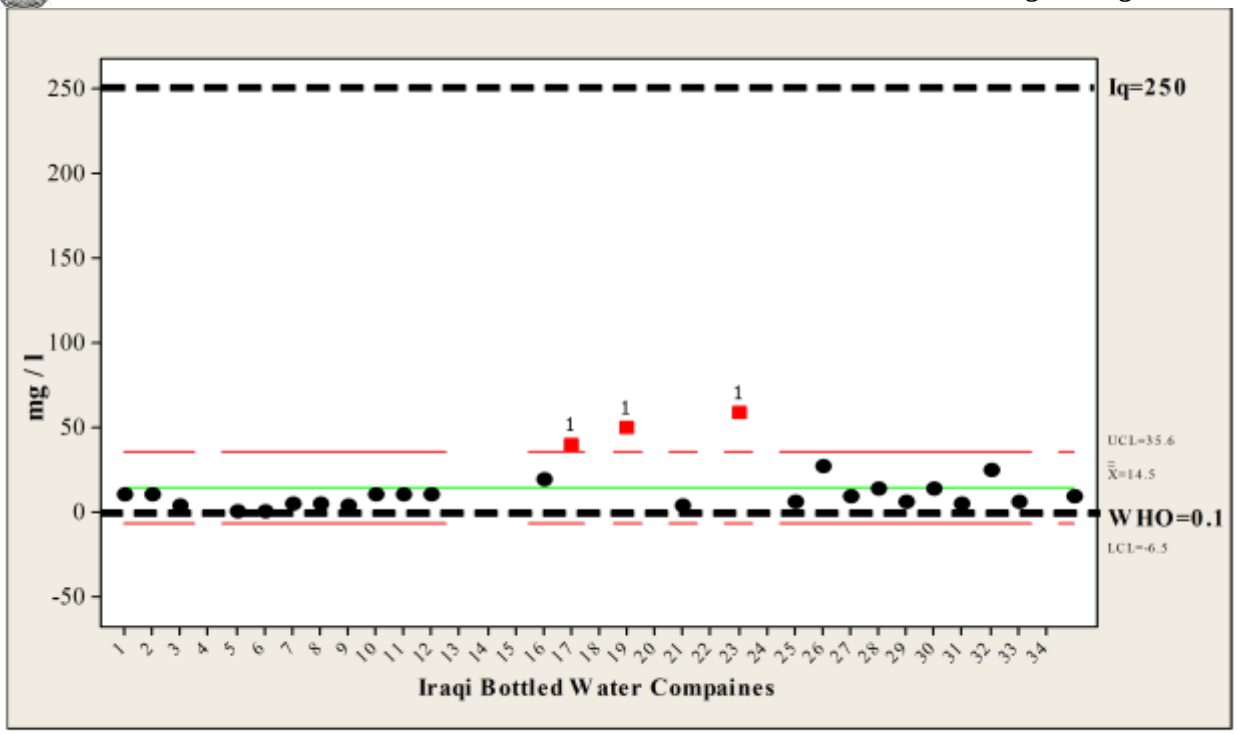


**Figure 10.** X-bar of Cl concentration in bottled water companies.

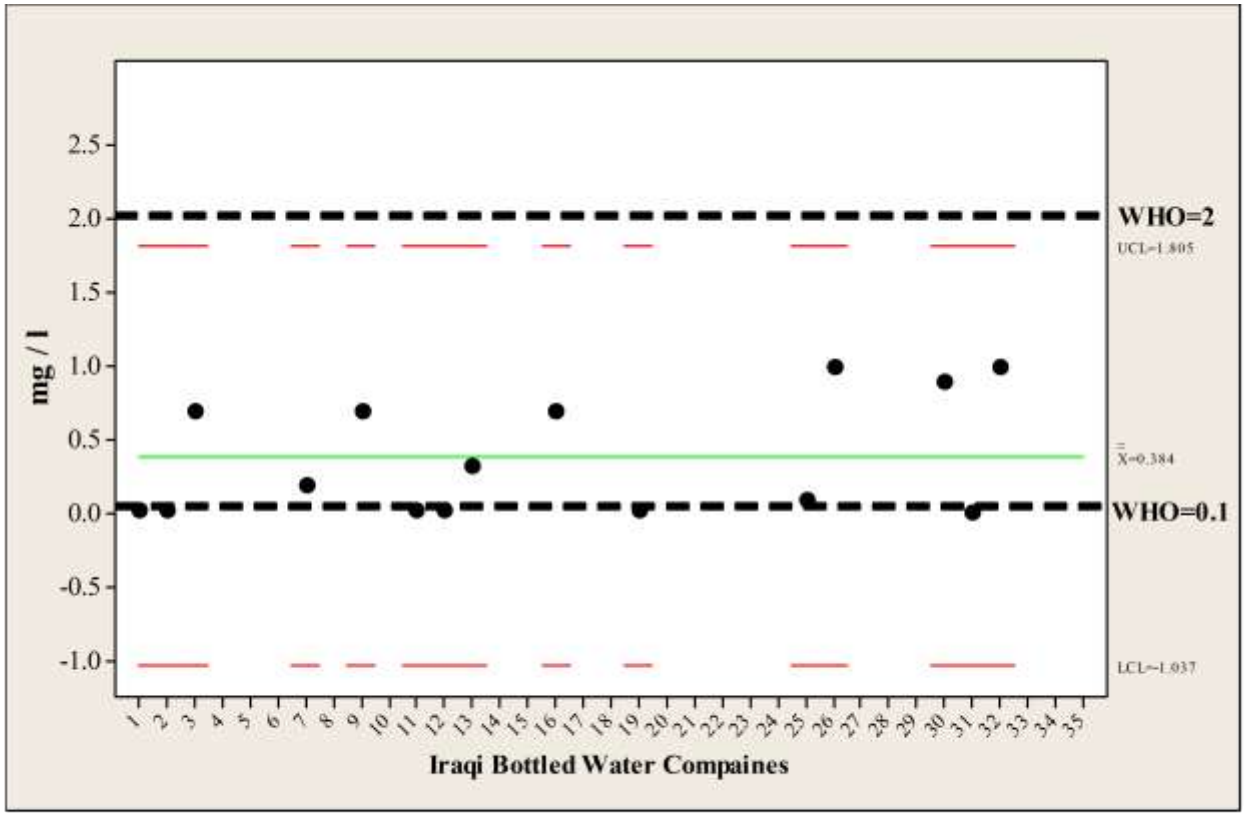


**Figure 11.** X-bar of F concentration in bottled water companies.

# Study of Energy Gains by Orientation of Solar Collectors in Baghdad City

**Hussein Mohammed Taqi Al-Najjar – Lecturer**

Department of Energy Engineering – College of Engineering –University of Baghdad

Email:quality_electric61@yahoo.com

## ABSTRACT

Firstly, in this study, a brief updated description and applications of different solar collectors used in renewable energy systems for supplying electric and thermal energy was presented. Secondly, an attempt was made to utilize tilting orientation of solar collector for maximizing collector energy with time in respect to horizontal orientation. For energy calculation, global solar radiation was used since they are directly related. For that purpose, field measurements of half-hourly radiation on two flat panels of tilting and horizontal orientations were carried out throughout 8-month period under local climate of Baghdad. Then, energy gain and radiation level averages were calculated based on the field radiation data using Excel programming. The tilting orientation was found to be more effective for the winter months with significant energy gains of larger than 40% and maximum gain of 58%. On the contrary, the radiation levels on collector were lower during winter months. Finally, for clear sky condition, the average solar radiations for tilting and horizontal orientations of collector were of 910 W/m$^2$ and 713 W/m$^2$ respectively.

**Key words:** solar collector, PV, thermal, tilting orientation, horizontal orientation, energy gain.

# دراسة أرباح الطاقة من توجيه المجمعات الشمسية في مدينة بغداد

**حسين محمد تقي النجار – مدرس**

قسم هندسة الطاقة - كلية الهندسة – جامعة بغداد

## الخلاصة

في هذه الدراسة تم أولا وصف موجز ومحدّث لأنواع وتطبيقات المجمعات الشمسية في أنظمة الطاقة المتجددة لتجهيز الطاقة الكهربائية والحرارية. وثانياً، أستخدم توجيه الأمالة لزيادة طاقة المجمع مع الزمن مقارنة مع التوجيه الأفقي. لحساب الطاقة، أستخدم الأشعاع الشمسي الكلي لأنهما متناسبين بصورة مباشرة. لهذا الغرض، تم أجراء القياسات الحقلية للأشعاع كل نصف ساعة على لوحين مستويين ذوا توجيه الأمالة والأفقي ولمدة ثمان شهور وفق البيئة المحلية لمدينة بغداد. ثم، تم حساب معدلات ربح الطاقة ومستوى الأشعاع وفق البيانات الحقلية بطريقة برمجة أكسل. وجد بأن توجيه الأمالة ذو فعالية أكبر في شهور الشتاء بأرباح طاقة أعلى من 40% وأقصى ربح 58%. وعلى العكس، فأن مستويات الأشعاع للمجمع كانت أوطأ في شهور الشتاء .أخيرا، في ظروف السماء الصافية، كان معدل الأشعاع الشمسي لتوجيه الأمالة والأفقي للمجمع هو 910 واط/م$^2$ و713 واط/م$^2$ على التوالي.

**كلمات رئيسية**: مجمع شمسي، كهروضوئي، حراري، توجيه الأمالة، توجيه أفقي، ربح الطاقة.

## 1. INTRODUCTION

Renewable energy systems utilizing solar collectors, including photovoltaic (PV) or thermal panels, are being one of the important technologies in supplying electric, heating and cooling energy for power systems and buildings, **Herrando, et al., 2014**, **Fang,** and **Li, 2013**, **Cao, et al., 2014**.

In fact, in 2007, global renewable power accounted for 18% of the total power generation in the world. The total operating capacity of solar PV power and solar thermal power was 10 GW and 425 MW respectively. The world solar heating and cooling capacity was 125 $GW_{th}$ , **REN21, 2013**.

The amount of output energy of a solar collector depends on several parameters such as design, material and structure of collector, local meteorological condition, geographic location, time and the relative orientation of the collector to both the sun and the sky. The latter parameter directly affects the energy input to the associated solar energy system, **Lubitz, 2011**. Different orientation mechanisms of solar collectors are available such as: adjusting of tilt angle, azimuth angle, both, inclined axis or other. Adjustment can be made continuously, daily or per other selected time step. The effectiveness of an orientation mechanism can be evaluated by calculating the corresponding energy gain as compared to a reference collector. Different studies have been carried out around the world to evaluate various orientation methods of PV and thermal collectors under site-related conditions.

In Saudi Arabia, **Ahmed, et al., 2015** found by analytical modeling of an on-site PV system in Dhahran city, that the yearly energy gain of continuous and monthly tilting was 43% and 19% respectively as compared to horizontal system.

For main Syrian zones, **Skeiker, 2009** used a mathematical model to estimate the incident solar radiation on a solar collector. The results revealed that the solar gain of 12 times tilting in a year was 30% with respect to horizontal collector.

In Jordan, **Al Tarabsheh, et al., 2012** simulated the solar radiation, neglecting diffuse and reflected components, near the Hashemite University for 10% efficiency PV modules using the Meteonorm 5.0 software. The annual energy gain of hourly tilting was calculated as 5.87% compared to fixed PV modules.

At university of Bechar Algeria, **Rebhi, et al., 2010** studied the performance of a prototype system for permanent orientation of PV module. An efficiency gain of 27.48% was found for a particular day compared to fixed system.

**Khorasanizadeh, et al., 2014** established a diffuse model to calculate the solar gain of monthly adjustable tilt–angle collector in Tabass city, Iran. The yearly gain was found to be 23.15% compared to horizontal collector.

For different areas in china, **Li, et al., 2010** suggested a mathematical procedure based on solar geometry to estimate the annual collectible radiation on solar panels. The gain using an orientation method about inclined axis was found to be 20-30% compared to fixed panels.

**Chang**, **2009** investigated the yearly gains for solar collectors in Taiwan from observed data of global radiation during ten years (1990-1999). The gain using single-axis adjustment was found to lie between 14.3 to 25.3% as compared to fixed collector.

In Malaysia, **Sunderan, et al., 2011** utilized monthly average of daily solar data for estimating the total radiation on PV panel. The annual energy gain was calculated to be 6.4% for monthly tilting as compared to horizontal PV panel.

For the European continent, **Huld, et al., 2010** presented a method for estimating energy output from PV systems using solar radiation and temperature data bases with PV performance models. The gain of inclined orientation compared to fixed system was approximately 30% in southern Europe, about 20-25% in central Europe and up to 50% in northern Scandinavia.

The present work aimed firstly to present a brief updated description of solar collector types and applications. Secondly to find the energy gains and radiations level by orientation of solar collectors under local climate condition of Baghdad city. Calculations are to be based on field measurements of half-hourly global solar radiations on tilting and horizontal dummy panels for 8-month period: October to May.

## 2. TYPES OF SOLAR COLLECTORS, Duffie, and Beckman, 2013, Kalogirou, 2013, Twidell, and Weir, 2005.

A solar collector transforms solar incident energy of wavelengths 0.3-3.0 μm into some other energy form: thermal, electric or both according to the optical characteristics of the energy-absorbing surface of the collector, called receiver which could be of flat, concave or convex geometry. In this respect, solar collectors can be classified according to the form of its output energy.

On the other hand, solar collectors can be classified according to the level of incident radiation on the receiver. A concentrator is added to the collector structure such that to direct the solar radiation onto the receiver. The concentrator could be reflectors or refractors of different geometries: two-dimensional (linear) such as flat or cylindrical or three-dimensional (circular). Consequently, a concentrating collector can operate at higher solar radiation level. In this case, the receiver will have smaller area compared to non-concentrating collector.

An important characteristic parameter for concentrating collector is its concentration ratio $C$. It is the ratio of the aperture area $A_a$ of the concentrator to the area of the receiver $A_r$, which is approximately the factor by which the solar radiation on the receiver is increased from its normal level that is of an average maximum 1.1kW/m$^2$ as in non-concentrating collectors.

The input energy to the collector, $E_i$ (kWhr) is

$$E_i = G_{ir}\, A_r \tag{1}$$

Where: $G_{ir}$ is the incident solar radiation (kWhr/m$^2$) on the receiver. Thus, the variable parameter for the input energy is the solar radiation. The $G_{ir}$ is related to the incident solar radiation on the aperture $G_{ia}$ (kWhr/m$^2$) by the concentration ratio $C$ as:

$$G_{ir} = C \,.\, G_{ia} \tag{2}$$

Where

$$C = \frac{A_a}{A_r} \tag{3}$$

The $G_{ia}$ is also called the global incident radiation. Different mathematical models can be found in literature as in **Sen, 2008** for estimating the radiation components of $G_{ia}$ including the view factors of a particular collector orientation for each radiation component. The amount of the absorbed energy per unit area of the receiver $S_r$ (kWhr/m$^2$) depends on the optical properties of the collector:

$$S_r = \alpha \,.\, G_{ir} \tag{4}$$

Where $\alpha$ is a lumped parameter for collector optical characteristics. A different $\alpha$ is associated with each radiation component. According to the specific design and structure of the solar collector, part of the absorbed energy is transformed into useful output energy $E_o$ (kWhr) as thermal, electric or both. The types of solar collectors will be explained according to above classifications as follows:

### 2.1 Solar Thermal Collectors, Kalogirou, 2004, Mills, 2004.

In this type of collectors, the receiver is a black absorber surface which could be provided with glass cover to reduce convection and radiation losses to the atmosphere. Also, the receiver might be enclosed in an evacuated space to obtain low loss coefficients. Absorbed thermal energy by the receiver is transferred by forced convection to working fluid, using tubes or ducts, as useful output energy.

Non-concentrating thermal collectors can deliver thermal energy at moderate temperatures up to 100$^o$C above ambient. The major applications of these collectors are in water heating, industrial process heat and air conditioning for buildings (space heating and cooling).

For applications of higher energy-delivery temperatures up to 1500$^o$C, concentrating thermal collectors are used. Depending on its particular geometry, higher concentration ratios provide higher solar radiation, lower heat losses and higher working temperatures. Concentration ratio of the order

of $10^5$ can be obtained. The major applications of such collectors are in solar power systems where steam is utilized to convert thermal energy to mechanical and then to electrical energy. Different configurations of thermal collectors can be constructed as shown in **Fig.1** and **Fig.2**.

### 2.2 Solar PV Collectors, Tiwari, and Dubey, 2010.

For this type of collectors, the receiver is photovoltaic (PV) cell which is a junction semiconductor that converts part of solar radiation directly to electric energy by photoelectric effect. The other part will be converted into thermal energy. PV collector is an array of identical PV modules that are arrayed in series and parallel to obtain the desired current and voltage for the load to which it is connected. A power conditioning equipment is usually needed to match the operating characteristic of the PV collector with that of the load. For ac loads, inverters of desired frequency will be required. **Fig.3** shows the electric circuit for PV collector.

Obviously, the electric energy is removed by external circuit (the electric load). On the other hand, the thermal energy should be removed by some heat transfer mechanism so PV cell will operate at lowest possible temperature, otherwise its electrical efficiency will be reduced.

For non-concentrating PV collectors, the incident solar radiation is of normal level. Thus, output power per unit area of collector is limited. Thermal losses may be removed by natural convection. The application of such collectors is in on-site or on-grid power systems, **Al-Najjar, 2013**.

The high costs of PV cells led to consideration of operation of these cells at high levels of solar radiation. Concentrating PV (CPV) collectors use multi-junction PV cells of flat or concave geometry with concentration ratios up to 400. Cell materials must be able to withstand high operating temperatures. In addition, sufficient cooling of PV collector should be assured. Application of such collectors is in on-grid power systems as a promising technology for future power. Typical configurations of PV collectors are shown in **Fig.4** and **Fig.5**.

### 2.3 Solar Photovoltaic-Thermal Collectors (PVT)

As explained above, PV receiver produces combination of electric and thermal energy. Thus, a PVT collector is a hybrid solar device. The thermal energy is treated as in thermal collectors. PVT collectors could be non-concentrating or concentrating (CPVT). In both types, the electrical energy can be used for supplying power systems, whether off-grid or on-grid; while the thermal energy can be utilized for water heating, air conditioning or for thermal power systems, **Tiwari,** and **Dubey, 2010**, **Amori,** and **Al-Najjar, 2012**.

## 3. ORIENTATION OF SOLAR COLLECTORS

As explained, different orientations of solar collector changes the energy input to the associated solar energy system and in turn changes its energy output. In fact, collector orientation aims to get maximum possible incident radiation with time such that to maximize output energy.

The orientation of a solar collector is specified by two angles: the tilt angle $\beta$ and the azimuth angle $\gamma$; see **Fig.6**. The figure shows a non-concentrating collector however it also applies to a concentrating collector. Each of the two angles can be adjusted using different mechanisms within some selected time step such as continuously, daily, weekly, monthly and so on. Three mechanisms of collector orientation are explained below, **Duffie,** and **Beckman, 2013**, **Kalogirou, 2013**.

Tilting mechanism:

For continuous tilting, the tilt angle is adjusted to optimum $\beta_o$ according to:

$$\beta = \theta_z = \beta_o \tag{5a}$$

Otherwise, for tilting in daily, weekly, monthly basis… and so on, the tilt angle is:

$$\beta = |\phi - \delta| = \beta_o \tag{5b}$$

The azimuth angle is determined by:

$$\gamma = \begin{cases} 0° & if \quad \phi - \delta > 0 \\ 180° & if \quad \phi - \delta \leq 0 \end{cases} \tag{6}$$

Where the zenith angle $\theta_z$ is calculated by:

$$cos\theta_z = cos\phi \cos\delta \cos\omega + sin\phi \sin\delta \tag{7}$$

The hour angle $\omega$ in degrees is found as:

$$\omega = 15°(t_s - 12) \tag{8}$$

Solar time in hours $t_s$ is approximately equal to local time for this study. Where $\phi$ is the site latitude and $\delta$ is the solar declination angle and is given by:

$$\delta = 23.45° \sin\left[\frac{360}{365}(284 + n)\right] \tag{9}$$

where n is the nth day of the year.

Azimuthal mechanism:

The tilt angle is

$$\beta = constant \tag{10}$$

Which needs to be optimized such that it gives maximum energy over the whole period of evaluation.

The azimuth angle is adjusted to optimum $\gamma_o$ according to:

$$\gamma = \gamma_s = \gamma_o \tag{11}$$

The sign of $\gamma$ is the same as that of $\omega$ as given by Eq. (8). The solar azimuth angle $\gamma_s$ is found by:

$$\cos\gamma_s = \frac{cos\theta_z \ sin\phi - \sin\delta}{sin\theta_z \ cos\phi} \tag{12}$$

Two-angle mechanism:

Both angles are adjusted to optimum $\beta_o$ and $\gamma_o$ as:

$$\beta = \theta_z = \beta_o \tag{13}$$

And

$$\gamma = \gamma_s = \gamma_o \tag{14}$$

To evaluate a certain orientation mechanism for a given solar collector, the corresponding percentage gain $g\%$, which is the energy increase in respect to the energy of a reference orientation, is calculated as:

$$g\% = (r - 1) \times 100 \quad (15)$$

Where $r$ is energy ratio given by:

$$r = \frac{collector\ energy\ of\ an\ orientation\ mechanism}{collector\ energy\ of\ a\ reference\ orientation} \quad (16)$$

The energy in the ratio $r$ above could be input energy or output energy of the collector over a specified time. Output power could also be used. The denominator of Eq. (16) represents the reference for energy comparison which could be of horizontal or other fixed orientation. For horizontal reference, the two angles are:

$$\beta = 0 \ \ and \ \ \gamma = 0 \quad (17)$$

The gain equation, Eq. (15), is based on half-hourly results of the present study. Then, as required, daily, monthly and annual average gains can be obtained.

## 4. EXPERIMENTAL WORK

The experimental study presented in this paper involves four objectives as follows:

Firstly, the solar collector under study is a non-concentrating type. Thus, aperture and receiver of the collector are identical and the concentration ratio $C$, Eq. (3), is unity.

Secondly, energy gains are to be found using the input energy to solar collector rather than its output energy. Thus, for a given area $A_r$ of the receiver, the energy ratio $r$ of Eq. (16) for gain calculation will be the ratio of the corresponding incident solar radiations as can be found using Eq. (1). In this respect, solar collectors will not discriminate between thermal and PV collectors.

Thirdly, the orientation of collector that to be evaluated for gain is of tilting mechanism with weekly adjustment as described by Eq. (5b) and Eq. (6).

Fourthly, the calculated gains are to be obtained as compared to the horizontal orientation of collector as described by Eq. (17).

For the purpose of applying above issues, two structures of wooden panels are fabricated. One is of adjustable tilt angle $\beta$ such that it can be set manually, at each day of experiment, to optimum value $\beta_o$ according to Eq. (5b) with site latitude $\phi$ equal to 33° for Baghdad city. However, the panel is fixed at zero azimuth angle $\gamma$ according to Eq. (6) since $\phi > \delta$ as given by Eq. (9) for all n. Thus, this panel represents the collector orientation that to be evaluated; see **Fig.7a**.

The other panel is fixed at horizontal orientation, i.e. of zero tilt angle and zero azimuth angle as given by Eq. (17). This panel represents the reference collector for gain calculation; see **Fig.7b**.

Field measurements of global solar radiation on each of the two collector orientations of **Fig.7** are carried out simultaneously at every half-hour from 8:00 am – 4:00 pm. This work is conducted in eight months (17 October 2013 to 15 May 2014) on a weekly basis at the solar laboratory of energy engineering department at Baghdad/Al-Jadriya. These half-hourly data are used to find daily and monthly averages of energy gains of the solar collector. Different climate conditions were encountered, during the 8-month period, such as sunny, windy, cloudy and rainy. This will definitely affect gain values.

## 5. RESULTS AND DISCUSSION

The whole experimental data obtained for a period of eight months were tabulated in Excel sheets according to half-hour measurements of each day of experiment. Excel sheets were programmed to calculate the energy gain from the measured data for the two orientations, tilting and horizontal, of the solar collector. First, the individual gain per each half-hour was calculated by Eq. (15). Then, daily average gains were found. Finally, monthly average gain for each of the eight months, October to May, was determined. In addition, Excel sheets calculate daily and monthly averages of solar radiation for each of the two collector orientations.

In respect to daily average gains within the whole 8-month period, a maximum value of 82% was obtained on 27 December 2013 with half-hourly variation as shown in **Fig. 8**. In fact, during this month the solar declination $\delta$ is at its maximum negative $\approx -23^{o}$. Thus, tilting collector is set at maximum angle of $\beta_o = 56^{o}$ as compared to zero angle of the horizontal collector. This will give maximum energy gain. **Fig. 8** indicates larger gains at hours far from solar noon due to high reflections from surroundings in addition to temporary climate conditions. The corresponding solar radiations are shown in **Fig. 9**. It shows normal profiles of large relative radiation for the two orientations giving large gain as explained above.

On the other hand, a minimum daily average gain of 11.5% was found on 18 April 2014. This low energy gain is due to small declination of about $10^{o}$ during this month which results in a small difference between the two orientations of collector. The variation of energy gain is shown in **Fig.10** which displays larger gains at 2:30 and 3:00 afternoon due to partly cloudy local condition. The half-hourly variation of solar radiations for that day is shown in **Fig. 11**. Owing to small energy gain, the two radiation profiles are close to each other.

Solar radiations on each of the tilting and horizontal collector as monthly average values are shown in **Fig. 12**. Higher levels were obtained for the month of May. Comparable values were also found for the other months except November and January. However, it is expected that maximum radiation will be at June and July. Radiation levels larger than 700 $W/m^2$ were observed on the tilting collector. Whereas for the horizontal collector, measured solar radiations were larger than 450 $W/m^2$. This corresponds to an average sunny climate condition during these months.

For the two months of November and January, lower radiation levels were noticed of smaller than 400 W/m$^2$ on the tilting collector and smaller than 250 W/m$^2$ on the horizontal collector. This is due to cloudy and rainy conditions during most of the two months. Furthermore, **Fig. 12** shows that the relative radiation of the two orientations was larger in winter months than that in the other months. This will be explained below. The relative radiation lies in the range of 1.11 to 1.57.

Monthly average energy gains for the months of October to May are plotted in **Fig. 13**. The gain values were found to be approximately within 12% to 60%. For five months, October to February, the gain was larger than 40%. The profile of energy gain is governed by tilt-angle setting, as determined by the solar declination in Eq. (5b), and the local climate condition. Thus, the profile of **Fig. 13** is increasing for October to December as tilting is being larger. Maximum gain value of 57.8% was obtained at December. Then, gain is decreasing as tilting is being smaller. A minimum gain was noticed in May of 12.2%. It is expected that energy gain will further decrease to its minimum value at June and July when tilting is about 11$^o$. Finally, the data of **Fig. 13** are listed in **Table 1**.

## 6. CONCLUSION

In this study, a brief updated description of solar collector types and applications were presented. Then, based on field measurements of global solar radiation for tilting and horizontal orientations of collector throughout 8-month period in Baghdad, energy gain and radiation level averages were found, see **Fig. 12**, **Fig. 13** and **Table 1**. On the basis of this study, the following conclusions have been drawn:

1- The tilting mechanism of solar collector is more effective for the winter months as compared to the other months.
2- On the contrary, radiation levels for the solar collector are lower for the winter months than that for the other months.
3- There is a significant energy gain of larger than 40% for October to February with a maximum gain of about 58%.
4- For clear sky condition, the tilting and horizontal orientations of collector are of monthly average solar radiation 910 W/m$^2$ and 713 W/m$^2$ respectively.

## REFERENCES


- Ahmed, N., Sheikh, A. K., Gandhidasan, P., and Elshafie, E., 2015, *Modeling, Simulation and Performance Evaluation of a Community Scale PVRO Water Desalination System Operated by Fixed and Tracking PV Panels: A Case Study for Dhahran City, Saudi Arabia*, Renewable Energy, Vol.75, PP.433-447.

- Al-Najjar, H. M. T., 2013, *Experimental Evaluation of the Performance of One-Axis Daily Tracking and Fixed PV Module in Baghdad, Iraq*, Journal of Engineering, Vol.19, No.9, PP.1145-1157.

- Al Tarabsheh, A., Etier, I., and Nimrat, A., 2012, *Energy Yield of Tracking PV Systems in Jordan,* International Journal of Photoenergy, Vol.2012, Article ID890183, 5 pages.

- Amori, K. E., and Al-Najjar, H. M. T., 2012, *Analysis of Thermal and Electrical Performance of a Hybrid (PV/T) Air Based Solar Collector for Iraq,* Applied Energy, Vol.98, PP.384-395.

- Cao, S., Hasan, A., and Sireu, K., 2014, *Matching Analysis for On-site Renewable Energy Systems of Office Buildings with Extended Indices*, Applied Energy, Vol.113, PP. 230-247.

- Chang, T. P., 2009, *Performance Evaluation for Solar Collectors in Taiwan*, Energy, Vol.34, Issue 1, PP. 32-40.

- Duffie, J. A., and Beckman, W. A., 2013, *Solar Engineering of Thermal Processes*, John Wiley and Sons Inc., 4th edition.

- Fang, X., and Li, D, 2013, *Solar Photovoltaic and Thermal Technology and Applications in China*, Renewable and Sustainable Energy Reviews, Vol.23, PP. 330-340.

- Herrando, M., Markides, C. N., and Hellgardt, K., 2014, *A UK-Based Assessment of Hybrid PV and Solar–Thermal Systems for Domestic Heating and Power: System Performance*, Applied Energy, Vol.122, PP.288-309.

- Huld, T., Cebecauer, T., Suri, M., and Dunlop, E., 2010, *Analysis of One Axis Tracking Strategies for PV Systems in Europe*, Progress in Photovoltaics: Research and Applications, Vol.18, Issue 3, PP. 183-194.

- Kalogirou, S. A., 2004, *Solar Thermal Collectors and Applications,* Progress in Energy and Combustion Science, Vol.30, PP.231-295.

- Kalogirou, S. A., 2013, *Solar Energy Engineering: Processes and Systems*, Elsevier Inc., 2nd edition.
- Khorasanizadeh, H., Mohammadi, K., and Mostafaeipour, A., 2014, *Establishing a Diffuse Solar Radiation Model for Determining the Optimum Tilt Angle of Solar Surfaces in Tabass, Iran*, Energy Conversion and Management, Vol. 78, PP.805-814.
- Li, Z., Liu, X., and Tang, R., 2010, *Optical Performance of Inclined South-North Single Axis Tracked Solar Panels*, Energy, Vol.35, Issue 6, PP.2511-2516.
- Lubitz, W. D., 2011, *Effect of Manual Tilt Adjustments on Incident Irradiance on Fixed and Tracking Solar Panels,* Applied Energy, Vol.88, PP. 1710-1719.
- Mills, D., 2004, *Advances in Solar Thermal Electricity Technology*, Solar Energy, Vol.76, PP. 19-31.
- Rebhi, M., Sellam, M., Belghachi, A., and Kadri, B., 2010, *Conception and Realization of Sun Tracking System in the South-West of Algeria,* Applied Physics Research, Vol.2, No.1, PP.66-75.
- REN21, 2013, *Renewables 2013: Global Status Report*.
- Sen, Z., 2008, *Solar Energy Fundamentals and Modeling Techniques*, Spring-Verlag.
- Skeiker, K., 2009, *Optimum Tilt Angle and Orientation for Solar Collectors in Syria,* Energy Conversion and Management, Vol.50, Issue 9, PP. 2439-2448.
- Sunderan, P., Ismail, A. M., Singh, B., and Mohamed, N. M., 2011, *Optimum Tilt Angle and Orientation of Stand-Alone Photovoltaic Electricity Generation Systems for Rural Electrification*, Journal of Applied Sciences, Vol. 11, No. 7, PP. 1219-1224.
- Tiwari, G. N., and Dubey, S., 2010, *Fundamentals of Photovoltaic Modules and Their Applications*, RSC publishing.
- Twidell, J., and Weir, T., 2005, *Renewable Energy Resources*, Taylor & Francis, 2nd edition.


## NOMENCLATURE

$A_a$ = surface area of concentrator aperture, $m^2$.

$A_r$ = surface area of collector receiver, $m^2$.

$C$ = concentration ratio, dimensionless.

CPV= concentrating photovoltaic collector.

CPVT= concentrating photovoltaic thermal collector.

$E_i$ = input energy to collector, kWhr.

$E_o$ = useful output energy, kWhr.

$G_{ia}$ = global solar radiation incident on the aperture, kWhr/m$^2$.

$G_{ir}$ = incident solar radiation on the receiver, kWhr/m$^2$.

g = energy gain of collector, dimensionless.

n = nth day of the year, $1 \leq n \leq 365$.

PV= photovoltaic.

PVT= photovoltaic thermal collector.

r = energy ratio of collector, dimensionless.

$S_r$ = absorbed energy per unit area of the receiver, kWhr/m$^2$.

$t_s$ = Solar time, hours.

$\alpha$ = lumped parameter for collector optical characteristics: $0 < \alpha < 1$, dimensionless.

$\beta$ = tilt angle: the angle between the plane of collector surface and the horizontal, $0° \leq \beta \leq 90°$.

$\beta_o$= optimum tilt angle of collector, degrees.

$\gamma$ = azimuth angle: the deviation of the projection on a horizontal plane of the normal to collector surface from the solar noon, $-180° \leq \gamma \leq 180°$.

$\gamma_o$= optimum azimuth angle of collector, degrees.

$\gamma_s$= solar azimuth angle: the angular displacement from south of the projection of beam radiation on the horizontal plane, degrees.

$\delta$ = solar declination angle: the angular position of the sun at solar noon with respect to the plane of the equator, $-23.45° \leq \delta \leq 23.45°$.

$\theta_z$ = zenith angle: the angle between the vertical and the line to the sun, degrees.

$\phi$ = site latitude: the angular location north or south of the equator, $-90° \leq \phi \leq 90°$.

$\omega$ = hour angle: the angular displacement of the sun east or west of the solar noon due to earth rotation, degrees.

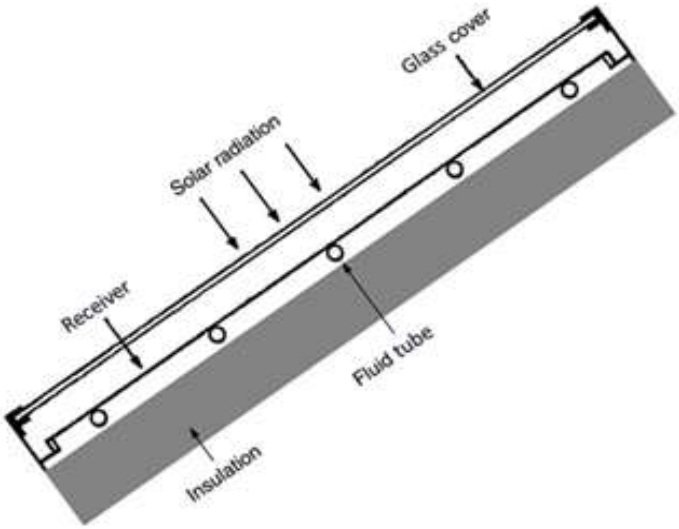


**Figure 1.** Non-concentrating thermal collector.

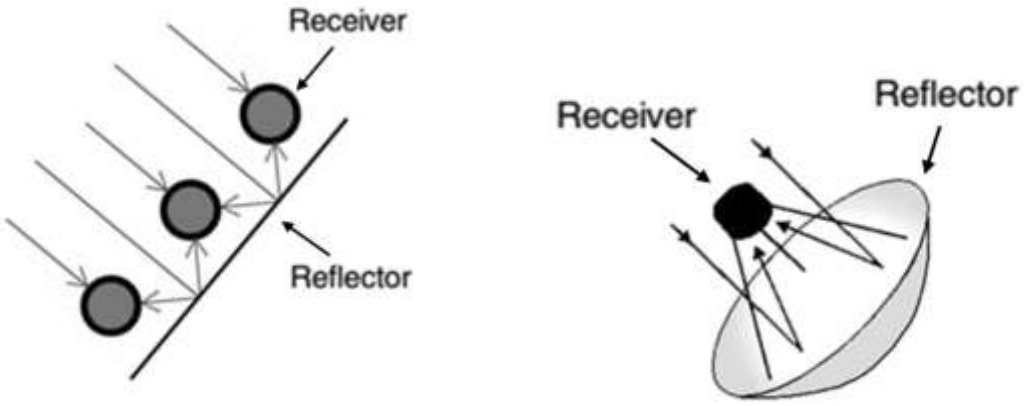


(a) (b)

**Figure 2.** Concentrating thermal collector (a) with linear concentrator (b) with circular concentrator.

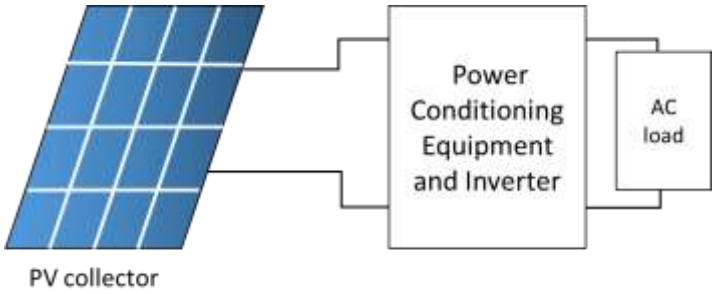


**Figure 3.** Electric circuit for PV collector.

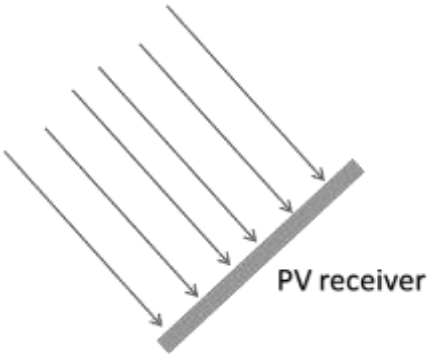


**Figure 4.** Non-concentrating PV collector.

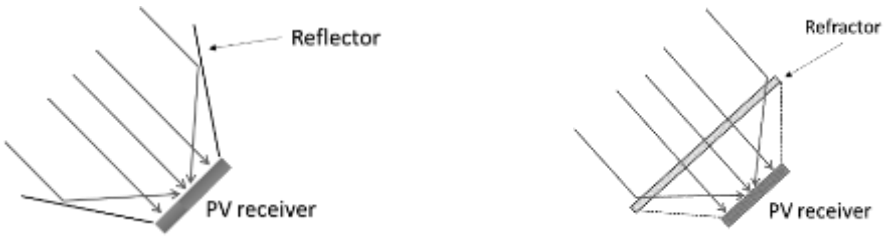


(a) (b)

**Figure 5.** CPV collector (a) with reflector (b) with refractor.

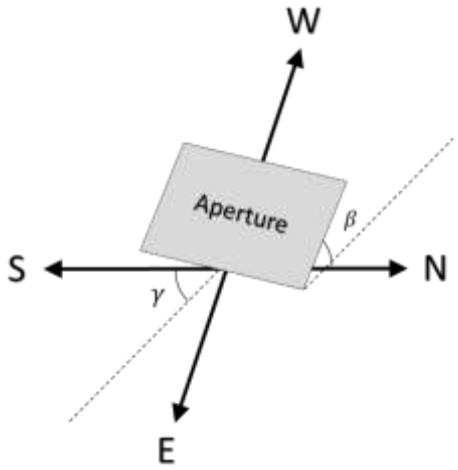


**Figure 6.** Tilt and the azimuth angles of solar collector.

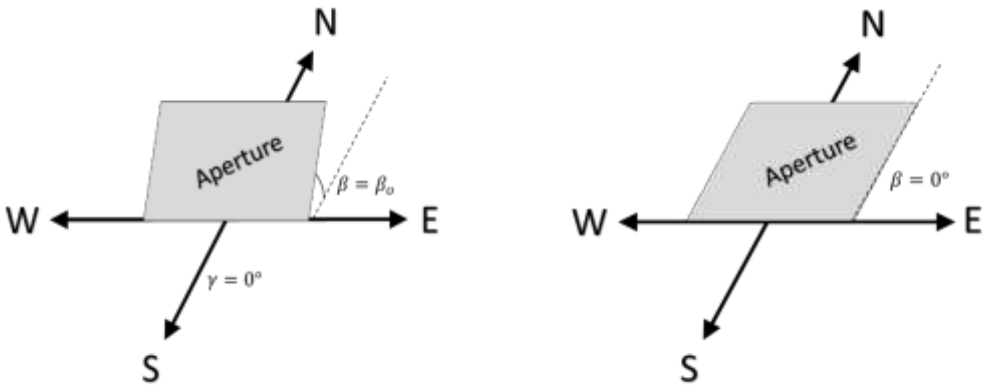


(a) (b)

**Figure 7.** Orientations of the solar collector under study: (a) tilting orientation (b) horizontal orientation.

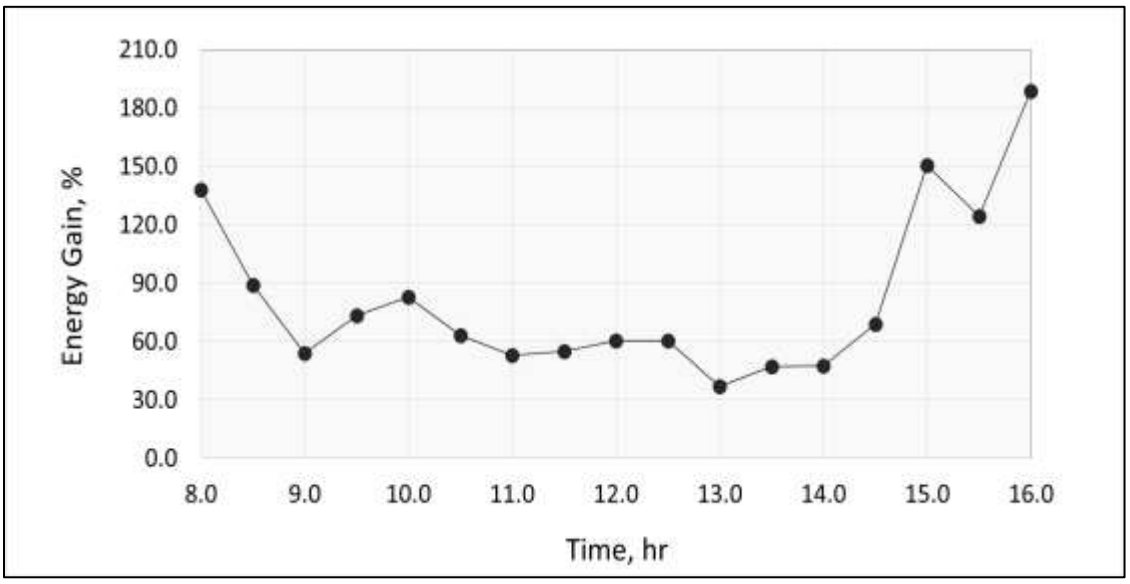


**Figure 8.** Variation of energy gain on 27 December 2013.

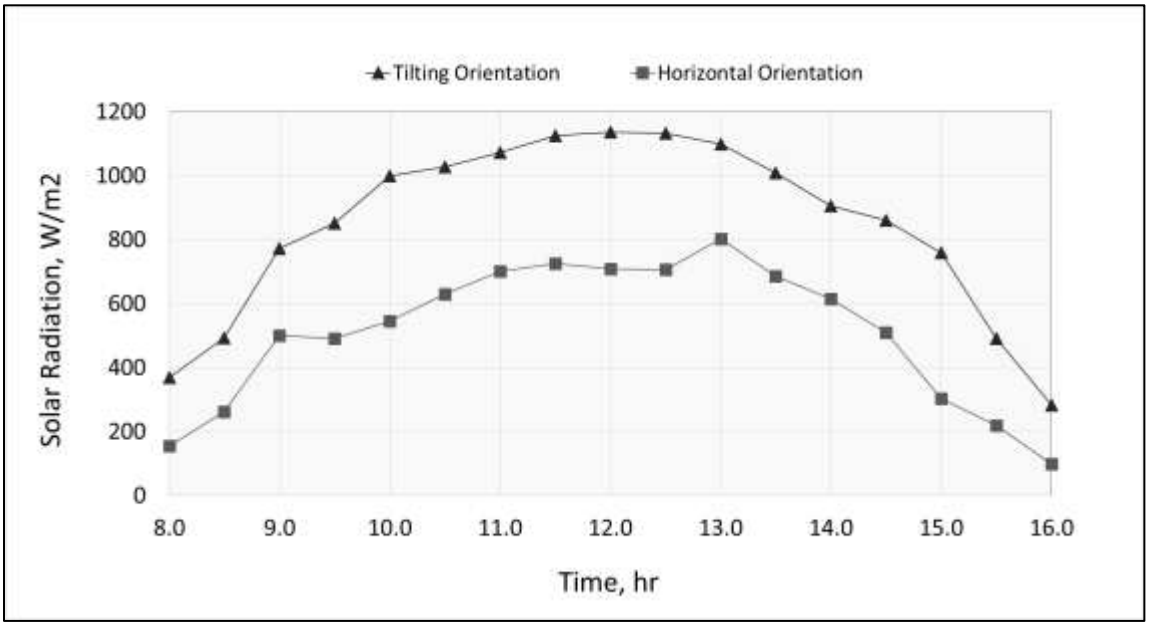


**Figure 9.** Variation of incident solar radiation on 27 December 2013.

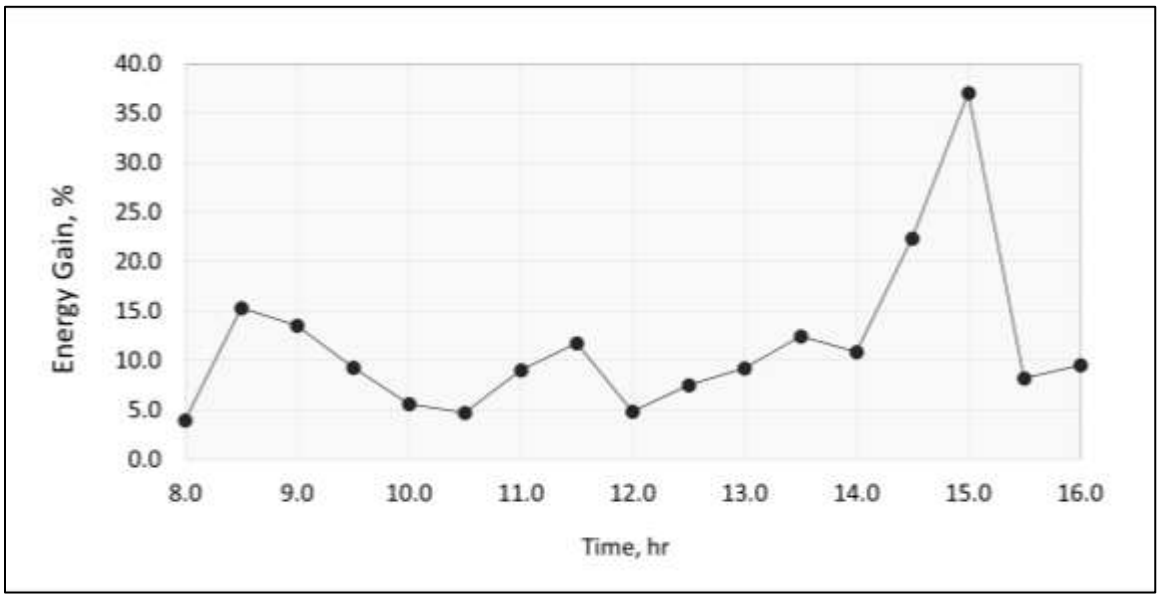


**Figure 10.** Variation of energy gain on 18 April 2014.

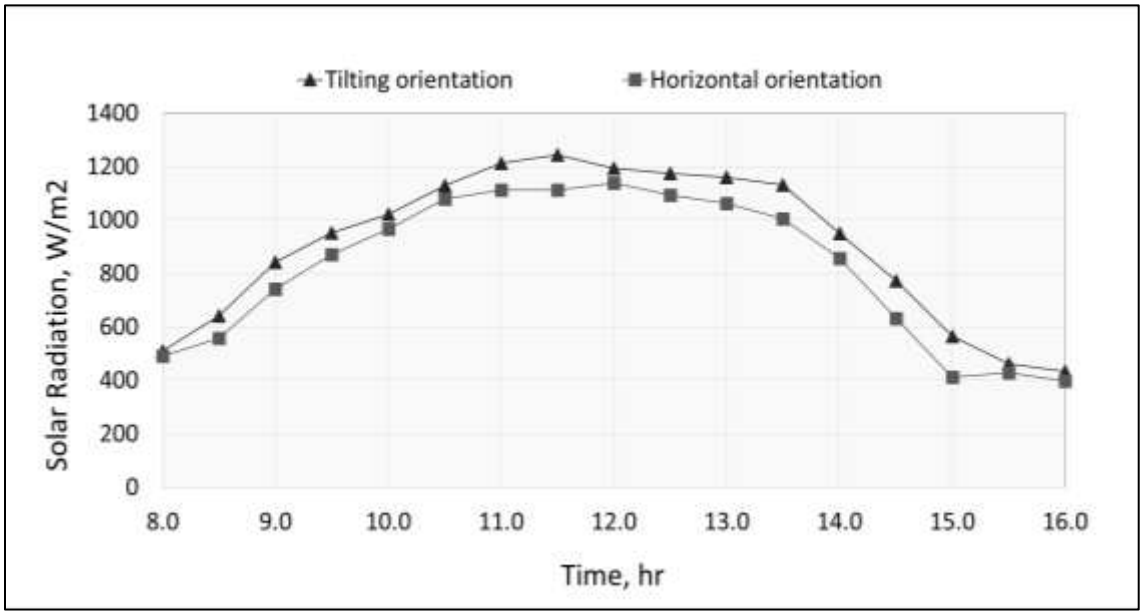


**Figure 11.** Variation of incident solar radiation on 18 April 2014.

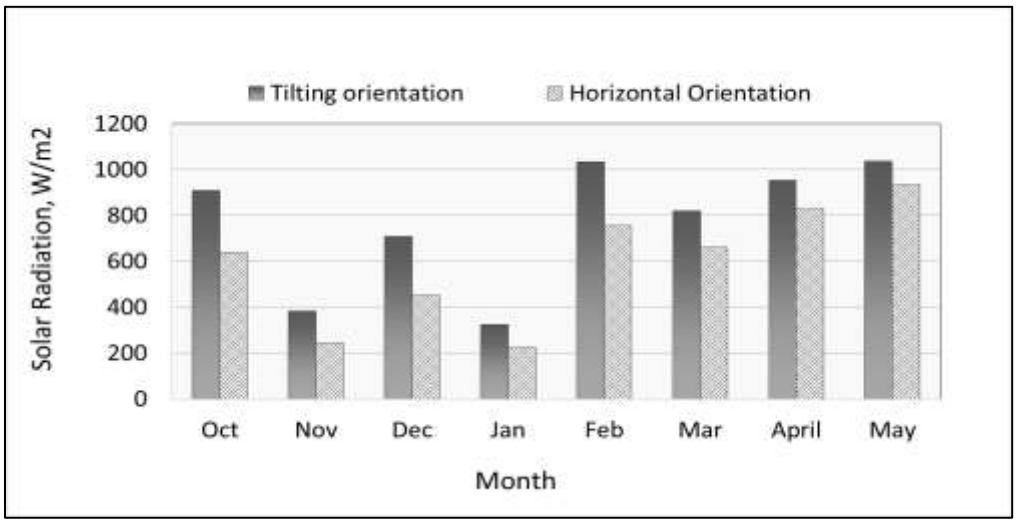


**Figure 12.** Variation of monthly average solar radiation.

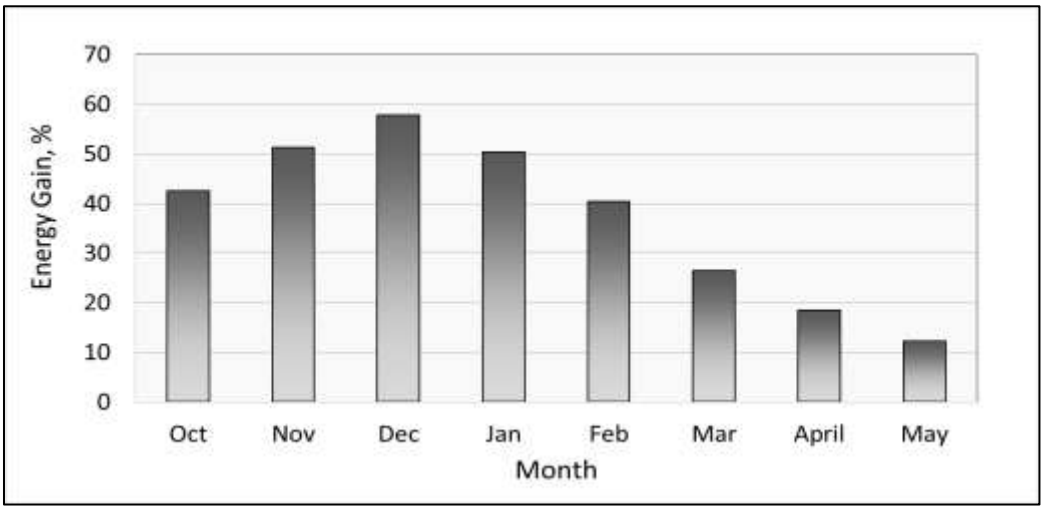


**Figure 13.** Variation of monthly average energy gain.

**Table 1.** List of monthly average gain.

| Month | Energy Gain, % |
|---|---|
| October | 42.5 |
| November | 51.3 |
| December | 57.8 |
| January | 50.3 |
| February | 40.4 |
| March | 26.4 |
| April | 18.5 |
| May | 12.2 |

# Development of Spatial Data Infrastructure based on Free Data Integration

**Dr. Maythm al-Bakri**
Lecturer
Department of Surveying
College of Engineering
University of Baghdad
Email: m.m.m.s.albakri@gmail.com

## ABSTRACT

In recent years, the performance of Spatial Data Infrastructures for governments and companies is a task that has gained ample attention. Different categories of geospatial data such as digital maps, coordinates, web maps, aerial and satellite images, etc., are required to realize the geospatial data components of Spatial Data Infrastructures. In general, there are two distinct types of geospatial data sources exist over the Internet: formal and informal data sources. Despite the growth of informal geospatial data sources, the integration between different free sources is not being achieved effectively. The adoption of this task can be considered the main advantage of this research. This article addresses the research question of how the integration of free geospatial data can be beneficial within domains such as Spatial Data Infrastructures. This was carried out by suggesting a common methodology that uses road networks information such as lengths, centeroids, start and end points, number of nodes and directions to integrate free and open source geospatial datasets. The methodology has been proposed for a particular case study: the use of geospatial data from OpenStreetMap and Google Earth datasets as examples of free data sources. The results revealed possible matching between the roads of OpenStreetMap and Google Earth datasets to serve the development of Spatial Data Infrastructures.

**Key words:** SDI; OSM; Google Earth; Geospatial Data Integration; Data Quality

# تطوير البنى التحتية للمعلومات المكانية بتكامل البيانات المجانية

**م.د. ميثم مطشر شرقي**
قسم هندسة المساحة
كلية الهندسة / جامعة بغداد

## الخلاصة

لقد نالَ تطور منظومة البنى التحتية للمعلومات المكانية (SDIs) في السنوات الأخيرة اهتماماً كبيراً من قبل الحكومات والشركات ذات العلاقة. هنالك أنواع وفئات مختلفة من المعلومات المكانية مثل الخرائط الرقمية ، الاحداثيات ، الخرائط على الشبكة العنكبوتية ، الصور الجوية والفضائية يجب توفرها من اجل تحقيق المقومات الاساسية لمنظومة البنى الاساسية للمعلومات المكانية (SDI). بصورة عامة هناك مصدران اساسيان للمعلومات المكانية على الشبكة العنكبوتية: المصادر الرسمية والغير الرسمية والتي عادة ماتكون مجانية. على الرغم من النمو السريع للبيانات المكانية المجانية على الشبكة العنكبوتية ، الا ان تكامل وادماج هذه البيانات مع بعضها البعض للاستفادة منها في تطبيقات مختلفة كبناء منظومة SDI لم يتحقق بشكل فعال لحد الان. إن تبني هذه المهمة يمكن أن تعتبر الميزة الرئيسة لهذه الدراسة. يتضمن هذا البحث الاجابة عن السؤال في كيفية دمج البيانات الجغرافية المكانية الحرة وتوظيفها بحيث تكون مفيدة في مجالات مختلفة مثل تطوير (SDI).

لتنفيذ هذه المهمة تم اقتراح منهجية عامة تستخدم المعلومات الهندسية الخاصة بشبكات الطرق مثل الاطوال ، النقاط الوسطية ، احداثيات نقاط البداية والنهاية ، عدد العقد ، الاتجاهات من أجل مقارنتها وبيان امكانية دمجها. اقترحت هذه المنهجية لدراسة حالة معينة : استخدام البيانات الجغرافية من خريطة الشارع المفتوح (OSM) وبرنامج Google Earth (GE) كأمثلة على مصادر البيانات المجانية. اظهرت النتائج امكانية تكامل بيانات شبكات الطرق من المصادر المجانية للمعلومات المكانية وتوظيفها لخدمة وتطوير منطومة البنى الأساسية للمعلومات المكانية (SDIs).

## 1. INTRODUCTION

During the past decade the development of the World Wide Web (www) has led to a massive increase of geospatial information by non-specialist users. This kind of information was termed by **Goodchild, 2007** as volunteered geographic information (VGI). Various VGI applications exist that allows users to upload and browse information in various media (text, pictures, videos, documents, etc.), where such information becomes 'spatial' through links to a spatial reference**, DeLongueville, et al., 2010**. Nowadays, there is a wide variety of geospatial data sources available on the Internet such as the Google Map service, the OpenStreetMap (OSM) project, the Yahoo imagery, the Google Earth (GE) software and many others. Inconsistent data quality is expected in a VGI datasets which makes data integration more challenging task.

Data integration is generally defined as the process of combing different datasets to improve one of them or to enhance the visual presentation of overlaid spatial datasets, **Koukoletsos, et al., 2012**. Integrated geospatial datasets may have different quality issues, often due to the way that each was compiled. Therefore, the data quality issue becomes important when integrating spatial data. A number of authors have considered the effects of geospatial data quality on data integration. For example, **Neis,** and **Zielstra, 2014** studied the current developments in VGI research, focusing on the different methods that were applied to analyze the VGI data quality. They concluded that the development of new methods that compute a trust factor, contributor reputation or individual contributor data quality is required. **Koukoletsos, et al., 2012** proposed an automated feature-based matching method specifically designed for VGI. It is applied to the OSM dataset using the official data from Ordnance Survey as the reference dataset. The results are then used to evaluate data completeness of OSM in several case studies in the UK. In the same view, **Pourabdollah, et al., 2013** presented a method for conflating road attributes, namely the name and reference code, of OSM with the open data provided by Ordnance Survey. It was shown that the best correspondence between attributes exists in the very dense areas, followed by the very low density areas, and lastly in the middle to large sized cities.

The main goal of the current study was to create a program which can assess and report on linear geospatial data quality. This program requires the inclusion of a range of linear data quality measures (e.g. lengths, centeroids, start and end points, number of nodes and directions) which will be coded and tested to ensure the creation of a data quality index. This index will be applied to a number of geospatial data sets and an assessment based on it will be made of the possible data integration of such data sets. The types of data set to be used include OpenStreetMap (OSM) and Google Earth (GE). The result will be a working system or potentially a report on linear data quality, which can be used to integrate data sets.

## 2. BACKGROUND

### 2.1 Spatial Data Infrastructure: Development and Concepts

In general, a spatial data infrastructure (SDI) can be defined as the implementation of a framework of geographic data, technology, human resources, software, and polices that are linked in order to process, disseminate and share geospatial data in effective way. Over the last few years, various authors have been defined the term "SDI" differently. For instance, according to **Williamson, 2004** the SDI means a special case of Information Infrastructure, specifically geared towards geographic information. In a follow-up study, **Hjelmager, et al., 2008** wrote that the SDI is an evolving concept about facilitating and coordinating the exchange and sharing of spatial data and services between stakeholders from different levels in the spatial data community. In a study conducted by **Mohammadi, et al., 2010**, it was shown that the SDI aims to better address the technical and nontechnical issues and facilitate data integration. The SDIs aim to provide a holistic platform for users to interact with spatial data through technical and nontechnical tools.

In their analysis of SDI, **Rajabifard,** and **Williamson, 2006** identified the main components of SDI as a data, policy, network, standards and people, as shown in **Fig. 1**. In general, a data component represents various layers of geospatial data. The layers may include satellite images, geographic names, coordinates, administrative boundaries and elevation for a country or jurisdiction. These geospatial data sources are managed by different communities and their geospatial data quality are different as well. For instance, maps for necessary purposes such as land use maps, topographic mapping for the military applications and cadastral maps have been produced by formal or governmental institutions. In many countries, much of these data are protected by the data license due to their high quality. At the same time, the maps which have been performed by these institutions are invested and considered as a source of economy. This

can be easily recognised through pricing policies and legal copyright, **Perkins,** and **Dodge, 2008.** Whereas, the recent development in communication technologies allowed for establishing open source collaborative map projects which usually free datasets, **Geller, 2007**. The differences between various sources of free datasets can cause some integration problems for SDI applications. Hence, this investigation has attempted to resolve data integration problem of linear features from OSM and GE sources to serve SDI management.

### 2.2 OpenStreetMap Project

The OpenStreetMap (OSM) project (www.openstreetmap.org) was started by Steve Coast in England in 2004, and its aim is to create a free world map. In many ways the OSM is similar to Wikipedia, the free encyclopaedia. Anyone can contribute (edit, add or delete data) to Wikipedia, just as anyone can contribute to OSM. The central purpose of OSM is to collect geodata, and make that data available to anybody in its raw form. In addition to that, the project also offers a number of different maps on the web, which are created from this raw data. By looking at OSM one can be able to select different map layer such as Standard, Cycle Map, Transport Map, MapQueqst Open and Humanitarian, **Ramm,** and **Chilton, 2011**.

Objects drawn on an OSM map are called map features. A map features have a geographic coordinates and descriptions. OSM project includes several groups of features such as roads and railways; forests, lakes and rivers; coastline and islands; buildings and land use areas. The most important group of objects in OSM are, of course, streets. They are tagged using the highway key, with a value describing the type of street or way. The road classification in OSM service was based on the road types in the world, as illustrated in **Table 1, Ramm,** and **Chilton, 2011.** In this analysis, the road network of all OSM ways was used for integrating with the correspondence ways of GE datasets.

### 2.3 Google Earth Software

Google Earth (GE) is the most popular 3-dimension virtual globe system that offers free access to high resolution imagery for most of the global. It was launched in 2005 by Google. The GE can also provide digital elevation data, which is collected by NASA's Shuttle Radar Topography Mission. In recent years, the using of GE has become more popular by general public and scientific communities. This is due to the fact that the GE is user friendliness, free of charge, wide availability, minimal system and computing power requirements. In addition, GE do not

need for extensive training compared with popular geographic information systems (GIS) software, **Benker, et al., 2011**. One of the most gorgeous features of GE is the use of one coordinate system for the whole of the world, that is, WGS84 (World Geodetic System which was found in 1984). This means that every position on the Earth can be stored by the value of geographic coordinates (latitude / longitude). Therefore, GE has been used, for example, to collect ground control points (GCPs), for orthorectification of satellite imagery, to estimate urban vegetation cover, to visualize the output of scientific experiments, and as reference data to evaluate land cover datasets, **Hernández, et al., 2013**.

Although these are positive aspects, however, the resolution of GE images is vary for different areas of the globe. Besides, the 3D viewer modelling is limited for some countries and cities, for instance there is no 3D data for Iraq, while other places such as UK have a detailed 3D data for all cities and countryside. Another limitation of GE is that the inconsistency of positional accuracy of GE data. Therefore, a series of accuracy assessments of GE's imagery have been undertaken by different researchers. For example, **Benker, et al., 2011** assessed the accuracy of GE imagery in the Big Bend region of Texas, USA based on high precision field measurements (<1 m). They found that GE's imagery has a horizontal mean error of 6.95 m and Root Mean Square Error (RMSE) of 2.64 m. In an investigation into accuracy assessment of GE data, **Mohammed, et al., 2013** estimated the GE horizontal and vertical accuracy in Khartoum state. The finding showed that the (RMSE) for horizontal coordinates was 1.59 m and for height measurement was 1.7 m. In another major analysis, **Pulighe, et al., 2015** examined the horizontal accuracy of very-high resolution GE images for the Rome / Italy. The results revealed that very-high resolution GE images have an overall positional accuracy to 1 meter.

To the best of our knowledge, there is a lack of evaluating the integration of GE data with other open source data; therefore this research attempts to contribute to the presenting of a methodology for integrating linear features, such as roads, form GE and OpenStreetMap (OSM) data sources.

## 3. STUDY SITE AND DATASET

The study area of this case study is situated in the city of Al-Jadriya, placed in Baghdad the capital of Iraq **(Fig. 2)**. It covers approximately 18 $km^2$. The study area covers few centres of population (including the city centre), and some scattered green areas around them. The reason for selecting this area was to test the possibility of integrating open source geospatial data outside the cities where there are high levels of participation such as UK. The selected site is

located within the longitude ranging from 44.368694° E to 44.436500° E and the latitude ranging from 33.262502° N to 33.311578° N. From the map of the study area can see the details of the roads that were under analysis in the research (see **Fig. 2 and Table 1**).

In this study, the data of OpenStreetMap (OSM) service were downloaded from Geofabrik (www.geofabric.de) in 2015. This server has data extracts from the OSM project which are normally updated every day. Data on the download server is organised by region. The OSM data directory contains files that have a whole continent's data in them, and for some continents there are subdirectories in which you find individual files for various countries. Some countries again have their own subdirectories with data for administrative subdivisions. For instance, the OSM data for Iraq are available as a one directory with different layers for the whole country. The Geofabrik service can provide OSM data as shapfiles which can be processed directly by almost GIS software.

In order to enable a comparative analysis, the Google Earth (GE) roads dataset was used as other open source data. The GE makes it easy to search for the coordinates of any location and zooming in on them. There are many ways to obtain coordinates: move the mouse cursor to where you want, and note the coordinates displayed in the lower left-hand corner of the GE display window. Other useful way to obtain coordinates from GE is creating a place mark (probably in the temporary folder). Right-click or control-click on the place mark; one of the options is "Copy". Copy the place mark and paste it back to a text editor. The result is a KML (Keyhole Markup Language) description of the place mark, and since KML is XML, it's easily manipulable. The latest method has been adopted to acquire GE data for the study area of this research.

**Fig. 3** illustrates a sample of the road networks in OSM and GE. Red lines represent GE data and blue lines represent OSM data. It can be seen from the figure below that the roads from two data sources are almost similar. However, in some places there are some roads recorded in GE data whereas they are not recorded in OSM data. Therefore, adopting a convenient data integration process can improve and enrich OSM data based on GE data or vice versa.

## 4. PROGRAM DESIGN

A geospatial data from different sources contain various features. Data integration of multisource geospatial data, take advantage of the strengths of a single data source for improvement of visual interpretation and quantitative analysis. In order to achieve the main goal of this project (data

integration), the properties of tested data must be checked carefully. It is indispensable because the information of different free sources is often not complaint to any standard and each organisation is producing the datasets at various level of richness. There are different methods of properties quality assessment and several pieces of research have focused on evaluating them, **Tveite, 1999; Devillers, et al., 2006; Haklay, 2010**. In this investigate the assessment of the quality of data provided by open sources will depend on a comparison of the roads network parameters such as lengths, centeroids, start and end points, number of nodes and directions. The result will be a set of operators which can measure data quality, allow for the preparation of datasets prior to successful integration, and actually undertake the integration of data. This can be used to determine whether the integrated procedure can be achieved or whether the selected data should be changed. This will allow for purposes such as data updates between datasets, contribute to change detection strategies, and assuring map auditing for optimum data quality.

In order to implement the methodology of this research, a program was encoded using Matlab. The Matlab was adopted because it has the ability for producing and analysing scientific graphs, developing effective algorithms, and achieving efficient mathematical computations, in addition to involving tools for programming matrices operations. **Fig. 4** shows a diagram for the workflow of the designed program. In the first step, the program required calling or loading tested data. The tested roads network data extracted using ArcGIS software, and then exported from ArcGIS to save it as .xlsx in order to import into the coded program.

The open source data was designed to include different feature types such as roads, politics boundaries, buildings, lakes, rivers, etc. Therefore, in pre-processing phase the tested data was filtered to obtain only road data for integration test. The purpose of the primary filter is to quickly create a subset of the data and reduce the consuming of the processing time. Afterwards, it is required to enter the number of observations (number of tested roads) into the program. Subsequently, the program will check the integration parameters (conditional expression) such as lengths, centeroids, start and end points, number of nodes and directions to decide the proceeding into integration process or not. If the tested data pass the conditional expression, the program will go directly into successful integration, otherwise the program will return back into the previous step to select alternative dataset.

## 5. EXPERIMENT AND RESULTS ANALYSIS

### 5.1 The Roads Length

The intensity of mapping activities of open source data for any city can be reflected by road length characterization. Therefore, it is necessary to consider roads length as one parameter of roads network data integration processing. The assumption is that the length of compared features is approximately similar to the length of its matching feature(s). In this research, the roads length was imported from OSM and GE databases using ArcGIS 9.3. The roads lengths of 212 pairs of homologous roads were considered. It can be seen from **Fig. 5** that more than 70% of the differences in the length are within 5m. This is quite a good number for the matching length of roads from OSM and GE datasets.

### 5.2 The Centroid of the Roads

In mathematics and physics, the centroid or geometric centre of a two-dimensional region is the arithmetic mean (average) position of all the points in the shape. The definition extends to any object in n-dimensional space: its centroid is the mean position of all the points in all of the coordinate directions. Informally, it is the point at which a cardboard cut-out of the region could be perfectly balanced on the tip of a pencil, assuming uniform density and a uniform gravitational field. The centroid of any polyline ($X_c$ , $Y_c$) can be defined as follows:

$$X_c = \frac{1}{\int_l dL} \int_L x\, dL \quad (1)$$

$$Y_c = \frac{1}{\int_l dL} \int_L y\, dL \quad (2)$$

Where dL is the differential element of length, and it can be expressed as $d_L = \sqrt{dx^2 + dy^2}$. In this project, the centroid of the selected pairs of roads was calculated and the results are presented in **Fig. 6**. As can be seen from the bar chart below, there are no instances of the shift between the centroid of OSM and GM datasets lay between zero and less 3m, and nearly 70% of the shift lay between 3m and 9m and the rest has spread over a wide range up to 17m. Hence, this is an indication of an efficient judgment of roads integration from OSM and GE data sources.

### 5.3 Start and End Points

Regarding the accuracy of start and end points of roads, efforts to date have focused primarily on road intersections only, **Zielstra,** and **Zipf, 2010; Haklay, 2010; Girres,** and **Touya, 2010**, and

have not evaluated the accuracy of other point features such as start and end points of roads. In order to expand the current state-of-knowledge, this part of study has addressed point features representing the start and end points of the roads of OSM and GE datasets. **Fig. 7 and 8** illustrate the summary statistics for the differences between the coordinates of start and end points of the compared roads. It is clear from the data in charts that the distribution of both groups is similar. In addition, over sixty percent of those lay between 0 and 6 m which indicated that this comparison can be a good metric for integrating OSM and GE datasets.

### 5.4 Number of Nodes and Vertices

Shape points are the ends and bends that define the feature's outline. At the beginning and end of every line feature is a node, whereas at each bend (change of direction) is a vertex. A shape of any feature is recorded by using the coordinates of its shape points. In this study, the difference in node number of all OSM and GE object lines were determined. As shown in **Fig. 9**, almost two-third of the compared roads (68%) has the same number of nodes and vertices, while only 28% has one node different, which is quite acceptable for integrating linear features.

### 5.5 The Angle of Road Direction

A recent study by **Zhao, et al., 2015** suggested that the using of road direction can be a good measure for linear data integration. In this research, the measuring of the angle of direction was prepared according to the procedure used by **Zhao, et al., 2015**. Thus the road angles were measured based on a planer coordinates system joining the start and end points of the line and the vertical axis. **Fig. 10** shows the summary statistics for the preliminary analysis of the differences in the direction of roads between tested datasets. It is apparent from this data that nearly eighty percent of the differences in direction were within 5 degrees. According to these observations, we can infer that it is possible to choose 5 degrees as threshold values for integrating network roads from OSM and GE datasets.

## 6. DISCUSSION AND CONCLUSION

The free and online mapping sources have experienced increase in geospatial data contributions in recent years. This is due to the fact that profiting from the wide availability of online geo-data on the Internet. The amounts of free geographical information are increasing every day. For instance, a recent statistics showed that the geospatial information database project provides

1400 web map servers that provide over 200,000 map data layers. Profiting from the free accessibility of UGC data (licence, cost, sharing) and opening up a new paradigm of geo-data-people's SDI. Thousands of users are able to access to current volunteered geographic information (VGI) data without any charge whereas; in European countries formal geographical data is expensive and out of the reach of individuals, **Perkins,** and **Dodge, 2008**. Potential benefits in integration e.g. contributing to more informed decision and making videos of location. Nowadays, in any part of the world, the VGI sources let visitors to search a world map and download different portions remotely, **Haklay,** and **Weber, 2008**. The VGI content can also potentially fill in the gaps in places where formal data is scare, unreliable and unavailable. Hence, huge benefits can be gained by integrating open source datasets especially in developing SDI applications.

Conventionally, the geospatial data for an SDI have provided by official (governmental) mapping agencies. However, users usually pay to obtain official mapping data; therefore VGI becomes another way to contribute for spatial information management and SDI development. Today, the VGI is one of the embedding areas within SDI especially for applications need to update SDI quickly such as emergency services. For instance, the United Nations based on VGI from OSM as the most important source to collect geospatial data and create route maps when an earth quick hit Haiti in January 2010. Therefore, it is necessary to encourage volunteers to enlarge the free and open source maps and overcome the potential and limitations of their contributions.

The aim of this research was to investigate the integration of open source geospatial datasets and assess its quality. The method compared geometric properties of road networks such as lengths, centeroids, start and end points, number of nodes and directions. The majority of the tests were based on OpenStreetMap (OSM) and Google Earth (GE) datasets. The results showed that more than 70% of the differences in the length are within 5m. Also, there are no instances of the shift between the centroid of OSM and GM datasets lay between zero and less 3m, and nearly 70% of the shift lay between 3m and 9m and the rest has spread over a wide range up to 17m. In addition, over sixty percent of the differences in start and end points lay between 0 and 6m. Moreover, almost two-third of the compared roads (68%) has the same number of nodes and vertices, while only 28% has one node different. The comparison between the directions of the tested datasets reported that almost eighty percent of the differences in direction were within 5

degrees. The findings of this study suggest that in general it is possible to choose the obtained metrics as a threshold values for successful integration of network roads from OSM and GE data sources.

## REFERENCES


- Benker, S.C; Langford, R.P.; Pavlis, T.L., 2011, *Positional Accuracy of the Google Earth Terrain Model Derived from Stratigraphic Unconformities in the Big Bend Region, Texas*, USA. Geocarto International, 26(4), PP. 291-301.

- DeLongueville, B., G. Luraschi, P. Smits, S. Peedell, and T. De Groeve., 2010, Citizens as sensors for natural hazards: a VGI integration workflow. Geomatica, 64(1), PP. 41-59.

- Devillers, R. and R. Jeansoulin (eds), 2006, Fundamentals of Spatial Data Quality. Great Britain: Antony Rowe Ltd, Chippenham, Wiltshire.
- Geller, T., 2007, *Imaging the World: The State of Online Mapping*, IEEE Computer Graphics and Applications, March/April: 8-13.

- Girres, J., and G. Touya., 2010, *Quality Assessment of the French OpenStreetMap Dataset*, Transactions in GIS, 14 (4), PP. 435–459.

- Goodchild, M.F., 2007, *Citizens as Sensors: The World of Volunteered Geography*, Geojournal, 69 (4), PP. 211-221.

- Haklay, M., 2010, *How Good is Volunteered Geographical Information? A Comparative Study of OpenStreetMap and Ordnance Survey Datasets*, Environment and Planning B: Planning and Design, 37 (4), PP. 682–703.

- Haklay, M., and Weber, P., 2008, *OpenStreetMap: User-Generated Street Maps*, IEEE Pervasive Computing 7 (4): 12-18.

- Hernández, C., Salinas-Castillo, W., Guevara-cortina, F., and X. Martínez-Becerra, 2013, *Horizontal Positional Accuracy of Google Earth's Imagery over Rural Areas: A study Case in Tamaulipas, Mexico*, BCG - Boletim de Ciências Geodésicas.

- Hjelmager, J. et al., 2008, *An Initial Formal Model for Spatial Data Infrastructure*, International Journal of Geographical Information Science, 22(11), PP.1295-1309.

- Koukoletsos, T; Haklay, M; Ellul, C, 2012, *Assessing Data Completeness of VGI through an Automated Matching Procedure for Linear Data*, Transactions in GIS, 16 (4), PP. 478 - 498.

- Mohammed, N., Ghazi, A., and Mustafa, H., 2013, *Positional Accuracy Testing of Google Earth*, International Journal of Multidisciplinary Sciences and Engineering, 4 (6), PP. 6-9.

- Mohammadi, H., Abbas, R. and Ian P. Williamson, 2010, *Development of an Interoperable Tool to Facilitate Spatial Data Integration in The Context of SDI*, International Journal of Geographical Information Science, 24 (4), PP. 487–505.

- Neis, P. & Zielstra, D., 2014, *Recent Developments and Future Trends in Volunteered Geographic Information Research: The Case of OpenStreetMap*. Future Internet, 6, PP. 76- 106.

- Perkins, C., M. Dodge, 2008, *The Potential of User-Generated Cartography: A case Study of The OpenStreetMap Project and Mapchester Mapping Party*, North West Geography, 8, PP. 19-32.

- Pourabdollah, A.; Morley, J.; Feldman, S.; Jackson, M., 2013, *Towards An Authoritative OpenStreetMap: Conflating OSM and OS OpenData National Maps' Road Network*, ISPRS Int. J. Geo-Inf., 2, PP. 704–728.

- Pulighe Giuseppe, Valerio Baiocchi & Flavio Lupia, 2015, *Horizontal Accuracy Assessment of Very High-Resolution Google Earth Images in The City of Rome, Italy*, International Journal of Digital Earth

- Rajabifard, A. and I. Williamson, 2006, *The Integration of Built and Natural Environmental Datasets Within National SDI Initiatives*, Seventeenth United Nations Regional Cartographic Conference for Asia and the Pacific, New York**:** 7.
- Ramm, F., Topf, J. and Chilton, S., 2011, *OpenStreetMap - Using and Enhancing the Free Map of The World*, Cambridge, England: UIT Cambridge Ltd.
- Tveite, H. and S. Langass, 1999, *An Accuracy Assessment Method for Geographical Line Data Sets based on Buffering*, International Journal of Geographical Information Science, Vol. 13 (1): PP. 27-47.
- Williamson, I., 2004, *Building SDIs—The Challenges Ahead*, In Proceedings of the 7th International Conference: Global Spatial Data Infrastructure, 2–6 February, Bangalore, India.

- Zielstra, D., and A. Zipf., 2010, *A Comparative Study of Proprietary Geodata and Volunteered Geographic Information for Germany*, In 13th AGILE International Conference on Geographic Information Science.

- Zhao, P., Jia, T., Qin, K., Shan, J., and Jiao, C., 2015, *Statistical Analysis on The Evolution of OpenStreetMap Road Networks in Beijing*, Physica A, 420, PP. 59-72.

**Table 1**. Road classifications and descriptions by OpenStreetMap project, **Ramm,** and **Chilton, 2011**.

| Road type | Description |
|---|---|
| highway, motorway | A restricted access major divided highway, normally with 2 or more running lanes plus emergency hard shoulder. Equivalent to the Freeway, Autobahn, etc.. |
| highway, trunk | The most important roads in a country's system that aren't motorways. (Need not necessarily be a divided highway.) |
| highway, primary | The next most important roads in a country's system. (Often link larger towns.) |
| highway, secondary | The next most important roads in a country's system. (Often link smaller towns and villages.) |
| highway, tertiary | The next most important roads in a country's system. |
| highway, residential | Roads which are primarily lined with and serve as an access to housing. |
| highway, service | For access roads to, or within an industrial estate, camp site, business park, car park etc. |

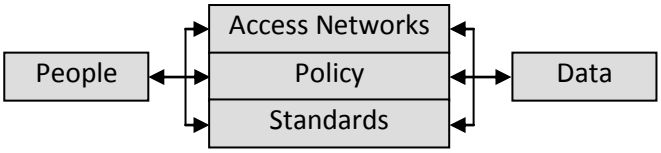


**Figure 1**. SDI components, **Rajabifard,** and **Williamson, 2006.**

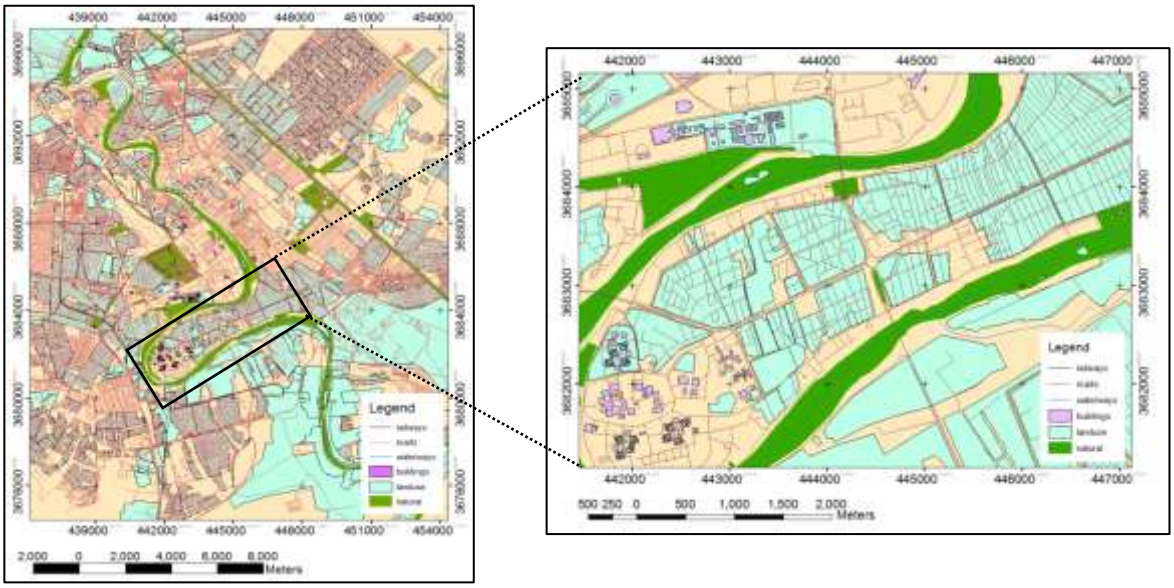


**Figure 2**. Geographical location of the study area with the studied roads.

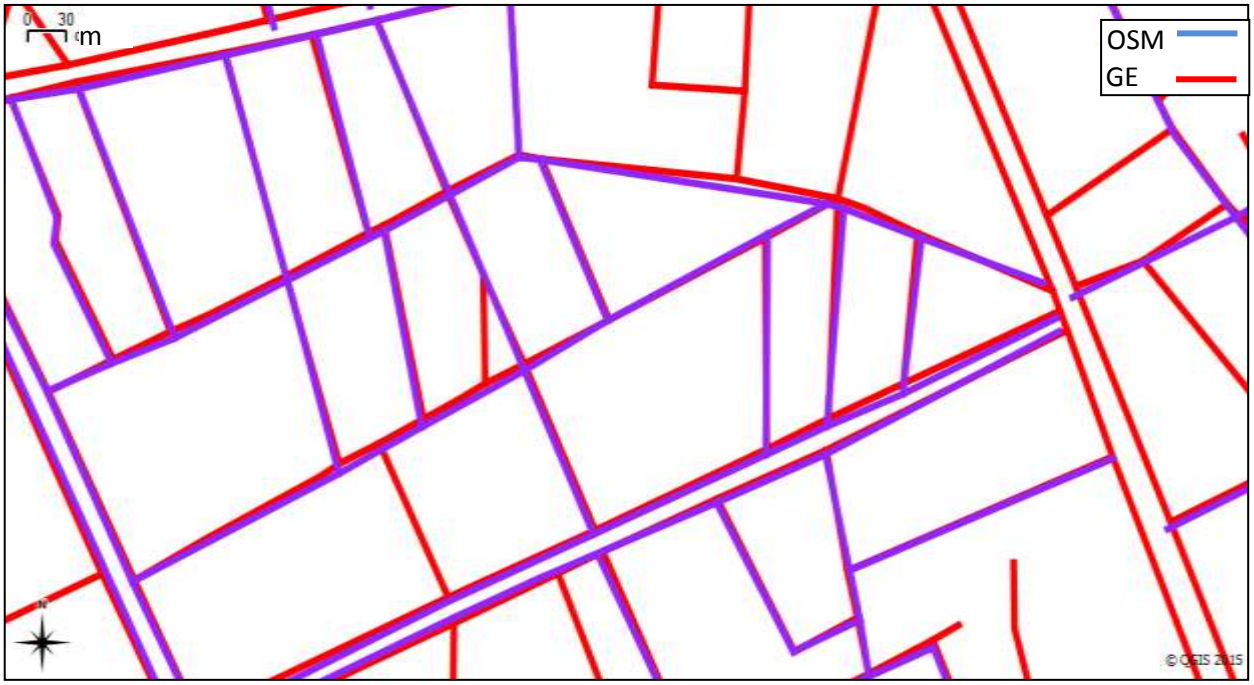


**Figure 3.** Example of matched and mismatched data.

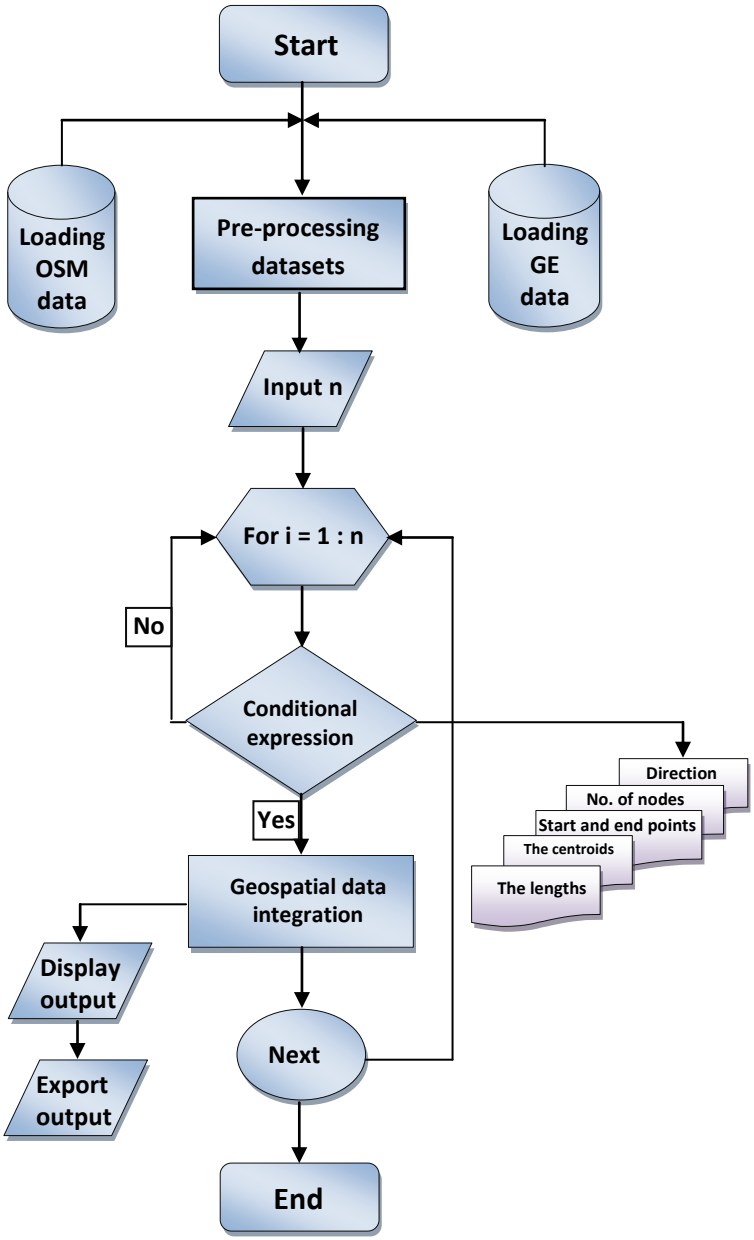


**Figure 4.** The workflow of the designed program

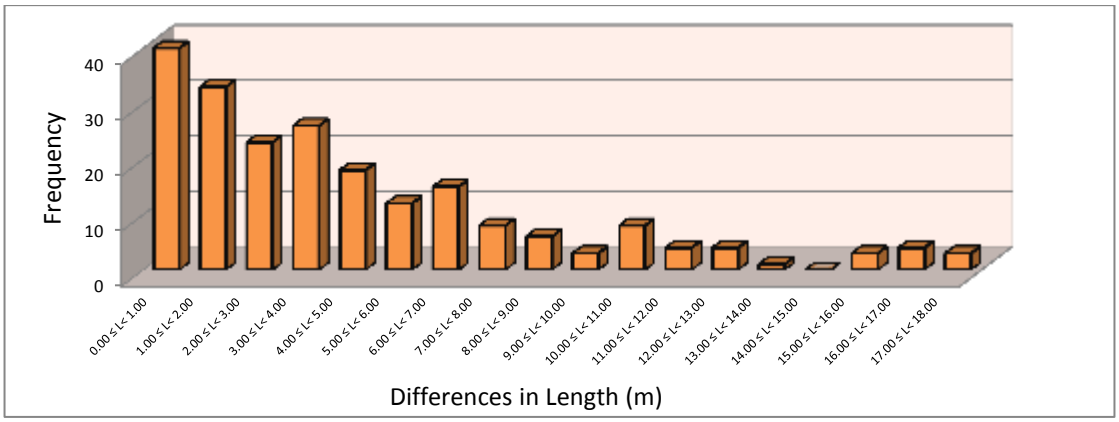


**Figure 5**. The diffrences in roads length.

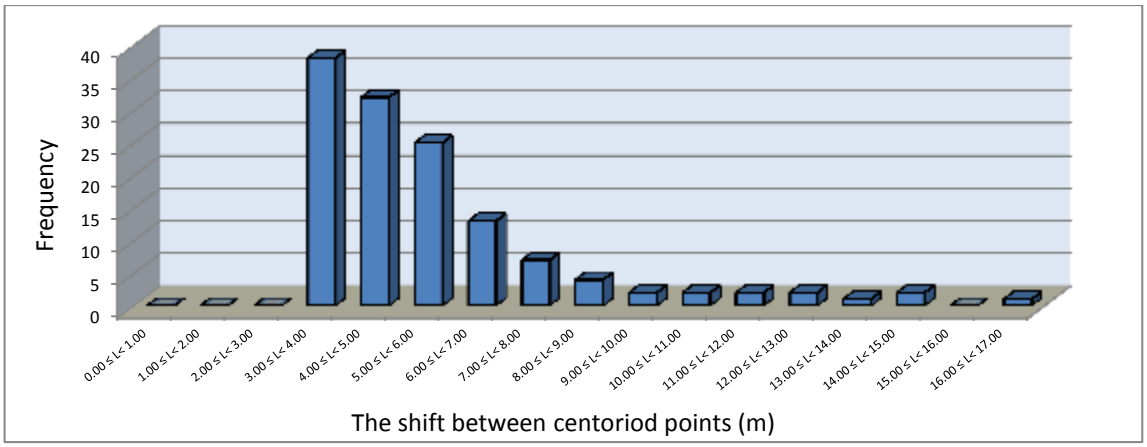


**Figure 6**. The differences in centoroid.

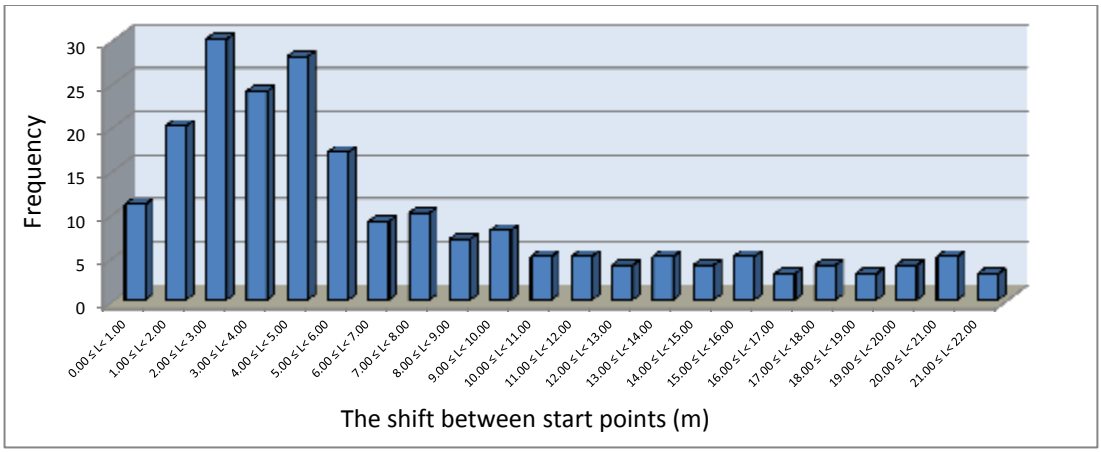


**Figure 7**. The differences in start points.

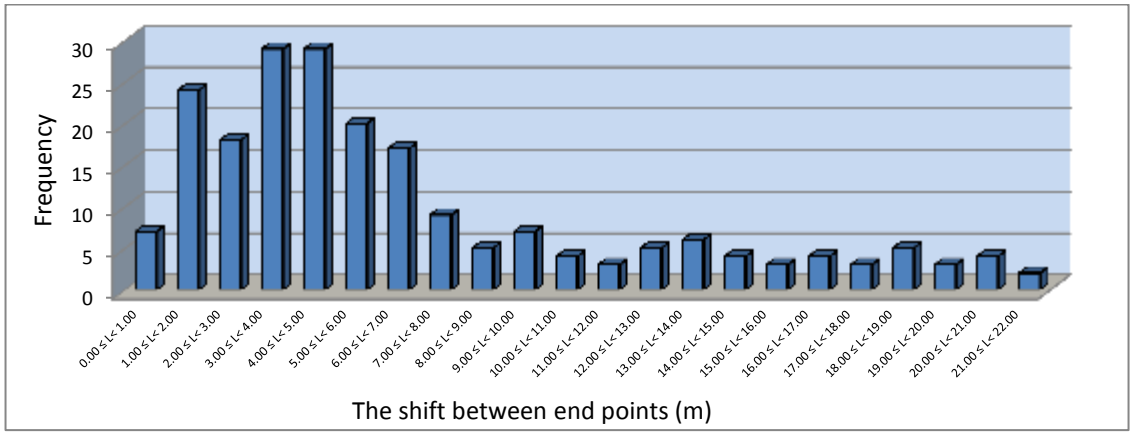


**Figure 8**. The differences in end points.

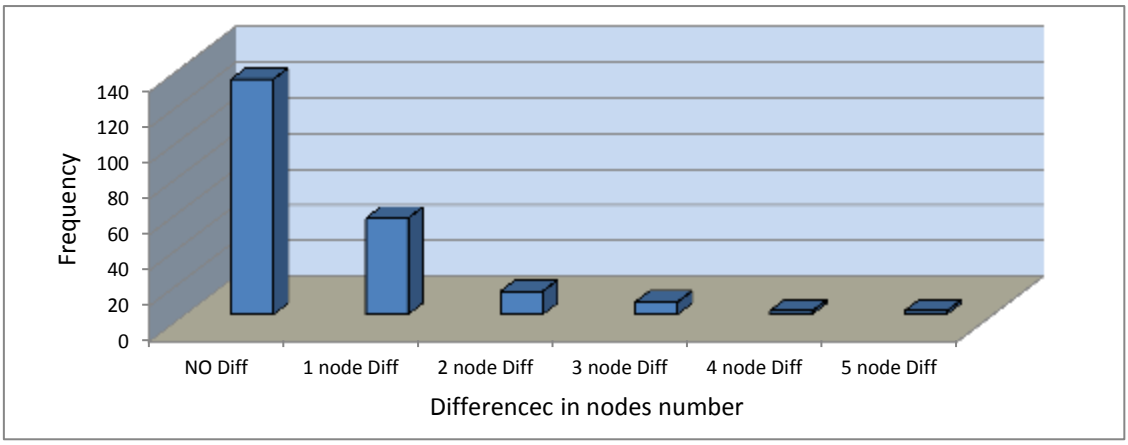


**Figure 9**. The differences between node numbers.

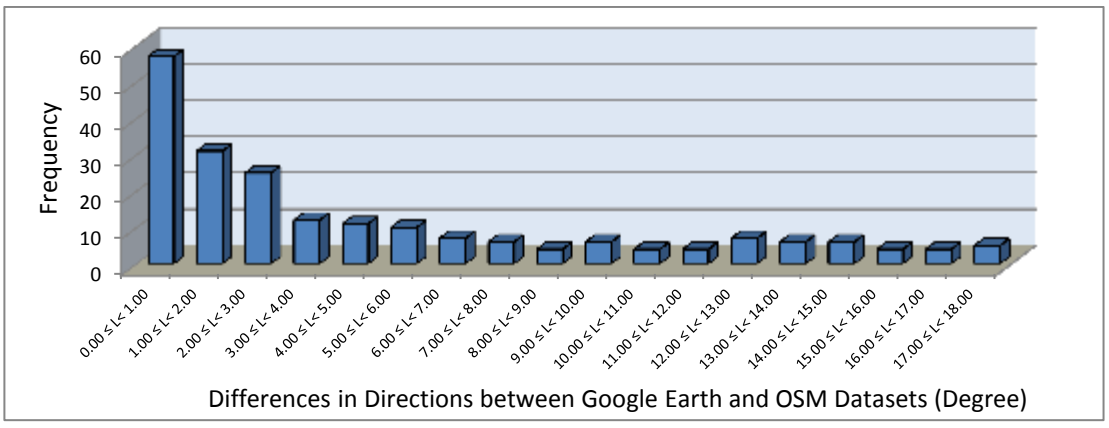


**Figure 10**. The differences in direction.